



## ORDERING INFORMATION

Requests for copies of this report should be directed to Research Reports Center (RRC), Box 50490, Palo Alto, CA 94303, (415) 965-4081. There is no charge for reports requested by EPRI member utilities and affiliates, contributing nonmembers, U.S. utility associations, U.S. government agencies (federal, state, and local), media, and foreign organizations with which EPRI has an information exchange agreement. On request, RRC will send a catalog of EPRI reports.

Copyright © 1980 Electric Power Research Institute, Inc.

EPRI authorizes the reproduction and distribution of all or any portion of this report and the preparation of any derivative work based on this report, in each case on the condition that any such reproduction, distribution, and preparation shall acknowledge this report and EPRI as the source.

## NOTICE

This report was prepared by the organization(s) named below as an account of work sponsored by the Electric Power Research Institute, Inc. (EPRI). Neither EPRI, members of EPRI, the organization(s) named below, nor any person acting on their behalf: (a) makes any warranty or representation, express or implied, with respect to the accuracy, completeness, or usefulness of the information contained in this report, or that the use of any information, apparatus, method, or process disclosed in this report may not infringe privately owned rights; or (b) assumes any liabilities with respect to the use of, or for damages resulting from the use of, any information, apparatus, method, or process disclosed in this report.

Prepared by  
Stanford University  
Stanford, California

## ABSTRACT

This study has examined the adsorptive/coprecipitation behavior of several inorganic cations and anions in systems containing freshly precipitated X-ray amorphous iron oxyhydroxide. The project examined experimentally several simple, well-characterized model systems to establish type behavior in sufficient detail to allow interpretation of subsequent experimental work on less well-characterized waste materials. A prominent feature of this project was evaluation of the feasibility of utilizing iron-bearing waste liquids as source materials for the precipitation of amorphous iron oxyhydroxide in trace element removal processes. The roles of complexing ligands and competing metals and ligands, and their significance in controlling the distribution of trace elements at the solution/oxide interface have been characterized. From this research a new semi-quantitative model of oxide surfaces has been proposed, as well as a model to describe adsorption of various metal-ligand complexes. Experimental results indicate the adsorption/coprecipitation process with amorphous iron oxyhydroxide is feasible for removing trace elements from a variety of power plant waste streams. In addition, the feasibility of using an acid-metal cleaning waste containing high concentrations of dissolved iron as the iron source for coprecipitation of trace elements has been confirmed. The adsorptive removal of trace elements from real waste streams in complex systems (real wastes) using either reagent iron sources or acid-metal cleaning waste can be interpreted in terms of the generalized behavior of model systems.

9 1 1 2 7 5 1 1 1 1 1 5 1 1 7 5

THIS PAGE INTENTIONALLY  
LEFT BLANK

## EPRI PERSPECTIVE

### PROJECT DESCRIPTION

This final report is the first in a sequence of research reports to be delivered under RP910. It documents the results of laboratory experiments evaluating the feasibility of employing freshly precipitated ferric oxyhydroxide to extract trace elements from power plant waste streams.

Precipitation and coagulation of ferric hydroxide has long been a conventional treatment for water clarification. Much is known regarding its formation, its sedimentation characteristics, and its ability to capture suspended material in solution; however, there is a lack of published literature addressing the compound's adsorptive property. Based on literature reviews of the subject, Stanford University researchers determined that freshly precipitating ferric iron can induce aqueous trace element insolubilization by adsorption. If such a means for reducing trace quantities of potentially toxic substances is determined to be technically and economically feasible, it will enable utilities to comply with current effluent regulatory controls governing inorganic pollutants.

The project is divided into successive phases of principal activities. In this initial phase, the behavior of trace metals in the presence of precipitated ferric hydroxide was examined under well-controlled laboratory conditions. The motivation for this effort was to determine the applicability and usefulness of this chemical-physical phenomenon. This report discusses the findings in detail.

Subsequent phases of work will be directed at the process and engineering application of this technique in the power plant cycle. If warranted, plans for field testing will be developed, a test facility fabricated, and tests conducted.

### PROJECT OBJECTIVES

The major objective of the present effort is to clearly define the capabilities and limitations of aqueous trace element insolubilization by freshly precipitated

ferric iron for a total of seven elements common to power plant waste streams. They are cadmium, copper, lead, zinc, arsenic, selenium, and chromium. More specifically, the project will: (1) establish the kinetics and equilibrium levels of trace element removal; (2) define a coprecipitation/adsorption model which permits prediction of the process behavior in other chemical environments, based on the acquired data set from laboratory studies; (3) determine the effect of using spent-metal cleaning wastewaters as the source of iron to generate the iron hydroxide adsorbent; and finally, (4) confirm the removal of trace elements from actual power plant waste stream samples.

#### PROJECT RESULTS

The results and conclusions confirmed the feasibility of employing iron hydroxide adsorption/coprecipitation for reducing trace-metal concentrations. With the exception of wastes bearing chelating agents, such as ethylenediaminetetraacetic acid (EDTA), adsorption removal ratios in excess of 90% for a number of trace metals were achieved on freshly precipitated iron. These are encouraging results. Although not as dramatic, the substitution of spent-metal cleaning wastewaters as the iron-reactant feed source did promote reasonable removal ratios.

To fully accomplish the goal of this project, further research and studies are recommended. Continued support of this research is necessary to resolve remaining uncertainties and to generate specific process performance data. In order to make this process available to the utility industry as a usable option, the method must be put into practice. Engineering, operating, and detailed economic feasibility must be established. This requires development of system design and operating criteria, assessment of possible treatment strategies and configurations, and formulation of a pilot-scale demonstration plan. These will be the objectives in Phase II.

Roger M. Jorden, Project Manager  
Winston Chow, Project Manager  
Coal Combustion Systems Division

#### ACKNOWLEDGMENTS

This work has been greatly aided by discussions with G. A. Parks of Stanford University, R. O. James of CSIRO of Australia, and J. A. Davis of the Swiss Federal Institute for Water Resources and Water Pollution Control. The technical assistance of R. Appleton and B. Honeyman are acknowledged.

6  
1  
1  
1  
5  
3  
1  
1  
6

THIS PAGE INTENTIONALLY  
LEFT BLANK

## CONTENTS

<u>Section</u>	<u>Page</u>
1 INTRODUCTION	1-1
Project Objectives	1-1
2 ADSORPTION OF METALS AT THE SOLID/SOLUTION INTERFACE	2-1
Introduction	2-1
The Solid/Solution Interface	2-1
Adsorption Patterns and Models for Hydrolyzable Metals	2-2
Empirical Studies of Metal Adsorption from Solution	2-5
Adsorption Isotherms	2-6
Effects of Complexing Ligands	2-10
Effects of Competing Metals	2-10
Adsorption Stoichiometry	2-13
References	2-15
3 EQUILIBRIUM METAL ADSORPTION AND COPRECIPITATION IN LIGAND-FREE SYSTEMS	3-1
Introduction	3-1
Adsorption vs. Coprecipitation	3-1
Kinetics of Adsorption and Coprecipitation	3-3
Adsorption Isotherms--Theoretical Considerations	3-7
Adsorption Isotherms for Individual Metal Ions	3-7
Isotherms in Models of Metal Adsorption at the Oxide/ Solution Interfaces	3-13
Experimental Results: Adsorption Isotherms and the Need for a Multi-Site Model	3-14
Experimental Isotherm	3-14
Possible Causes for Non-Langmuir Behavior	3-19
A Model of Adsorption on a Multi-Site Surface	3-23
Mathematical Development	3-23
Comparison of the Model with Experimental Results	3-28
Estimating the Surface Density and Binding Strength of High-Energy Sites	3-33

<u>Section</u>		<u>Page</u>
3	Testing the Model with Amorphous and Crystalline Systems	3-34
	Estimating the "Instantaneous" Adsorption Constant	3-44
	Comparison of $K_{e,o}$ with $K_1$ Values from the SGMA Model	3-46
	Continuous vs. Discrete Distribution of Surface Sites	3-48
	Summary	3-49
	Competitive Adsorption Studies	3-50
	Adsorption Stoichiometry	3-53
	Prospects for Improving Adsorption Models	3-56
	References	3-57
4	EQUILIBRIUM ANION ADSORPTION AND COPRECIPITATION	4-1
	Importance of Adsorbent Concentration	4-2
	Kinetics	4-7
	Competitive Anion Adsorption	4-10
	Modeling of Anion Adsorption Experiments by the SGMA Model	4-16
	References	4-18
5	EFFECTS OF COMPLEXING LIGANDS ON METAL ION ADSORPTION: EXPERIMENTAL RESULTS AND A CONCEPTUAL MODEL	5-1
	Introduction	5-1
	Arguments Supporting Adsorption of Complexes	5-1
	A Semi-Quantitative Model of Metal Adsorption in Systems Containing Complexing Ligands	5-3
	Conceptual Basis of the Model	
	Chemical Reactions and Equilibria in Me/L/S Systems	5-4
	Surface Speciation	5-9
	Re-Evaluation of the Assumptions of the Model	5-12
	Summary of the Model	5-21
	Correlation of the Model with Experimental Results	5-22
	Stereochemistry of Adsorbed Complexes	5-26
	Summary	5-28
	References	5-29
6	LABORATORY STUDIES WITH COAL-FIRED POWER PLANT WASTE STREAMS	6-1
	General Discussion of Power Plant Wastes	6-1
	Introduction	6-1
	Review of Power Plant Wastes	6-1
	Wastes and Waste Characteristics	6-7
	Characterization of the Fly Ashes	6-7
	Preparation and Handling of Fly-Ash Solutions	6-7

<u>Section</u>	<u>Page</u>
Preparation and Handling of Power Plant Wastes	6-7
Analysis of Selected Constituents in Power Plant Wastes	6-9
Characteristics of the Fly Ash, Bromate, Vertan, and Acid-Iron Wastes	6-9
6 Coprecipitation of Trace Elements Using Waste Materials	6-16
Zinc Adsorption	6-16
Cadmium Adsorption	6-21
Copper Adsorption	6-24
Selenite Adsorption: Bromate Waste	6-35
Anion Removal	6-28
Selenite Adsorption	6-28
Selenite Adsorption: Fly-Ash Waste	6-30
Selenite Adsorption: Vertan Waste	6-37
Chromate Adsorption	6-37
Chromate Adsorption: Fly-Ash Waste	6-39
Chromate Adsorption: Bromate Waste	6-41
Chromate Adsorption: Vertan Waste	6-41
Arsenate Adsorption	6-41
Arsenate Adsorption: Fly-Ash Waste	6-41
Arsenate Adsorption: Bromate and Vertan Wastes	6-44
Anions: Ion-Pair and Complex Formation	6-45
Summary: Anion Removal from Wastes	6-46
Mixing Studies	6-46
Characteristics of Amorphous Iron Oxyhydroxide	6-47
Results of Mixing Experiments	6-48
Coagulation and Settling Studies	6-54
Technical Feasibility	6-54
Economic Feasibility	6-58
References	6-61
7 SUMMARY, CONCLUSIONS, AND SUGGESTIONS FOR FUTURE WORK	7-1
Summary	7-1
Conclusions	7-3
Suggestions for Further Work	7-4
References	7-6
APPENDIX A EXPERIMENTAL DATA	A-1
APPENDIX B EXPERIMENTAL METHODS AND MATERIALS	B-1
Reagents and Instrumentation	B-1

	<u>Page</u>
Experimental Procedures	B-2
Preparation of the Adsorbents	B-2
Characterization of the Adsorbents	B-2
Amorphous Iron Oxyhydroxide	B-3
Adsorption Kinetics	B-9
Procedures for Equilibrium Adsorption and Coprecipitation Experiments	B-10
APPENDIX B	
Analytical Procedures	B-12
Radioisotopes	B-12
Copper and Lead	B-13
pH Measurement	B-13
Mixing Studies	B-14
Experimental Procedures for Coagulation and Sedimentation Experiments	B-14
References	B-15

## ILLUSTRATIONS

<u>Figure</u>	<u>Page</u>
3-1 Adsorption and coprecipitation of cadmium onto am-Fe(OH) <sub>3</sub>	3-4
3-2 Adsorption and coprecipitation of selenate onto am-Fe(OH) <sub>3</sub>	3-4
3-3 Kinetics of coprecipitation of zinc onto am-Fe(OH) <sub>3</sub>	3-5
3-4 Kinetics of adsorption of silver onto am-Fe (OH) <sub>3</sub>	3-5
3-5 Kinetics of adsorption of copper onto SiO <sub>2</sub>	3-6
3-6 Kinetics of adsorption of cadmium onto $\gamma$ Al <sub>2</sub> O <sub>3</sub>	3-6
3-7a Relationship between adsorption bond energy and adsorption density of the Freundlich and Langmuir isotherms	3-11
3-7b Typical plots of $\log (\Gamma/\Gamma_{\max})$ vs. $\log C_{\text{eq}}$ for a) Langmuir and b) Freundlich isotherms	3-11
3-8 Fractional adsorption of Cd on am-Fe(OH) <sub>3</sub> as a function of Fe <sub>T</sub> and pH	3-15
3-9 Fractional adsorption of Cd on am-Fe(OH) <sub>3</sub> as a function of Cd <sub>T</sub> and pH	3-15
3-10 Adsorption isotherm for Cd on am-Fe(OH) <sub>3</sub> for Cd <sub>T</sub> /Fe <sub>T</sub> > 2 x 10 <sup>-5</sup> mole/mole	3-16
3-11 Adsorption edge for Cd adsorbing on am-Fe(OH) <sub>3</sub> at very low adsorption density	3-17
3-12 Adsorption isotherm for Cd on am-Fe(OH) <sub>3</sub> at very low adsorption density	3-17
3-13 Effects of metal ion concentration on fraction adsorption: Comparison of experimental with SGMA model prediction	3-21
3-14 Log K <sub>e</sub> vs. log $\Gamma_{\text{Cd}}$ for x = 1.8	3-29
3-15 Log K <sub>e</sub> vs. log $\Gamma_{\text{Cd}}$ for x = 2.0	3-29
3-16 Apparent proton release accompanying adsorption of Cd on am-Fe(OH) <sub>3</sub> assuming constant K <sub>e</sub>	3-32
3-17 Log K <sub>e</sub> vs. log Cu for x = 1.88	3-35
3-18 Log K <sub>e</sub> vs. log $\Gamma_{\text{Pb}}$ for x = 1.65	3-36
3-19 Log $\Gamma_{\text{Ag}}$ vs. log [Ag <sup>+</sup> ] <sub>eq</sub> for pH equal to 6.5 and 10.0	3-36
3-20 Log K <sub>e</sub> vs. log $\Gamma_{\text{Zn}}$ for x = 3.2	3-37
3-21 Adsorption isotherm for Hg on am-Fe(OH) <sub>3</sub>	3-39
3-22 Log K <sub>e</sub> vs. log $\Gamma_{\text{Hg}}$ for x = 2.0	3-39
3-23 Fractional adsorption of Cd on $\gamma$ -Al <sub>2</sub> O <sub>3</sub> as a function of Cd <sub>T</sub> and pH	3-40
3-24 Fractional adsorption of Cd on $\gamma$ -Al <sub>2</sub> O <sub>3</sub> as a function of Cd <sub>T</sub> and pH at very low adsorption density	3-40

<u>Figure</u>	<u>Page</u>
3-25 Log $K_e$ vs. log $\Gamma_{Cd}$ for $x = 1.6$	3-41
3-26 Fractional adsorption of Cu on $\alpha\text{-SiO}_2$ as a function of $Cu_T$ and pH	3-42
3-27 Effect of $5 \times 10^{-7}M$ Cu on the adsorption edge for $5 \times 10^{-5}M$ Cd on am-Fe(OH) <sub>3</sub>	3-51
3-28 Effect of Cu on the adsorption edge for Cd on am-Fe(OH) <sub>3</sub> when $Cu_T > Cd_T$	3-51
3-29 Effect of $5 \times 10^{-7}M$ Pb, Cu, or Zn on the adsorption edge for $5 \times 10^{-7}M$ Cd on $\gamma\text{-Al}_2\text{O}_3$	3-53
4-1 Percent selenate adsorbed versus pH	4-4
4-2 Percent selenite adsorbed versus pH	4-4
4-3 Percent arsenate adsorbed versus pH	4-6
4-4 Kinetics of adsorption of chromate onto amorphous iron oxyhydroxide	4-8
4-5 Kinetics of coprecipitation of selenite onto amorphous iron oxyhydroxide	4-8
4-6 Kinetics of adsorption/desorption of chromate onto amorphous iron oxyhydroxide	4-9
4-7 Effects of addition of iron on selenate adsorption in pre-equilibrated system	4-10
4-8 Partitioning of selenate and sulfate anion in a competitive adsorption experiment	4-13
4-9 Effects of sulfate addition on chromate adsorption	4-15
4-10 Comparison of the effects of sulfate and selenate addition on chromate adsorption	4-16
5-1 Possible pH-adsorption edges for different types of systems	5-4
5-2 Effect of ligand concentration and equilibrium constants on pH-adsorption curves	5-11
5-3 Expected dependence of adsorption edges for metals and ligands on total adsorbate concentration	5-14
5-4 Effect of total metal concentration on pH	5-16
5-5 Total fractional metal sorption on non-homogeneous surfaces	5-16
5-6 Effect of adsorbate concentration on adsorption edge in cases where site-limitation is suspected	5-18
5-7 Effect of total adsorbate concentration on adsorption edge for ligands which significantly shift the IEP	5-18

<u>Figure</u>	<u>Page</u>
5-8 Adsorption edges for ligand-like, metal-like, and metal-or-ligand-like complexes	5-19
5-10a Effects of $\text{SO}_4^{2-}$ and $\text{Cl}^-$ on Cd adsorption	5-24
5-10b Effects of $\text{S}_2\text{O}_3^{2-}$ on Cd adsorption	5-24
5-11 Effects of $\text{Cl}^-$ on Ag adsorption	5-25
5-12 Effects of $\text{S}_2\text{O}_3^{2-}$ on Ag adsorption	5-25
6-1 Complexation of copper ion in solution as a function of bromate addition	6-12
6-2 Complexation of copper ion in solution as a function of vertan addition	6-12
6-3 Variation in the pH of various fly-ash solutions as a function of water:ash ratios. 4 days contact	6-14
6-4 Variation of the conductivity of various fly-ash solutions as a function of water:ash ratios	6-14
6-5 Percent adsorption of zinc onto waste am- $\text{Fe}(\text{OH})_3$ as a function of pH in a coprecipitating system	6-17
6-6 Percent zinc adsorbed onto waste am- $\text{Fe}(\text{OH})_3$ as a function of pH and iron dose	6-17
6-7 Percent zinc adsorbed onto waste am- $\text{Fe}(\text{OH})_3$ as a function of pH and fly-ash leachate	6-19
6-8 Percent zinc adsorbed onto waste am- $\text{Fe}(\text{OH})_3$ in fly-ash 1 leachate as a function of pH and iron dose	6-19
6-9 Percent zinc adsorbed onto waste am- $\text{Fe}(\text{OH})_3$ in fly ash 2 as a function of pH and iron dose	6-20
6-10 Percent zinc adsorbed onto waste am- $\text{Fe}(\text{OH})_3$ in fly ash 3 as a function of pH and iron dose	6-20
6-11 Percent zinc adsorption on waste am- $\text{Fe}(\text{OH})_3$ in fly ash 1 as a function of time at constant pH	6-22
6-12 Percent zinc adsorption onto am- $\text{Fe}(\text{OH})_3$ as a function of pH and bromate waste addition	6-22
6-13 Percent zinc adsorbed onto waste am- $\text{Fe}(\text{OH})_3$ from a vertan waste diluted 1:500	6-23
6-14 Percent cadmium adsorbed onto waste am- $\text{Fe}(\text{OH})_3$ as a function of pH and iron dose	6-23
6-15 Comparison of cadmium adsorption onto waste am- $\text{Fe}(\text{OH})_3$ from fly-ash waste and distilled water	6-24

<u>Figure</u>	<u>Page</u>
6-16 Percent Cu adsorbed onto waste am-Fe(OH) <sub>3</sub> in fly-ash 1 solution as a function of pH and iron dose	6-26
6-17 Percent Cu adsorbed onto waste am-Fe(OH) <sub>3</sub> as a function of pH and bromate concentration (dilution ratio given as volume bromate waste per volume distilled water)	6-26
6-18 Percent Cu adsorbed onto waste am-Fe(OH) <sub>3</sub> as a function of pH and iron dose	6-27
6-19 Percent Cu adsorbed onto waste am-Fe(OH) <sub>3</sub> in 0.2% vertan as a function of pH and iron dose	6-27
6-20 Percent adsorption of selenite onto am-Fe(OH) <sub>3</sub> as a function of pH in a coprecipitating system	6-29
6-21 Adsorption of selenite onto waste am-Fe(OH) <sub>3</sub> from fly-ash 1 waste solution	6-31
6-22 Adsorption of selenite onto waste am-Fe(OH) <sub>3</sub> from fly-ash 2 waste solution	6-31
6-23 Adsorption of selenite onto waste am-Fe(OH) <sub>3</sub> from fly-ash 3 waste solution	6-32
6-24 Selenite adsorption onto am-Fe(OH) <sub>3</sub> from various sources	6-32
6-25 Adsorption of selenite onto waste am-Fe(OH) <sub>3</sub> from a bromate waste solution	6-35
6-26 Adsorption of selenite onto am-Fe(OH) <sub>3</sub> from vertan waste solution	6-38
6-27 Percent chromate adsorbed onto am-Fe(OH) <sub>3</sub> as a function of pH	6-38
6-28 Chromate adsorption onto waste am-Fe(OH) <sub>3</sub> from fly ash 1 and in a model system	6-40
6-29 Chromate adsorption onto waste am-Fe(OH) <sub>3</sub> from fly ash 2 and in a model system	6-40
6-30 Chromate adsorption onto waste am-Fe(OH) <sub>3</sub> from bromate waste	6-42
6-31 Chromate adsorption onto waste am-Fe(OH) <sub>3</sub> from a vertan waste solution	6-42
6-32 Arsenate adsorption onto am-Fe(OH) <sub>3</sub> in a model system	6-43
6-33 Adsorption of arsenate onto am-Fe(OH) <sub>3</sub> as a function of pH	6-43
6-34 Arsenate adsorption onto waste am-Fe(OH) <sub>3</sub> from fly-ash 2 waste solution	6-44

<u>Figure</u>	<u>Page</u>
6-35 Mixing characteristic curves for ideal case and four experimental systems	6-50
6-36 Elapsed time versus residence time at constant $C/C_0$ (0.367) for various experimental mixing rates	6-51
6-37a Kinetics of Cd adsorption on am-Fe(OH) <sub>3</sub> formed in mixing chamber with $\bar{t} = 5$ sec	6-52
6-37b Kinetics of Cd adsorption on am-Fe(OH) <sub>3</sub> formed in mixing chamber with $\bar{t} = 30$ sec	6-52
6-38 pH-adsorption and pH-coprecipitation edges for Cd on am-Fe(OH) <sub>3</sub> formed under varying mixing regimes	6-53
6-39 Variation of residual turbidity with iron dose for 1:10 bromate and 1:100 vertran solutions	6-55
6-40 Variation of residual turbidity as a function of polymer dose for 1:10 bromate and 1:100 vertran solutions	6-55
6-41 Variation of residual turbidity as a function of pH for 1:10 bromate and fly-ash solutions	6-56
6-42 Variation of residual turbidity as a function of bromate dilution	6-57
6-43 Residual turbidity as a function of settling time for 1:10 bromate and fly-ash solutions	6-57
A-1 pH-adsorption edge for Cd on am-Fe(OH) <sub>3</sub> : Effect of total iron	A-4
A-2 pH-adsorption edge for Cd on am-Fe(OH) <sub>3</sub> : Effect of total Cd	A-4
A-3 Adsorption isotherm for Cd on am-Fe(OH) <sub>3</sub>	A-5
A-4 Cadmium removal as a function of am-Fe(OH) <sub>3</sub> dosage at varying pH	A-5
A-5 pH-adsorption edge for Cd on Fe(OH) <sub>3</sub> : Results at low adsorption densities	A-6
A-6 Adsorption isotherm for Cd on am-Fe(OH) <sub>3</sub> : Very low adsorption density	A-6
A-7 pH-adsorption edge for Cu on am-Fe(OH) <sub>3</sub> : Effect of total Cu	A-7
A-8 pH-adsorption edge for Cu on am-Fe(OH) <sub>3</sub> : Effect of total iron	A-7
A-9 Adsorption isotherm for Cu on am-Fe(OH) <sub>3</sub>	A-8
A-10 Copper removal as a function of am-Fe(OH) <sub>3</sub> dosage at varying pH	A-8
A-11 pH-adsorption edge for Zn on am-Fe(OH) <sub>3</sub> : Effect of total Zn	A-9
A-12 pH-adsorption edge for Zn on am-Fe(OH) <sub>3</sub> : Effect of total Zn	A-9
A-13 pH-adsorption edge for Zn on am-Fe(OH) <sub>3</sub> : Effect of total iron	A-10
A-14 Adsorption isotherm for Zn on am-Fe(OH) <sub>3</sub>	A-10

<u>Figure</u>	<u>Page</u>
A-15 pH-adsorption edge for Pb on am-Fe(OH) <sub>3</sub> : Effect of total-Pb	A-11
A-16 pH-adsorption edge for Pb on am-Fe(OH) <sub>3</sub> : Effect of total iron	A-11
A-17 Adsorption isotherm for Pb on am-Fe(OH) <sub>3</sub>	A-12
A-18 pH-adsorption edge for Cd on γ-Al <sub>2</sub> O <sub>3</sub> : Effect of total Cd	A-12
A-19 pH-adsorption edge for Cd on γ-Al <sub>2</sub> O <sub>3</sub> : Effect of total Cd at very low adsorption density	A-13
A-20 pH-adsorption edge for Cu on γ-Al <sub>2</sub> O <sub>3</sub> : Effect of total Cu	A-13
A-21 pH-adsorption edge for Zn on γ-Al <sub>2</sub> O <sub>3</sub> : Effect of total Zn	A-14
A-22 pH-adsorption edge for Pb on γ-Al <sub>2</sub> O <sub>3</sub> : Effect of total Pb	A-14
A-23 pH-adsorption edge for Cd on α-SiO <sub>2</sub> : Effect of total Cd	A-15
A-24 pH-adsorption edge for Cd on α-SiO <sub>2</sub> : Effect of total SiO <sub>2</sub> and total Cd	A-15
A-25 Adsorption isotherm for Cd on α-SiO <sub>2</sub> : Effect of pH	A-16
A-26 pH-adsorption edge for Cu on α-SiO <sub>2</sub> : Effect of total Cu	A-16
A-27 pH-adsorption edge for Pb on α-SiO <sub>2</sub> : Effect of total Pb	A-17
A-28 pH-adsorption edge for Zn on α-SiO <sub>2</sub> : Effect of total Zn	A-17
A-29 pH-adsorption edge for arsenate on am-Fe(OH) <sub>3</sub> : Effects of total iron and total arsenate	A-18
A-30 Adsorption isotherm for arsenate on am-Fe(OH) <sub>3</sub> : Effect of pH	A-18
A-31 Arsenate removal as a function of am-Fe(OH) <sub>3</sub> dosage at pH = 9.5 and pH = 10.5	A-19
A-32 pH-adsorption edge for chromate on am-Fe(OH) <sub>3</sub>	A-19
A-33 pH-adsorption edge for chromate on am-Fe(OH) <sub>3</sub>	A-20
A-34 pH-adsorption edge for selenate on am-Fe(OH) <sub>3</sub> : Effect of total SeO <sub>4</sub> <sup>2-</sup>	A-20
A-35 Adsorption isotherm of selenate on am-Fe(OH) <sub>3</sub> : Effect of pH	A-21
A-36 Selenate removal as a function of am-Fe(OH) <sub>3</sub> dosage at pH = 4.5 and pH = 6.5	A-21
A-37 pH-adsorption edge for selenite on am-Fe(OH) <sub>3</sub> : Effect of total iron and total SeO <sub>3</sub> <sup>2-</sup>	A-22
A-38 pH-adsorption edges for Cd on am-Fe(OH) <sub>3</sub> : Effect of NaCl concentration	A-22

<u>Figure</u>	<u>Page</u>
A-39 pH-adsorption edge for Cd on am-Fe(OH) <sub>3</sub> : Effect of SO <sub>4</sub> <sup>2-</sup> concentration	A-23
A-40 pH-adsorption edge for Cu on am-Fe(OH) <sub>3</sub> : Effect of swamping media anion (Cl <sup>-</sup> on NO <sub>3</sub> <sup>-</sup> )	A-23
A-41 pH-coprecipitation edge for Cu on am-Fe(OH) <sub>3</sub> : Effect of NH <sub>3</sub> concentration	A-24
A-42 pH-coprecipitation edge for Zn on am-Fe(OH) <sub>3</sub> : Effect of NaCl concentration	A-24
A-43 pH-coprecipitation edge for Zn on am-Fe(OH) <sub>3</sub> : Effect of SO <sub>4</sub> <sup>2-</sup> concentration	A-25
A-44 pH-adsorption edge for Cd on am-Fe(OH) <sub>3</sub> : Effect of SO <sub>4</sub> <sup>2-</sup> , Cl <sup>-</sup> concentration	A-25
A-45 pH-adsorption edge for Cd on am-Fe(OH) <sub>3</sub> : Effect of S <sub>2</sub> O <sub>3</sub> concentration	A-26
A-46 pH-adsorption edge for Cd on am-Fe(OH) <sub>3</sub> : Effect of S <sub>2</sub> O <sub>3</sub> concentration	A-26
A-47 pH-adsorption edge for Cd on am-Fe(OH) <sub>3</sub> in presence of Cu	A-27
A-48 pH-adsorption edge for Cd on am-Fe(OH) <sub>3</sub> in presence of Zn	A-27
A-49 pH-adsorption edge for Cd on am-Fe(OH) <sub>3</sub> in presence of Pb	A-28
A-50 pH-adsorption edge for Zn on am-Fe(OH) <sub>3</sub> in presence of Cd	A-28
A-51 pH-adsorption edge for Zn on am-Fe(OH) <sub>3</sub> in presence of Pb	A-29
A-52 pH-adsorption edge for Zn on am-Fe(OH) <sub>3</sub> in presence of Cu	A-29
B-1 Change in pH ( $\Delta$ pH) upon addition of sodium nitrate to amorphous iron oxide suspensions as a function of pH measured in low ionic strength medium (1.5 x 10 <sup>-3</sup> M NaNO <sub>3</sub> ). p <sub>H</sub> PZC is ~ 7.9	B-6
B-2 Surface charge density ( $\sigma_0$ ) of amorphous iron oxide as a function of pH at various ionic strengths. BET surface area of 182 m <sup>2</sup> /g and p <sub>H</sub> PZC of 7.9 used in the calculation of surface charge density	B-6
B-3 Surface charge density curves for goethite, hematite, and amorphous iron oxide in 0.1M KNO <sub>3</sub> . After Yates (3)	B-7
B-4 Mixing tank diagram (cross section)	B-14

THIS PAGE INTENTIONALLY  
LEFT BLANK

1  
0  
1  
1  
1  
5  
3  
7  
1  
1  
6

TABLES

<u>Table</u>	<u>Page</u>
2-1 Summary of Published Literature from Which Adsorption Isotherms for Metals Have Been Derived	2-7
2-2 Summary of Published Literature Relating to the Effects of Dissolved Ligands on Metal Adsorption	2-11
2-3 Summary of Published Studies of Competitive Adsorption Between Pairs of Metal Ions	2-12
3-1 Characteristics of Theoretical Adsorption Isotherms	3-13
3-2 Summary of Results--Adsorption in One-Metal Systems in the Absence of Complexing Ligands	3-18
3-3 Fractional Surface Coverage in Typical Experimental Systems	3-20
3-4 Apparent Equilibrium Constants for Various Metals on am-Fe(OH) <sub>3</sub>	3-47
3-5 Proton Release Accompanying Adsorption of Metal Ions on am-Fe(OH) <sub>3</sub>	3-54
4-1 Competitive Adsorption Between SO <sub>4</sub> <sup>2-</sup> and CrO <sub>4</sub> <sup>2-</sup>	4-16
4-2 Apparent Equilibrium Constants for Various Anions on am-Fe(OH) <sub>3</sub>	4-17
5-1 Adsorption in Complex Systems	5-7
5-2 Analysis of the Assumptions of the Proposed Model for Adsorption of Complexes	5-20
5-3 Characteristics of CdL <sub>x</sub> and AgL <sub>x</sub> Sorption on Various Adsorbents	5-22
5-4 Speciation of Dissolved Cadmium in Systems Containing Various Ligands	5-27
6-1 Typical Waste Streams from Coal-Fired Power Plants	6-2
6-2 Waste Disposal Characteristics of Typical Cooling Tower Inhibitor Systems	6-5
6-3 Characteristics of Once-Through Ash Pond Discharges	6-6
6-4 Chemical Composition of Fly Ashes Used in Study	6-8
6-5 Characterization of Fly-Ash Transport Water and Boiler-Cleaning Wastes from a Coal-Fired Power Plant	6-10
6-6 Comparison Between Typical Trace Metals in Ammoniacal Bromate and Hydrochloric Acid Wastes Produced at Allen Steam Station vs. Those Produced at Marshall Steam Station	6-11
6-7 Trace Element Content of Various Fly Ashes and Water Solutions	6-15
6-8 Acid-Iron Waste Constituent Concentration in Experimental System	6-29
6-9 Constituent Concentrations under Given Experimental Conditions	6-33
6-10 Comparison of the Constituent Concentrations of Acid-Iron Waste/ Fly-Ash Systems and Acid-Iron Waste/Na <sub>2</sub> SeO <sub>3</sub> System	6-34

<u>Table</u>	<u>Page</u>
6-11 Constituent Concentrations of Bromate Acid-Iron Waste System Under Experimental Conditions	6-36
6-12 Comparison of Constituent Concentrations ( $Fe_T$ $5.0 \times 10^{-4}M$ )	6-36
6-13 Constituent Concentrations of Vertan Waste/Acid-Iron Waste System Under Given Experimental Conditions	6-39
6-14 Possible Ion Pairs and Complexes for Arsenate, Chromate, and Selenite	6-45
6-15 Comparative Costs of Using Acid-Iron Waste vs. Ferrous Sulfate for Trace Element Removal	6-59
6-16 Estimated Annual Costs--Central Treatment Plant for Coal-Fired Power Plants (Based on Flow of 220 GPD/MW)	6-60
B-1 Specific Surface Area of $\alpha\text{-Fe(OH)}_3$	B-3
B-2 Specific Surface Area of $\gamma\text{-Al}_2\text{O}_3$ Measured by 3 Different Methods	B-9
B-9 Summary of Surface Properties of the Adsorbents	B-9

## SUMMARY

This project was concerned with understanding the dominant processes and mechanisms responsible for entrapment and release of trace elements present in liquid effluent discharges from coal-fired power plants when iron is used as a precipitating and coagulating agent. The specific objectives of the project were to establish the capacity and limitations for trace element removal by freshly precipitated amorphous ferric oxyhydroxide. Although the determination was for a selected group of trace elements requiring removal from waste liquid streams generated in coal-fired power plants, the potential for application of the new information is much broader.

The research objectives were realized through technical review of the pertinent chemical and engineering literature, specific experimental work, and appropriate mathematical modeling. The scope of the research was limited to a study of the behavior of Cd, Cu, Pb, Zn, As, Se, and Cr in well-characterized heterogeneous model systems containing amorphous iron oxyhydroxide and limited experimental work on removal of trace elements from selected real waste liquids from coal-fired power plants. The approach to this project involved proceeding from simple, well-defined model systems to more complex model systems to experimental work utilizing iron-bearing waste liquid to treat typical waste streams from coal-fired power plants.

The terms adsorption and coprecipitation are used interchangeably. No significant difference was noted in the rate and equilibrium data for removal of trace elements on preformed iron oxyhydroxide (adsorption) and simultaneous precipitation (coprecipitation). Reversibility was achieved in both adsorption and coprecipitation systems with the contact time studied (4-6 hours). Thus, trace element adsorption onto and coprecipitation with amorphous iron oxyhydroxide are considered to be operationally the same.

Adsorption of cadmium, zinc, copper, lead, silver, arsenic, selenium, and chromium onto amorphous iron oxyhydroxide and  $\gamma$ -alumina was studied as a function of adsorbent and adsorbate concentrations, solution composition, and pH. All systems were studied under well-controlled conditions.

Fractional adsorption of dissolved metal increases abruptly in a narrow pH range. The pH of abrupt adsorption increases in the order  $Pb < Cu < Zn < Cd \approx Ag$  and  $SeO_4 < CrO_4 < SeO_3 < AsO_4$  under otherwise identical conditions. At extremely low surface coverage, for a given adsorbent concentration, fractional adsorption is independent of total metal concentration. However, at greater adsorption densities, fractional sorption decreases with increasing adsorbate concentration. The Langmuir isotherm cannot model the data.

The adsorption density at which fractional sorption first becomes dependent on total adsorbate concentration varies over several orders of magnitude for different metals on the same adsorbent. The behavior can be modeled by postulating that the surface consists of a wide distribution of surface-site types. Competitive adsorption experiments indicate that in many cases different metal ions preferentially adsorb to different groups of sites. Therefore, adsorption of one metal often may have only a small effect on adsorption of a second ion.

Ligands which form dissolved complexes with metal ions can either increase or decrease metal adsorption. Chloride, sulfate, and ammonia generally decrease fractional adsorption of cadmium at a given pH. The decrease is consistent with the hypothesis that the complexed metal adsorbs somewhat less strongly than the uncomplexed metal. For example, cadmium thiosulfate complexes adsorb in a qualitatively different manner and, on oxides with sufficiently positive surface charge, they can adsorb more strongly than free aquo cadmium. On highly negative surfaces there is negligible adsorption of these complexes. On the other hand, sulfato and chloro complexes of cadmium always adsorbed more weakly than aquo cadmium.

The James-Healy, surface-complexation, and SGMA (Stanford General Model for Adsorption) adsorption models all assume that oxide surfaces are composed of only one type of site. They fail to totally predict the observed variations in adsorption with changing adsorbate concentration. The SGMA adsorption model has been used to model adsorption in this study.

Experimental work to evaluate removal of trace elements from typical waste streams indicated feasibility for removal of trace anions and cations from power-plant fly-ash transport water as well as an ammonia bromate cleaning waste. Results indicated that the adsorption/coprecipitation process would not be feasible for treating trace elements contained in an EDTA vertan cleaning waste. Experimental results from studies using real power-plant waste materials have been interpreted

in terms of the general behavior characteristics of well-characterized model systems. Complete verification of the behavior of trace element removal in complex real wastes was not achieved.

The major conclusions from this research have significance for both fundamental and practical purposes.

Trace elements, in both anionic and cationic form can potentially be removed from very dilute solutions utilizing either a preformed solid ( $\text{Fe}(\text{OH})_3$ ) or by precipitating the solid in situ. The removal behavior of the trace elements studied appeared to be identical regardless of the mode of preparation of the freshly precipitated amorphous iron oxyhydroxide.

The presence or absence of competing ligands for trace metal cations can have a dramatic effect on the removal of the trace metals. This effect is directly correlated to the chemical behavior of the solution complex of the trace metal, where the complex may adsorb or not adsorb, altering the adsorption behavior of the trace metal accordingly. Similar behavior is expected but not confirmed for trace metal anions and major electrolyte cation (e.g.,  $\text{AsO}_4^{2-}$  and  $\text{Ca}^{2+}$  or  $\text{Mg}^{2+}$ ). Thus, solution species which compete for coordination with the trace element species may enhance or retard removal of the trace element on  $\text{Fe}(\text{OH})_3$ .

The presence or absence of major or minor solute species which compete for surface sites can displace the equilibrium concentration of the adsorbing trace element. For example, sulfate competes for the same sites as selenate and chromate causing a decrease in the amount of Se or Cr adsorbed under specific conditions. The presence of a second strongly adsorbing trace metal appears not to strongly influence the adsorption characteristics of a trace metal at very dilute concentrations (e.g., simultaneous adsorption of Pb and Cd).

The rate at which iron reagents are mixed does not appear to affect the partitioning of trace metals after one-hour contact time.

Feasibility of using an acid-metal cleaning waste containing high concentrations of dissolved iron as the iron source for coprecipitation of trace elements has been confirmed.

The adsorptive removal of trace elements from real waste streams in complex systems using either reagent iron sources or acid-metal cleaning waste can be interpreted in terms of the generalized behavior of model systems.

The adsorptive removal characteristics of each trace element of concern must be experimentally verified. Thus, each trace element must be tested experimentally to understand both the qualitative and quantitative aspects of removal by amorphous ferric oxyhydroxide.

Because the removal characteristics of each trace element is a function of the speciation of the trace element and the degree of competition for surface sites on the solid, rather complete chemical characterization of waste streams is required before quantitative prediction will be possible.

Basic work on clean model systems has led to important information concerning the process mechanisms:

- Oxide surfaces consist of sites of varying energy. The variation may be estimated as at least  $\pm 1$  to  $\pm 5$  Kcal/mole, depending on which model of the interface is used. Metals adsorb preferentially to the high-energy sites.
- The density of high-energy sites varies from solid to solid, and from trace element to trace element for a given oxide.
- The high-energy sites represent a small fraction, often less than 0.1 percent, of the total number of surface sites available for trace element adsorption.
- Adsorption of metal ions often has a very small effect on adsorption of other cations, suggesting that high-energy sites can be metal-specific. On the other hand, adsorption of anions can have major effects on adsorption of other anions indicating a more general overlap of site occupancy for anions than cations.
- Complex metal-ligand moieties can adsorb to amorphous iron oxyhydroxide. Under some circumstances the complex can adsorb more strongly than the free metal ion.
- Adsorption of metal-ligand complexes can be analogous to that of either free ligand or free metal. The distinction between the two may be related to the stereochemical orientation of the adsorbed complex.
- All systems were reversible in the contact times studied.

The need for further study in several areas has been realized during the conduct of this research. In some cases, an interpretation of the results of this study awaits clarification by further experimental work. However, the feasibility of removal of trace elements from dilute solutions has been confirmed.

## Section 1

### INTRODUCTION

Assessment, management, and control of man's impact on the environment and the environment's impact on man through release and dispersal of toxic substances are among the high-priority objectives of our day. Success depends partly on our ability to describe, predict, and design for entrapment and removal of these trace contaminants at the source, whenever possible. In order to adequately describe and predict release, transport, and entrapment of trace elements, a fundamental understanding of the controlling processes and mechanisms must be available.

The entrapment, release, and transport of trace elements in heterogeneous aqueous systems is controlled by numerous physical, chemical, and biological processes. The overall objective of this project was concerned with gaining greater insight into the physical-chemical behavior in heterogeneous aqueous environments of such trace elements as Cd, Cu, Pb, Zn, As, Se, and Cr--all of which are known to be trace contaminants (among others) in waste fluids from various operations in coal-fired power plants. Removal of many of these trace elements is possible by adsorption or coprecipitation with hydrous metal oxides. However, there are many factors which affect the efficiency of removal of a trace substance from solution, such as speciation of the trace element, oxidation state, pH, competing ligands and cations, type and characteristics of solid substrate, general composition of solution, temperature, competition for adsorption sites, time of contact, etc. It is, therefore, important to understand the processes and mechanisms controlling the behavior of the specific compounds of interest before reliable predictions can be made. The major focus of this EPRI project, RP-910, was to study and describe the behavior of selected trace elements in the presence of amorphous iron oxyhydroxide.

#### PROJECT OBJECTIVES

This project was concerned with understanding the dominant processes and mechanisms responsible for entrapment and release of trace elements present in liquid effluent discharges from coal-fired power plants when iron is used as a precipitating and coagulating agent. The specific objectives of the project were to establish the capacity and limitations for trace element removal by freshly precipitated ferric

hydroxide. Although the determination was for a selected group of trace elements requiring removal from waste liquid streams generated in coal-fired power plants, the potential for application of the new information is much broader.

The research objectives were realized through technical review of the pertinent chemical and engineering literature, specific experimental work, and appropriate mathematical modeling. The scope of the research was limited to a study of the behavior of Cd, Cu, Pb, Zn, As, Se, and Cr in well-characterized heterogeneous model systems containing amorphous iron oxyhydroxide and limited experimental work on removal of trace elements from selected real waste liquids from coal-fired power plants. The approach to this project involved proceeding from simple, well-defined model systems to more complex model systems to experimental work utilizing iron-bearing waste liquid to treat typical waste streams from coal-fired power plants.

This report is organized in the following manner: Section 2 presents a short summary of literature on adsorption/coprecipitation processes and pertinent literature on available models for these phenomena. Section 3 presents experimental work on metal-ion adsorption and coprecipitation in ligand-free systems, while Section 4 is concerned with anion adsorption and coprecipitation. Section 5 presents experimental work on adsorption and coprecipitation in systems containing both cationic and anionic adsorbates. The first five sections are concerned with elucidating general behavioral phenomena in model systems. Section 6 presents results from experiments on adsorption and coprecipitation of trace elements from power plant waste liquids. Included in this section is a short study on the effect of mixing on removal efficiency and preliminary economic analysis of a potential process for trace element removal. Section 7 presents a summary, conclusions, and suggestions for further study.

## Section 2

### ADSORPTION OF METALS AT THE SOLID/SOLUTION INTERFACE

#### INTRODUCTION

Adsorption from solution is an important process in natural systems and has also been exploited for use in analytical chemistry and engineering processes. It finds application in electro-analytical chemistry, ion exchange, froth flotation, coagulation, and concentration and collection of trace contaminants. Early adsorption theory focused on the response of inert electrodes in aqueous solutions. The Guoy-Chapman description of the double layer, with refinements proposed by Stern to allow for specific adsorption, proved adequate to describe electrode characteristics. However, serious deviations from theoretical behavior are observed when applying this model to adsorption from aqueous solution onto oxide surfaces. No generally accepted model of the oxide/water interface has yet been advanced. In this section models of adsorption at the oxide/water interface are summarized and their strengths and weaknesses are compared vis-à-vis laboratory and field data.

#### THE SOLID/SOLUTION INTERFACE

With any solid/solution interface there is associated a surface charge and a gradient in electrical potential extending from the interface into the solution phase. The charge originates by non-stoichiometric dissolution of the solid, substitution for an atom in the solid lattice by one of unequal charge, or adsorption of charged species from solution (1). The electrical potential at the surface is fixed by the requirement that, at equilibrium, the electrochemical potential of a species must be the same in all phases in a system. Generally, a pair of ions which are present in both the surface phase and in bulk solution are used to calculate the surface potential and these are called potential-determining ions (PDI). For oxide surfaces,  $H^+$  and  $OH^-$  are almost always chosen to be the PDI. In any system there is a unique concentration of PDI at which potential-determining cations and anions are adsorbed equally. This condition is known as the point of zero charge (PZC). In ideal pure systems (those containing only solid, inert electrolyte, and water), surface charge and surface potential are zero at the PZC. For oxides the PZC is usually expressed as a pH, so in pure systems when  $pH > PZC$ , the surface is negatively charged, and

when  $\text{pH} < \text{PZC}$ , the surface carries a positive charge. Ions of opposite charge accumulate near the interface while those of like charge are repelled. The potential decays with distance from the interface, and the concentrations of ions approach their values in bulk solution. The region including the surface and the adjacent volume in which ionic concentrations are different from bulk solution is known as the electrical double layer (EDL).

By assuming that ions can be represented by point charges, Guoy and Chapman (1,2) independently derived theoretical expressions for surface charge, interfacial concentrations of PDI, and surface potential as functions of bulk PDI concentrations and distance from the interface. Since the Guoy-Chapman model considers only electrical interactions, it cannot account for specific adsorption, i.e., adsorption involving chemical, Van der Waals, or other non-electrostatic bonding. Also, the point-charge model of ions leads to unrealistically large ionic concentrations near the interface. Stern (2) refined the theory by including a term to account for specific adsorption and suggesting that ions retain their hydration sphere during adsorption and therefore can approach the surface no more closely than their hydrated radii. Grahame (2) altered Stern's treatment slightly by suggesting that only specifically sorbed ions lose their hydration spheres and can approach to a distance equal to their unhydrated radii. As modified, the Guoy-Chapman-Stern-Grahame (GCSG) adsorption model is still an oversimplification in that it treats the charge in the double layer as diffuse rather than discrete, and lumps all non-electrostatic terms into a single specific adsorption potential. However, it does an adequate job of predicting electrical phenomena at many solid/liquid interfaces. When the model is applied to the metal oxide/aqueous solution interface anomalies arise. The observed surface charge is considerably greater than that predicted, and the electrokinetic potential and colloidal stability do not bear the same relationship to surface charge as in model systems (3,4,5). Yates (6) was able to resolve many of the anomalies by assuming that adsorbed ions form interfacial ion pairs with discrete charged surface and his model considers adsorption only of the PDI and the specifically sorbed metal, has been developed by Schindler and Stumm and their co-workers (7,8,9). Davis and co-workers (10,11,12) have synthesized and refined aspects of both models into a generalized model that can account for adsorption of trace metals and bulk electrolyte ions and for electrokinetic phenomena. This model will be referred to as the Stanford Generalized Model for Adsorption (SGMA).

#### ADSORPTION PATTERNS AND MODELS FOR HYDROLYZABLE METALS

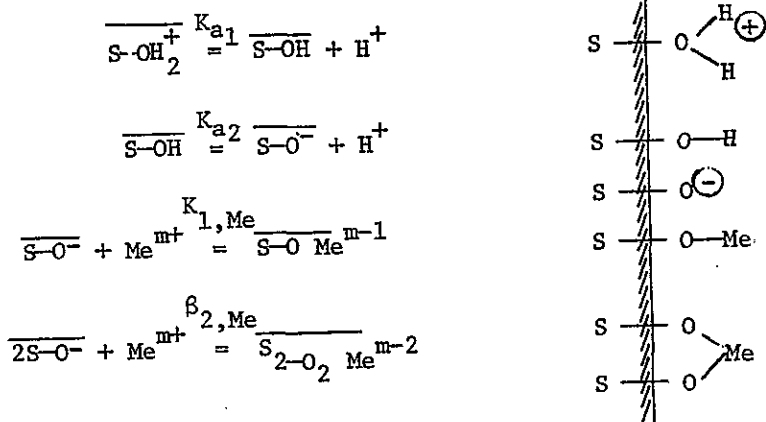
Adsorption of metal ions onto oxide surfaces from dilute aqueous solution is highly pH-dependent. The amount adsorbed expressed as a fraction of the total metal in

solution increases abruptly from nil to near 100 percent in a narrow pH range, 1 to 2 units wide. The analogies with hydrolysis reactions in solution and precipitation reactions have been noted by a number of workers. The pH at which abrupt adsorption takes place increases or does not change with increasing metal concentration, a trend opposite that for precipitation reactions. Therefore, it has been proposed that adsorption is a direct result of hydrolysis and that the hydrolyzed metal ion,  $\text{Me}(\text{OH})^{+m-1}$ , is the adsorbing species (13). Further evidence for the theory is provided by the observation that the pH of abrupt adsorption is apparently affected only weakly by the identity of the solid (14). Small deviations from one system to the next have been attributed to specific chemical interactions between the solid and the adsorbate.

The most complete mathematical description of this model is provided in a series of papers by James and Healy (15,16,17). Adsorption is viewed as a physical process in which the ions retain their inner hydration spheres and a single layer of water molecules separates the adsorbate from the surface. The representation of the electrical double layer in their model is very simplified. All solution species are potential adsorbates, and the extent to which each adsorbs is governed by a combination of coulombic, solvation, and chemical terms. The coulombic term can either favor or oppose adsorption, depending on the sign of the surface charge. The solvation term expresses the energy required to remove part of the outer hydration sphere of the metal ion and replace it with "structured water" of low dielectric constant near the surface. It opposes adsorption and is proportional to the square of the charge of the sorbing species. The third term represents a chemical interaction between sorbate and sorbent. It favors enhanced adsorption and is used as a fitting parameter. In most cases, when a hydrous oxide is the adsorbent, the solvation term dominates the coulombic term. This leads to enhanced adsorption of hydrolyzed, lower-charged species over that of free aquo ions. A variation of this model involves adsorption of the unhydrolyzed species which then hydrolyzes on the surface. While the two models differ conceptually, the configurations at equilibrium are identical and the models are thermodynamically indistinguishable.

The assumption that the adsorbate retains its hydration sphere may require unreasonably large values for the chemical free energy of adsorption in some systems. To alleviate this problem, Stumm et al. (9) and Schindler et al. (7) have proposed a chemical adsorption model in which the oxide surface is treated analogous to an amphoteric, polyprotic acid which can form covalent bonds with the adsorbate. Potential surface reactions included in the model are given schematically as shown

below. Depending on the pH of the solution, the surface acidity constants, and the number of adsorptive bonds per metal ion, the adsorption of one metal ion can be accompanied by release of 0 to 4 protons. The equilibrium expressions are written to be analogous to reactions in solution, e.g.  $\beta_{2,Me} \equiv \frac{(\overline{S_2O_2Me})}{(\overline{SO})^{-2}(Me)^{-1}}$ .



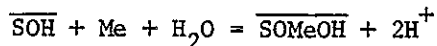
Since the strengths of the surface- $H^+$  and surface- $Me^{2+}$  bonds depend on the potential near the surface, which changes with pH,  $\beta_2$  and  $K_1$  are conditional constants, not true thermodynamic constants. Each is a combination of two energy terms, one of which describes the strength of the bond in the absence of an electrical potential gradient from the surface to bulk solution. The second describes the electrostatic energy required to move ions from bulk solution ( $\psi = 0$ ) to the surface ( $\psi \neq 0$ ) and vice versa. The first term, called the intrinsic equilibrium constant,  $K^{int}$ , is unique for each solid-metal pair, and is independent of adsorbed and dissolved metal concentrations. It is not a true constant either since it varies with ionic strength of the solution, but it is approximately constant in solutions of swamping electrolyte.

Methods for measuring the intrinsic and conditional constants associated with metal/silica and metal/ $\gamma$ -alumina systems are described by Stumm et al. (9), Hohl and Stumm (18), and Scindler et al. (7,8). Based on the surface complexation model these workers claim that in most systems the unhydrolyzed free metal ion is the reactive species.

Conceptually, the surface complexation model is an elaboration and refinement of the ion-exchange model first proposed by Dugger et al. (13). Both models yield linear relationships between the adsorption equilibrium constants and first hydrolysis constants for several metals, despite the assumption that hydrolyzed metals

do not take part in the adsorption reaction. Further evidence for this model has been provided by Dalang and Stumm (19), who have shown that when the inner hydration sphere is replaced by a slowly reacting ligand (e.g. as in  $\text{Co}(\text{NH}_3)_6^{3+}$ ) metal complexes do not specifically sorb, suggesting that direct metal-surface bonding is required for specific adsorption.

The SGMA expands the number of potential adsorption reactions to include simultaneous adsorption and hydrolysis:



Protons are assumed to bind directly to and be located in the same plane as the surface oxide group, i.e., they experience the surface potential,  $\psi_0$ . In the layer adjacent to the surface, and still capable of forming direct chemical bonds with the surface, are specifically adsorbed ions, including weakly sorbed electrolyte ions. In the diffuse layer, separated from the surface by at least one water molecule, are non-specifically sorbed ions. By assuming that bulk electrolyte ions can specifically adsorb, Davis et al. (10) are able to define intrinsic complexation and acidity constants which are independent of solution ionic strength. Davis and Leckie (11) analyzed the results of Hohl and Stumm (18) and found that two stoichiometries involving adsorption of both free and hydrolyzed Pb ions are required to model the data. In much of the debate as to whether metals are physically or chemically adsorbed onto oxides, a single type of bonding is assumed to dominate in all systems. There is no conceptual limitation preventing different types of bonds from forming under different conditions. Physical adsorption may be dominant in some systems while under different solution conditions direct bonding of the free metal to the surface may dominate. A resolution of the issue must await improved techniques for analyzing surface bonding. Although both physical and chemical models can adequately describe much of the published trace metal adsorption data, the SGMA model is most complete, because it is able to account for electrokinetic phenomena as well. However, all the models have serious deficiencies when applied over wide ranges of adsorbate concentration.

#### EMPIRICAL STUDIES OF METAL ADSORPTION FROM SOLUTION

The number of laboratory studies of metal adsorption reported in the literature is very large and expanding rapidly. The variation in techniques, solution conditions, and range of parameters studied is enormous. In the following discussion, the studies have been placed into one or more of four groups, depending on whether they

report

1. Adsorption isotherms
2. Effects of complexing ligands
3. Effects of competing metals
4. Adsorption stoichiometry

Each group is discussed in terms of its theoretical aspects, experimental findings, and the way it is treated by the various adsorption models.

### Adsorption Isotherms

Expressions describing the partitioning of adsorbate between the dissolved and adsorbed phases at constant temperature are known as adsorption isotherms. A number of theoretical isotherms have been developed to model adsorption from the gas phase, and with some minor assumptions and modifications, can be applied to adsorption from aqueous solution (20).

The isotherms most commonly used to model adsorption at the solid solution interface are the Langmuir and Freundlich isotherms. They differ with respect to how the free energy of adsorption is assumed to vary with adsorption density. In systems that obey Langmuir isotherms, adsorption density is a linear function of  $C_{eq}$  at low surface coverage and is independent of  $C_{eq}$  at large surface coverage. In systems obeying Freundlich isotherms, a plot of adsorption density vs. equilibrium dissolved adsorbate concentration has no linear region (except in the special case where  $n = 1$ ) and no maximum adsorption density. The isotherms are discussed more thoroughly in Section 3.

Table 2-1 summarizes the literature in which information about adsorption isotherms has been reported or can be derived. Both Freundlich and Langmuir isotherms have been reported for almost every combination of adsorbent-type (clay, natural sediments, oxides) and metal-ion identity. In a study by Bingham et al. (21) even the identity of a complexing salt was able to change the isotherm type. In a number of studies two or more types of bonding have been inferred for one metal-solid system. These include multi-site Langmuir bonding (22,23), specific and non-specific bonding depending on pH (24), reversible and irreversible sorption (25), and multiple Freundlich-type isotherms (26,27). In many cases the experiments were designed to mimic a specific system and the range of variables studied was small. Particularly in the case of Freundlich-type isotherms, considerably more information could have been gained by extending the conditions studied to very low or high surface coverage.

Table 2-1

Summary of Published Literature from Which Adsorption Isotherms for Metals Have Been Derived

ADSORBATE		ADSORBENT		pH	Electrolyte Matrix	Notes on Isotherm	Reference
Identity	Conc. Range	Identity	Conc.				
Hg	$10^{-9}$ - $10^{-3}$ M	am-Fe(OH) <sub>3</sub>	$5 \times 10^{-4}$ M	6-11	0.1M NaClO <sub>4</sub>	Freundlich slopes: 1.0 low $\Gamma$ 0.5 high $\Gamma$	(27)
Ca, Zn, Co	$10^{-4}$ - $10^{-3}$ M	MnO <sub>2</sub>	0.10 g/l	4.0	$10^{-3}$ M NaNO <sub>3</sub>	Multi-site Langmuir; each metal was capable of replacing different surface species	(23)
Cd, Zn	$0-5 \times 10^{-4}$ M	MnO <sub>2</sub>	10 mg/l	4-8	$10^{-3}$ M NaNO <sub>3</sub>	2-site Langmuir for Cd, Zn. 1-site Langmuir for Ca	(22)
Cu, Zn, Cd	0-15 mg/l	MnO <sub>2</sub>	0-80 mg/l	1-6	$10^{-3}$ M KAc	Langmuir; $\Gamma_{\max}$ Cu = $2\Gamma_{\max}$ Cd = $2\Gamma_{\max}$ Zn	(28)
Ag	0.185- $1.85 \times 10^{-3}$ M	20-150 mg/l	0.2 g/l	3-7	0.08M NaClO <sub>4</sub>	Langmuir	(29)
Co	$10^{-7}$ - $10^{-3}$ M	NiFe <sub>2</sub> O <sub>4</sub> ; ZrO <sub>2</sub> ; TiO <sub>2</sub>		3-11		Freundlich: slopes 0.3 to 0.6; slope decreases as T increases	(30)
Co	$6 \times 10^{-8}$ - $10^{-5}$ M	am-Fe(OH) <sub>3</sub>	$1.2 \times 10^{-4}$ - $3.0 \times 10^{-3}$ M	8.0	0.03M NH <sub>4</sub> Cl	Langmuir: to at least $\Gamma \sim 0.1$ to 0.4 mol/mol	(31)
Cd	$0-10^{-5}$ M	MnO <sub>2</sub> ; am-Fe(OH) <sub>3</sub> ; Al <sub>2</sub> O <sub>3</sub>	$10^{-5}$ - $2 \times 10^{-4}$ M	5-9	0.01M	Langmuir	(32)
Ag, Cu	$10^{-7}$ - $10^{-3}$ M	am-Fe(OH) <sub>3</sub>	$10^{-4}$ - $10^{-2}$ M	2.12	0.1M NaNO <sub>3</sub>	Freundlich: slopes 0.5-0.7	(33)
Cd, Pb, Zn	$0-4 \times 10^{-3}$ M	MnO <sub>2</sub> ; am-Fe(OH) <sub>3</sub>	$4 \times 10^{-3}$ M	2-8		Cd, Zn reached $\Gamma_{\max}$ ; Pb did not	(34)

Table 2-1 cont.

2-7

Table 2-1 continued

ADSORBATE		ADSORBENT		pH	Electrolyte Matrix	Notes on Isotherm	Reference
Identity	Conc. Range	Identity	Conc.				
Cu	$10^{-6}$ - $10^{-3}$ M	SiO <sub>2</sub>	0.1-100 mg/l	3.8-5.8	DI Water	Freundlich: slope ~0.5	(35)
12 metals	0.01-10 µg/l	am-Fe(OH) <sub>3</sub>	0.003-1.0 g/l	7.7-8.2	Seawater	Percent adsorption decreased as C <sub>T</sub> increased for Co,Cr,Mo,Hg	(36)
Co	$10^{-7}$ - $10^{-3}$ M	SiO <sub>2</sub>		2-12	DI water	Freundlich: slope .67 going to ~ 0	(24)
Co,Cu	50-100 µg/l	Illite	70 m <sup>2</sup> /l	4-8	Seawater; 0.7M NaCl	Langmuir	(37)
Cu	$4 \times 10^{-6}$ to $3 \times 10^{-4}$ M	Bentonite	5 g/l	4-6	CaAc	2 sites: 1 OH and 1 from adsorbed organics	(38)
Zn,Co	$1 \times 10^{-6}$	Several clays	1.6-3.3 g/l	5-8	0.1M CaCl <sub>2</sub>	Bond energy decreased with increasing C <sub>T</sub>	(39)
Co	0-2000	Montmorillonite	2 g/l	5-7	0.1M CaCl <sub>2</sub>	Langmuir: exchangable Co plus nonexchangable with is f(time)	(25)
Cu,Zn	0-5 meq/l	Montmorillonite	0.1 g/l	4-8	DI water	Langmuir when chloro-salt used; Freundlich when acetate-salt used	(21)
Cu,Zn,Cd	10 mg/l	Bentonite	50 mg/l	1-6	$10^{-3}$ M KAc	Freundlich slopes .65 Cu, .64 Cd .60 Zn	(28)
Mo	2-8 mg/l	Bentonite	20 g/l	7.7-8.2	Seawater	35% adsorbed at 2 ppm C <sub>T</sub> 25% adsorbed at 8 ppm C <sub>T</sub>	(36)

Table 2-1 cont.

Table 2-1 continued

ADSORBATE		ADSORBENT		pH	Electrolyte Matrix	Notes on Isotherm	Reference
Identity	Conc. Range	Identity	Conc.				
Pb	9-400 mg/l	Kaolinite; montmorillonite	10-20 g/l	4-7	DI water 0.1M NaCl	Authors say Langmuir; appears to be Freundlich	(26)
Cd,Pb	5-100 mg/l	Alkaline soil	2.5 g/l	7-9	0.1M KCl	Langmuir	(40)
Zn	1-10 mg/l	Suspended river sediments	171 mg/l	7.3	River water	Freundlich: slope 0.61	(41)
Cd	0-2x10 <sup>-4</sup> M	Solid humic acid	10 g/l	5.5		Langmuir	(42)
Cu	0-10 mg/l	soil	5 g/l	5.5	0.05M CaCl <sub>2</sub>	Langmuir	(43)
Cd	2-200 µg/l	River mud	7-210 mg/l	7.5-8.0	River water	Freundlich: slope 0.5; data not self-consistent	(44)
Ag,Zn,Cd	0-200 µg/l	River sediments		2-9	River and seawater	Langmuir	(45)
Hg	0-20 mg/l	River sediments	5 g/l	~7(?)	DI water (?)	Langmuir for 4 of 6 sediments tested	(46)

### Effects of Complexing Ligands

All natural systems and waste streams contain ligands which can form soluble complexes with metal ions. Conceptually, an adsorbent in such a system can interact with the metal or ligand separately or with the complex, and adsorption of any species could affect the surface and its affinity for other solution species.

Table 2-2 summarizes published reports of ligand effects on metal adsorption. In simple systems, the net effect of inorganic complexing ligands is generally to decrease adsorption of the metal. MacNaughton and James (47) and Avotins (27) found that the presence of chloride dramatically reduces adsorption of mercury on silica and amorphous iron hydroxide, respectively. Their results are consistent with the hypothesis that chloro-complexes of Hg do not sorb at all. Bruninx (48) reported that both dissolved cyanide and chloride decrease coprecipitation of Zn, Cd, and Hg with amorphous iron hydroxide. Chloride ion has also been shown to desorb Cd and Pb in alkaline soils (40). However, particularly in the presence of organic ligands, heavy metal sorption can increase when a complexing ligand is present. Siegel (49) found that  $Zn^{2+}$  and Zn-glycine<sup>+</sup> (Zn-gly<sup>+</sup>) species are equally sorbed but (Zn-gly<sub>2</sub>)<sup>0</sup> is sorbed much less strongly by several ion-exchange resins and clays. Huang et al. (50) reported that phosphate, glycine, tartrate, NTA, and humic acid all increase the adsorption of Cu and Cd onto Metapeka, a Delaware soil. Forbes et al. (51) claim that Cl<sup>-</sup> increases Cd sorption on goethite and Davis and Leckie (52) have shown that several organics can variously increase, decrease, or have no effect on silver and copper adsorption onto am-Fe(OH)<sub>3</sub> and α-SiO<sub>2</sub>, depending on the identity and concentration of the ligands and metals and the solution pH. It is likely that in such systems metal ion sorption is affected both by adsorption of the free ligand (53) and by the formation of solid-metal-ligand complexes.

There is no conceptual or theoretical limitation precluding adsorption of ligands or metal-ligand complexes and these reactions have been included in the SGMA model.

### Effects of Competing Metals

As with complexing ligands, all natural systems contain a wide variety of dissolved metal ions. Except for some of the alkali and alkaline earth metals, most are present in trace concentrations ( $< 10^{-6}M$ ). For this reason, and because specific adsorption is usually greatest for transition and p-block elements, most studies of competitive adsorption have involved trace metals in the presence of a large excess of Ca<sup>2+</sup> or Mg<sup>2+</sup> (Table 2-3). It appears that under these conditions Mg<sup>2+</sup>

Table 2-2

## Summary of Published Literature Relating to the Effects of Dissolved Ligands on Metal Adsorption

Adsorbate	Adsorbate	pH	Ligand Identity	Ligand Effects	Reference
Hg	am-Fe(OH) <sub>3</sub>	6-10	Cl	Large decrease in adsorption with increased Cl <sup>-</sup>	(27)
Cu, Pb, Zn, Cd, Co	α-FeOOH	5-8	Cl	Increases adsorption of Cd + Pb	(51)
Cd, Cu, Zn, Ni	am-Fe(OH) <sub>3</sub>	8.5	ethylene-diamine	Cd(en) and Zn(en) adsorb; Ni(en) + Cu(en) do not	(54)
Cu	MnO <sub>2</sub>	2-6	EDTA, tartrate, CO <sub>3</sub> , humic acid	Decreased adsorption	(55)
Cd	MnO <sub>2</sub> , am-Fe(OH) <sub>3</sub> , Al <sub>2</sub> O <sub>3</sub>	5	Cl	Decreased adsorption on MnO <sub>2</sub>	(32)
Ag, Cu	am-Fe(OH) <sub>3</sub>	2-12	several	Some ligands increased adsorption, some decreased it	(33)
Cu, Zn, Cd, Pb	γ-Al <sub>2</sub> O <sub>3</sub> , α-SiO <sub>2</sub>	2-10	several organic ligands	Increased adsorption	(50)
Cu	Kaolinite	4-9	several organic ligands	Decreased adsorption	(56)
Cu, Zn	Montmorillonite	4-8	acetate or chloride	More adsorbed from acetate than from chloride salt	(21)
Zn	several clays	8.0	glycine	Zn-gly adsorbed; Zn-gly <sub>2</sub> did not	(49)
Cd	solid humic acid	4.0	EDTA	Prevented adsorption	(42)
Cd	River mud	7.5-8.0	EDTA	Desorbed Cd	(44)

Table 2-3

## Summary of Published Studies of Competitive Adsorption Between Pairs of Metal Ions

Adsorbent	PRIMARY METAL		COMPETING METAL		Effects	Reference
	Identity	Conc. Range	Identity	Conc.		
am-Fe(OH) <sub>3</sub>	Cd	130-900 µg/l	Cu	800 mg/l	Both metals present as ethylenediamine complex. Cu has no effect	(54)
MnO <sub>2</sub>	Cd, Zn	$5 \times 10^{-5}M$	Zn, Cd	$5 \times 10^{-5}M$	Each decreases sorption of the other	(22)
MnO <sub>2</sub>	Cu	$\sim 10^{-4}M$ (?)	Ca	0-60 mg/l	Very slight desorption of Cu	(55)
MnO <sub>2</sub>	Cd	$10^{-5}M$	Ca	$0-2 \times 10^{-3}M$	Cd sorption decreased 66% when Ca added	(32)
MnO <sub>2</sub>	Ca	$\sim 1.5 \times 10^{-4}M$	Mn	$0-2 \times 10^{-4}M$	Ca sorption decreased as Mn sorption increased; $\Gamma_{tot}$ increased	(57)
MnO <sub>2</sub>	Cd, Zn	$10^{-3}M$	Pb	$10^{-3}M$	Pb decreased sorption of Cd and Zn	(34)
Illite	Ca	50-100 µg/l	Mg	1000 mg/l	Mg decreased Co sorption	(37)
Several clays	Co	$10^{-6}$ to $10^{-5}M$	Mg	0.1M	Mg decreased Co sorption	(58)
River sediments	Zn	1 to 10 mg/l	Ca	40 mg/l	Ca had no effect on Zn sorption	(41)

has a greater effect on trace metal sorption (37,58) than does  $\text{Ca}^{2+}$  (41,55). However, effects of the two alkaline earth elements have not been compared directly under controlled conditions.

It is not clear whether strong specific adsorption of some ions occurs because they bind more strongly to the same sites as  $\text{Ca}^{2+}$  and  $\text{Mg}^{2+}$ , or because they attach to a group of strong binding sites unavailable to the alkaline earths. If the multi-site hypothesis is true, competition between two strongly adsorbing ions may be evident at much lower adsorption densities than between a strongly sorbed and a weakly sorbed ion. Very few studies have been reported of competition between two metals which both adsorb strongly. Gadde and Laitinen (34) reported a significant decrease in adsorption of  $10^{-4}\text{M}$  Cd or Zn on  $\text{MnO}_2$  when an equal concentration of Pb was added to the system. Zasoski (22) found that adsorption of either Cd or Zn onto  $\text{MnO}_2$  decreases when the other is added at equimolar concentration (1 to 30  $\mu\text{M}$ ). An equivalent decrease in adsorption of either metal occurs in the presence of  $10^{-4}\text{M}$  Ca. Copper, Co, Zn, Fe, Mn, and Ni are all able to replace more of the Co previously adsorbed on montmorillonite than either Ca or Mg (25). There is at present no way to predict which solids have several distinct groups of surface sites, or the variation of metal-binding strengths among these groups. Therefore most adsorption models include the tacit assumption that surface sites are all equivalent. As a result, competitive effects are predicted to be important only when full surface coverage is approached. This requires much larger concentrations of adsorbate for the onset of competitive effects than is often observed.

#### Adsorption Stoichiometry

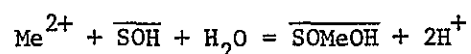
Oxide surfaces are visualized as consisting of exposed hydroxyl groups which can undergo reversible protolysis reactions in response to solution conditions (59). When a metal ion adsorbs, it may bond to either one or two surface sites (60). When the possibility of metal ion hydrolysis accompanying adsorption is included, even in the absence of complexing ligands, the potential number of surface reactions is fairly large. Because several reactions may occur simultaneously, adsorption stoichiometry is very complex. Until recently, attempts to model stoichiometry have been largely confined to determining the number of protons released when an ion adsorbs. Although this number can theoretically vary from zero to at least three, most studies report values between one and two. On manganese oxides, release of structural and weakly sorbed ions as well as protons accompanies adsorption (23). Measurements of proton release are potentially of great value, but the interpretation of data is often clouded by uncertainties regarding the concomitant exchange

of electrolyte ions and the fact that proton release is expected to vary with pH and concentration of adsorbents and adsorbate.

Since the James-Healy adsorption model does not involve formation of direct surface-metal bonds, it cannot be used in any simple way to predict stoichiometry of surface species.

Schindler et al. (7) and Hohl and Stumm (18) claim that by applying adsorption and proton release data to mass-action-type equilibrium expressions, the surface complexation model can distinguish between mono- and bidentate surface complexes. However, as will be shown later, their mass-action expressions for adsorption of one metal ion to two oxide sites is questionable. James et al. (61) attempted to determine surface hydrolysis constants for cadmium on several crystalline oxides. They fit the metal adsorption data by the James-Healy model, and then adjusted surface-hydrolysis constants so as to be consistent with measurements of proton release accompanying adsorption. According to this model, cadmium hydrolyzes at a lower pH on the surface than in bulk solution.

The SGMA model can account for stoichiometry somewhat better than the other models because it allows for adsorption of any dissolved species by any of several different mechanisms. Davis and Leckie (11) have shown that for many metal/oxide systems, the data are modeled most closely when the following reaction is dominant:



However, regardless of which model is used, dispute about adsorption stoichiometry and the merits of the various models will undoubtedly continue until the confirmation and speciation of adsorbed ions can be determined unambiguously.

An alternate approach to studying surface stoichiometry is by infrared spectroscopy. Parfitt and Russell (62) adsorbed several dissolved anions onto goethite, then dried the solid and analyzed the surface species using infrared spectroscopy. They found that  $\text{HPO}_4^{2-}$ ,  $\text{SO}_4^{2-}$ ,  $\text{C}_2\text{O}_4^{2-}$ ,  $\text{SeO}_3^{2-}$ , benzoic acid and the halides all bound to surface oxide sites which were singly coordinated to Fe. The doubly charged species were all bidentate and the singly-charged species were monodentate. Spectroscopic studies of surfaces with adsorbed metal ions could probably provide much information about surface stoichiometry. The major drawback to such studies is that the solids must be removed from the aqueous environment for analysis.

In summary, several models of adsorption at the oxide/aqueous solution interface have been proposed in recent years, but none is completely successful in accounting for surface phenomena. In most models, the Langmuir isotherm is assumed to apply, adsorption of metal/ligand complexes is treated in an over-simplified manner, and metal ion competition is presumed to be significant only when surface coverage approaches a monolayer. In many cases, predictions based on the models are in error. Detailed studies of surface site-binding energy and density distributions, and of the effect of dissolved and adsorbed complexing ligands are required to provide a basis for improving the models.

#### REFERENCES

1. G. A. Parks. "Adsorption in the Marine Environment." Chemical Oceanography, 2d ed., Chap. 4. J. P. Riley and G. Skirrow (eds.). New York: Academic Press, 1975.
2. D. C. Grahame. "The Electrical Double Layer and the Theory of Electrocapilarity." Chem. Rev., 41, 441-489 (1947).
3. J. Lyklema. "The Electrical Double Layer on Oxides." Croat. Chim. Acta, 43, 249-274 (1971).
4. S. M. Ahmed. Oxides and Oxide Films, Vol. 1, Chap. 4. J. W. Diggle (ed.). New York: Marcel Dekker, Inc., 1972.
5. R. J. Hunter and H. J. L. Wright. "Dependence of Electrokinetic Potential on the Concentration of Electrolyte." J. Coll. Interface Sci., 37, 564-574 (1971).
6. D. E. Yates. "The Structure of the Oxide/Aqueous Electrolyte Interface." Ph.D. Thesis, University of Melbourne, Australia, 1975.
7. P. Schindler, E. Wälti and B. Fürst. "The Role of Surface Hydroxyl Groups in the Surface Chemistry of Metal Oxides." Chimia, 30(2), (1976).
8. P. W. Schindler, B. Fürst, R. Dick and P. U. Wolf. "Ligand Properties of Surface Silanol Groups. I. Surface Complex Formation with  $Fe^{3+}$ ,  $Cu^{2+}$ ,  $Cd^{2+}$ , and  $Pb^{2+}$ ." J. Coll. Interface Sci., 55, 469-475 (1976).
9. W. Stumm, C. P. Huang and S. R. Jenkins. "Specific Chemical Interaction Affecting the Stability of Dispersed Systems." Croat. Chem. Acta, 42, 223-245 (1970).
10. J. A. Davis, R. O. James and J. O. Leckie. "Surface Ionization and Complexation at the Oxide/Water Interface: 1. Computation of Electrical Double Layer Properties in Simple Electrolytes." J. Coll. Interface Sci., 63(3), 480-499 (March 1978).
11. J. A. Davis and J. O. Leckie. "Surface Ionization and Complexation at the Oxide/Water Interface: 2. Surface Properties of Amorphous Iron Oxyhydroxide and Adsorption of Metal Ions." J. Coll. Interface Sci., 67(1), 90-107 (1978).
12. J. A. Davis and J. O. Leckie. "Surface Ionization and Complexation at the Oxide/Water Interface: 3. Adsorption of Anions." J. Coll. Interface Sci., accepted for publication (1979).

13. D. Dugger, L. J. Stanton, B. Irby, W. McConnell, W. Cummins and R. Maatman. "The Exchange of Twenty Metal Ions with the Weakly Acidic Silanol Group of Silica Gel." J. Phys. Chem., 68, 757 (1964).
14. J. O. Leckie and R. O. James. "Control Mechanisms for Trace Metals in Natural Waters." Aqueous Environmental Chemistry of Metals, A. V. Rubin (ed.). Ann Arbor, Mich.: Ann Arbor Science Publ., 1974.
15. R. O. James and T. W. Healy. "Adsorption of Hydrolyzable Metal Ions at the Oxide-Water Interface. I. Co(II) Adsorption of SiO<sub>2</sub> and TiO<sub>2</sub> as Model Systems." J. Coll. Interface Sci., 40, 42-52 (1972).
16. R. O. James and T. W. Healy. "Adsorption of Hydrolyzable Metal Ions at the Oxide-Water Interface. II. Charge Reversal of SiO<sub>2</sub> and TiO<sub>2</sub> Colloids by Adsorbed Co(II), La(III) and Th(IV) as Model Systems." J. Coll. Interface Sci., 40, 53-64 (1972).
17. R. O. James and T. W. Healy. "Adsorption of Hydrolyzable Metal Ions at the Oxide-Water Interface. III. A Thermodynamic Model of Adsorption." J. Coll. Interface Sci., 40, 65-81 (1972).
18. H. Hohl and W. Stumm. "Interaction of Pb<sup>2+</sup> with Hydrous  $\gamma$ -Al<sub>2</sub>O<sub>3</sub>." J. Coll. Interface Sci., 55, 281-288 (1976).
19. F. Dalang and W. Stumm. "Comparison of the Adsorption on Hydrous Oxide Surfaces of Aquo Metal Ions with That of Inert Complex Cations." Colloid and Interface Science, Vol. 4, Hydrosols and Rheology. New York: Academic Press, 157-168, 1976.
20. A. W. Adamson. Physical Chemistry of Surfaces, 3d ed. New York: John Wiley and Sons, 1976.
21. F. Bingham, A. Page and J. Simms. "Retention of Cu and Zn by H-Montmorillonite." Soil Sci. Soc. Amer. Proc., 28, 351-354 (1964).
22. R. J. Zasoski. "Sorption and Sorptive Interactions of Cadmium and Zinc on Hydrous Manganese Oxide." Ph.D. Thesis, University of California at Davis, 1974.
23. P. Loganathan and R. Burau. "Sorption of Heavy Metal Ions by a Hydrous Manganese Oxide." Geochim. Cosmochim. Acta, 37, 1277-1293 (1973).
24. T. W. Healy, R. O. James and R. Cooper. "The Adsorption of Aqueous Co(II) at the Silica-Water Interface." Adv. Chem. Series, 79, 62-73 (1968).
25. J. F. Hodgson. "Cobalt Reactions with Montmorillonite." Soil Sci. Soc. Amer. Proc., 24, 165-168 (1960).
26. R. A. Griffin and N. F. Shimp. "Effect of pH on Exchange Adsorption or Precipitation of Lead from Landfill Leachate by Clay Minerals." Environ. Sci. Tech., 10(13), 1256-1261 (1976).
27. P. V. Avotins. "Adsorption and Coprecipitation Studies of Mercury on Hydrous Iron Oxides." Ph.D. Thesis, Stanford University, Stanford, Calif., 1975.
28. R. D. Guy, C. L. Chakrabarti and L. L. Schramm. "The Application of a Simple Chemical Model of Natural Waters to Metal Fixation in Particulate Matter." Can. J. Chem., 53, 661-669 (1975).

29. B. J. Anderson, E. A. Jenné and T. T. Chao. "The Sorption of Silver by Poorly Crystallized Manganese Oxides." Geochim. Cosmochim. Acta, 37, 611-622 (1973).
30. P. Tewari and W. Lee. "Adsorption of Co(II) at the Oxide-Water Interface." J. Coll. Interface Sci., 52, 77-88 (1975).
31. M. H. Kurbatov, G. Wood and K. Kurbatov. "Isothermal Adsorption of Cobalt from Dilute Solutions." J. Phys. Chem., 55, 1170-1182 (1951).
32. H. Posselt. "Environmental Chemistry of Cadmium in Aqueous Systems." Ph.D. Thesis, University of Michigan, Ann Arbor, Mich., 1971.
33. J. A. Davis. "Adsorption of Trace Metals and Complexing Ligands at the Oxide/Water Interface." Ph.D. Thesis, Stanford University, Stanford, Calif., 1977.
34. R. R. Gadde and H. A. Laitinen. "Studies of Heavy Metal Adsorption by Hydrous Iron and Manganese Oxides." Anal. Chem., 46, 2022 (1974).
35. P. W. Richardson and H. E. Hawkes. "Adsorption of Copper on Quartz." Geochim. Cosmochim. Acta, 15, 6-9 (1958).
36. K. B. Krauskopf. "Factors Controlling the Concentrations of Thirteen Rare Metals in Seawater." Geochim. Cosmochim. Acta, 9, 1-32 (1956).
37. T. P. O'Connor and D. R. Kester. "Adsorption of Copper and Cobalt from Fresh and Marine Systems." Geochim. Cosmochim. Acta, 39, 1531-1543 (1975).
38. H. F. Steger. "On the Mechanism of the Adsorption of Trace Copper by Bentonite." Clays and Clay Minerals, 21, 429-436 (1973).
39. K. G. Tiller and J. F. Hodgson. "The Specific Sorption of Cobalt and Zinc by Layer Silicates." 9th National Conf. on Clays and Clay Minerals, 9, 393-411 (1962).
40. B. Singh and G. Sekhow. "Adsorption, Desorption and Solubility Relationships of Lead and Cadmium in Some Alkaline Soils." J. Soil Sci., 28, 271-275 (1977).
41. J. O'Connor and C. Renn. "Soluble-Adsorbed Zinc Equilibrium in Natural Waters." J. Amer. Water Works Assoc., 56, 1055-1061 (1964).
42. R. Riffaldi and R. Levi-Minzi. "Adsorption and Desorption of Cd on Humic Acid Fraction of Soils." Water, Air, and Soil Pollution, 5, 179-184 (1975).
43. R. G. McLaren and D. V. Crawford. "Studies on Soil Copper. II. Specific Adsorption of Copper by Soils." J. Soil Sci., 24, 443-452 (1973).
44. J. Gardiner. "The Chemistry of Cadmium in Natural Waters. II. The Adsorption of Cadmium on River Muds and Naturally Occurring Solids." Water Res., 8, 157-164 (1974).
45. C. Murray and L. Murray. "Adsorption-Desorption Equilibria of Some Radio-nuclides in Sediment-Freshwater and Sediment-Seawater Systems." Presented at the Symposium on the Interaction of Radioactive Contamination with Constituents of the Marine Environment, Seattle, Wash., July 10-14 (1972).
46. S. Ramamoorthy and B. R. Rust. "Mercury Sorption and Desorption Characteristics of Some Ottawa River Sediments." Can. J. Earth Sci., 13, 530-536 (1976).

47. M. G. MacNaughton and R. O. James. "Adsorption of Aqueous Mercury(II) Complexes at the Oxide/Water Interface." J. Coll. Interface Sci., 47, 431-440 (1974).
48. E. Bruninx. "The Coprecipitation of Zn, Cd and Hg with Ferric Hydroxide." Phillips Research Reports, 30, 177-191 (1975).
49. A. Siegel. "Equilibrium Binding Studies of Zinc-Glycine Complexes to Ion-Exchange Resins and Clays." Geochim. Cosmochim. Acta, 30, 757-768 (1966).
50. C. P. Huang, H. A. Elliott and R. M. Ashmead. "Interfacial Reactions and the Fate of Heavy Metals in Soil-Water Systems." J. Water Poll. Cont. Fed., 49, 745-756 (1977).
51. E. Forbes, A. Posner and J. Quirk. "The Specific Adsorption of Inorganic Hg(II) Species and Co(III) Complex Ions on Goethite." J. Coll. Interface Sci., 49, 403-408 (1974).
52. J. A. Davis and J. O. Leckie. "Effect of Adsorbed Complexing Ligands on Trace Metal Uptake by Hydrous Oxides." Environ. Sci. Tech., 12(12), 1309-1315 (1978).
53. A. Breeuwsma and J. Lyklema. "Physical and Chemical Adsorption of Ions in the Electrical Double Layer on Hematite ( $\alpha$ -Fe<sub>2</sub>O<sub>3</sub>)." J. Coll. Interface Sci., 43, 437-443 (1973).
54. B. Bhushan and K. Kar. "Certain Micro-Chemical Separations Using Hydrous Ferric Oxide as a Selective Sorbent. II. Separation and Determinations of Small Amounts of Cadmium from Copper and from Nickel." J. Radioanal. Chem., 33, 123-128 (1976).
55. R. D. Guy and C. L. Chakrabarti. "Studies of Metal-Organic Interactions in Model Systems Pertaining to Natural Waters." Can. J. Chem., 54, 2600-2611 (1976).
56. H. Farrah and W. Pickering. "The Sorption of Copper Species by Clays. I. Kaolinite." Aust. J. Chem., 29, 1167-1176 (1976).
57. H. S. Posselt, F. J. Anderson and W. Weber. "Cation Sorption on Colloidal Hydrous Manganese Dioxide." Environ. Sci. Tech., 2(12), 1087-1093 (Dec. 1968).
58. J. F. Hodgson, K. Tiller and M. Fellows. "The Role of Hydrolysis in the Reaction of Heavy Metals with Soil Forming Materials." Soil Sci. Soc. Amer. Proc., 28, 42-46 (1964).
59. G. A. Parks and P. L. DeBruyn. "The Zero Point of Charge of Oxides." J. Phys. Chem., 66, 967-976 (1962).
60. W. Stumm, H. Hohl and F. Dalang. "Interaction of Metal Ions with Hydrous Oxide Surfaces." Croat. Chim. Acta, 48, 491-502 (1976).
61. R. O. James, R. J. Stiglich and T. W. Healy. "Analysis of Models of Adsorption of Metal Ions at Oxide/Water Interfaces." Farad. Disc. Chem. Soc., 59, 142-156 (1975).
62. R. L. Parfitt and J. D. Russell. "Adsorption on Hydrous Oxides. IV. Mechanisms of Adsorption of Various Ions on Goethite." J. Soil Sci., 28, 297-305 (1977).

### Section 3

#### EQUILIBRIUM METAL ADSORPTION AND COPRECIPITATION IN LIGAND-FREE SYSTEMS

##### INTRODUCTION

Equilibrium adsorption and coprecipitation experiments were conducted using various combinations of the following constituents:

Adsorbents: am-Fe(OH)<sub>3</sub>, α-SiO<sub>2</sub>, γ-Al<sub>2</sub>O<sub>3</sub>.

Adsorbates: Cd<sup>2+</sup>, Zn<sup>2+</sup>, Cu<sup>2+</sup>, Pb<sup>2+</sup>, Ag<sup>+</sup>, S<sub>2</sub>O<sub>3</sub><sup>2-</sup>, CrO<sub>4</sub><sup>-</sup>, AsO<sub>4</sub><sup>-</sup>, SeO<sub>4</sub><sup>2-</sup>,  
SeO<sub>3</sub><sup>2-</sup>, SO<sub>4</sub><sup>2-</sup>.

Adsorption isotherms were derived for several adsorbates and adsorption in systems containing several pairs of adsorbate species was studied on all three adsorbents. In addition, proton release accompanying sorption of each metal onto am-Fe(OH)<sub>3</sub> was measured for one concentration of Me<sub>T</sub> and Fe<sub>T</sub>.

In this section the results of metal ion adsorption and coprecipitation experiments in systems free of complexing ligands are discussed and compared with predictions of adsorption models. It is shown that the assumption that all adsorption sites on a given surface have identical binding energy is not consistent with the results and leads to large errors in the predicted adsorption behavior of cadmium, zinc, copper, and lead on amorphous Fe(OH)<sub>3</sub> and two crystalline adsorbents. Evidence is presented that many solids have a distribution of adsorption site-types and that the free energy of adsorption of a metal ion varies depending on which site it binds. Adsorption at the strongest binding sites is limited by the availability of such sites at surface coverages orders of magnitude less than the mono-layer capacity. The selectivity of the sites for specific metal ions varies widely, possibly due to stereochemical factors.

##### ADSORPTION VS. COPRECIPITATION

The distinction between adsorption and coprecipitation is based solely on the sequence of addition of reagents to the reacting system. In coprecipitation, a solid is precipitated from solution containing several other dissolved species. These other species may be incorporated into the solid by adsorption on the surface of

growing particles, physical entrapment in pore spaces, or substitution in the crystal lattice. Examples of coprecipitation include the precipitation of solids in complex natural systems such as soils, rivers, lakes and oceans, and in domestic and industrial waste-processing streams. The solid may form in response to changes in redox potential, pH, solution composition, or other system parameters.

An adsorption process is one in which the adsorbate species are directly exposed only to the surface of preformed solids. In these systems solid-state diffusion is the only process by which adsorbate species can reach the interior of non-porous particles. Such systems may be found when two bodies or streams of water mix, during dredging operations, and in filtration, ion-exchange, and adsorption columns.

Since thermodynamic chemical equilibrium is independent of the sequence of reagent addition, the ultimate equilibrium condition of a given system does not depend on when the solid is precipitated. Nevertheless, since solid-state diffusion is often a very slow process, one may expect greater removal of adsorbate from solution by coprecipitation than by adsorption in short-term, non-equilibrium experiments. However, there are factors which mitigate the differences between the two processes. Most solids probably do not precipitate as well-formed crystals, but rather through a sequence of species including multi-nuclear and polymeric soluble forms, weakly structured colloids, and finally discrete particles. The degree of ordering of the atoms follows a continuous path from completely random to well-ordered. As crystallization proceeds, the specific surface area and number of adsorbent atoms in direct contact with the solution generally decrease. Amorphous clumps of atoms reorient themselves, gradually approaching a condition in which a flat crystal face is exposed. The distribution of pore spaces changes from many micro-pores to a much smaller number of larger pores. This process is known as "aging" and is critical to the relationship between adsorption and coprecipitation. If for instance, crystallization is very slow and the adsorbate is added as soon as the amorphous solid precipitates, the adsorbate molecules have easy access to almost all the adsorbent. In this case, one expects little difference between coprecipitation and adsorption in terms of removal efficiency of dissolved adsorbate ions. If, on the other hand, the solid crystallizes rapidly (a possibility that is enhanced if seed crystals are present in the system), and if adsorbate is added after the solid is well crystallized, a significant portion of the adsorbent may be unavailable to adsorbate ions except via solid-state diffusion. In such a case, one expects significantly more removal by coprecipitation than by adsorption in short-term experiments. If one considers adsorption or coprecipitation to be analogous to

complexation of metal ions in solution, then to a first approximation coprecipitation brings "solid ligands" into closer and more rapid contact with metal ions than does adsorption. The extent to which the two processes differ is related to the extent and rate of crystallization when the adsorbate is added. There is considerably more published data available from adsorption experiments than from coprecipitation experiments. However, in many waste treatment processes a solid is precipitated in the presence of potential adsorbates. Thus information on coprecipitation is needed to model these processes, and a quantitative model relating coprecipitation to adsorption would be extremely valuable to make much of the published literature data applicable to engineering systems.

Coprecipitation and adsorption on amorphous  $\text{Fe}(\text{OH})_3$  were studied in systems containing Cd, Zn, Cu,  $\text{SeO}_3$ , and  $\text{CrO}_4$ . In some systems a dissolved metal-complexing ligand was present ( $\text{Cd} + \text{Cl}$ ,  $\text{Cd} + \text{SO}_4$ ). In all cases adsorbate partitioning between the dissolved and solid phases was independent of the sequence of reagent addition for reaction times of 0-5 hours (Figures 3-1 and 3-2, and also Appendix A). In other words, in terms of adsorbate removal efficiencies, adsorption and coprecipitation are indistinguishable in these systems. Based on available information about the structure of rapidly precipitated  $\text{Fe}(\text{OH})_3$ , this result is not surprising. The exceptionally small particle size and the fact that the precipitate is X-ray amorphous suggest that within the time frame of the experiments and most engineering processes (0-6 hrs) almost all the iron oxyhydroxide surface is in relatively close contact with dissolved species.

There is an alternate possible explanation for the indistinguishability of adsorption and coprecipitation in the systems studied. If the precipitation reaction occurs on a much shorter time scale than adsorption, the entire precipitation/adsorption process may take place so rapidly that the two sequential processes appear to be simultaneous. At present there is no way to distinguish between the two mechanistic interpretations of the experimental evidence. From an engineering point of view, though, the chemical mechanism is not as important as the observation that when amorphous  $\text{Fe}(\text{OH})_3$  is the adsorbent, the order of addition of reagents has no effect on adsorbate removal efficiency. Based on this evidence, coprecipitation and adsorption are grouped together and are discussed as a single phenomenon in the remainder of this report.

#### KINETICS OF ADSORPTION AND COPRECIPITATION

Kinetics of adsorption and coprecipitation of several metals on am- $\text{Fe}(\text{OH})_3$ ,  $\alpha\text{-SiO}_2$ , and  $\gamma\text{-Al}_2\text{O}_3$  are shown in Figures 3-3 through 3-6. As is typical for metal sorption

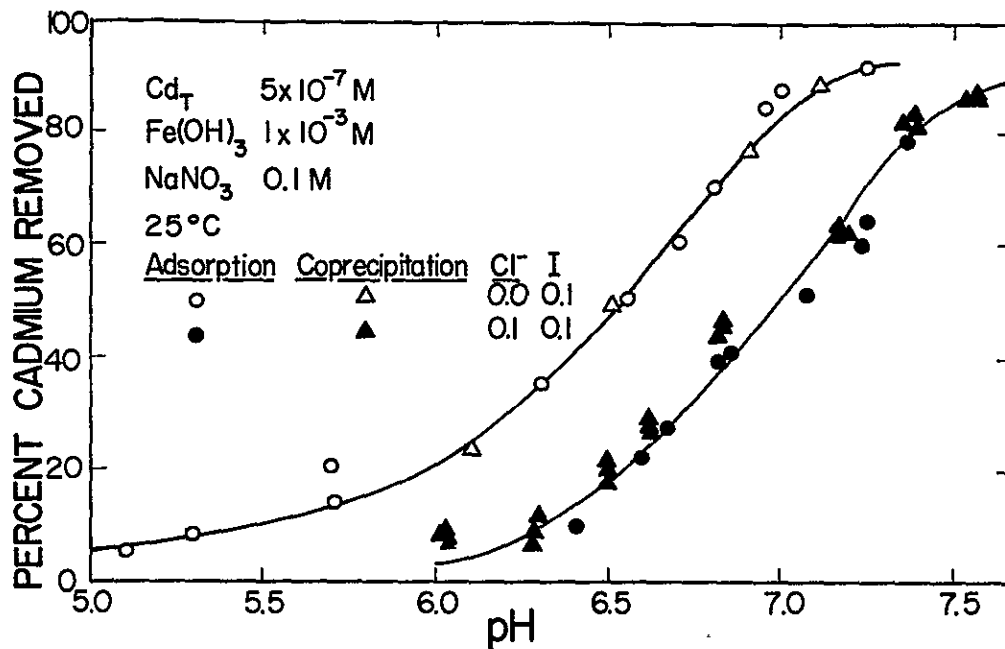


Figure 3-1. Adsorption and coprecipitation of cadmium onto am- $Fe(OH)_3$

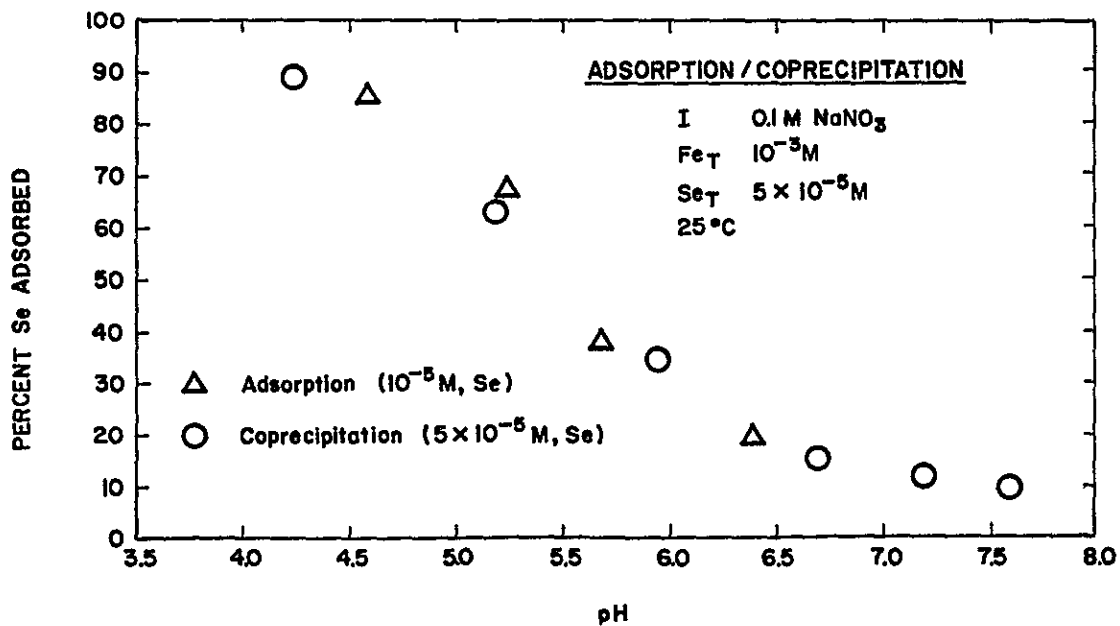


Figure 3-2. Adsorption and coprecipitation of selenate onto am- $Fe(OH)_3$

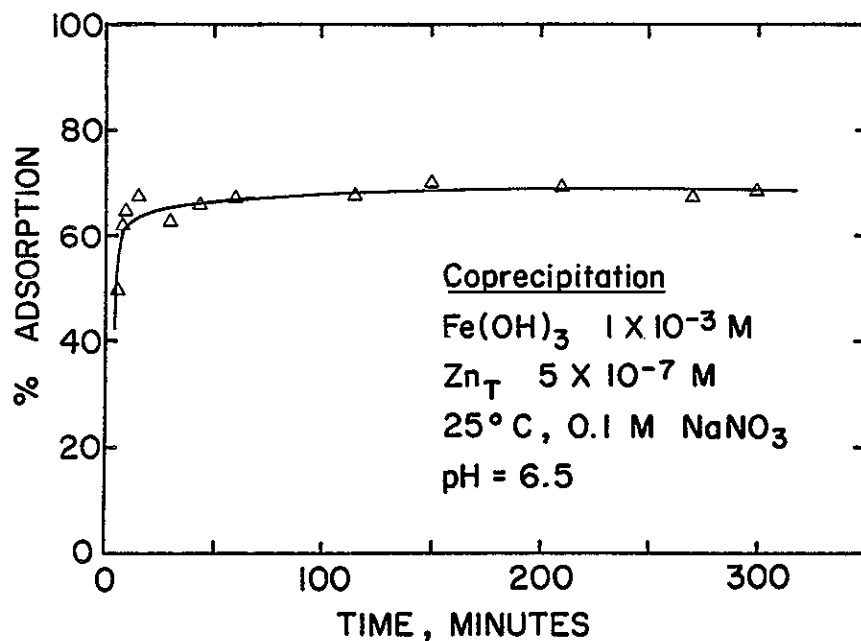


Figure 3-3. Kinetics of coprecipitation of zinc onto am- $\text{Fe}(\text{OH})_3$

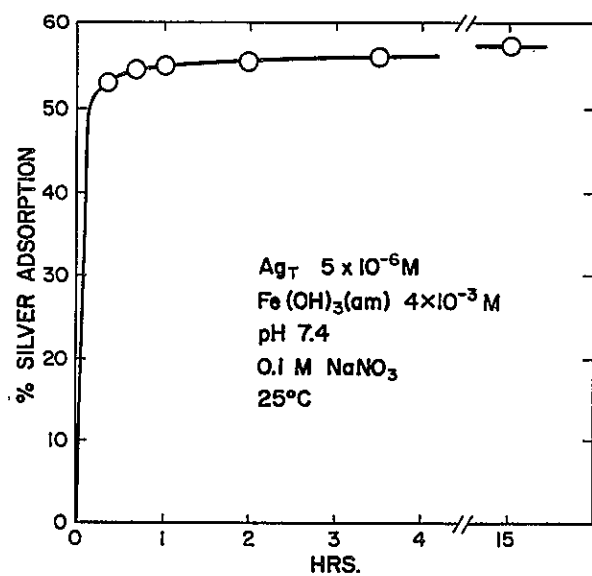


Figure 3-4. Kinetics of adsorption of silver onto am- $\text{Fe}(\text{OH})_3$

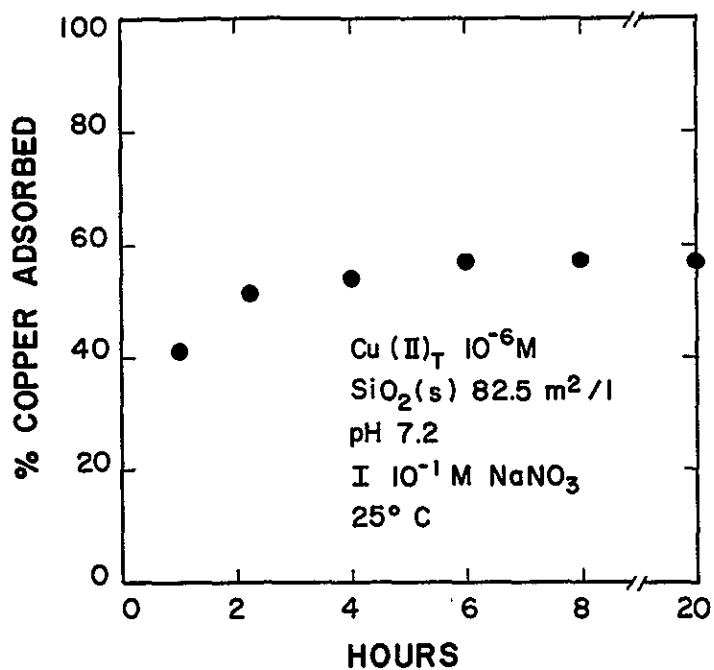


Figure 3-5. Kinetics of adsorption of copper onto SiO<sub>2</sub>

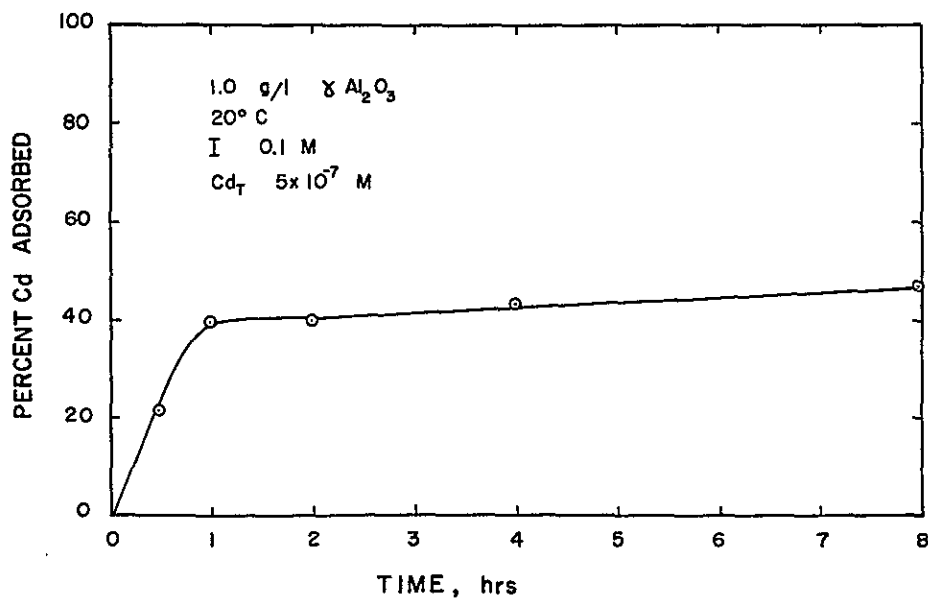


Figure 3-6. Kinetics of adsorption of cadmium onto  $\gamma$  Al<sub>2</sub>O<sub>3</sub>

onto hydrous oxides, there is a rapid initial uptake followed by a much slower adsorption step which may last several days or longer. As discussed earlier, the two steps are probably related to surface bonding and solid-state diffusion, respectively. Kinetics for adsorption experiments are nearly identical to those for coprecipitation. On a time scale typical of engineering processes, only the more rapid adsorption step is important. In a waste treatment operation, changing the detention time between 10 minutes and several hours would have very little effect on metal removal efficiencies.

## ADSORPTION ISOTHERMS--THEORETICAL CONSIDERATIONS

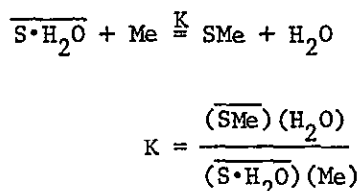
### Adsorption Isotherms for Individual Metal Ions

Adsorption isotherms describe the equilibrium partitioning of a chemical species between adsorbed and dissolved phases. Isotherms are often displayed graphically as plots of adsorption density  $\Gamma$ , versus equilibrium-dissolved concentration of adsorbate,  $C_{eq}$ .  $\Gamma$  and  $C_{eq}$  are usually concentration terms, not activities. Often an equilibrium constant is defined relating  $\Gamma$  to  $C_{eq}$ , implicitly assuming that activity coefficients in solution and on the surface are constant for the conditions of the experiment. In addition, there is often an unstated assumption that chemical speciation is unimportant or unchanging in the system. For example, in systems where a metal is the adsorbate,  $\Gamma$  and  $C_{eq}$  are often determined by techniques that do not differentiate among the various dissolved chemical species of the metal. A legitimate adsorption equilibrium constant can be measured by such techniques only if speciation of the metal is either the same under all experimental conditions or specifically accounted for.

In this section three commonly observed isotherms, the Langmuir, Freundlich, and BET, are outlined briefly. A more fundamental treatment is available in surface chemistry texts (e.g., Adamson (1)).

The Langmuir Isotherm. The Langmuir isotherm derives from the assumption that the free energy of adsorption is independent of surface coverage. That is, the driving force for adsorption onto an adsorbate-free surface is the same as that for adsorption onto a nearly filled surface. For gases, this assumption is often taken to mean that adsorbed molecules do not interact with one another at all. For adsorption from solution, a more acceptable model is that of an ideal surface solution, in which the interaction between adjacent surface species are all equivalent. That is, the affinity of the adsorbate for a given site is independent of whether the neighboring sites are occupied by solvent (water) or adsorbate species.

In the mathematical derivation of the Langmuir isotherm, the system is assumed to have a fixed concentration of sites to which adsorbate ions can sorb,  $S_T$  (moles of sites/l). The adsorption reaction is modeled analogous to solution phase reactions:



where (i) is the activity of species i in moles/l. Assuming activity coefficients on the surface to be constant, and using adsorption density as the measure of surface concentration (moles/m<sup>2</sup>), a mass balance on surface sites yields:

$$S_T = \Gamma_{\max} \cdot a = (\Gamma_{H_2O} + \Gamma_{Me}) a$$

where a is the surface concentration in m<sup>2</sup>/l. If solution phase activity coefficients are also constant, setting (H<sub>2</sub>O) = 1 :

$$K = \frac{\Gamma_{Me}}{[\Gamma_{\max} - \Gamma_{Me}][Me]}$$

where [Me] is the dissolved concentration of Me.

Rearranging,

$$\Gamma_{Me} = \frac{\Gamma_{\max}(K[Me])}{1 + K[Me]} \quad (3-1)$$

which is the Langmuir isotherm. The assumption that adsorption energy is independent of surface coverage means that K is independent of  $\Gamma_{Me}$ .

Metal ion adsorption data are often displayed as plots of fractional metal sorption versus pH. Fractional sorption is defined as the amount of metal adsorbed divided by the total metal concentration in the system (sorbed plus dissolved). An expression for fractional adsorption as a function of total metal concentration can be derived for Langmuir-type systems as follows:

$$\Gamma_{Me} = \Gamma_{\max} \frac{K[Me]}{1 + K[Me]}$$

The fractional adsorption is defined as

$$f = \frac{\text{adsorbed metal}}{\text{total metal}}$$

$$= \frac{\Gamma_{\text{Me}} A}{\Gamma_{\text{Me}} A + [\text{Me}]V}$$

where A and V are total surface area and total volume of the system, respectively. Substituting,

$$f = \frac{\Gamma_m K[\text{Me}]A / (1 + K[\text{Me}])}{\left( \frac{\Gamma_m K[\text{Me}]A}{1 + K[\text{Me}]} \right) + [\text{Me}]V}$$

At low concentration,

$$\Gamma \ll \Gamma_m \quad \text{and} \quad K[\text{Me}] \ll 1$$

so

$$f = \frac{\Gamma_m K[\text{Me}]A}{\Gamma_m K[\text{Me}]A + V[\text{Me}]} = \frac{\Gamma_m KA}{\Gamma_m KA + V}$$

Thus fractional adsorption is independent of total metal concentration at low adsorption densities.

At high adsorption densities ( $\Gamma \rightarrow \Gamma_m$ )

$$f = \frac{\Gamma A}{\Gamma A + [\text{Me}]V}$$

and fractional sorption decreases with increasing total metal concentration. These results are exactly analogous to complexation of a metal ion by a dissolved ligand. When the number of surface sites (or ligands) is in excess, the fractional adsorption (or complexation) is independent of total adsorbate (or metal ion) concentration. As the ratio of adsorbate concentration to total surface sites increases, a significant fraction of the available sites are occupied and the tendency for an additional molecule to adsorb is decreased in proportion to the lowered probability of finding an available site. However, when a molecule does

adsorb, the free energy change is the same as that for formation of previous adsorbate-surface bonds.

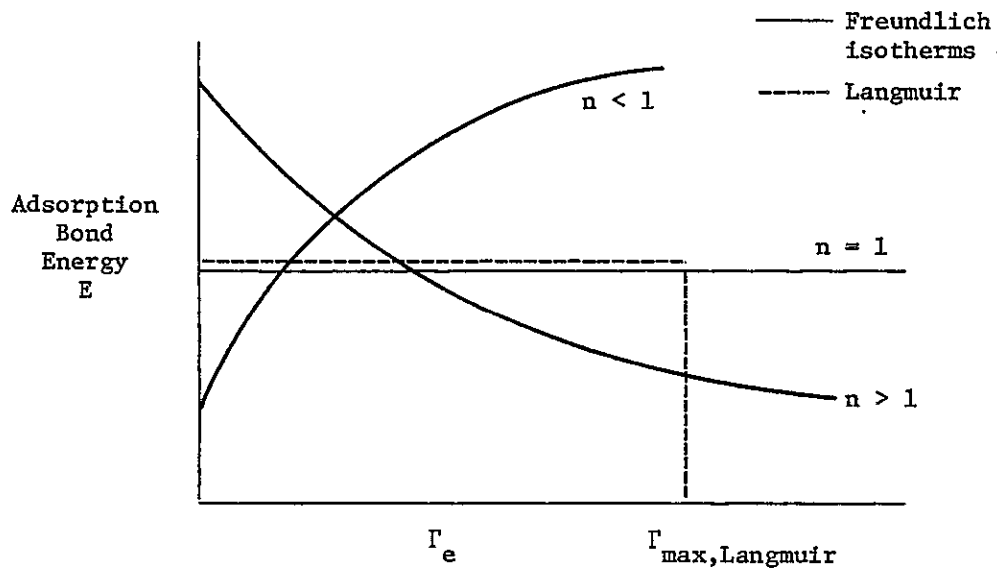
The Freundlich Isotherm. The Freundlich isotherm can be derived from the assumption that the probability of an adsorption bond having energy between  $\Delta G$  and  $(\Delta G + d\Delta G)$  is proportional to  $\exp(-\Delta G/RT)$  (2). This model of the relationship between free energy and surface coverage is chosen for its mathematical tractability and has no theoretical basis.

The mathematical expression of the Freundlich isotherm is

$$\Gamma = K C_{eq}^{1/n} \quad (3-2)$$

where  $n$  and  $K$  are constants. In a qualitative way  $K$  is related to the strength of the sorptive bond and  $n$  is related to the distribution of bond strengths. If  $n = 1$ , all surface sites are equivalent and the Freundlich isotherm is identical to a Langmuir isotherm where  $\Gamma_{max} \rightarrow \infty$ . If  $n \neq 1$ , the average strength of surface-adsorbate bonds varies with adsorption density. The greater the difference between  $n$  and 1.0, the wider is the distribution of surface bond energies. If  $n < 1$ , bond energies increase with adsorption density. This may occur, for instance, if there are favorable adsorbate-adsorbate interactions on the surface. The more common situation of  $n > 1$  may be due to unfavorable adsorbate-adsorbate interactions, a distribution of surface site types, or any factor that causes an increase in surface activity coefficient with increasing surface density. Relationships between adsorption bond energy and adsorption density are illustrated in Figure 3-7a. Typical Langmuir and Freundlich isotherms are plotted in Figure 3-7b.

The BET Isotherm. The BET isotherm is a modified form of the Langmuir expression in which multi-layer adsorption is allowed. As molecules adsorb on the surface, they form a new surface layer onto which additional molecules can sorb. Subsequent layers are formed in the same way, and each layer is assumed to obey a Langmuir isotherm (1). There is no maximum adsorption density, but there is a maximum concentration attainable in solution. This concentration is fixed by the condition of saturation with respect to a condensed surface phase which may be a solid, liquid, or micelle-type structure. If all the layers are assumed to have the same adsorption energy parameter, the isotherm is



$\Gamma_e$  = number of sites for which bond energy is  $E$  .

Figure 3-7a. Relationship between adsorption bond energy and adsorption density of the Freundlich and Langmuir isotherms

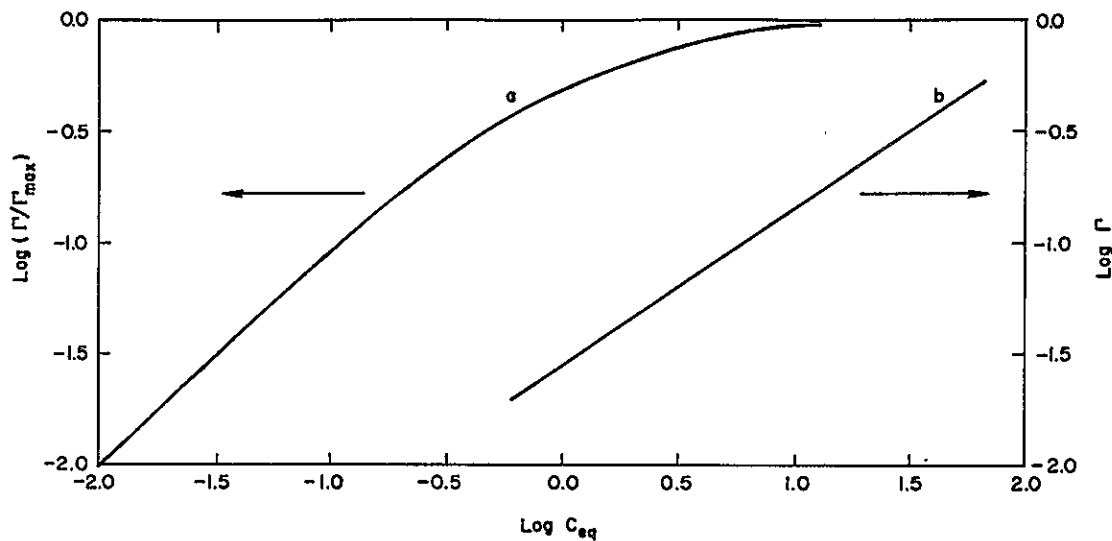


Figure 3-7b. Typical plots of  $\log(\Gamma/\Gamma_{\max})$  vs.  $\log C_{eq}$  for a) Langmuir and b) Freundlich isotherms

$$\Gamma = \frac{BC_{eq} \Gamma_o}{(C_s - C_{eq}) [1 + (B - 1)(C_{eq}/C_s)]} \quad (3-3)$$

where

- $\Gamma$  = adsorption density,
- $\Gamma_o$  = maximum adsorption density of the first layer,
- $B$  = adsorption energy parameter;  $B/C_s$  corresponds to  $K$  in the Langmuir isotherm,
- $C_{eq}$  = equilibrium adsorbate concentration in solution,
- $C_s$  = saturation adsorbate concentration in solution.

For  $B \gg 1$  and  $C \ll C_s$ , the BET isotherm reduces to the Langmuir expression. If  $B$  is different on different layers, the BET isotherm is conceptually similar to the Freundlich isotherm in that adsorption energy varies as surface coverage changes. The main differences are 1) the assumed location of adsorbing species, and 2) in the Freundlich derivation all sites are available initially while in the BET system some sites are not formed until others have filled. There is at this time no model which combines the multi-layer BET hypothesis with continuously variable adsorption energies characteristic of Freundlich systems.

Comparison and Summary. All three isotherms relate adsorption density to dissolved adsorbate concentration, assuming other solution conditions are constant. That is, variables such as ionic strength, temperature, and pH must be held constant when fitting data to one of the isotherms. The effects of these parameters on adsorption must be specified in addition to the adsorption isotherm in a complete adsorption model.

A critical difference between the various isotherms is that only the Langmuir predicts a maximum adsorption density. According to the Freundlich and BET isotherms the number of sites is unlimited.

Finally, it should be remembered that the fact that data fit a certain model is not proof that the assumptions of the model are met. The salient aspects of each isotherm are summarized in Table 3-1.

Table 3-1

## CHARACTERISTICS OF THEORETICAL ADSORPTION ISOTHERMS

Isotherm Type	$\Gamma = f(C_{eq})$	Basic Assumptions	Characteristic Features
Langmuir	$\Gamma = \Gamma_{max} \left( \frac{KC_{eq}}{1 + KC_{eq}} \right)$	$\Delta G_{ads} =$ constant (i.e., ideal surface solution); $\Gamma_{max}$ corresponds to monolayer coverage	At low $C_{eq}$ , $\Gamma \propto C_{eq}$ ; At high $C_{eq}$ , $\Gamma \rightarrow \Gamma_{max}$ ; K is a measure of bond strength
Freundlich	$\Gamma = kC_{eq}^{1/n}$	Probability of a site having binding energy $\Delta G$ is $k_1 \exp(-k_2 \Delta G)$	Adsorption density theoretically unlimited; no linear region in plot of $\Gamma$ vs. $C_{eq}$
BET	$\Gamma = \frac{BC_{eq} \Gamma_o}{(C_s - C_{eq}) [1 + (B-1)(C_{eq}/C_s)]}$	Multi-layer adsorption; $\Delta G_{ads}$ generally assumed constant on all layers	Adsorption density theoretically unlimited. At low $\Gamma$ , identical to Langmuir isotherm

Isotherms in Models of Metal Adsorption at the Oxide/Solution Interfaces

Because the Langmuir isotherm has a well-developed theoretical basis, it is generally included in models of metal adsorption at oxide/water interfaces. It is possible, of course, to apply other isotherms as well. The James-Healy adsorption model, for instance, could be combined with the Freundlich isotherm by allowing the fitting parameter  $\Delta G_{chem}$  to vary with surface coverage. However, such a change without any theoretical basis would strip the model of its predictive value and render it entirely empirical. Therefore, the Langmuir isotherm is assumed to be applicable to metal/oxide adsorption systems in the James/Healy model. Because they assume the surface to be analogous to a dissolved ligand, the surface complexation and site-binding models also predict Langmuir isotherms. Actually, the surface complexation and site-binding models predict slightly modified Langmuir

isotherms. The modification results because surface charge varies as ions sorb, altering the coulombic attraction between the surface and adsorbate. The electrostatic correction term is calculated by assuming a homogeneous surface charge over the entire surface and is approximately constant for small changes in surface coverage in swamping electrolyte solution at constant pH.

## EXPERIMENTAL RESULTS: ADSORPTION ISOTHERMS AND THE NEED FOR A MULTI-SITE MODEL

### Experimental Isotherm

Adsorption density can be varied by changing either the total metal or the total surface area in a system. Results of experiments in which these parameters are varied independently are shown in Figures 3-8 and 3-9, and are plotted as fractional adsorption of cadmium onto am-Fe(OH)<sub>3</sub> versus pH. The curves are steep and approximately parallel, and shift to higher pH with increasing adsorbate or decreasing adsorbent concentration. When plotted as log  $\Gamma$  vs. log  $C_{eq}$ , the isotherm is linear with slope of 0.66 (Figure 3-10). When the ratio  $Cd_T/Fe_T$  is very low, fractional adsorption is independent of pH (Figure 3-11), and the adsorption isotherm has unit slope (Figure 3-12). The adsorption behavior of cadmium on am-Fe(OH)<sub>3</sub> is typical of all metal/oxide systems studied. Plots of fractional sorption vs. pH and log  $\Gamma$  vs. log  $Me_{eq}$  for all the other systems studied are included in Appendix A, and are summarized in Table 3-2.

A relationship between log  $\Gamma$  and log  $C$  for a Langmuir-type system can be derived as follows. In a single-site Langmuir system:

$$\frac{\Gamma}{\Gamma_m} = \frac{KC_{eq}}{1 + KC_{eq}} \quad (3-1)$$

$$\log \frac{\Gamma}{\Gamma_m} = \log \frac{KC_{eq}}{1 + KC_{eq}}$$

Taking the derivative of both sides, and dropping the subscript:

$$d \left( \log \frac{\Gamma}{\Gamma_m} \right) = d \left( \log \frac{KC}{1 + KC} \right)$$

Since  $d \log x = \frac{1}{x} dx$ ,

$$d \log \Gamma - d \log \Gamma_m = \frac{1 + KC}{KC} d \left( \frac{KC}{1 + KC} \right)$$

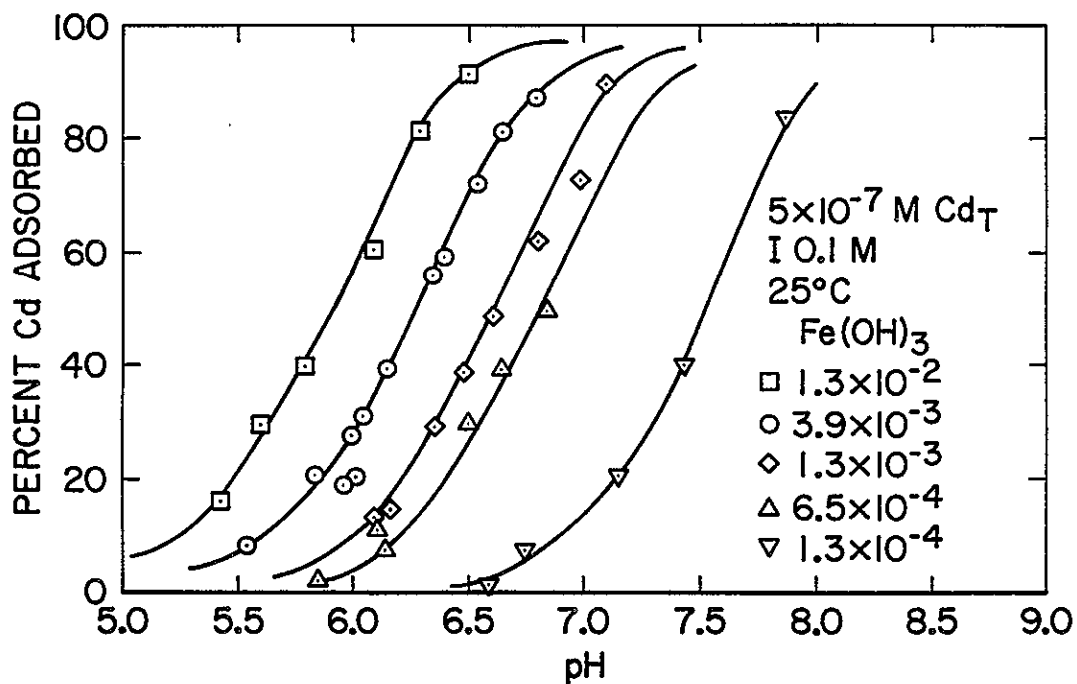


Figure 3-8. Fractional adsorption of Cd on am-Fe(OH)<sub>3</sub> as a function of Fe<sub>T</sub> and pH

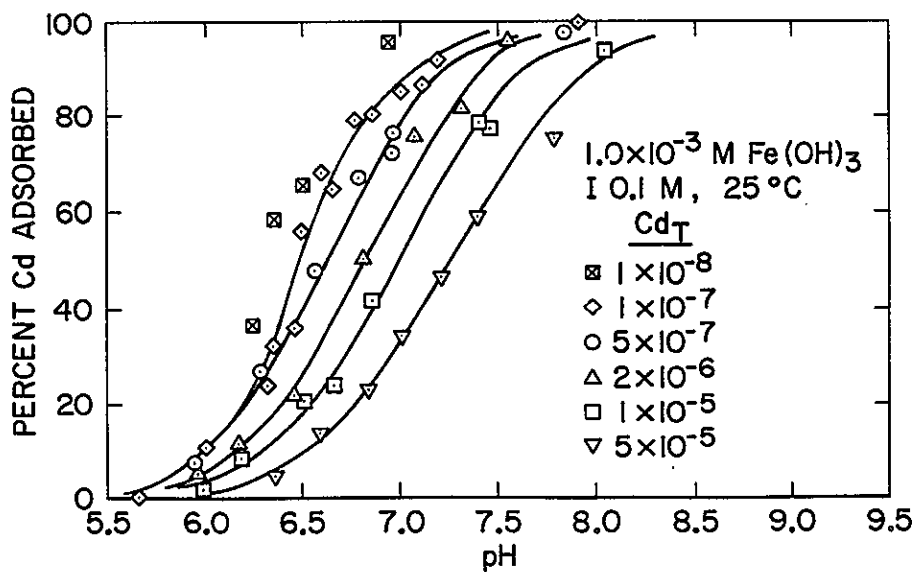


Figure 3-9. Fractional adsorption of Cd on am-Fe(OH)<sub>3</sub> as a function of Cd<sub>T</sub> and pH

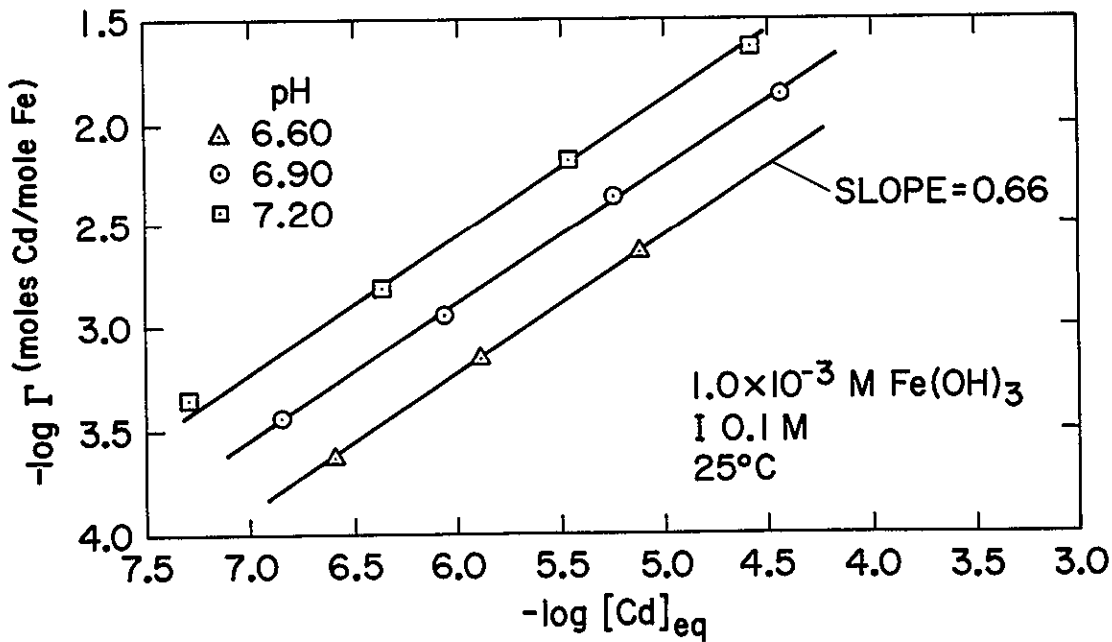


Figure 3-10. Adsorption isotherm for Cd on am- $Fe(OH)_3$  for  $Cd_T/Fe_T > 2 \times 10^{-5}$  mole/mole

Since  $\Gamma_m$  is constant,  $d \log \Gamma_m = 0$ . Expanding the right side of the equation,

$$\begin{aligned} d \log \Gamma &= \left( \frac{1 + KC}{KC} \right) \left( \frac{K}{1 + KC} - \frac{K^2 C}{(1 + KC)^2} \right) dC \\ &= \left( \frac{1}{C} - \frac{K}{1 + KC} \right) dC \\ &= \frac{1 + KC - KC}{C(1 + KC)} dC \\ &= \frac{1}{1 + KC} \frac{dC}{C} \end{aligned}$$

$$d \log \Gamma = \frac{1}{1 + KC} d \log C \quad (3-4)$$

$$\left( \frac{d \log \Gamma}{d \log C} \right)^{-1} = 1 + KC \quad (3-5)$$

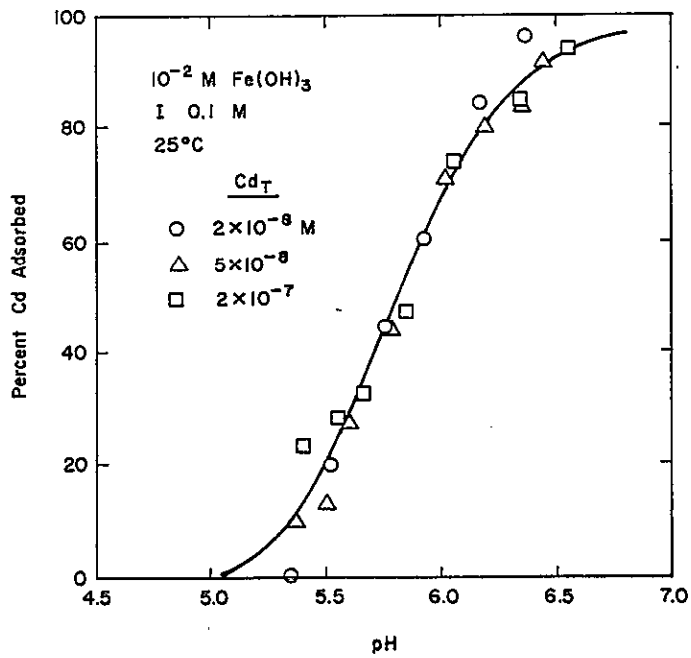


Figure 3-11. Adsorption edge for Cd adsorbing on am- $\text{Fe}(\text{OH})_3$  at very low adsorption density

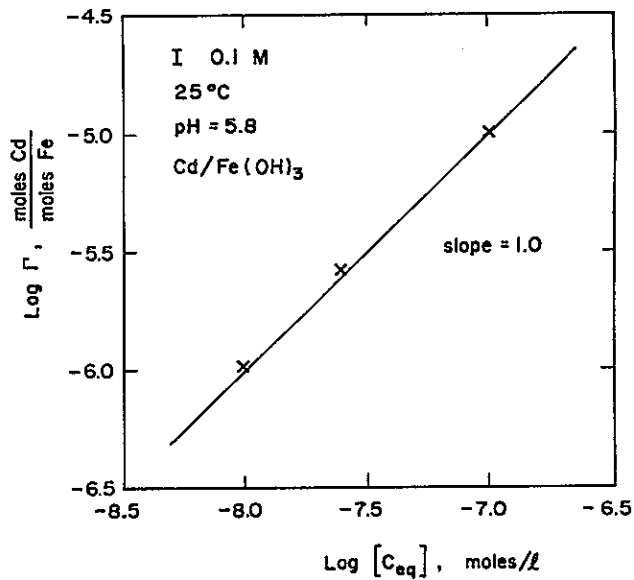


Figure 3-12. Adsorption isotherm for Cd on am- $\text{Fe}(\text{OH})_3$  at very low adsorption density

Table 3-2

SUMMARY OF RESULTS  
 ADSORPTION IN ONE-METAL SYSTEMS IN THE ABSENCE OF COMPLEXING LIGANDS

Adsorbate	Adsorbent	Range of log $\Gamma^a$	Range of pH for 50% Adsorption	Slope of log $\Gamma$ vs. log[Me]
Cd	am-Fe(OH) <sub>3</sub>	-8.6 to -6.1 <sup>c</sup>	5.9 to 7.3	0.66
		-11.9 to -9.3	~5.8	1.0
	$\gamma$ -Al <sub>2</sub> O <sub>3</sub>	-9.4 to -6.4	7.0 to 7.8	<1.0 <sup>b</sup>
	$\alpha$ -SiO <sub>2</sub>	-11.8 to -9.8	~6.0	1.0
		-9.0 to -5.5	8.5 to 10.0	1.0
Zn	am-Fe(OH) <sub>3</sub>	>-6.6	6.1 to 6.7	<1.0 <sup>b</sup>
		-8.9 to -6.6	~6.4	1.0
	$\gamma$ -Al <sub>2</sub> O <sub>3</sub>	-9.4 to -6.4	6.1 to 6.6	<1.0 <sup>b</sup>
	$\alpha$ -SiO <sub>2</sub>	-9.3 to -6.3	6.6 to 6.9	<1.0 <sup>b</sup>
Cu	am-Fe(OH) <sub>3</sub>	-7.9 to -5.9	5.2 to 5.8	0.7
		-9.6 to -7.9	~5.2	1.0
	$\gamma$ -Al <sub>2</sub> O <sub>3</sub>	-9.4 to -6.4	5.5 to 6.0	<1.0 <sup>b</sup>
	$\alpha$ -SiO <sub>2</sub>	-9.3 to -6.3	6.6 to 7.3	<1.0 <sup>b</sup>
Pb	am-Fe(OH) <sub>3</sub>	-8.9 to -5.9	4.1 to 5.0	0.5
		-9.4 to -6.4	5.0 to 6.2	<1.0 <sup>b</sup>
	$\alpha$ -SiO <sub>2</sub>	-9.3 to -6.3	~6.3	1.0
Ag	am-Fe(OH) <sub>3</sub>	-9.1 to -8.5	5.7 to 6.0	>1.0
		-7.9 to -6.9	7.0 to 8.5	0.6
	$\alpha$ -SiO <sub>2</sub>	-9.2 to -8.6	7.6 to 9.9	<1.0
		-8.6 to -7.6	9.9 to 11.4	0.67

<sup>a</sup>Dimensions of  $\Gamma$  are moles/m<sup>2</sup>.

<sup>b</sup>Insufficient data at fixed pH to quantify.

<sup>c</sup>Based on 350 m<sup>2</sup>/g Fe(OH)<sub>3</sub>.

Based on Eq. 3-4, a plot of  $\log \Gamma$  vs.  $\log C$  for a single-site Langmuir system has slope  $S = 1/(1 + KC)$ . The linearized form (Eq. 3-5) indicates that a plot of  $[(d \log \Gamma)/(d \log C)]^{-1}$  vs.  $C$  must be a line of slope  $K$  and intercept 1.0. Values for  $C$  and  $d \log \Gamma/d \log C$  according to Eq. 3-5 are shown below:

$C :$	$<10^{-2}K^{-1}$	$10^{-2}K^{-1}$	$10^{-1}K^{-1}$	$K^{-1}$	$10K^{-1}$	$10^2K^{-1}$	$>10^2K^{-1}$
$d \log \Gamma/d \log C :$	$>0.99$	$0.99$	$0.91$	$0.5$	$0.09$	$0.01$	$<0.01$

The results indicate that over a range of 2 orders of magnitude of  $C$ , a log-log plot of  $\Gamma$  vs.  $C$  for a Langmuir-type system must have one of the following traits:

1. It has a region of slope  $>0.9$  (if  $C < 0.1 K^{-1}$ ).
2. It has a region of slope  $<0.1$  (if  $C > 10K^{-1}$ ).
3. It is highly non-linear; the slope decreased from near 0.9 at low concentration to near 0.1 at high concentration (if  $0.1K < C < 10K$ ).

When tested by these criteria, adsorption of Cd, Ag, Cu, and Pb on am-Fe(OH)<sub>3</sub> cannot be described by a single-site Langmuir model. This is also true for adsorption of the four metals studied on  $\gamma$ -Al<sub>2</sub>O<sub>3</sub>. Fractional adsorption of Cd and Pb on  $\alpha$ -SiO<sub>2</sub>, and Zn on Fe(OH)<sub>3</sub> is approximately independent of  $Me_T$  in the range studied. It is possible that if  $Me_T$  is increased further in these systems, a maximum adsorption density would be attained as expected from the Langmuir analysis. However, for cadmium sorption onto  $\alpha$ -SiO<sub>2</sub>, the maximum observed fractional surface coverage was 283 percent, if the hydrated ion is assumed to be the adsorbing species (Table 3-3). According to the Langmuir expression, significant decreases in fractional adsorption should be observed at such high surface coverage, but no such decrease occurs. Thus, even in some of the systems where fractional adsorption is approximately independent of  $Me_T$ , the assumption of Langmuir-type adsorption is dubious.

#### Possible Causes for Non-Langmuir Behavior

Metal adsorption in all systems studied is modeled much more closely by the Freundlich isotherm. This suggests that for each metal/solid system, there is a distribution of adsorption bond energies. The tendency for an ion to sorb decreases slightly each time another ion adsorbs. There are at least three possible causes for this:

1. The coulombic attraction between the solid and adsorbate decreases as metal ions sorb, because the surface charge becomes more positive.

Table 3-3

## FRACTIONAL SURFACE COVERAGE IN TYPICAL EXPERIMENTAL SYSTEMS

Adsorbate	Adsorbent (Data Given as Percent Coverage)		
	$\alpha$ -SiO <sub>2</sub>	am-Fe(OH) <sub>3</sub>	$\gamma$ -Al <sub>2</sub> O <sub>3</sub>
	100 m <sup>2</sup> /1 4.5 sites/nm <sup>2</sup>	53.5 m <sup>2</sup> /1 9.8 sites/nm <sup>2</sup>	125 m <sup>2</sup> /1 8 sites/nm <sup>2</sup>
Cd <sup>a</sup>	0.47 (283) <sup>d</sup>	0.88 (44)	0.37 (19)
Cd <sup>b</sup>	0.02 (11)	0.03	0.01
Cd <sup>c</sup>	0.13 (78)	0.11	0.06
Zn <sup>a</sup>	0.66	1.2	0.53
Zn <sup>b</sup>	0.01	0.02	0.01
Zn <sup>c</sup>	0.13	0.11	0.06
Cu <sup>a</sup>	0.68	1.3	0.53
Cu <sup>b</sup>	0.01	0.02	0.01
Cu <sup>c</sup>	0.13	0.11	0.06
Pb <sup>a</sup>	0.52	0.78	0.35
Pb <sup>b</sup>	0.03	0.05	0.02
Pb <sup>c</sup>	0.13	0.11	0.06

<sup>a</sup>Based on 10<sup>-6</sup> moles/l hydrated Me<sup>2+</sup> sorbed.

<sup>b</sup>Based on 10<sup>-6</sup> moles/l unhydrated Me<sup>2+</sup> sorbed.

<sup>c</sup>Fraction of total surface sites occupied, based on 10<sup>-6</sup> moles/l Me sorbed.

<sup>d</sup>Numbers in parentheses indicate maximum adsorption density observed.

- There may be unfavorable chemical interactions between adjacent adsorbed species.
- There may be a variety of site types on the solid, of varying affinity for the adsorbate.

The first possibility is a well-known phenomenon, and its effect can be calculated within certain limits. Surface charge changes only slightly when a divalent metal adsorbs because adsorption is generally accompanied by release of between 1.5 and 2.0 protons. There may also be some release of electrolyte ions from the surface layer. The SCMA model can be used to calculate the change in surface charge when a trace metal adsorbs, and the effect on additional adsorption. The model indicates that the coulombic effect causes no noticeable shift in the adsorption edge

for the ranges of  $Me_T$  and  $\bar{S}_T$  studied. The predicted effect on fractional adsorption of increasing  $Cd_T$  from  $5 \times 10^{-7}M$  to  $5 \times 10^{-5}M$  in a system consisting of  $10^{-3}M$   $Fe(OH)_3$  and  $0.1M$   $NaNO_3$  is shown in Figure 3-13, based on the assumptions of the SGMA model. Clearly, the change in coulombic attraction between the surface and adsorbate cannot be solely responsible for the observed isotherms.

The possibility that chemical interactions with other adsorbate ions decrease the tendency to adsorb is not reasonable at low surface coverages. Obviously, if it is unfavorable for an ion to sorb near one that is already sorbed, at low surface coverage it would tend to locate at a site farther away, beyond the range of chemical interactions with the previously sorbed ion. By the same argument, BET-type adsorption in which an ion binds to a lower-energy second-layer site is unlikely at low surface coverage, when many higher-energy first-layer sites are still available.

The only reasonable explanation for a Freundlich isotherm in the systems studied is a variation in surface site types and their affinities for sorbate ions. The idea that not all surface sites are identical is entirely reasonable. Crystalline

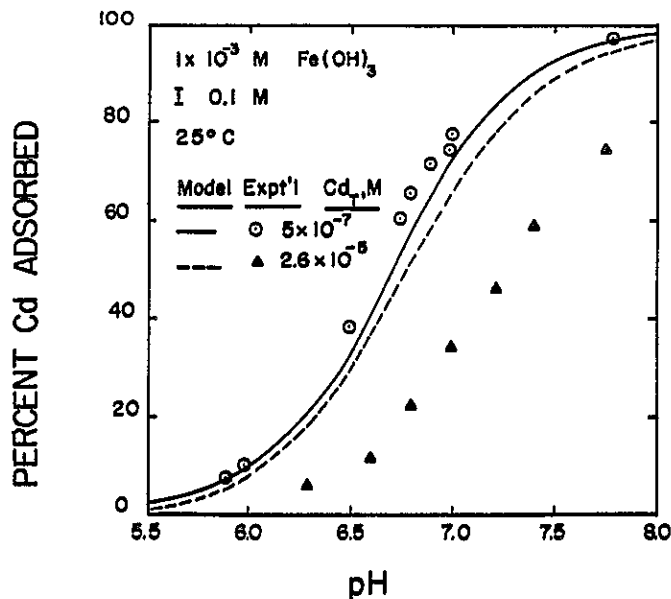


Figure 3-13. Effects of metal ion concentration on fraction adsorption: Comparison of experimental with SGMA model prediction

surfaces are known to have pits, edges, and other discontinuities as a result of surface defects. The potential for surface non-homogeneities are at least as large on amorphous solids, where stereochemical variations from one site to the next may be much greater. Even on a theoretically perfect crystal, there are several distinct potential binding sites. Schindler et al. (3) suggested that a metal ion may bind to one or two oxide sites simultaneously. They implied that the sites involved in bidentate bonding are identical to those which form monodentate bonds. However, it is equally reasonable to assume that ideal surfaces consist of a surface solution of distinct monodentate and bidentate sites. Three different types of OH groups have been identified on the 100 face of goethite by IR spectroscopy (Parfitt and Russell (4)). The groups differ from one another according to whether the oxygen is singly-, doubly-, or triply-coordinated to iron. Benzoic acid adsorbs strictly as a monodentate species and replaces singly-coordinated OH groups. Doubly- and triply-coordinated hydroxo-sites are altered by the presence of the benzoic acid on the singly-coordinated sites, as indicated by a change in the intensity of their OH stretching bands. Thus, the affinity of a given surface site type for an adsorbate may be altered by sorption onto other types of sites.

The presence of multiple distinct sites on a given solid has also been invoked occasionally to explain adsorption of heavy metals at the oxide/water interface. Loganathan and Bureau (5) and Zasoski (6) hypothesized the presence of two types of sites on  $MnO_2$  for adsorption of Cd, Zn, and Co. Guy et al. (7) and Gadde and Laitinen (8) showed that Cu and Pb have adsorption capacities different from Cd and Zn on  $MnO_2$  suggesting the presence of multiple sites, although the authors did not propose that explanation of their data. Thus, the concept that several types of surface sites may coexist on a solid is reasonable and has been suggested to a limited extent by several authors.

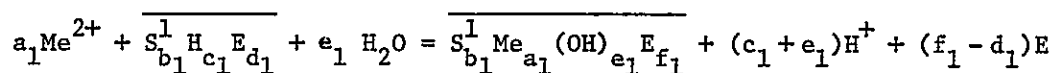
Based on the experimental data, it is proposed that many oxides have several distinct groups of sites to which chemical species may adsorb. The surface density of each type of site is fixed for a given surface, and is independent of that of any other site type. In addition, the strength of the adsorptive bonds may be different for each site type. If each type of site fills according to the Langmuir isotherm, then for each  $i$ ,  $\Gamma_i = K_i C_{eq} \Gamma_{i,max} / (1 + K_i C_{eq})$ , where  $\Gamma_i$  is the surface density of type  $i$  sites. At any equilibrium concentration  $C_{eq}$ , all types of sites are partially occupied. Fractional coverage,  $\Gamma_i / \Gamma_{i,max}$  is greatest for the sites with the greatest adsorption constant and decreases monotonically with  $K_i$ .

If adsorption of metal onto different surface site types were measurable, this model could be experimentally tested. Unfortunately, only the overall adsorption density  $\Gamma_{\text{tot}}$  can be measured, and from it an apparent overall equilibrium constant is derived. In this section, relationships between the true, thermodynamic equilibrium constants and the measurable, apparent equilibrium constant are investigated. It is then shown that the experimental results are consistent with the model.

#### A MODEL OF ADSORPTION ON A MULTI-SITE SURFACE

##### Mathematical Development

A generalized equation for adsorption of metal to a single site type can be written as follows:



where

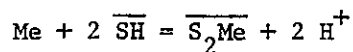
$S^{(1)}$  = a surface site, type 1,

E = bulk electrolyte ion (may be either cation or anion),

$a_1, b_1, \dots, f_1$  = stoichiometric coefficients for the reaction.

This equation allows for simultaneous adsorption, hydrolysis, and exchange of surface protons and inert electrolyte. The subscript 1 on the coefficients indicate that the reaction is with site type 1. Similar reactions involving other site types occur simultaneously.

Bidentate adsorption is modeled here as a reaction between a metal ion and a single, bidentate site, i.e.,



The stability constant for formation of the bidentate complex by each reaction is:

$$\beta \equiv \frac{\overline{(\text{S}_2\text{Me}^{(i)})} (\text{H}^+)^2}{(\text{Me}) \overline{(\text{S}_2^{(i)}\text{H}_2)}} \quad (\text{This work})$$

$$\beta = \frac{\overline{(\text{S}_2\text{Me})} (\text{H}^+)^2}{(\text{Me}) \overline{(\text{SH})}^2} \quad (\text{Hohl and Stumm (9)})$$

Since 2 sites must be adjacent to form a bidentate complex the reaction is more analogous to formation of a dissolved bidentate complex than to complexation by two independent ligand molecules. In addition, for the same reason the concentration of bidentate binding sites is proportional to total surface area not to the square of surface area.

The equilibrium constant for the generalized reaction is:

$$K'_{e,1} = \frac{\overline{(S_{b_1}^1 Me_{a_1} (OH)_{e_1} E_{f_1}) (H^+)^{c_1+e_1} (E)^{f_1-d_1}}}{(Me)^{a_1} \overline{(S_{b_1}^1 H_{c_1} E_{d_1})}} \quad (\text{EDL}) \quad (3-6)$$

where EDL is the term accounting for coulombic interactions in the electrical double layer. The expression has several non-measurable terms which must be estimated or eliminated.

A number of simplifications can be made in the equation: 1) The magnitude of the EDL term depends on the adsorption stoichiometry and the electrical potential at the plane where the adsorbed ions reside. In swamping electrolyte solutions (e.g.,  $10^{-1}M$ ), it varies with pH but is insensitive to the extent of adsorption of a trace element (e.g.,  $10^{-5}M$ ). Thus we can assume EDL is a function of pH only (call it  $D(pH)$ ). 2) The activity of inert electrolyte (E) is assumed constant. 3) Assuming that not more than one metal ion binds to a site,  $a_1 = 1$ . A site may be either mono- or multi-dentate, so this does not necessarily imply  $a_1 = b_1$ . 4) Activity coefficients, both in bulk solution and at the surface, are assumed constant for a given solution ionic strength.

To simplify the notation, let

$$c_1 + e_1 = x_1$$

$$\overline{S_{b_1}^1 H_{c_1} E_{d_1}} = \overline{S^{(1)}}$$

and

$$\overline{S_{b_1}^1 Me_{a_1} (OH)_{e_1} E_{f_1}} = \overline{SMe^{(1)}}$$

so

$$K'_{e,1} = \frac{[\overline{SMe^{(1)}}] (H^+)^{x_1}}{[Me] [\overline{S^{(1)}}]} D_1 (E)^{f_1 - d_1} \gamma_T = \frac{[\overline{SMe^{(1)}}] (H^+)^{x_1}}{[Me] [\overline{S^{(1)}}]} z_1 D_1 \quad (3-7)$$

where  $[ ]$  = the concentration of a species (moles/l),  $\gamma_T$  is a composite activity coefficient including the activity coefficients of  $\overline{SMe^{(1)}}$ ,  $\overline{S^{(1)}}$ , and Me, and  $z_1 = (E)^{f_1-d_1}\gamma_T = \text{constant}$ . Placing all constants on the left of the equal sign,

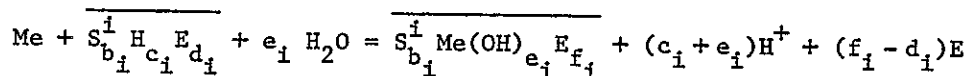
$$K'_{e,1} z_1^{-1} = \frac{\overline{[SMe^{(1)}]}(H^+)^{x_1}}{[Me][\overline{S^{(1)}}]} D_1 \quad (3-8)$$

Thus far a number of simplifications in the adsorption equilibrium expression have been made, and justification for the simplifications has been given. The resulting conditional stability constant has two measurable quantities,  $[Me^{2+}]$  and  $(H^+)$ . The remaining parameters,  $\overline{[S^{(1)}]}$  and  $x_1$ , relate to adsorption onto specific sites and cannot be measured. Only average values which include sorption onto all site types are measurable experimentally. Next, an apparent equilibrium constant based on these average values will be defined and compared qualitatively with the thermodynamic equilibrium constant.

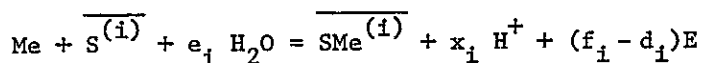
Consider the case where several site types are filling simultaneously. If for each site type the assumptions of the model are met, then the equilibrium constant for site type  $i$  is

$$K'_{e,i} = \left( \frac{\overline{[SMe^{(i)}]}(H^+)^{x_i}}{[Me][\overline{S^{(i)}}]} \right) (z_i) D_i \quad (3-9)$$

The relevant reaction is



or, more simply,



Define  $F_i$  as the fraction of adsorbed metal bound to sites  $S^i$ . Thus,

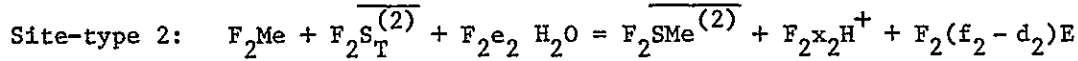
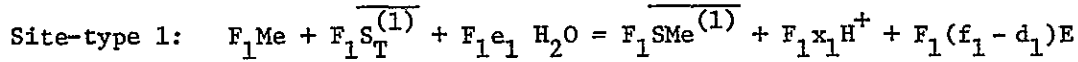
$$F_i = \overline{[SMe^{(i)}]} / \left( \sum_j \overline{[SMe^{(j)}]} \right)$$

and

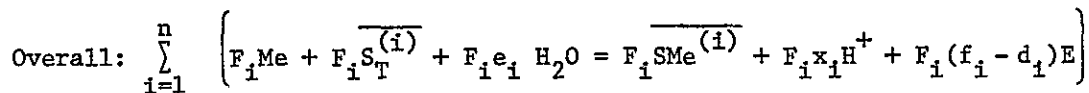
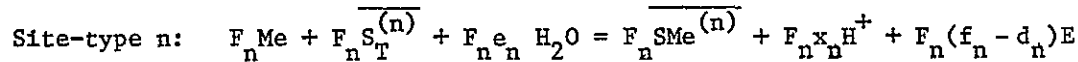
$$\sum F_i = 1.0$$

The overall reaction stoichiometry is the weighted sum of adsorption to all possible site types:

Reaction



⋮



This net reaction includes all the individual sorption reactions occurring simultaneously. The overall equilibrium constant  $K'_{e,o}$  is given by the product of the individual constants raised to the appropriate power:

$$K'_{e,o} = \prod_{i=1}^n (K'_{e,i})^{F_i}$$

or

$$K'_{e,o} = \prod_{i=1}^n \left( \frac{[\overline{\text{SMe}^{(i)}}] (\text{H}^+)^{x_i} D_i}{[\text{Me}] [\overline{S_T^{(i)}}]} \right)^{F_i} \cdot \prod_{i=1}^n (z_i)^{F_i} \quad (3-10)$$

At very low dissolved metal concentrations, all site types are in excess, so the number of available sites of type  $i$  is approximately equal to the total number of such sites,  $[\overline{S_T^{(i)}}]$ . Type  $i$  sites represent a fixed fraction  $A_i$  of the total surface sites, so  $[\overline{S_T^{(i)}}] = A_i [S_T]$ .

Furthermore, assuming that the pH dependence of all site types is approximately equivalent,  $x_i$ ,  $z_i$ , and  $D_i$  are independent of the identity of a site, e.g. for constant solution conditions ( $x_1 = x_2 = \dots = x_n = x$ ). Then,

$$F_i = \frac{[\overline{SMe}^{(i)}]}{[\overline{SMe}_T]} = \frac{[\overline{SMe}^{(i)}]}{\sum_j [\overline{SMe}^{(j)}]} = \frac{K'_{e,i} [\overline{Me}] [\overline{S}_T^{(i)}] / (H^+)^x}{\sum_j \left\{ K'_{e,j} [\overline{Me}] [\overline{S}_T^{(j)}] / (H^+)^x \right\}} = \frac{K'_{e,i} [\overline{S}_T^{(i)}]}{\sum_j K'_{e,j} [\overline{S}_T^{(j)}]} \quad (3-11)$$

That is, the number of sites of a given type occupied by metal ions is proportional to the total number of occupied sites.

Substituting  $[\overline{SMe}_T] F_i = [\overline{SMe}^{(i)}]$  and  $[\overline{S}_T] A_i = [\overline{S}_T^i] = [\overline{S}^i]$  in Eq. 3-10,

$$K'_{e,o} = \prod_{i=1}^n \left( \frac{[\overline{SMe}_T] (H^+)^x}{[\overline{Me}] [\overline{S}_T]} \right)^{F_i} \cdot \prod_{i=1}^n \{ (z_i) (F_i / A_i) \}^{F_i} \quad (3-12)$$

Since

$$\prod_{i=1}^n N^{F_i} = N^{\sum F_i}$$

$$K'_{e,o} = \left( \frac{[\overline{SMe}_T] (H^+)^x D}{[\overline{Me}] [\overline{S}_T]} \right)^{\sum F_i} \cdot \alpha \quad (3-13)$$

where

$$\alpha = \prod_{i=1}^n \{ (z_i) (F_i / A_i) \}^{F_i}$$

and is constant for a given system.

Since  $\sum F_i = 1.0$ ,

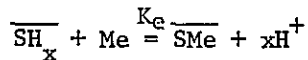
$$K'_{e,o} = \frac{[\overline{SMe}_T]}{[\overline{S}_T]} \cdot \frac{1}{[\overline{Me}]} \cdot (H^+)^x \cdot \alpha D \quad (3-14)$$

The ratio  $[\overline{SMe}_T] / [\overline{S}_T]$  is the overall adsorption density,  $\Gamma_{Me}$ . Letting  $K_{e,o} = K'_{e,o} \alpha^{-1} D^{-1}$ :

$$K_{e,o} = \Gamma_{Me} (H^+)^x / [\overline{Me}] \quad (3-15)$$

$K_{e,o}$  is the overall apparent equilibrium constant and can be evaluated from directly measurable experimental quantities.

An expression similar to Eq. 3-15 can be derived based on a very simple single-site model ignoring surface electrical properties. If sites are in excess the equilibrium constant for the reaction



is

$$K_e \equiv \frac{[\overline{SMe}](H^+)^x}{[\overline{SH}_x][Me]} = \Gamma_{Me} (H^+)^x / [Me]$$

The longer, more general derivation is provided here to emphasize some critical assumptions and, in particular, to define the conditions under which the expression is valid for multi-site adsorption.

#### Comparison of the Model with Experimental Results

Values of  $\Gamma_{Me}$ ,  $(H^+)$ , and  $[Me]$  were determined under widely varying conditions.  $x$  was measured only under one set of conditions for Cd, Cu, Zn, and Pb, and only on  $Fe(OH)_3$ .

For the system that was studied most extensively, Cd sorption onto amorphous  $Fe(OH)_3$ , a plot of  $\log K_{e,o}$  vs.  $\log \Gamma_{Cd}$  has two distinct ranges (Figure 3-14). At very low  $\Gamma$ ,  $\log K_{e,o}$  is constant, as it should be if the assumptions of the derivation are valid and if it is approximately constant over the pH range studied. At higher adsorption density,  $\log K_{e,o}$  decreases with increasing  $\Gamma$ , indicating that at least one of the assumptions fails in this region. To compute  $K_{e,o}$  in Figure 3-14, the experimentally determined value  $x = 1.8$  was used.

Figure 3-15 shows that if  $x = 2$  instead of 1.8, the absolute value of  $K_e$  changes, but the shape of the curve does not. The assumptions considered most suspect are: 1) that the value of  $D$  is constant in the pH range studied; 2) that the value of  $x$  is independent of pH; 3) that the value of  $x$  is the same for all site types; 4) that  $\gamma_T$  is constant; and 5) that all site types are in excess. These assumptions will be considered individually.

The calculated variation of  $D$  with pH depends on which adsorption model is used. According to the surface complexation model,  $D$  is approximately independent of pH because the electrical energy required to remove protons from a charged surface

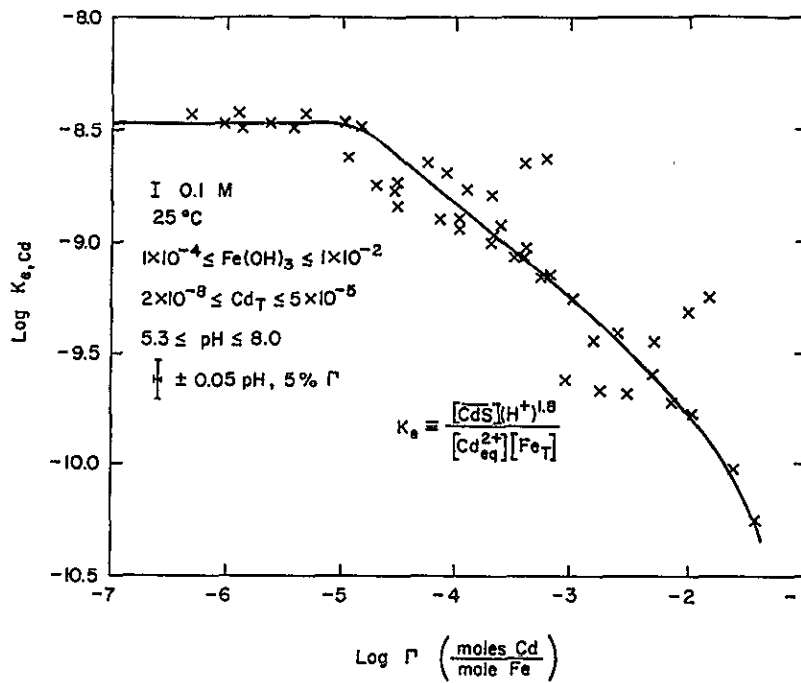


Figure 3-14.  $\text{Log } K_e$  vs.  $\text{log } \Gamma_{\text{Cd}}$  for  $x = 1.8$

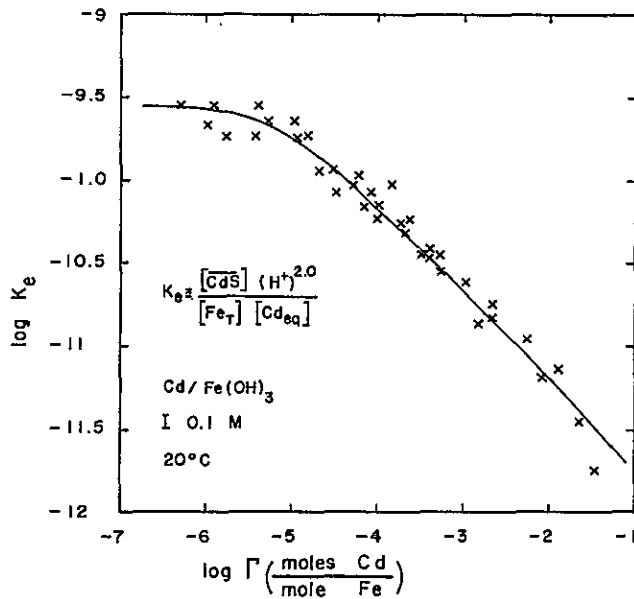


Figure 3-15.  $\text{Log } K_e$  vs.  $\text{log } \Gamma_{\text{Cd}}$  for  $x = 2.0$

is exactly compensated by the energy gained when the protons are replaced by a cation, as long as net surface charge is conserved. In the SGMA model electrical energy change associated with moving a proton to or from the surface is greater than that for any other singly-charged cation, since protons are assumed to approach the surface more closely. This leads to the somewhat surprising conclusion that, in most cases, the net electrical interaction term describing a cation adsorption reaction becomes less attractive (or more repulsive) as pH is increased. The magnitude of the effect is a function of how closely the cations approach the surface, and other interfacial parameters such as the dielectric constant.

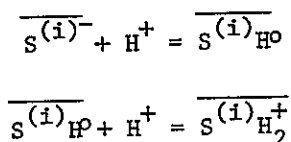
If changes in  $D$  are the sole reason for the variation of  $K_{e,o}$  with  $\Gamma$ , then  $K_{e,o}$  (and  $K'_{e,o}$ ) should be constant for constant  $D$ . Since for a given adsorbent/adsorbate pair,  $D$  is a function of pH only, this is equivalent to saying  $K'_{e,o}$  must be constant in all systems at fixed pH. At fixed pH,

$$K'_{e,o} = \frac{[\overline{SMe}_T]}{[\overline{S}_T][Me]} \cdot (H^+)^x \cdot D \cdot \alpha$$

$$= \frac{[\overline{SMe}_T]}{[Me]} \cdot \frac{1}{[\overline{S}_T]} \cdot \beta$$

where  $\beta = (H^+)^x \cdot D \cdot \alpha = \text{constant}$ .  $[\overline{SMe}]/[Me]$  is related to the fractional metal adsorption and, at fixed  $[\overline{S}_T]$ , is independent of  $Me_T$  if sites are not limiting. Thus, if the variation in  $K_{e,o}$  is due solely to variation in  $D$ , fractional adsorption must be independent of  $Me_T$  for fixed adsorbent concentration and pH. This is contrary to experimental evidence. While such reasoning does not rule out the possibility that changes in  $D$  contribute to the variability of  $K_{e,o}$ , it does indicate that changes in  $D$  cannot fully explain the phenomenon.

The variable  $x$  is the number of protons released, on the average, when a metal ion adsorbs. It gives no information about the source of the protons. If the surface undergoes reversible protolysis characterized by the reactions (ignoring the inert electrolyte):

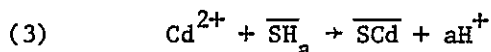
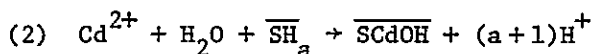
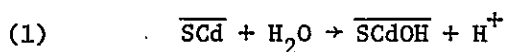


9 1 1 3 0 7 1 2 1 7

then at a given pH and ionic strength, the average number of protons bound to an  $S^{(i)}$  site is fixed. By analogy to solution chemistry of mononuclear complexes the ratio of hydrolyzed to unhydrolyzed adsorbed metal is assumed constant at a given pH, independent of total metal concentration. Thus,  $x_i$ , which is the sum of the average number of protons per  $S^{(i)}$  site and the fractional hydrolysis of adsorbed ions, is a function of pH but not of  $S^{(i)}$  or  $Me_T$ .

There are two ways in which  $x$  can change as a function of pH, if all site types are in excess. First, the average number of protons bound to the sorption sites,  $c_i$ , may change, and secondly, the extent of hydrolysis of adsorbed metal may change. Yates (10) has shown that the average number of protons per surface site changes only 10 percent in the pH range from the PZC to 3 units above or below the PZC. In the present study, for each metal the pH range investigated is approximately 2 units wide. It is, therefore, likely that the average number of surface protons per binding site changes only slightly.

The assumption that the extent of hydrolysis of adsorbing ions is independent of pH can be tested indirectly as follows. At pH 7.0,  $10^{-2}M Fe_T$ , and  $8.1 \times 10^{-5}M Cd_T$  the experimentally determined value of  $x$  is 1.8, and  $\log K_{e,o} = -10.06$ . If the sole cause for the decrease in  $K_{e,o}$  is a change in  $x$ , then the value of  $x$  under other conditions is given by  $x = -10.06 - \log \Gamma + (\log [Cd^{2+}] / (\log (H^+)))$ . As shown in Figure 3-16, the value of  $x$  calculated from this equation decreases with increasing pH. This is exactly opposite what would be expected if hydrolysis of adsorbed species were increasing with increasing pH. Consider, for example, the following reactions:



Reactions (1) and (2) are mechanisms by which hydrolyzed metal ions are formed on or bind to the surface. The left side of reaction (1), and reaction (3) involve unhydrolyzed adsorbed species. Regardless of the mechanism, reactions forming hydrolyzed surface species release more protons than those in which unhydrolyzed surface species are formed. Therefore, increasing surface hydrolysis tends to increase the value of  $x$  and cannot be invoked to explain the variation in  $K_{e,o}$ .

This analysis is based on the assumption that  $D$  is independent of pH. Some of the apparent decrease in  $x$  may in fact be due to decreasing values of  $D$  with increasing pH. However, as noted earlier, variation in  $D$  can account at most for only a portion of the decrease in  $K_{e,o}$ , and cannot account for the decrease in fractional adsorption with increasing  $[Me_T]$  at constant pH and  $[S_T]$ . The same argument can be made for the effect of changes in the hydrolysis of adsorbed species.

Activity coefficients of adsorbed species may change as the surface composition changes. However, it is unlikely that such changes in activity coefficients can explain the apparent decrease in  $K_{e,o}$ . Activity coefficients are thought to arise primarily from electrical interactions and are therefore relatively insensitive to parameters other than net ionic charge (11). Thus activity coefficients of adsorbed Hg, Cd, Zn, Cu, and Pb are expected to be approximately equal. Since the adsorption density at which  $K_{e,o}$  starts decreasing varies by several orders of magnitude among this group of metals, it is unlikely that the variation in  $K_{e,o}$  can be accounted for by changes in activity coefficients.

The possibility that surface sites are not in excess but are in fact limiting, is consistent with the smooth curve obtained in Figure 3-14. At very low surface

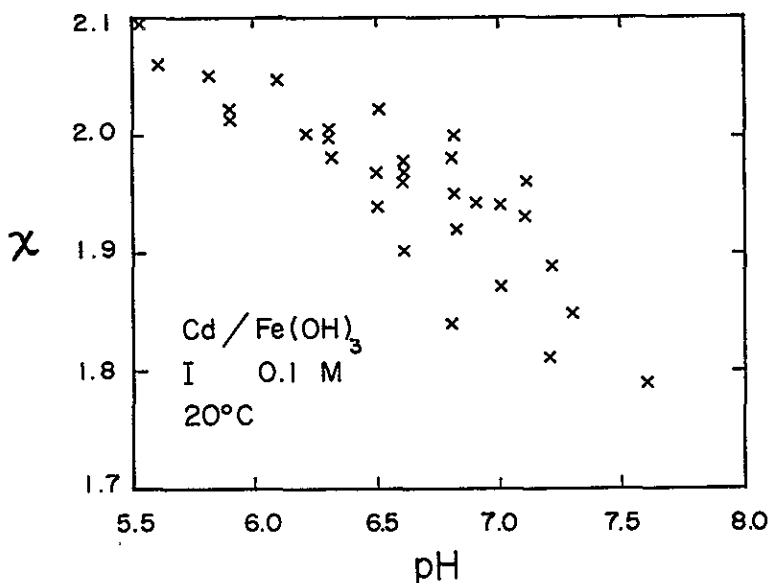


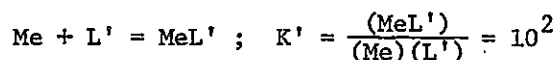
Figure 3-16. Apparent proton release accompanying adsorption of Cd on am-Fe(OH)<sub>3</sub> assuming constant  $K_e$

coverages, all sites are in excess, and  $K_{e,o}$  is constant. The metal ions bind preferentially to sites where the interaction energy is maximum, so  $K_{e,o}$  is greatest at low  $\Gamma$ . As surface coverage increases, adsorption to the highest energy sites becomes site-limited and adsorbing ions are forced, on the average, to bind to sites of lower interaction energy.

#### Estimating the Surface Density and Binding Strength of High-Energy Sites

The conditions when  $K_{e,o}$  starts decreasing are such that the "highest energy" sites are becoming limiting. Call the adsorption density under these conditions  $\Gamma^*$ . At  $\Gamma < \Gamma^*$ , sites of all binding energies are filling simultaneously. There is no way to measure what portion of the total adsorption density at  $\Gamma = \Gamma^*$  is attributable to the strongest binding sites.

An example from solution chemistry will help clarify this point. Consider a metal in solution with two potential complexing ligands, L and L'. Say the concentrations and stability constants are given as



$$(\text{L})_{\text{tot}} = 10^{-6}\text{M}; \quad (\text{L}')_{\text{tot}} = 10^{-2}\text{M}$$

The apparent overall stability constant in this system is

$$K_{\text{app}} = \frac{(\text{Complexed Me})}{(\text{Free Me})(\text{Free Ligand})} = \frac{(\text{MeL}) + (\text{MeL}')}{(\text{Me})(\text{L} + \text{L}')}$$

The equilibrium conditions for several different free metal concentrations are given below:

Case	Me	MeL	L	MeL'	L'	$K_{\text{app}}$
1	$10^{-9}$	$10^{-9}$	$10^{-6}$	$10^{-9}$	$10^{-2}$	200
2	$10^{-8}$	$10^{-8}$	$10^{-6}$	$10^{-8}$	$10^{-2}$	200
3	$10^{-7}$	$9.0 \times 10^{-8}$	$9.1 \times 10^{-7}$	$10^{-7}$	$10^{-2}$	190
4	$10^{-6}$	$5.0 \times 10^{-7}$	$5.0 \times 10^{-7}$	$10^{-6}$	$10^{-2}$	150
5	$10^{-5}$	$9.1 \times 10^{-7}$	$9.0 \times 10^{-8}$	$10^{-5}$	$10^{-2}$	109
6	$10^{-4}$	$10^{-6}$	$10^{-8}$	$10^{-4}$	$10^{-2}$	101
7	$10^{-3}$	$10^{-6}$	$10^{-9}$	$9 \times 10^{-4}$	$9 \times 10^{-3}$	99

Several important features emerge from this example. The apparent binding constant is much less than the stability constant of the strongest complex ( $K = 10^6$ ), even under conditions where all ligands are in excess (cases 1 and 2). Secondly, the apparent stability constant starts decreasing when the strongest complex (MeL) becomes limited by the availability of ligands (case 3), even though the absolute value of  $K_{app}$  is much closer to  $K'$  than  $K$ . Third, the concentration of complexed metal at this point is considerably greater than the total concentration of strongly complexing ligand.

If one extends this example to include many more ligands of varying complexing strength, it would be very nearly analogous to the proposed model of the surface. Now consider that on a given type of surface, the ratios of site densities are fixed. That is, for a given adsorbent, the ratio of the surface densities of site type A to site type B is the same in all systems. Returning to the example, this is analogous to fixing the ratio  $(L)_{tot}/(L')_{tot}$ . For all practical consideration then, the absolute value of individual stability constants become irrelevant. In the example, the fact that  $K_{MeL} = 10^6$  has little importance, because the greatest net overall stability constant that will be realized in any system is 200. From a chemical point of view it is important that a species exists with a very strong binding constant and that the apparent binding constant is not a good approximation for its strength. But in any real system, the maximum overall constant and not any individual constant controls the ratio of complexed (adsorbed) to free (dissolved) metal at equilibrium.

By analogy, then  $\Gamma^*$  is an important parameter measuring the adsorption density when the strongest binding sites become limiting, but it is not directly a measure of the density of high energy sites. Similarly, the maximum value of  $K_{e,o}$  is a measure of the maximum overall binding strength, but is not a direct measure of the strength of the strongest binding sites. Therefore, it should be remembered that adsorption sites referred to as "high-energy" sorption probably represent composite binding of several chemically different surface species. For  $\Gamma > \Gamma^*$  the effective adsorption binding strength is reduced, most probably because the assumption  $\frac{\overline{SMe}^{(i)}}{\overline{S}_T^{(i)}} \ll 1$  fails.

#### Testing the Model with Amorphous and Crystalline Systems

Systems Where am-Fe(OH)<sub>3</sub> Is the Adsorbent. A plot of  $K_{e,o}$  vs.  $\Gamma_{Cu}$  for sorption onto Fe(OH)<sub>3</sub> is shown in Figure 3-17. For these calculations the value of  $x$  is 1.88. Because it adsorbs at lower pH, the values of  $K_{e,o}$  for copper are greater

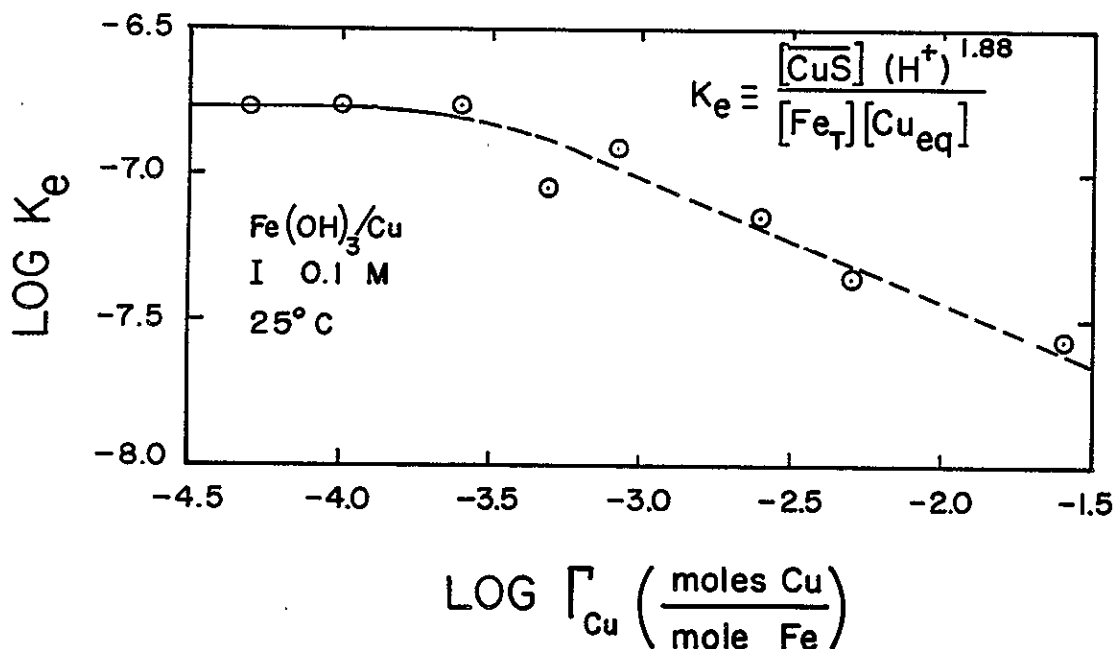


Figure 3-17.  $\text{Log } K_e$  vs.  $\text{log Cu}$  for  $x = 1.88$

than for cadmium. For  $\Gamma > \Gamma^*$  the distribution of surface sites is approximately the same for the two metals, i.e., the slopes of Figures 3-14 and 3-17 are approximately equal. The value of  $\Gamma^*$  for copper is approximately 20 times as large as that for cadmium. It is possible that copper sorbs strongly to sites unavailable to cadmium, or that the metals sorb to the same sites but that some of the moderate energy Cd sites are high-energy sites for Cu. These possibilities are addressed in the discussion of competitive sorption.

Adsorption of lead onto  $\text{Fe(OH)}_3$  was not studied as intensively at low adsorption density as that of Cd or Cu. Figure 3-18 is a plot of  $\text{log } K_{e,o}$  vs.  $\text{log } \Gamma_{\text{Pb}}$ , for  $x = 1.65$ . The value of  $K_{e,o}$  for lead is larger than for copper or cadmium, but for the data are less precise than those for the other metals. The value of  $\Gamma^*$  for lead was not determined but since the lead adsorption isotherm is linear with slope  $< 1$  for  $\Gamma_{\text{Pb}} \geq 10^{-3.5}$  moles Pb/mole Fe,  $\Gamma_{\text{Pb}}^*$  is probably less than this value.

Silver behaves similarly to Cd and Pb in that fractional adsorption decreases continuously as the ratio  $\text{Ag}_T:\text{Fe}_T$  increases from  $1.7 \times 10^{-5}$  to  $3 \times 10^{-3}$  mole Ag/mole Fe in 0.1M  $\text{NaNO}_3$ . The slope of a plot of  $\text{log } \Gamma_{\text{Ag}}$  vs.  $\text{log } C_{\text{eq}}$  is 0.6 at pH 6.5 and pH 10.5 (Figure 3-19). Therefore,  $\Gamma_{\text{Ag}}^*$  is at least as small as  $\Gamma_{\text{Cd}}^*$  and may be less.

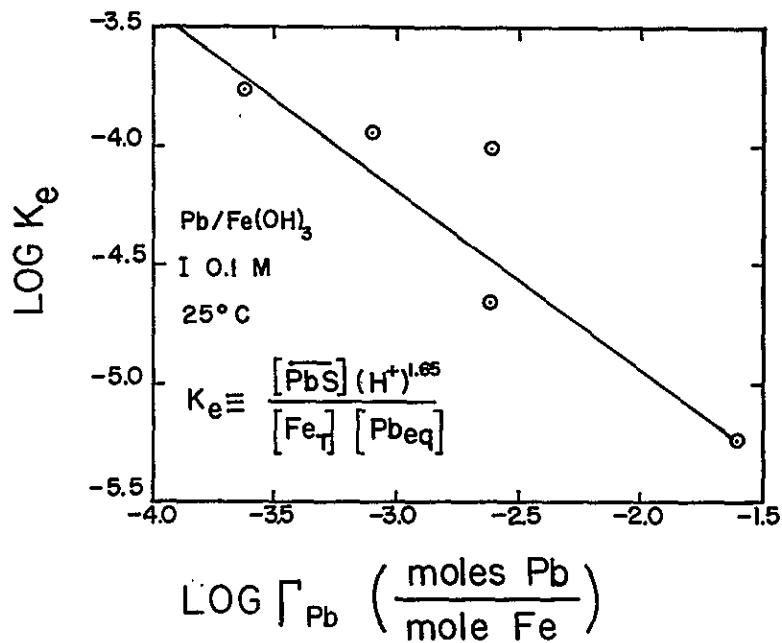


Figure 3-18.  $\text{Log } K_e$  vs.  $\text{log } \Gamma_{\text{Pb}}$  for  $x = 1.65$

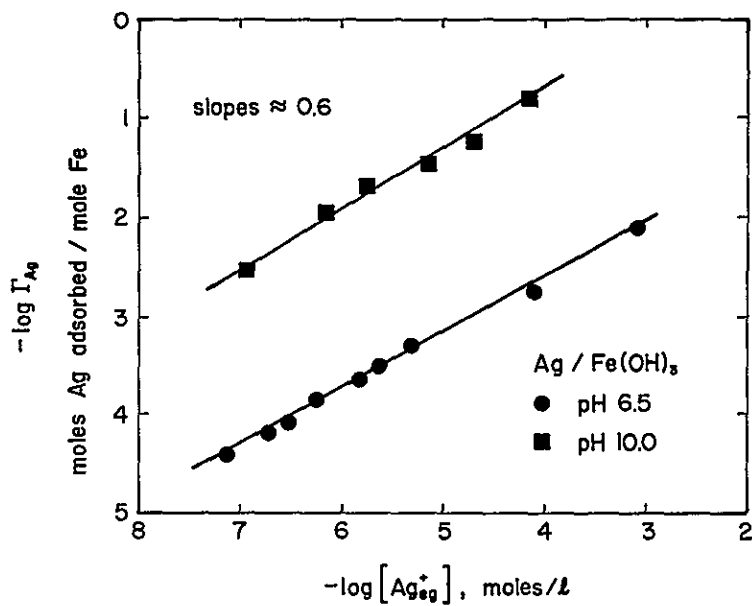


Figure 3-19.  $\text{Log } \Gamma_{\text{Ag}}$  vs.  $\text{log}[\text{Ag}_{\text{eq}}^+]$  for pH equal to 6.5 and 10.0

Zinc behaves differently from Cd, Cu, and Pb in several respects. First,  $\Gamma^*$  is approximately  $10^{-2}$  moles Zn/mole Fe, considerably greater than that for any of the other metals. Secondly, the proton release accompanying Zn adsorption is almost twice that of the other metals ( $3.2 \text{ H}^+$  per Zn). A plot of  $\log K_{e,0}$  vs.  $\log \Gamma_{\text{Zn}}$  is shown in Figure 3-20. Despite the chemical similarities between Zn and Cd or Cu, it is possible that Zn adsorbs to am-Fe(OH)<sub>3</sub> by a different mechanism than the other three metals studied.

A few studies reported in the literature are sufficiently similar to those described above to allow direct comparison. In all cases cited, the adsorbent was nearly identical to that used in these experiments.

Kurbatov et al. (12) studied coprecipitation of Co with am-Fe(OH)<sub>3</sub> and found the fraction removed from solution to be independent of  $\text{Co}_T$  for the range  $2 \times 10^{-7} < \Gamma_{\text{Co}} < 0.28$  Co/mole Fe in 0.26M NH<sub>4</sub>Cl. At " $\Gamma_{\text{Co}}^*$ "  $> 0.28$  mole Co/mole Fe, fractional coprecipitation of Co decreased with increasing  $\text{Co}_T$ . Studies by Dyck (13) show that Ag, Cd, Zn, and Cu are removed from solution equally well by coprecipitation or adsorption onto am-Fe(OH)<sub>3</sub>. Kurbatov's data suggest that, if a  $\Gamma_{\text{Co}}^*$  exists, it is even larger than that for Zn.

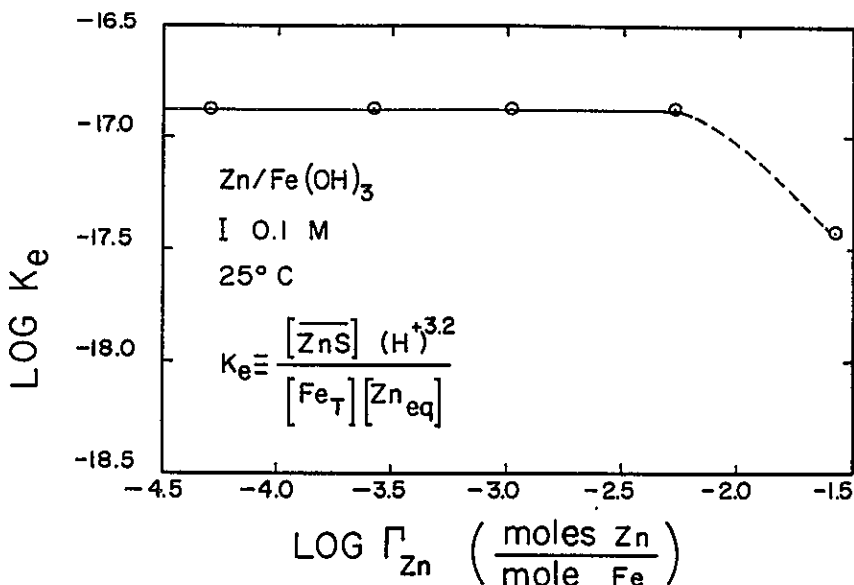


Figure 3-20.  $\log K_e$  vs.  $\log \Gamma_{\text{Zn}}$  for  $x = 3.2$

The Zn results reported here are qualitatively confirmed by Bruninx (14) who coprecipitated Zn with  $\text{Fe}(\text{OH})_3$  in mixed electrolyte ( $\text{NH}_4^+$ ,  $\text{K}^+$ ,  $\text{NO}_3^-$ ,  $\text{Cl}^-$ ) at total ionic strength of 0.05M. He found that fractional coprecipitation of Zn is identical at " $\Gamma_{\text{Zn}}^*$ " of  $2 \times 10^{-3}$  and  $2 \times 10^{-2}$  mole Zn/mole Fe, but less at " $\Gamma_{\text{Zn}}^*$ " =  $2 \times 10^{-1}$  mole Zn/mole Fe.

In the most strikingly similar study to that reported here, Avotins (15) found Hg fractional sorption onto am- $\text{Fe}(\text{OH})_3$  to be independent of  $\Gamma_{\text{Hg}}$  for  $10^{-6.2} < \Gamma_{\text{Hg}} < 10^{-2.7}$  mole Hg/mole Fe, and to decrease for  $\Gamma_{\text{Hg}} > 10^{-2.7}$  (Figure 3-21). A plot of  $\log K_{e,o}$  vs.  $\log \Gamma$  for Hg, assuming  $x = 2.0$ , is shown in Figure 3-22. Thus,  $\Gamma_{\text{Hg}}^* \approx 2 \times 10^{-3}$  mole Hg/mole Fe. For  $\Gamma_{\text{Hg}} > \Gamma_{\text{Hg}}^*$ , Avotins found  $\log \Gamma_{\text{Hg}}$  vs.  $\log C_{\text{eq}}$  plots to have slopes of 0.5 at pH 6.0 and 0.6 at pH 9.0. He gave no explanation of the results at  $\Gamma_{\text{Hg}} < \Gamma_{\text{Hg}}^*$  and did not include them in his model. Summarizing all the reported values,  $\Gamma^*$  for adsorption onto am- $\text{Fe}(\text{OH})_3$  increases in the order Pb, Ag, Cd < Cu < Hg < Zn < Co.

Systems Involving Well-Crystallized Absorbents. Since the micro-structure of amorphous hydrous iron oxide is open to speculation, it is important to determine whether high-energy surface sites can be found on other solids. In the only other system studied over a wide range of adsorption densities, Cd sorption on  $\gamma\text{-Al}_2\text{O}_3$  followed the same trend as on am- $\text{Fe}(\text{OH})_3$  (Figures 3-23 and 3-24). To determine  $K_e$ , an estimate of proton release from  $\gamma\text{-Al}_2\text{O}_3$  accompanying Cd adsorption is needed. Hohl and Stumm (9) reported that an average of 1.5 protons are released from  $\gamma\text{-Al}_2\text{O}_3$  when a  $\text{Pb}^{2+}$  ion adsorbs. This is approximately 10 percent less than the proton release accompanying adsorption of Pb onto am- $\text{Fe}(\text{OH})_3$ . As a first estimate it is assumed that the ratio of proton release accompanying Cd adsorption on the two solids is the same as that for Pb. Thus, the apparent overall equilibrium constant for Cd sorption on  $\gamma\text{-Al}_2\text{O}_3$  can be defined as

$$K_{e,o} = \Gamma_{\text{Cd}} \frac{(\text{H}^+)^{1.6}}{[\text{Cd}^{2+}]}$$

The shape of the  $\log \Gamma$  vs.  $\log K_e$  curve is the same as that for Cd sorption onto  $\text{Fe}(\text{OH})_3$ , and the value of  $\Gamma_{\text{Cd}}^*$  on  $\gamma\text{-Al}_2\text{O}_3$  is  $\sim 10^{-7}$  moles Cd/m<sup>2</sup> (Figure 3-25). Based on specific surface area of 350 m<sup>2</sup>/g for  $\text{Fe}(\text{OH})_3$ ,  $\Gamma_{\text{Cd}}^*$  on  $\text{Fe}(\text{OH})_3$  is  $1.2 \times 10^{-7}$  moles Cd/m<sup>2</sup>. Thus, the capacity for strong cadmium binding on am- $\text{Fe}(\text{OH})_3$  is somewhat less than on  $\gamma\text{-Al}_2\text{O}_3$ .

Although  $\Gamma^*$  was not determined for Cu, Pb, or Zn on  $\gamma\text{-Al}_2\text{O}_3$ , the isotherms for Cd, Cu, and Pb on this adsorbent are Freundlich type with slopes between 0.5 and

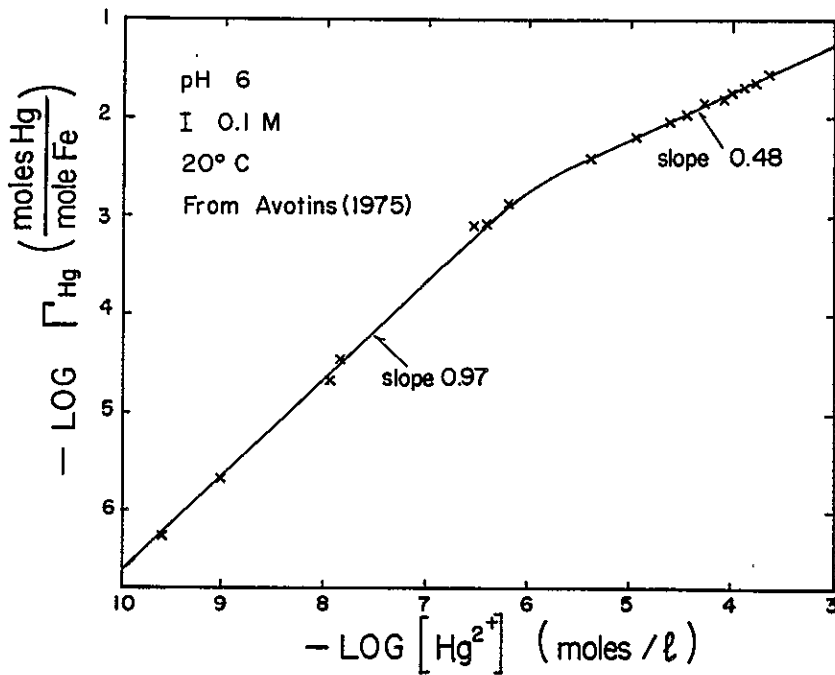


Figure 3-21. Adsorption isotherm for Hg on am-Fe(OH)<sub>3</sub>

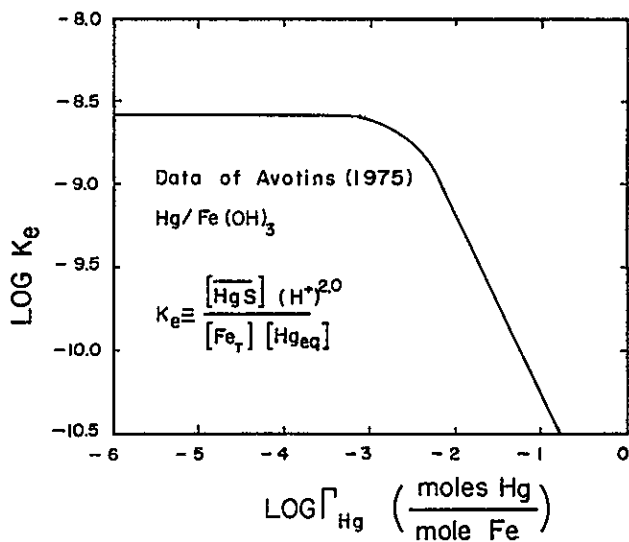


Figure 3-22. Log  $K_e$  vs. log  $\Gamma_{\text{Hg}}$  for  $x = 2.0$

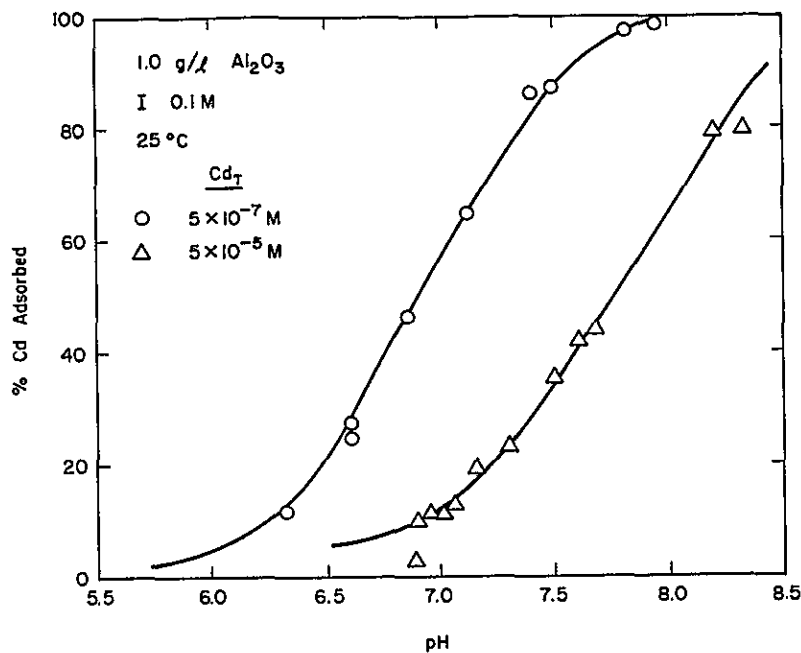


Figure 3-23. Fractional adsorption of Cd on  $\gamma\text{-Al}_2\text{O}_3$  as a function of  $\text{Cd}_T$  and pH

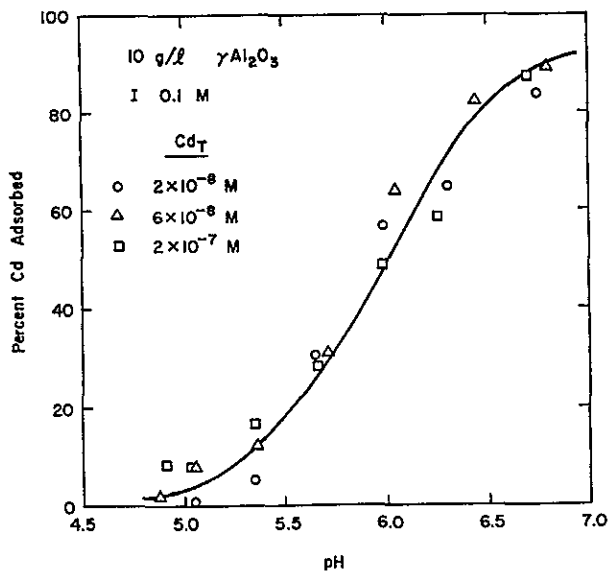


Figure 3-24. Fractional adsorption of Cd on  $\gamma\text{-Al}_2\text{O}_3$  as a function of  $\text{Cd}_T$  and pH at very low adsorption density

0.8. It is probable that at some adsorption density less than the lowest studied, high-energy sites for each metal/solid system are in excess.

Detailed studies of Cd sorption on  $\alpha$ -SiO<sub>2</sub> indicate the fractional adsorption and therefore the average adsorption energy are independent of adsorption density in the range  $1.5 \times 10^{-9}$  mole/m<sup>2</sup> <  $\Gamma_{\text{Cd}}$  <  $3 \times 10^{-6}$  mole/m<sup>2</sup>. Fractional surface coverage calculated in three different ways for this system is shown in Table 3-3. At the upper limit of adsorption densities studied surface sites should be limiting according to the Langmuir isotherm, but the expected behavior is not observed. Apparently either the fractional surface coverage has been overestimated, or a second layer of Cd can sorb on top of the first, bonding with approximately equal strength as the  $\alpha$ -SiO<sub>2</sub>-to-Cd bond. Studies of Pb sorption onto  $\alpha$ -SiO<sub>2</sub> were not as extensive, but the similarity with Cd sorption onto  $\alpha$ -SiO<sub>2</sub> and the contrast with Pb and Cd sorption onto the other solids studied is clear. On am-Fe(OH)<sub>3</sub> and  $\gamma$ -Al<sub>2</sub>O<sub>3</sub>, the shift in pH<sub>50%</sub> for Pb is approximately 1.0 pH unit for an increase in Pb<sub>T</sub> from  $5 \times 10^{-7}$ M to  $5 \times 10^{-5}$ M. On  $\alpha$ -SiO<sub>2</sub>, there is no shift at all for a similar change in Pb<sub>T</sub>. If there is a limited number of high-energy sites for Pb sorption onto  $\alpha$ -SiO<sub>2</sub>, the surface concentration of those sites is considerably greater than for any other solid studied. Based on the similarities between sorption of Cd and

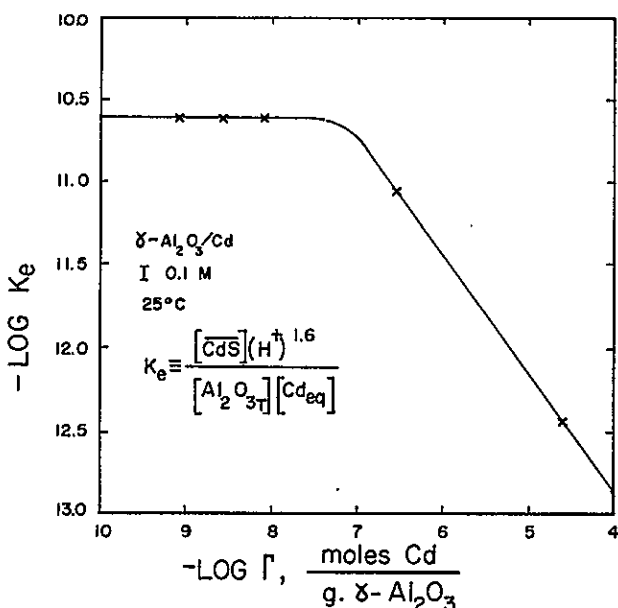


Figure 3-25. Log  $K_e$  vs. log  $\Gamma_{\text{Cd}}$  for  $x = 1.6$

that of Pb on all the adsorbents studied, it is unlikely that the limit is less than  $10^{-6}$  mole Pb/m<sup>2</sup>.

Copper sorption onto  $\alpha$ -SiO<sub>2</sub> is unique among all the systems studied in that increasing Cu<sub>T</sub> increases fractional adsorption (Figure 3-26). Such a relationship is expected if copper precipitates in bulk solution or on the  $\alpha$ -SiO<sub>2</sub> surface or if the adsorbing species are polynuclear.

In the pH range of interest, copper forms the least soluble hydroxide salt of the four metal adsorbates studied. Baes and Mesmer (16) estimate the solubility product of Cu(OH)<sub>2</sub> to be  $(\text{Cu}^{2+})(\text{OH}^-)^2 = 10^{-19.36}$ . They give the following constants for soluble hydroxo-complexes of copper

$$\log \frac{(\text{CuOH}^+)(\text{H}^+)}{(\text{Cu}^{2+})} = -8.0 \quad (\text{I} \rightarrow 0)$$

$$\log \frac{\text{Cu}_2(\text{OH})_2^{2+}(\text{H}^+)^2}{(\text{Cu}^{2+})^2} = -10.36 \quad (\text{I} \rightarrow 0)$$

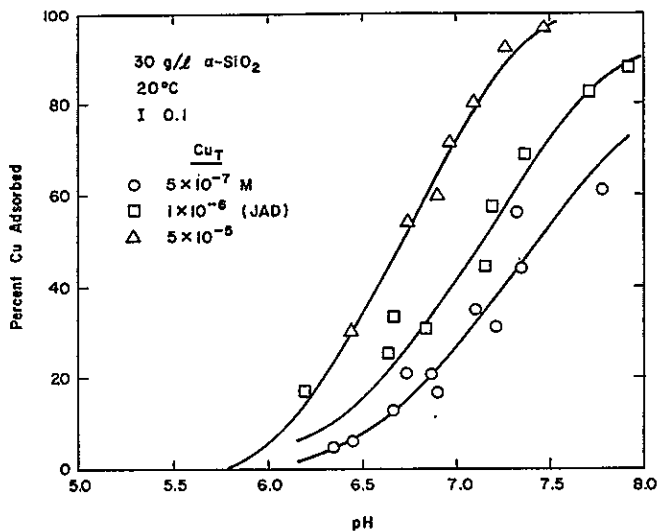


Figure 3-26. Fractional adsorption of Cu on  $\alpha$ -SiO<sub>2</sub> as a function of Cu<sub>T</sub> and pH

9 1 1 2 2 9

The data from the  $\text{Cu}/\alpha\text{-SiO}_2$  systems are consistent with the hypothesis that precipitation and not adsorption controlled copper solubility in the experiments with high  $\text{Cu}_T$ , as shown below:

Data Source	pH	$K_{SP}$	$Q_{SP} = (\text{Cu}^{2+})(\text{OH})^2$ Experimental <sup>a</sup>
"Δ", Fig. 3-26	6.72	$10^{-19.36}$	$10^{-19.6}$
"o", Fig. 3-26	7.35	$10^{-19.36}$	$10^{-20.3}$

<sup>a</sup>Activity coefficients estimated from Stumm and Morgan (11).

The empirical ion product in the system containing  $5 \times 10^{-5} \text{M Cu}_T$  is within experimental error of the solubility product. At the lower  $\text{Cu}_T$  concentration, the system is undersaturated with respect to  $\text{Cu}(\text{OH})_2$  solid, and the dissolved copper concentration is apparently controlled by adsorption. The high  $\text{Cu}_T/\alpha\text{-SiO}_2$  system is the only system studied in which experimental or theoretical evidence suggests precipitation of the metal hydroxide was occurring. It is quite likely that this is the cause for the apparent increase in adsorption with increasing metal concentration.

The evidence from zinc sorption studies on  $\alpha\text{-SiO}_2$  indicates that, as on  $\text{Fe}(\text{OH})_3$ , zinc adsorption sites may be quite different from those for the other metals. On the iron oxides the Zn adsorption edge shifts only at much greater adsorption densities than Cd, Cu, and Pb, whereas on  $\alpha\text{-SiO}_2$  the high energy zinc sites are apparently limiting at much lower surface coverage than the other metals.

It is difficult to explain why Zn adsorption behavior is so different from that of the other metals studied. Its electronic structure is analogous to Cd, and along with Pb and Cu, it is classified as a borderline acid according to Hard and Soft Acid and Base (HSAB) theory. The unhydrated radii of the metals increase in the order  $\text{Zn} \approx \text{Cu} < \text{Cd} > \text{Pb}$ . The surface density of high-energy sites on  $\text{Fe}(\text{OH})_3$  increases in the order  $\text{Pb} < \text{Cd} < \text{Cu} < \text{Zn}$ . Thus, the order may be partially explained if more sites are available to Zn simply because it can fit into smaller spaces at the surface and internally than the other three metals. This argument is particularly appealing since the other metal for which a very high  $\Gamma^*$  has been estimated from published data is Co, which has an ionic radius slightly smaller than Zn. However, it is unlikely that metal ions completely shed their waters of hydration when they sorb, so ranking adsorbate size based on unhydrated radii is probably inaccurate. In

addition, on  $\alpha\text{-SiO}_2$   $\Gamma^*$  for Zn is smallest of the four metals studied. Stereochemical factors such as preferred crystal structure and bond angles are undoubtedly involved in determining the strength and capacity of surface/metal interactions. Thus it is unlikely that any simple explanation will fully account for the relative magnitudes of  $\Gamma^*$  for several metals on all oxides.

#### Estimating the "Instantaneous" Adsorption Constant

At any  $\Gamma > \Gamma^*$ , the adsorption reactions occurring must have a lower average equilibrium constant than the overall average equilibrium constant. That is, if  $\Gamma$  is greater than  $\Gamma^*$ , the value of  $K$  for the sites being filled is less than the value of  $K_{e,o}$ . It is useful to determine these "instantaneous" average equilibrium constants  $K^{\text{inst}}$  to get a feel for the range of binding strengths among the various site types.

In the following section it is shown how instantaneous equilibrium constants can be derived from cumulative average equilibrium constants for a system where several reactions are occurring simultaneously. The derivation is based on thermodynamic relationships and is only valid if true thermodynamic equilibrium constants are used (i.e.,  $K'_{e,o}$ , not  $K_{e,o}$ ). Therefore, instantaneous constants are derived as a function of the thermodynamic constants,  $K'_{e,o}$ . Analysis of this relationship then allows one to speculate about the relationship between the instantaneous constants and the measured, apparent constants,  $K_{e,o}$ .

The free energy change accompanying adsorption of  $\Gamma$  moles of cadmium per mole of iron, onto sites of type  $i$ , is  $\Gamma_i \Delta G_i$ , where  $\Delta G_i$  is the molar free energy of adsorption onto sites  $i$ . For simultaneous adsorption onto several types of sites the overall free energy change is  $\Delta G_{\text{tot}} = \sum_i (\Gamma_i \Delta G_i)$  and the average free energy change is  $\Delta G_{\text{avg}} = \Delta G_{\text{tot}} / \Gamma_{\text{tot}} = [\sum_i (\Gamma_i \Delta G_i)] / \sum_i \Gamma_i$ . Now consider the case where equilibrium is perturbed slightly so a small number of Cd ions moves from solution to the surface (the group of sites may include more than one "site type"). The molar free energy change for this reaction,  $\Delta G_j$ , is

$$\Delta G_j = \frac{\left[ \sum_i \Gamma_i \Delta G_i \right]_2 - \left[ \sum_i \Gamma_i \Delta G_i \right]_1}{\left[ \sum_i \Gamma_i \right]_2 - \left[ \sum_i \Gamma_i \right]_1} = \frac{\left[ \Gamma_{\text{tot}} \Delta G_{\text{avg}} \right]_2 - \left[ \Gamma_{\text{tot}} \Delta G_{\text{avg}} \right]_1}{\left[ \sum_i \Gamma_i \right]_2 - \left[ \sum_i \Gamma_i \right]_1} \quad (3-16)$$

where the subscripts 1 and 2 indicate before and after the perturbation, respectively. If the perturbation is differentially small:

$$\Delta G_j = \frac{d(\Gamma_{\text{tot}} \Delta G_{\text{avg}})}{d \Gamma_{\text{tot}}} \quad (3-17)$$

For any chemical reaction,  $\Delta G = -RT \ln K$ , so (dropping the subscript "tot"):

$$-RT \ln K'_{e,j} = -RT \frac{d(\Gamma \ln K'_{e,o})}{d\Gamma} \quad (3-18)$$

Cancelling the  $RT$  term and expanding,

$$\begin{aligned} \ln K'_{e,j} &= \ln K'_{e,o} + \frac{\Gamma}{d\Gamma} d \ln K'_{e,o} \\ &= \ln K'_{e,o} + \frac{d \ln K'_{e,o}}{d \log \Gamma} \end{aligned}$$

$$\log K'_{e,j} = \log K'_{e,o} + \frac{1}{2.3} \frac{d \log K'_{e,o}}{d \log \Gamma} \quad (3-19)$$

Substituting  $K'_{e,o} = \alpha K_{e,o}$ ,  $K'_{e,j}$  is the average adsorptive equilibrium constant of sites being filled at a given adsorption density, i.e.,  $K'_{e,j} = K^{\text{inst}}$ ,

$$\log K'_{e,j} = \log \alpha K_{e,o} + \frac{1}{2.3} \frac{d \log \alpha K_{e,o}}{d \log \Gamma}$$

$$\log K'_{e,j} = \log \alpha + \log K_{e,o} + \frac{1}{2.3} \frac{d \log K_{e,o}}{d \log \Gamma} + \frac{1}{2.3} \frac{d \log \alpha}{d \log \Gamma}$$

$$\log K'_{e,j} = \log K_{e,o} + \frac{1}{2.3} \frac{d \log K_{e,o}}{d \log \Gamma} + \log \alpha + \frac{1}{2.3} \frac{d \log \alpha}{d \log \Gamma} \quad (3-20)$$

Thus, if overall thermodynamic equilibrium constants can be measured in an adsorption system, instantaneous constants can be calculated from a log-log plot of the overall constant versus adsorption density and Eq. 3-19. If the system involves metal complexation, instead of adsorption, the analysis is identical with adsorption density being replaced by the concentration of complexed species.

Unfortunately, in the systems under study, only an apparent constant  $K_{e,o}$  can be calculated and the value of the thermodynamic constant  $K'_{e,o}$  is unknown. It is important to know how much error results from using values of  $K_{e,o}$  instead of  $K'_{e,o}$  in Eq. 3-19.

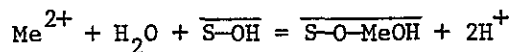
Equation 3-20 indicates that this error is equal to  $(\log \alpha + 1/2.3[(d \log \alpha)/(d \log \Gamma)])$ . If  $\alpha$  is constant,  $\log \alpha$  is constant and  $(d \log \alpha)/(d \log \Gamma)$  equals 0. Then, all the calculated values of  $K^{\text{inst}}$  are shifted by an amount  $\log \alpha$  relative to the true values, but the range of the calculated values is exactly as great as the range of the true values. In other words, if we are just interested

in learning how widely overall, average binding constants vary, using  $K_{e,o}$  instead of  $K'_{e,o}$  in Eq. 3-19 causes no error as long as  $\alpha$  is constant. It has been argued that most terms included in " $\alpha$ " are approximately constant for the experimental conditions. The only factor expected to vary is the ratio  $(A_1/F_1)$ , which is not constant under conditions of site limitation. It is not clear how much or even in which direction this ratio varies. However, because it is felt that  $K_{e,o}$  bears a strong relationship to  $K'_{e,o}$ , it is proposed that the terms in Eq. 3-20 involving  $\alpha$  are much less variable over the range of experimental conditions than the terms involving  $K_{e,o}$ .

The term  $(d \log K_{e,o}) / (d \log \Gamma)$  is the slope of a plot of  $\log K_{e,o}$  vs.  $\log \Gamma$ . Estimating the slope of Figure 3-14 to be 0 at  $\log K_{e,o} = -8.5$  and  $-1.5$  at  $\log K_{e,o} = -10.2$ , the range of apparent instantaneous equilibrium constants found for adsorption of cadmium onto amorphous  $\text{Fe}(\text{OH})_3$  is  $-10.9 \leq \log K'_e \leq -8.5$ , or about 2-1/2 orders of magnitude, for  $10^{-6.3} \leq \Gamma \leq 10^{-10.5}$  moles Cd/mole Fe. It is recognized that this conclusion is rigorous only to the extent that the assumptions of the derivation are correct, but also that some of the assumptions are open to question. Nevertheless, it does give a reasonable estimate of the range of overall surface-binding constants required to model the data.

#### Comparison of $K_{e,o}$ with $K_1$ Values from the SGMA Model

The SGMA model can model adsorption behavior of several metals on oxide surfaces. Generally, experimental data are modeled most accurately if one assumes that hydrolyzed metal ions sorb as a monodentate species (17). If unhydrolyzed metal is assumed to be the sorbing species or if the surface complex is bidentate, the adsorption edge predicted by the model is much less steep than that observed. Modeling the adsorption reaction by the equation:



the SGMA model can reproduce the observed adsorption edge for any single experiment from this study. However, the model does not predict the observed decrease in fractional adsorption with increasing  $\text{Me}_T$ . To model this trend one must assume the average surface complex formation constant decreases with increasing adsorption density. Table 3-4 shows the surface complexation equilibrium constants required to fit the cadmium data for an adsorption density range from  $10^{-6.0}$  mole Cd/mole Fe to  $10^{-1.6}$  mole Cd/mole Fe. The stability constants for Zn, Cu, and Pb sorption onto  $\text{Fe}(\text{OH})_3$  for one set of experimental conditions are also shown. The adsorption stability "constant,"  $K_1$ , increases with decreasing  $\text{Cd}_T$ , and attains a

Table 3-4

Apparent Equilibrium Constants for Various Metals on am-Fe(OH)<sub>3</sub>

$\text{Cd}^{2+} + \overline{\text{SOH}} + \text{H}_2\text{O} \stackrel{K_1}{=} \overline{\text{SO-CdOH}} + 2\text{H}^+$					
$\text{Fe}_T$	Metal	Concentration (moles/l)	$\log K_1^a$	$\log K_{e,o}^b$	$\log \Gamma$ at 50% Adsorbed (moles Cd/mole Fe)
$10^{-2}$	Cd	$2 \times 10^{-8}$	-10.4	-8.5	-6.0
$10^{-3}$		$5 \times 10^{-7}$	-10.6	-9.1	-3.6
$10^{-3}$		$2 \times 10^{-6}$	-10.9	-9.3	-3.0
$10^{-3}$		$5 \times 10^{-5}$	-11.2	-10.0	-1.6
$10^{-3}$	Zn	$5 \times 10^{-7}$	-10.3	-16.8	-3.6
$10^{-3}$	Cu	$5 \times 10^{-7}$	-8.7	-6.75	-3.6
$10^{-3}$	Pb	$5 \times 10^{-7}$	-7.3	$\geq -3.7$	-3.6
$10^{-3}$	Ag	$5 \times 10^{-7}$	-12.1	-10.2	-3.6

<sup>a</sup> $\log K_1$  estimated using the SGMA model for the reaction

$$\text{Cd}^{2+} + \overline{\text{SOH}} + \text{H}_2\text{O} \stackrel{K_1}{=} \overline{\text{SOCdOH}} + 2\text{H}^+$$

<sup>b</sup>Using the following experimentally determined values for the proton release parameter  $x$ :  $x_{\text{Cd}} = 1.80$ ,  $x_{\text{Zn}} = 3.20$ ,  $x_{\text{Cu}} = 1.88$ ,  $x_{\text{Pb}} = 1.65$ ,  $x_{\text{Ag}} = 1.9$ .

maximum value at very low  $\text{Cd}_T$ . This constant differs in two ways from the overall apparent stability constant  $K_{e,o}$  defined earlier. First, terms accounting for the effects of the gradient in electrical potential near the surface and for sorption of bulk electrolyte are explicitly included in the equilibrium expression and are not included in the intrinsic constants.

Secondly, the model assumes that all surface sites are equivalent and therefore adsorption of a metal ion to  $n$  sites releases  $nI_1$  protons from the surface, where  $I_1$  is the average number of protons per surface site. In addition, protons may be released by hydrolysis reactions. For most systems, Davis (18) finds the data are modeled best by setting  $n = 1$  and assuming 1 proton is released by hydrolysis of the adsorbing metal ion. In the pH range of interest, Yates (10)

and Davis (18) report that for  $\text{Fe}(\text{OH})_3$  and most other oxides  $I_1 = 1.0 \pm 0.1$ . Thus, the model almost always predicts that  $2.0 \pm 0.1$  protons are released per metal ion sorbed. Empirically, proton release is generally less than this. Possible causes for the discrepancy will be suggested later. When comparing  $K_{e,o}$  with  $K_1$ , the difference in the parameter characterizing proton release and the quantification of the EDL term may account for the fact that  $\log K_1$  decreases somewhat less than  $\log K_{e,o}$  as  $\Gamma_{\text{Cd}}$  increases.

The expression relating the instantaneous equilibrium constant to the average equilibrium constant holds regardless of whether the constant is defined as  $K_{e,o}$  or  $K_1$ . That is,

$$\log K_1^{\text{inst}} = \log K_1 + \frac{1}{2.3} \frac{d \log K_1}{d \log \Gamma}$$

where  $K_1^{\text{inst}}$  is the site-binding equilibrium constant for sites being filled when the adsorption density is  $\Gamma$  and the average SCMA equilibrium constant is  $K_1$ . The range of instantaneous average equilibrium constants based on the SCMA model is a little greater than one order of magnitude for the range of variables studied. This range is considerably smaller than that based on the model proposed earlier because, according to the site-binding model, much of the variation in the apparent binding constant can be attributed to electrostatic effect. However, it should be noted that at constant ionic strength and pH, the electrostatic correction is approximately independent of the concentration of an adsorbate present at trace levels. Therefore electrostatics cannot possibly account for decreased metal sorption with increasing total metal concentration under these conditions. From all indications, equilibrium constants continue to decrease at greater adsorption densities.

#### Continuous vs. Discrete Distribution of Surface Sites

The distribution of surface-site energies on  $\text{Fe}(\text{OH})_3$  and  $\gamma\text{-Al}_2\text{O}_3$  may be either discrete or continuous. As used here, a discrete distribution means that there is a relatively small number ( $< 5$ ) of distinct site types. The data presented cannot distinguish the two possibilities unambiguously. In the limit, of course, there is no such thing as a continuous distribution of surface site energies but only a large number of discrete values. Thus a Freundlich isotherm is equivalent to a linear combination of an infinite number of Langmuir isotherms.

One can always get good fit of adsorption data by modeling it as a series of Langmuir isotherms. The larger the range of  $C_{\text{eq}}$  and the greater the deviation of the

isotherm slope from unity, the greater will be the number of Langmuir-type equations required to get good fit. For a given set of data, the goodness-of-fit will improve with each additional site type proposed, but so will the complexity of the model. Each site type requires two empirical constants, one for the binding energy and another for the site density. From a practical viewpoint, it can be shown that a Freundlich isotherm of slope 0.7 over a range of one order of magnitude in  $C_{eq}$ , can be fit poorly by a one-site model, moderately well by a two-site model, and extremely well by a three-site model. Therefore, for data which fit a Freundlich-type isotherm, unless specific sites can be demonstrated to exist and identified by independent means, there is little point in trying to establish the surface concentration and energy of site types by fitting empirical data with multiple-site Langmuir isotherms. This is not to say that discrete groups of surface sites do not exist. Rather, the problem is that with four or more independent fitting parameters available, almost any data set can be modeled. It is difficult to justify attaching much significance to this many parameters, given the rather small data set available.

#### Summary

Adsorption data for single-metal/single-solid systems have been explained in terms of a distribution of surface sites. Data for four different metals and four solid surfaces have been compared. Amorphous  $Fe(OH)_3$  and  $\gamma-Al_2O_3$  surfaces are composed of sites which vary widely in their ability to bond metal ions. For Cd, Cu, Hg, and presumably Pb, there is a finite number of sites capable for forming high-energy adsorptive bonds. When fractional occupancy of these sites is small ( $\ll 100\%$ ), the overall equilibrium constant,  $K_{e,o}$  is maximum. The capacity to bind metal with maximum  $K_{e,o}$  differs by at least two orders of magnitude from one metal to another on the same solid. Orders of magnitude more metal can sorb with lower average equilibrium constant. An apparent equilibrium constant for adsorption has been defined, and shown to decrease significantly as adsorption density increases.

Despite its chemical similarity to the other metals studied, zinc may adsorb by a different mechanism or to different groups of sites than cadmium, copper, and lead.

The results can be modeled using a multi-site Langmuir model if at least 4 site types are postulated. Independent tests are required to determine the exact number of distinct, identifiable site types actually present.

## COMPETITIVE ADSORPTION STUDIES

A great deal of information about surface-site distribution can be obtained by studying the extent to which adsorption of one metal is affected by the presence of a second metal adsorbate. If two metals compete for the same sites, adsorption of the more strongly binding metal should force the less strongly bound metal to attach to lower-energy sites, shifting the adsorption edge to higher pH. On the other hand, if the metals bind to distinct different groups of sites, adsorption of one metal should have only a small, predominantly electrostatic effect on adsorption of another.

The results for adsorption of Cd on  $\text{Fe}(\text{OH})_3$  in the presence of much greater concentrations of Zn, Cu, or Pb indicate that competition for surface sites is very limited. If, for example, the order of increasing affinity of different sites for Cu is the same as for Cd (i.e.  $K^{(1)} > K^{(2)} > \dots > K^{(n)}$  for both Cu and Cd), Cu would preferentially fill the high-energy sites because copper adsorptive bonds are stronger than those of cadmium. This assumes that  $K_{\text{Cu}} > K_{\text{Cd}}$  for the individual site types. This is reasonable based on analogies to complexation in solution and the fact that for the overall average constants,  $K_{e,\text{Cu}} > K_{e,\text{Cd}}$ . If these conditions are set, the adsorption edge for  $5 \times 10^{-7} \text{ M Cd}$  is expected to shift to higher pH when Cu is added to the system. The magnitude of the effect can be predicted as follows. From the single metal adsorption experiments fractional copper adsorption is greater than 85 percent at  $\text{pH} \geq 6.2$  in systems containing  $10^{-3} \text{ M Fe}(\text{OH})_3$  and  $5 \times 10^{-5} \text{ M Cu}_T$ . The Cd adsorption edge in the competitive system ( $5 \times 10^{-7} \text{ M Cd}_T + 5 \times 10^{-5} \text{ M Cu}_T$ ) is in the range  $6.2 \leq \text{pH} \leq 7.3$ . Since the cadmium is expected to have a negligible effect on Cu sorption under these conditions (viz. Figure 3-27) the total adsorption density is  $\sim (4.5 \times 10^{-5} / 10^{-3}) \pm 10\% = 4.5 \times 10^{-2} \pm 0.5 \times 10^{-2}$  moles metal/mole Fe in the entire pH range of the cadmium sorption edge. The instantaneous average equilibrium constant for adsorption of cadmium onto am- $\text{Fe}(\text{OH})_3$  for  $\Gamma = 4.5 \times 10^{-2}$  mole/mole Fe is  $\log K^{\text{inst}} \approx -11.0$ . This is the expected value of  $K^{\text{inst}}$  for cadmium in the two-metal system if Cd and Cu compete for the same sites. Since adsorption density is approximately constant throughout the pH range where cadmium adsorbs,  $K^{\text{inst}}$  is also constant. From this value, the predicted adsorption edge for  $5 \times 10^{-7} \text{ M Cd}$  in the presence of  $5 \times 10^{-5} \text{ M Cu}$  can be derived. It is compared with the experimental curve in Figure 3-28.

The same general approach can be used if pH ranges of the individual adsorption edges overlap significantly. The calculations are slightly more complicated in this case because  $K^{\text{inst}}$  varies significantly as the low-concentration metal sorbs.

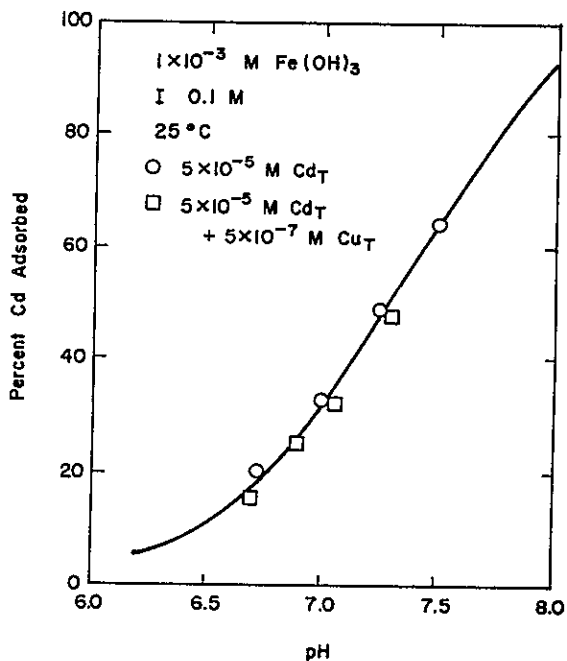


Figure 3-27. Effect of  $5 \times 10^{-7} \text{ M Cu}$  on the adsorption edge for  $5 \times 10^{-5} \text{ M Cd}$  on  $\text{am-Fe(OH)}_3$

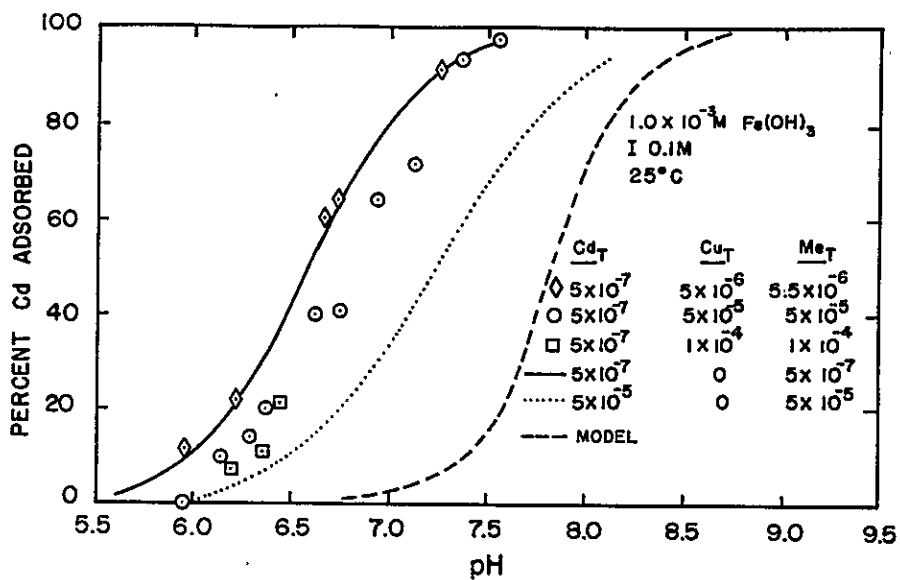


Figure 3-28. Effect of Cu on the adsorption edge for Cd on  $\text{am-Fe(OH)}_3$  when  $\text{Cu}_T > \text{Cd}_T$

There are two points to note about Figure 3-28. First, the presence of Cu has a much smaller effect than expected on Cd sorption. Secondly, the predicted adsorption edge is at a pH even higher than that for  $5 \times 10^{-5}$  M Cd in the absence of competition. A measure of the amount of copper bound to preferred cadmium-binding sites can be estimated from the instantaneous average equilibrium constant for cadmium in the two-metal system. Using these data at 25 percent and 75 percent Cd adsorbed (Figure 3-28) to estimate  $d \log K_{e,o} / d \log \Gamma_{Cd}$ ,  $K^{inst}$  for Cd in the bimetal system at 50 percent adsorbed ( $\log \Gamma_{Cd} = -3.6$ ) is  $\log K^{inst} = -9.36$ . From Figure 3-14, this corresponds to  $\log \Gamma \approx -3.0$  in a system containing only cadmium. Therefore, as a first estimate only  $\sim (10^{-3.0} - 10^{-3.6}) = 7.5 \times 10^{-4}$  moles Cu/mole Fe, or about 1.7 percent of the total adsorbed copper, "interferes" with cadmium sorption. Apparently, the combination of site densities and binding constants are such that most of the preferred Cu-binding sites are distinct from the high-energy Cd-binding sites. Results of other competitive experiments in which am-Fe(OH)<sub>3</sub> was the adsorbent are presented in Appendix A.

Competition between Pb and Cd is nearly identical, qualitatively and quantitatively, to that between Cu and Cd. Zinc appears to adsorb in a qualitatively different manner from Cd, so excess Zn is expected to have little or no effect on Cd sorption. Even when the  $(Zn)_T:(Cd)_T$  ratio is 100, no competitive effects are observed. Since Cu and Pb have equivalent effects on Cd sorption, one could conclude that they may tend to adsorb to the same sites. However, this is not the case, since  $5 \times 10^{-5}$  M Pb does not affect sorption of  $5 \times 10^{-7}$  M Cu at all.

These are extremely important results for modeling and predicting behavior in complex systems. It means that adsorption of metals on am-Fe(OH)<sub>3</sub> from a solution containing several different metal ions at widely different concentrations can, to a first approximation, be treated as though each metal were in solution by itself. Effects of Cu or Pb competing with Cd for sorption sites on  $\gamma$ -Al<sub>2</sub>O<sub>3</sub> are equivalent, and are similar to those on am-Fe(OH)<sub>3</sub> (Figure 3-29). Large excesses of either Cu or Pb have a small effect on sorption of  $5 \times 10^{-7}$  M Cd.

In contrast to the results with am-Fe(OH)<sub>3</sub>, Zn competes strongly with Cd for sites on  $\gamma$ -Al<sub>2</sub>O<sub>3</sub>. The shift in the adsorption edge of  $5 \times 10^{-7}$  M Cd is as great, or perhaps slightly greater, in the presence of  $5 \times 10^{-5}$  M Zn as when  $Cd_T$  concentration is changed from  $5 \times 10^{-7}$  M to  $5 \times 10^{-5}$  M in the absence of Zn. The difference between the competitive effects of zinc in Fe(OH)<sub>3</sub> and  $\gamma$ -Al<sub>2</sub>O<sub>3</sub> systems is not entirely surprising. Individual adsorption isotherms suggest that sorption of Zn onto am-Fe(OH)<sub>3</sub>

occurs by a different mechanism than sorption of Cd, Cu, or Pb. There is no such evidence when the adsorbent is  $\gamma\text{-Al}_2\text{O}_3$ .

In summary, the competitive adsorption studies support the hypothesis that oxide surfaces consist of discrete groups of sites and site energies. The preferred adsorption sites for Cd, Zn, Cu, and Pb are apparently distinct from one another on  $\text{Fe}(\text{OH})_3$ . On  $\gamma\text{-Al}_2\text{O}_3$ , Cu and Pb do not bind to the same high-energy sites as Cd, but Zn does.

#### ADSORPTION STOICHIOMETRY

The number of protons released when adsorbate ions bind to am- $\text{Fe}(\text{OH})_3$  was measured for each metal ion, and the results are summarized in Table 3-5. The most striking result is that while between 1.5 and 2.0 protons are released, on the average, per Cd, Cu, or Pb ion sorbed on  $\text{Fe}(\text{OH})_3$ , 3.2 protons are released for each Zn ion bonding to the surface. Mechanisms involving multiple hydrolysis and multi-dentate bonding can be invoked to explain the Zn data, e.g.  $(\text{SOH})_2 + \text{Zn}^{2+} + \text{H}_2\text{O} = (\text{SO})_2\text{-ZnOH} + 3\text{H}^+$ ; however, theoretical and empirical studies almost always predict a maximum release of 2 protons per metal ion sorbed. Considering that the Zn adsorption isotherms on am- $\text{Fe}(\text{OH})_3$  and  $\alpha\text{-SiO}_2$  are unusual in other respects, this supports the

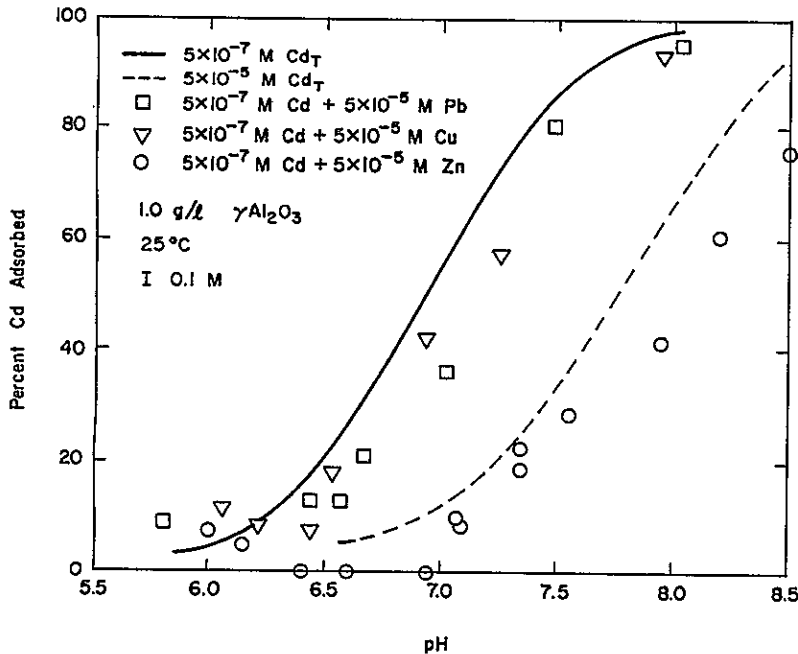


Figure 3-29. Effect of  $5 \times 10^{-7} \text{M}$  Pb, Cu, or Zn on the adsorption edge for  $5 \times 10^{-7} \text{M}$  Cd on  $\gamma\text{-Al}_2\text{O}_3$

Table 3-5

Proton Release Accompanying Adsorption of Metal Ions on am-Fe(OH)<sub>3</sub>

Adsorbate <sup>a</sup>	pH	Me <sub>T</sub>	Percent Me <sub>T</sub> Adsorbed	H <sup>+</sup> Ions Released per Me Sorbed
Cd	7.00	8.1 x 10 <sup>-5</sup>	78	1.80
Zn	6.75	7.7 x 10 <sup>-5</sup>	56	3.20
Cu	5.47	7.7 x 10 <sup>-5</sup>	88	1.88
Pb	5.35	8.8 x 10 <sup>-5</sup>	100	1.65

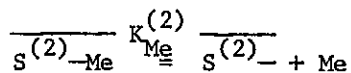
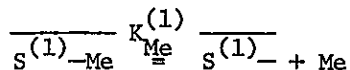
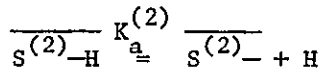
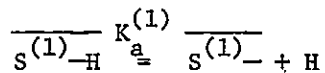
<sup>a</sup>All experiments except Zn run in duplicate. Zinc experiment run in quadruplicate. Variation between runs was < 5% in all cases.

hypothesis that the sorption mechanism operative for Zn is different from that for the other metals.

Mechanisms proposed for releasing two protons when one metal ion sorbs include bi-dentate bonding of the unhydrolyzed metal (9) and mono-dentate bonding accompanied by hydrolysis (18). Hohl and Stumm (9) measured proton release accompanying adsorption and calculated the fractions of lead bound in mono-dentate and bi-dentate complexes on  $\gamma$ -Al<sub>2</sub>O<sub>3</sub>. On the average 1.5 protons were released per Pb ion sorbed. However, as shown previously their formulation of the stability constant for the bi-dentate surface complex is questionable.

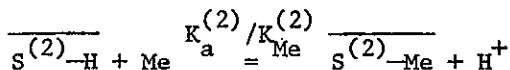
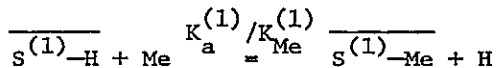
As noted earlier, use of the SGMA model leads to the conclusion that release of 2.0 protons generally accompanies sorption of a metal ion. One proton originates at the surface and the second is released by a hydrolysis reaction between the metal and a water molecule. Empirical evidence indicates that in most cases less than two protons are released per metal ion sorbed. Therefore, contrary to the SGMA model, either 1) much of the adsorbing metal does not hydrolyze; or 2) the average number of protons released per metal ion adsorbed is less than 1.0. The first possibility is self-explanatory. The second possibility does not necessarily imply that the average number of protons per surface site is less than 1.0. For instance, there may be a wide range of surface sites with varying acidities. Even if there is 1.0 surface proton per site on the average, Cd, Pb, and Cu ions may compete with H<sup>+</sup> more successfully on the more acid sites. On these sites the

average proton concentration is less than 1.0. For instance, consider two groups of sites,  $S^{(1)}$  and  $S^{(2)}$ , to which metal ions or protons can bind:



(For the purpose of this illustration, the question of metal ion hydrolysis is unimportant.)

The equilibrium constants for the proton-metal exchange reactions are



If  $\frac{K_a^{(1)}}{K_{Me}^{(1)}} > \frac{K_a^{(2)}}{K_{Me}^{(2)}}$  and  $K_a^{(1)} > K_a^{(2)}$ , then metal ions will preferentially bind to site (1), the more acid site. Note that this does not necessarily imply that  $K_{Me}^{(1)} > K_{Me}^{(2)}$ , but only that Me competes better with protons at site (1) than at site (2). Similarly, Zn, which releases more than the predicted number of protons, may hydrolyze and sorb to sites that are less acidic than the average. In view of evidence presented previously, it is quite likely that surface sites do have a range of acidities. Thus, even if the tritium exchange experiments of Yates (10) accurately measure proton exchange on all available sites, the results of his experiments may be inappropriate for modeling stoichiometry of metal adsorption.

At this time, no definite choice can be made among the various explanations for release of other than 2.0 protons when a metal ion sorbs. Quite possibly, all the mechanisms are operative under certain conditions.

#### PROSPECTS FOR IMPROVING ADSORPTION MODELS

It is reasonable to ask to what extent the SGMA and other adsorption models can be improved based on these studies. With respect to the variability of surface-site energies and effects of competing adsorbates, several alterations are required. At present the models are applicable only in situations where the ratio of total adsorbate to total adsorbent is approximately constant. This was apparently recognized by Hohl and Stumm. They studied adsorption of lead onto  $\gamma\text{-Al}_2\text{O}_3$  under conditions where the ratio  $(\text{Pb})_T:(\gamma\text{-Al}_2\text{O}_3)$  varied by a factor of ten, from  $8.3 \times 10^{-6}$  to  $8.3 \times 10^{-5}$  moles Pb/g  $\gamma\text{-Al}_2\text{O}_3$  (unpublished data). However, when developing the surface complexation model they presented only two sets of adsorption data, for which the adsorbate ratios were  $2.5 \times 10^{-5}$  and  $3.1 \times 10^{-5}$  moles Pb/g  $\gamma\text{-Al}_2\text{O}_3$  (9).

In summary, evidence has been presented for the existence of surface sites of wide-ranging adsorptive bonding strength on am- $\text{Fe}(\text{OH})_3$  and other solids. The distribution of site energies varies a great deal among adsorbents and adsorbates. A unifying theory explaining these variations is yet to be proposed. Such a theory would also be required to explain why some metals compete only slightly on am- $\text{Fe}(\text{OH})_3$ , but compete very strongly on other adsorbents. Considerably more laboratory investigation is required before such a theory is likely to emerge.

Adsorption and coprecipitation have engineering applications for collection of trace metals, and are important in natural systems which are perturbed by human activity, e.g. dredging. In systems which are near steady-state, or for which adsorbate and adsorbent concentrations usually vary by considerably less than a factor of 10, conditional adsorption equilibrium constants can be determined. When these are applied in conjunction with the SGMA or surface complexation model, changes in adsorption density as a function of  $\text{Me}_T$ , pH, and adsorbent concentration can be predicted fairly well. In systems where concentrations of the reactants can vary widely, a complete curve of average equilibrium constant ( $K'_e$ ) vs. adsorption density is required to model removal efficiency. In addition, since many engineering applications and all natural systems involve solutions containing several metals, additional competitive adsorption studies would be of value. Clearly, further experimental work in this area is in order. It is likely such work will help explain the difference between predicted and observed adsorption stoichiometry.



REFERENCES

1. A. W. Adamson. Physical Chemistry of Surfaces. 3d ed. New York: John Wiley and Sons, 1976.
2. A. G. Walton. The Formation and Properties of Precipitates. New York: Wiley Interscience, 1967.
3. P. Schindler, E. Wälti and B. Fürst. "The Role of Surface Hydroxyl Groups in the Surface Chemistry of Metal Oxides." Chimia, 30(2), (1976).
4. R. L. Parfitt and J. D. Russell. "Adsorption on Hydrous Oxides. IV. Mechanisms of Adsorption of Various Ions on Goethite." J. Soil Sci., 28, 297-305 (1977).
5. P. Loganathan and R. Burau. "Sorption of Heavy Metal Ions by a Hydrous Manganese Oxide." Geochim. Cosmochim. Acta, 37, 1277-1293 (1973).
6. R. J. Zasoski. "Sorption and Sorptive Interactions of Cadmium and Zinc on Hydrous Manganese Oxide." Ph.D. Thesis, University of California at Davis, 1974.
7. R. D. Guy, C. L. Chakrabarti and L. L. Schramm. "The Application of a Simple Chemical Model of Natural Waters to Metal Fixation in Particulate Matter." Can. J. Chem., 53, 661-669 (1975).
8. R. R. Gadde and H. A. Laitinen. "Studies of Heavy Metal Adsorption by Hydrous Iron and Manganese Oxides." Anal. Chem., 46, 2022 (1974).
9. H. Hohl and W. Stumm. "Interaction of  $Pb^{2+}$  with Hydrous  $\gamma-Al_2O_3$ ." J. Coll. Interface Sci., 55, 281-288 (1976).
10. D. E. Yates. "The Structure of the Oxide/Aqueous Electrolyte Interface." Ph.D. Thesis, University of Melbourne, Australia, 1975.
11. W. Stumm and J. J. Morgan. Aquatic Chemistry. New York: John Wiley and Sons, 1970.
12. M. H. Kurbatov, G. Wood and K. Kurbatov. "Isothermal Adsorption of Cobalt from Dilute Solutions." J. Phys. Chem., 55, 1170-1182 (1951).
13. W. Dyck. "Adsorption and Coprecipitation of Silver on Hydrous Ferric Oxide." Can. J. Chem., 46, 1441- (1968).
14. E. Bruninx. "The Coprecipitation of Zn, Cd and Hg with Ferric Hydroxide." Phillips Research Reports, 30, 177-191 (1975).
15. P. V. Avotins. "Adsorption and Coprecipitation Studies of Mercury on Hydrous Iron Oxides." Ph.D. Thesis, Stanford University, Stanford, Calif., 1975.
16. C. F. Baes, Jr. and R. E. Mesmer. The Hydrolysis of Cations. New York: Wiley-Interscience Publication, 1976.
17. J. A. Davis, R. O. James and J. O. Leckie. "Surface Ionization and Complexation at the Oxide/Water Interface: 1. Computation of Electrical Double Layer Properties in Simple Electrolytes." J. Coll. Interface Sci., 63(3), 480-499 (March 1978).
18. J. A. Davis. "Adsorption of Trace Metals and Complexing Ligands at the Oxide/Water Interface." Ph.D. Thesis, Stanford University, Stanford, Calif., 1977.

## Section 4

### EQUILIBRIUM ANION ADSORPTION AND COPRECIPITATION

15  
2  
3  
4  
5  
6  
7  
8  
9

In Section 3 it was shown that adsorption of metals on oxide surfaces can be modeled by a mass-law expression in which metal sorption is accompanied by release of protons to solution. The fractional metal adsorption decreases rapidly from near 100 percent to nil within approximately 2 pH units. In this section, corresponding results for adsorption of anions are presented and discussed. The conceptual model of the surface and surface reactions developed previously is consistent with the anion adsorption results. In Section 5 cation and anion results are combined in a generalized model which helps explain adsorption in complex systems containing metals, ligands, and metal-ligand complexes. Anion adsorption has not been studied nearly as extensively as that of cations. Nevertheless, some trends for the sorption behavior of anions are fairly well established. In general, anion adsorption patterns can be represented as a "mirror image" of those for cations. That is, anion adsorption often decreases from near 100 percent to near nil in a pH range about 2 units wide. Hingston et al. (1) found sorption of  $F^-$ ,  $Cl^-$ ,  $SO_4^{2-}$ , and  $MoO_4^{2-}$  was weak at  $pH > IEP$  and increased rapidly with decreasing pH below the IEP on gibbsite and goethite. Orthophosphate ( $o-PO_4^{3-}$ ) and silicate were more strongly specifically adsorbed, and significant quantities of these ions were removed from solution at  $pH > IEP$ . The authors claimed that the tendency for an anion to sorb is related to the strength of its conjugate acid. Only those anion acids with a  $pK_a > PZC$  adsorbed at  $pH > PZC$ . Anderson et al. (2) concluded that arsenate strongly specifically sorbs on amorphous aluminum hydroxide, since the pH of the iso-electric point decreases with increasing arsenate adsorption density. Fractional arsenate adsorption was near 100 percent at  $pH < IEP$  and decreased with increasing pH at  $pH > IEP$ . Whereas aspects of metal ion adsorption are analogous to hydrolysis reactions in solution, adsorption of anions appears to be similar to protonation of bases. That is, it appears to be closely coupled with the consumption of protons from or the release of hydroxyl ions to solution.

Examples of such reactions are:





For chemical reasons the breaking of a covalent metal/oxygen bond (Eq. 4-3) is considered much less likely than the reactions represented by Eqs. 4-1 and 4-2 (H. Taube, personal communication). Experimental evidence confirms that in many systems protons are consumed when anions sorb.

#### IMPORTANCE OF ADSORBENT CONCENTRATION

It is important to realize that if the ligand adsorption reaction is analogous to solution reactions, the proximity of the pH-adsorption edge to the IEP of the solid may be strictly an artifact of the experimental conditions. This can be seen most clearly by writing one possible generalized reaction for adsorption of an anion:



The  $\text{H}^+$  on the left side of Eq. 4-4 is included to account for the general shape of the pH-adsorption curve. Experimental evidence supports the contention that protons are consumed when an anion sorbs (unpublished data). Bulk electrolyte ions are omitted from the reaction equation for convenience.

The equilibrium expression for the reaction is

$$K = \frac{(\overline{\text{SOH}}_{x_1+x_2} \text{A}_a)}{(\overline{\text{SOH}}_{x_1})(\text{H}^+)^{x_2}(\text{A}^-)^a} \times \text{EDL} \quad (4-5)$$

where EDL is the correction accounting for electrostatic interactions resulting from the electrical potential in the double layer. Its magnitude depends on the particular mathematical model chosen to simulate the surface environment. Assuming activity coefficients in the bulk solution and at the surface are constant and that a single anion binds to a surface site, and letting  $\overline{\text{SOH}}_{x_1+x_2} \text{A}_a \equiv \overline{\text{SA}}$ , the equilibrium constant can be rewritten in logarithmic form:

$$\log \frac{[\overline{\text{SA}}]}{[\text{A}]} = \log K - x_2 \text{pH} - \log \text{EDL} + \log [\overline{\text{SOH}}_{x_1}] \quad (4-6)$$

$\overline{[SA]}/[A]$  is a measure of the partitioning of the ligand between the surface and solution. The value of the EDL term in most adsorption models is a function of ionic strength and pH. Thus for a system in which ionic strength is fixed,

$$\log \frac{\overline{[SA]}}{[A]} = \log K - f_2(\text{pH}) + \log [\overline{\text{SOH}}_{x_1}] \quad (4-7)$$

where  $f_2(\text{pH}) = -x_2\text{pH} - \log \text{EDL}$  and is strictly a function of pH. Thus for a given system the pH region of the adsorption edge can theoretically be chosen arbitrarily by appropriate adjustment of the adsorbent concentration ( $[\overline{\text{SOH}}_{x_1}]$ ). For instance, if in a given system, 50 percent of the anion is adsorbed ( $\log(\overline{[SA]}/[A]) = 0$ ) at the PZC, by using  $10^2$  or  $10^{-2}$  as much adsorbent one can adjust fractional anion adsorption at the PZC to 99 percent or 1 percent, respectively. Thus, correlation of the PZC or IEP with the pH-adsorption edge results from the choice of adsorbent concentration and not from any inherent relationship between the two. Nevertheless, most studies of adsorption on oxides are conducted using surface concentrations of  $10\text{-}100 \text{ m}^2/\text{l}$ , and in most such systems anion adsorption edges are in the range  $\text{IEP} \pm 2$ . Thus, in typical experimental systems it is empirically likely that anions will partition strongly to the surface at  $\text{pH} < (\text{IEP} - 2)$  and strongly toward the solution phase at  $\text{pH} > (\text{IEP} + 2)$ .

Adsorption and coprecipitation of  $\text{SO}_4^{2-}$ ,  $\text{S}_2\text{O}_3^{2-}$ ,  $\text{SeO}_4^{2-}$ ,  $\text{SeO}_3^{2-}$ ,  $\text{AsO}_4^{3-}$ , and  $\text{CrO}_4^{2-}$  on  $\alpha\text{-Fe}(\text{OH})_3$  were studied over wide ranges of adsorbate concentration, adsorbent concentration, and pH. In all cases the typical pattern of a steep pH-adsorption edge, with adsorption decreasing as pH increases, was observed (viz. Figure 4-1). At constant pH and total anion concentration,  $A_T$ , fractional adsorption increases with increasing adsorbent concentration. This is the same trend observed in metal-adsorption experiments, and is consistent with a model in which the adsorbent is treated analogous to a dissolved complexing agent. In all systems studied, as the ratio  $A_T:\text{Fe}_T$  is increased a point is reached at which the maximum fractional adsorption attainable is less than 100 percent (Figures 4-1 and 4-2). The most likely explanation for such behavior is that at large adsorption density the number of available surface sites is limiting. This behavior is consistent with a single-site Langmuir adsorption model. The availability of sites limits adsorption density in these systems, and if all adsorbates occupy the same number of surface sites, the effect should be independent of adsorbate identity. To a first approximation this is experimentally observed. In all systems studied, the maximum adsorption density at which 100 percent fractional adsorption is attained is near 0.1 mole A/mole Fe.

9 1 1 2 5 1 1 2 7 8

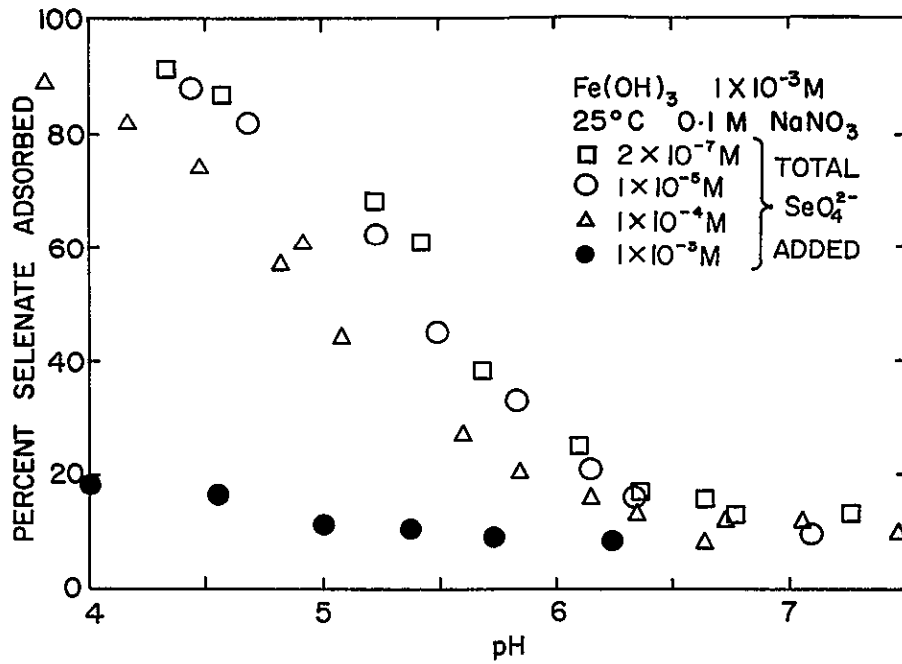


Figure 4-1. Percent selenate adsorbed versus pH

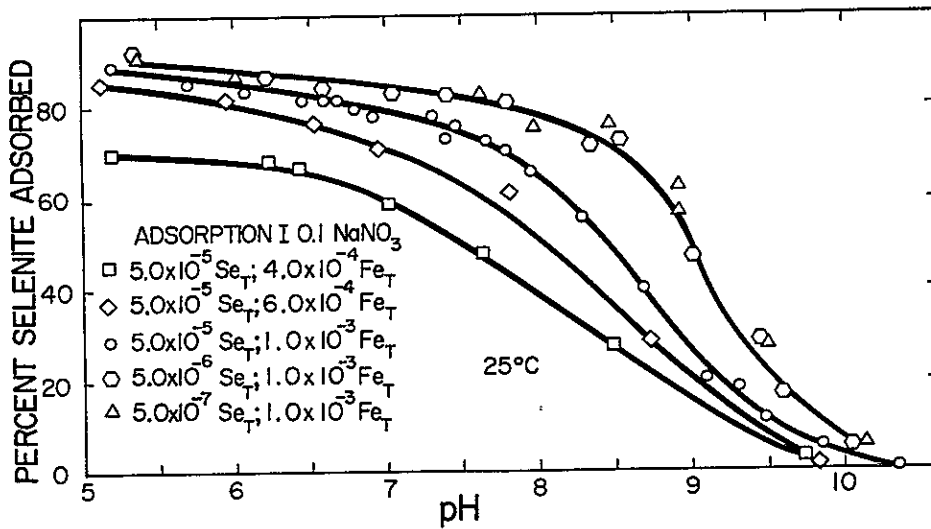


Figure 4-2. Percent selenite adsorbed versus pH

When  $A_T \leq 10^{-2} Fe_T$ , the anion is completely removed from solution at low pH and when  $A_T = Fe_T$ , the maximum observed fractional adsorption in any system is 0 to 20 percent. Small variations in the exact value of  $\Gamma_{max}$  among different anions may be partially explained by differences in the number of sites or surface area that individual molecules occupy. In the metal adsorption experiments the maximum ratio of adsorbate to adsorbent studied was 0.05 mole/mole. If the area and site-occupancy required by metal ions are comparable to or smaller than those for anions, one would expect 100 percent metal adsorption to be attainable in all systems studied. This was in fact the case. However, Swallow (3) was able to remove all the Cu from suspensions of am-Fe(OH)<sub>3</sub>, even when the ratio  $Me_T:Fe_T$  was  $\geq 0.1$ . This suggests that either metal ions require less surface area or sites than anions, or that at large adsorption densities metal ions are removed from solution by a different mechanism than anions. Possible alternative mechanisms are multi-layer adsorption and/or surface precipitation.

It is worthwhile to note at this time the extremely large adsorptive capacity of am-Fe(OH)<sub>3</sub>. Since all the anions studied have 3 or more oxygen atoms, a reasonable estimate may be that each anion occupies an equivalent surface area as that provided by a single Fe(OH)<sub>3</sub> unit cell of the surface. Based on this estimate, at least 10 percent of the Fe(OH)<sub>3</sub> groups in the solid are available to complex a dissolved species. It is extremely unlikely that anions would form a close-packed lattice at the surface due to mutual electrostatic repulsion. Thus a ratio of 1 adsorbed anion per 10 Fe(OH)<sub>3</sub> groups probably indicates that at least 20 percent and possibly more of the iron hydroxide groups are in direct contact with the solution phase. This is indicative of an extremely porous structure, and clearly illustrates the efficiency of am-Fe(OH)<sub>3</sub> as an adsorbent under appropriate solution conditions.

Recall that at fixed pH fractional metal adsorption decreased with increasing total metal concentration, even though there is no indication that total site availability is limited. That is, the pH-adsorption edge shifts to higher pH with increasing total metal concentration. Since typical pH-adsorption edges for anions are mirror images of those for metals, the analogous effect is for the edge to shift to lower pH with increasing anion concentration. Such shifts were observed for  $AsO_4^{3-}$  (Figure 4-3) and  $SeO_3^{2-}$  (Figure 4-2) at  $A_T:Fe_T$  ratios well below those at which site limitation occurs. In the  $S_2O_3^{2-}$  and  $SeO_4^{2-}$  systems, there was a slight shift observable only at  $A_T \geq 0.1 Fe_T$ . No shift was observable at all in  $CrO_4^{2-}$  systems. Insufficient data are available to evaluate the  $SO_4^{2-}$  system in this respect. However, in all comparable experiments  $SO_4^{2-}$  adsorption was identical to  $SeO_4^{2-}$  sorption,

so it is likely that a slight shift would be observed in the pH-adsorption edge for  $\text{SO}_4^{2-}$  in systems where  $(\text{SO}_4^{2-})_T \geq 0.1 \text{ Fe}_T$ . The shifting adsorption edge may be partially explained by changes in the electrical properties of the surface. As anions sorb, they alter the charge distribution near the surface in such a way that additional anion adsorption is repressed. Anderson et al. (2) found that shifts in the pH-adsorption edge for  $\text{AsO}_4^{3-}$  on am- $\text{Fe}(\text{OH})_3$  correlated with shifts in the IEP. Assuming that the anions studied adsorb by similar mechanisms and that the location of adsorbed anions is approximately independent of their identity, the shift of the IEP and its effect on adsorption should be approximately equivalent, and occur at the same adsorption density for all anions of a given charge. The adsorption density required for a given shift is expected to decrease with increasing negative charge on the anion. The observed and/or expected shifts in the pH-adsorption edges of  $\text{S}_2\text{O}_3^{2-}$ ,  $\text{SeO}_4^{2-}$ ,  $\text{SO}_4^{2-}$ , and  $\text{CrO}_4^{2-}$  are consistent with this behavior and explanation.

Adsorption of  $\text{AsO}_4^{3-}$  and  $\text{SeO}_3^{2-}$  is very similar to metal adsorption in that when the ratio  $A_T:\text{Fe}_T$  is small, fractional sorption is independent of adsorbate concentration at fixed adsorbent concentration and pH. At higher adsorbate concentration, fractional sorption decreases with increasing total adsorbate concentration, even

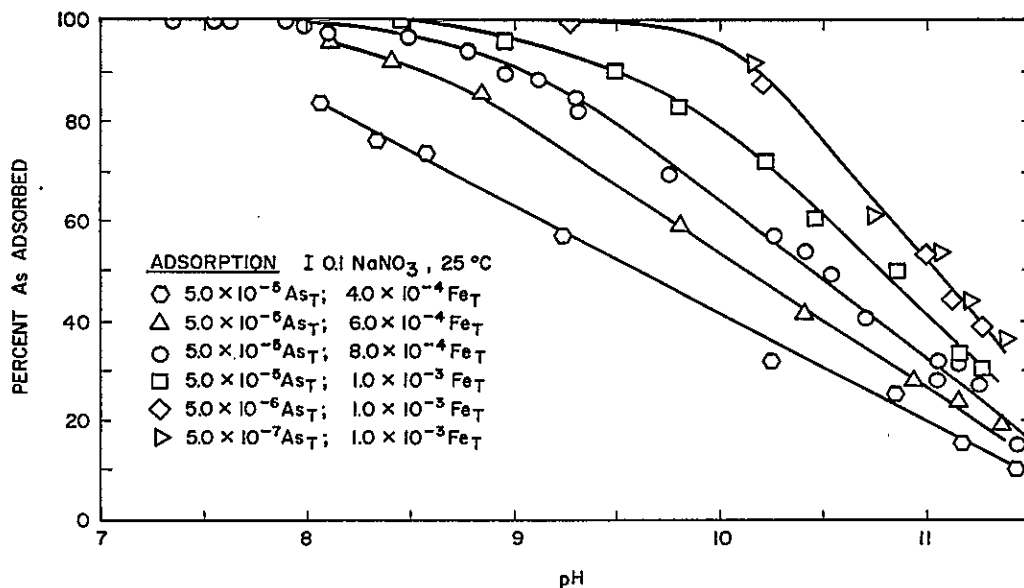


Figure 4-3. Percent arsenate adsorbed versus pH

though the concentration of available sites is apparently not a limiting factor. In the case of metal adsorption, the most likely explanation for this behavior is the presence of a variety of surface site types. At low adsorption density the strongest-binding sites are in excess and the average adsorptive binding energy is maximum. As adsorption density increases, the number of available strong-binding sites decreases and the adsorbate is forced on the average to bind to sites of weaker-binding constant. It is interesting to note that for both anions which exhibit this effect, fractional adsorption does not change when the ratio  $A_T:Fe_T$  is increased from  $5 \times 10^{-4}$  mole/mole to  $5 \times 10^{-3}$  mole/mole. However, when the ratio is increased to  $5 \times 10^{-2}$  mole/mole, the adsorption edges shift to lower pH (by about 0.4-0.5 pH units) in both cases. Since availability of the high-energy sites becomes a limiting factor at the same adsorption density for both anions, it is possible that they share the same group of high-energy sites.

The reason that some anions exhibit a pH-adsorption edge shift at lower adsorption density compared to others is not clear at this time. If anions, by virtue of their much larger size, require more binding sites per molecule than do metal ions, it is reasonable to expect that the strong specific site-binding typical of metal ions would not be detected for anions. If anions bind to, or at least cover, several sites simultaneously, the measured binding constant would be an average based on all the surface-adsorbate bonds formed. The influence of a single strong-binding site would then be diluted compared to the case where an ion binds to it exclusively. This may explain the most common case for anion adsorption, in which the pH-adsorption edge shifts only at large adsorption density. However, if this is the sole reason for the difference between typical cation and typical anion adsorption, it is difficult to explain the adsorptive behavior of  $AsO_4^{3-}$  and  $SeO_3^{2-}$ . A fully satisfactory explanation of the observations must await further and more detailed studies of adsorptive bonding energy and mechanisms.

#### KINETICS

Anions reach equilibrium with am- $Fe(OH)_3$  rapidly in both adsorption and coprecipitation systems (Figure 4-4 and 4-5). Removal efficiencies are generally  $\geq 90$  percent of their equilibrium value within minutes after all the reagents are added and removal is essentially complete within 1 hour. Although there were occasional exceptions (Figure 4-6), rapid kinetics were also generally observed for adsorption or desorption in systems which had been pre-equilibrated at a slightly higher or lower pH.

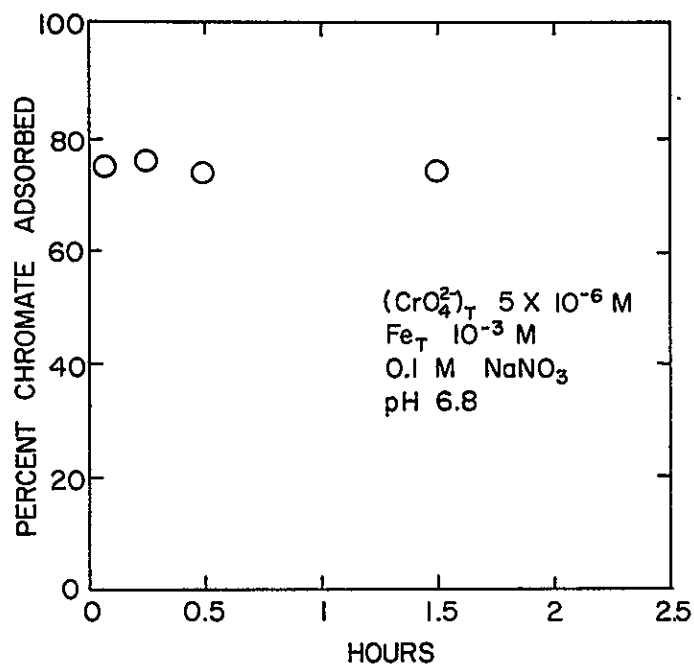


Figure 4-4. Kinetics of adsorption of chromate onto amorphous iron oxyhydroxide

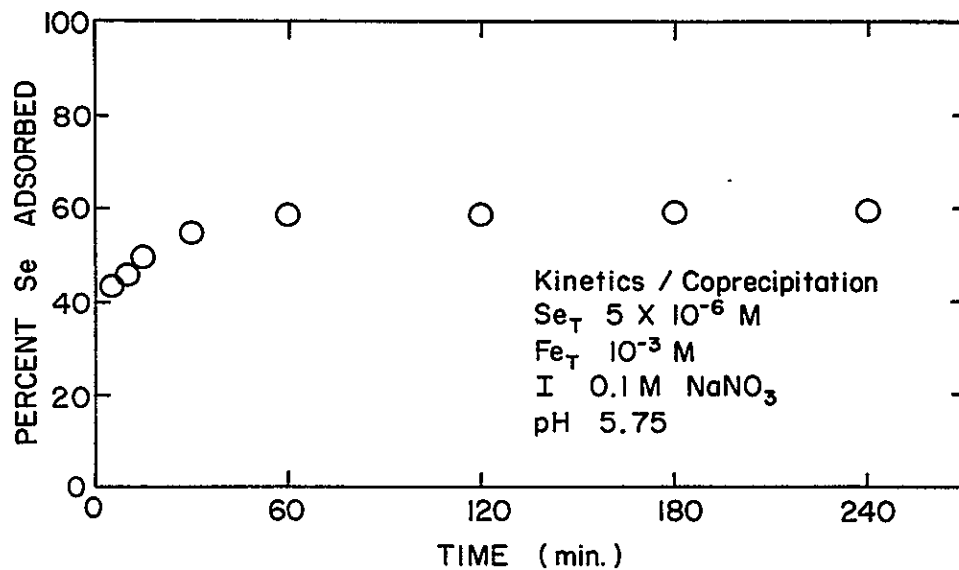


Figure 4-5. Kinetics of coprecipitation of selenite onto amorphous iron oxyhydroxide

In designing treatment processes, it may be desirable to induce and take advantage of transient, non-equilibrium solution conditions. For instance, if one could "trap" anions on a surface by coating the surface with a new layer of adsorbent, and then adsorb metal ions onto the second layer by raising the pH, it may be possible to remove both metals and anions from solution simultaneously, despite the fact that such removals would not occur in a system at equilibrium. To test this theory a system with  $10^{-3}M$   $Fe_T$  and  $10^{-5}M$   $(SeO_4^{2-})_T$  was equilibrated at pH 5. Then aliquots of  $Fe(NO_3)_3$  and NaOH were added so that the new solution conditions were  $Fe_T = 2 \times 10^{-3}M$  and  $pH \sim 6.5$ . Within 3 minutes the pH had dropped to  $\sim 6.1$  and fractional  $SeO_4^{2-}$  adsorption had decreased from the initial equilibrium value of  $\sim 75$  percent to  $\sim 40$  percent, which is approximately the equilibrium value for the new conditions (Figure 4-7). Further additions of NaOH rapidly desorbed  $SeO_4^{2-}$ . Apparently adsorbate molecules cannot be trapped on am- $Fe(OH)_3$  particles by adding more Fe to solution. This may be either because the additional Fe forms new particles rather than coating those already present or because the am- $Fe(OH)_3$  matrix is so porous that adding a few layers to a particle with ions previously sorbed does not significantly hinder the adsorption/desorption exchange process. While this result probably eliminates one possible way to take advantage of non-equilibrium solution conditions, it does not preclude the possibility that a different coating material may be found which achieves the same objective.

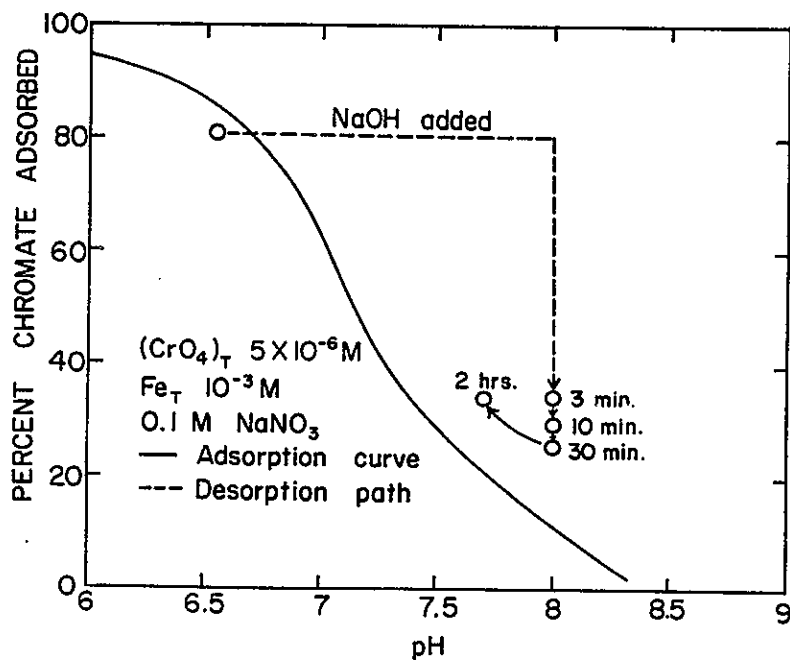


Figure 4-6. Kinetics of adsorption/desorption of chromate onto amorphous iron oxyhydroxide

COMPETITIVE ANION ADSORPTION

When a system contains multiple adsorbates which compete for the same group of sites, the adsorption of each ion may be less than in a comparable single-adsorbate system. Consider an ideal Langmuir system in which two potential adsorbates are present. The adsorptive reactions and equilibrium constants are

$$\overline{SH}_{x_1} + A^{m-} + x_2 H^+ \stackrel{K_A}{=} \overline{SH}_{x_1+x_2}^A \quad (4-8)$$

$$\overline{SH}_{x_1} + B^{n-} + x_3 H^+ \stackrel{K_B}{=} \overline{SH}_{x_1+x_2}^B \quad (4-9)$$

$$K_A = \frac{(\overline{SH}_{x_1+x_2}^A)}{(\overline{SH}_{x_1})(A^{m-})(H^+)^{x_2}} \quad (4-10)$$

$$K_B = \frac{(\overline{SH}_{x_1+x_2}^B)}{(\overline{SH}_{x_1})(B^{n-})(H^+)^{x_3}} \quad (4-11)$$

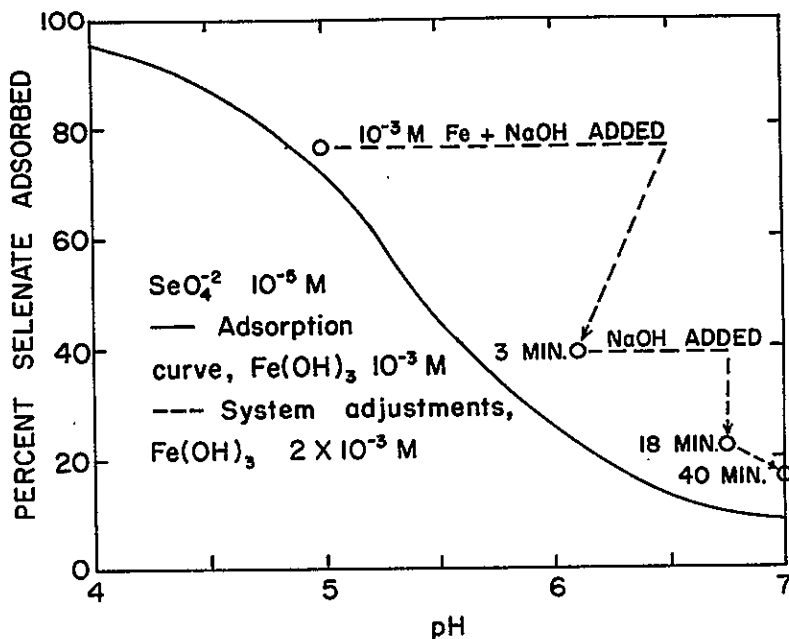


Figure 4-7. Effects of addition of iron on selenate adsorption in pre-equilibrated system

91120511304

If A and B are the only adsorbates, then

$$(\overline{S}_T) = (\overline{SH}_{x_1}) + (\overline{SH}_{x_1+x_2} A) + (\overline{SH}_{x_1+x_3} B)$$

Letting

$$(\overline{SA}) = (\overline{SH}_{x_1+x_2} A) \quad \text{and} \quad (\overline{SB}) = (\overline{SH}_{x_1+x_3} B)$$

and substituting into Eq. 4-10, we get

$$K_A = \frac{(\overline{SA})}{[(\overline{S}_T) - (\overline{SA}) - (\overline{SB})] (A^{m-})(H^+)^{x_2}} \quad (4-12)$$

Rearrangement yields

$$\frac{1}{K_A (A^{m-})(H^+)^{x_2}} = \frac{(\overline{S}_T) - (\overline{SA}) - (\overline{SB})}{(\overline{SA})} \quad (4-13)$$

and

$$= \frac{(\overline{S}_T)}{(\overline{SA})} - 1 - \frac{(\overline{SB})}{(\overline{SA})} \quad (4-14)$$

Combining Eqs. 4-10 and 4-11 yields

$$\frac{(\overline{SB})}{(\overline{SA})} = \frac{K_B}{K_A} \cdot \frac{(B^{n-})}{(A^{m-})} \cdot \frac{(H^+)^{x_3}}{(H^+)^{x_2}} \quad (4-15)$$

Substituting Eq. 4-15 into Eq. 4-14 and rearranging yields

$$\begin{aligned} \frac{(\overline{S}_T)}{(\overline{SA})} &= \frac{1}{K_A (A^{m-})(H^+)^{x_2}} + 1 + \frac{K_B (B^{n-})(H^+)^{x_3}}{K_A (A^{m-})(H^+)^{x_2}} \\ &= \frac{1 + K_A (A^{m-})(H^+)^{x_2} + K_B (B^{n-})(H^+)^{x_3}}{K_A (A^{m-})(H^+)^{x_2}} \end{aligned} \quad (4-16)$$

Inverting:

$$\frac{(\overline{SA})}{(\overline{S_T})} \cong \Gamma_A = \frac{K_A (A^{m-}) (H^+)^{x_2}}{1 + K_A (A^{m-}) (H^+)^{x_2} + K_B (B^{n-}) (H^+)^{x_3}} \quad (4-17)$$

where  $\Gamma_A$  is in terms of fractional site occupancy. In a single-adsorbate system, the expression for  $\Gamma_A$  is

$$\Gamma_A = \frac{K_A (A^{m-}) (H^+)^{x_2}}{1 + K_A (A^{m-}) (H^+)^{x_2}}$$

Thus the effect of the second adsorbate (B) is to reduce the concentration of available sites for bonding  $A^{m-}$  ions. Clearly then, if the second adsorbate binds to a different group of sites, the adsorption of A should be unaffected when B is added to the system.

Since adsorption of  $SO_4^{2-}$  is identical to that of  $SeO_4^{2-}$  under all conditions studied, the  $SO_4^{2-}/SeO_4^{2-}$  competitive system was chosen for study as the one most likely to exhibit ideal competitive effects. The similarity of the adsorption behavior of these anions in single-adsorbate systems indicates that to a first approximation  $K_{SO_4} = K_{SeO_4}$  and  $x_{SO_4} = x_{SeO_4}$ . Equation 4-17 then reduces to

$$\begin{aligned} \Gamma_{SeO_4} &= \frac{K_{SeO_4} (SeO_4^{2-}) (H^+)^{x_{SeO_4}}}{1 + K_{SeO_4} (SeO_4^{2-}) (H^+)^{x_{SeO_4}} + K_{SO_4} (SO_4^{2-}) (H^+)^{x_{SO_4}}} \\ &= \frac{K_{SeO_4} (SeO_4^{2-}) (H^+)^{x_{SeO_4}}}{1 + K_{SeO_4} [(SeO_4^{2-}) + (SO_4^{2-})] (H^+)^{x_{SeO_4}}} \end{aligned} \quad (4-18)$$

Equation 4-18 is identical to that for sorption of  $SeO_4^{2-}$  in a single-adsorbate system with the exception that in the denominator the equilibrium  $SeO_4^{2-}$  concentration is replaced by the total equilibrium dissolved adsorbate concentration  $[(SeO_4^{2-}) + (SO_4^{2-})]$ . Thus,  $SeO_4^{2-}$  partitioning in a system (call it #1) containing  $SO_4^{2-}$  is the same as in a second system (#2) containing  $(SeO_4^{2-})_2 = (SeO_4^{2-})_1 + (SO_4^{2-})_1$ , and

$(SO_4^{2-})_2 = 0$ , if the assumptions of the competitive Langmuir derivation are valid. This prediction has been experimentally verified (Figure 4-8). Apparently  $SeO_4^{2-}$  and  $SO_4^{2-}$  do bind to the same group of surface sites.

The expected results in a competitive system between two adsorbates of unequal binding strength are somewhat more complicated. Consider competition between a small concentration of  $CrO_4^{2-}$  and a much larger concentration of  $SO_4^{2-}$ . In single-adsorbate systems  $CrO_4^{2-}$  is more strongly sorbed than  $SO_4^{2-}$ , i.e., the  $CrO_4^{2-}$  adsorption edge is in a more alkaline pH range than that of  $SO_4^{2-}$ . Consider Eq. 4-18 for this system:

$$\Gamma_{CrO_4} = \frac{K_{CrO_4} (CrO_4^{2-}) (H^+)^{x_{CrO_4}}}{1 + K_{CrO_4} (CrO_4^{2-}) (H^+)^{x_{CrO_4}} + K_{SO_4} (SO_4^{2-}) (H^+)^{x_{SO_4}}} \quad (4-19)$$

or, equivalently,

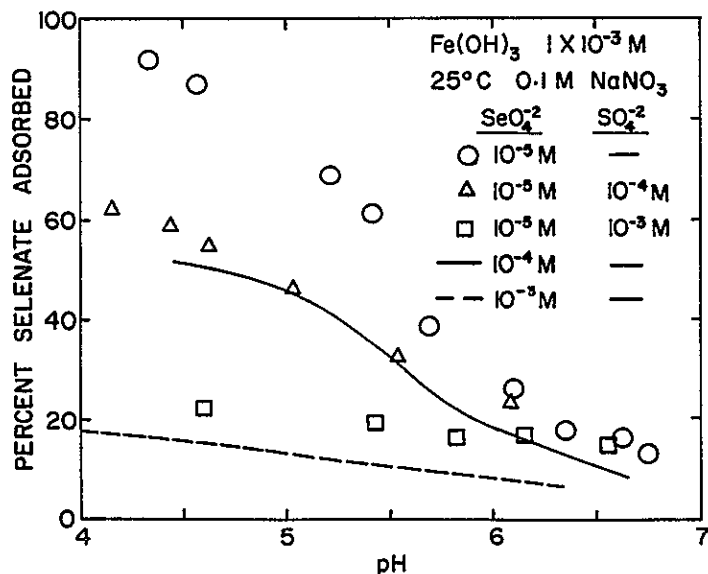


Figure 4-8. Partitioning of selenate and sulfate anion in a competitive adsorption experiment

$$\Gamma_{\text{CrO}_4} = \frac{K(\text{CrO}_4^{2-})(\text{H}^+)^x \text{CrO}_4}{1 + \frac{(\overline{\text{SCrO}_4})}{(\overline{\text{SH}}_{x_1})} + \frac{(\overline{\text{SSO}_4})}{(\overline{\text{SH}}_{x_1})}} \quad (4-20)$$

$(\overline{\text{SCrO}_4})$  and  $(\overline{\text{SSO}_4})$  are the activities of bound  $\text{CrO}_4^{2-}$  and  $\text{SO}_4^{2-}$ , respectively.

In the pH range more alkaline than the  $\text{SO}_4^{2-}$  adsorption edge but more acidic than the  $\text{CrO}_4^{2-}$  edge,  $(\overline{\text{SSO}_4})$  is negligible, so  $\Gamma_{\text{CrO}_4}$  is the same as in a  $\text{SO}_4^{2-}$ -free system. At lower pH, the term  $(\overline{\text{SSO}_4})/(\overline{\text{SH}}_{x_1})$  in the denominator of Eq. 4-20 becomes significant and  $\text{CrO}_4^{2-}$  sorption is reduced relative to the  $\text{SO}_4^{2-}$ -free system. Finally, if the concentration ratio  $(\text{SO}_4^{2-})_T/(\text{CrO}_4^{2-})_T$  is large enough, the  $(\overline{\text{SSO}_4})/(\overline{\text{SH}}_{x_1})$  term may dominate, so Eq. 4-19 reduces to

$$\Gamma_{\text{CrO}_4} = \frac{K_{\text{CrO}_4} (\text{CrO}_4^{2-})(\text{H}^+)^x \text{CrO}_4}{K_{\text{SO}_4} (\text{SO}_4^{2-})(\text{H}^+)^x \text{SO}_4} \quad (4-21)$$

Then, at fixed pH,

$$\frac{\Gamma_{\text{CrO}_4}}{(\text{CrO}_4^{2-})} = K' (\text{SO}_4^{2-})^{-1} \quad (4-22)$$

where

$$K' = K_{\text{CrO}_4} K_{\text{SO}_4}^{-1} (\text{H}^+)^x \text{CrO}_4^{-x} \text{SO}_4^x$$

Thus, at fixed pH, if surface sites are nearly all occupied by  $\text{SO}_4^{2-}$ , the ratio of bound-to-free  $\text{CrO}_4^{2-}$  should be inversely proportional to  $(\text{SO}_4^{2-})$  concentration. Results of  $\text{CrO}_4^{2-}/\text{SO}_4^{2-}$  competitive adsorption experiments are shown in Figure 4-9.

In single-adsorbate systems the pH-adsorption edges are in the range pH 4.5 to 7.0 for  $\text{SO}_4^{2-}$  and 6.0 to 8.0 for  $\text{CrO}_4^{2-}$  for  $10^{-3}\text{M Fe}_T$  and no site limitation. At pH  $\geq$  6.8, the presence of 0 to  $10^{-1}\text{M SO}_4^{2-}$  has a negligible effect on sorption of  $5 \times 10^{-6}\text{M CrO}_4^{2-}$ . However, as pH decreases below 6.8,  $\text{SO}_4^{2-}$  sorbs and reduces  $\text{CrO}_4^{2-}$  adsorption.

At a given pH < 6.8,  $\text{CrO}_4^{2-}$  decreases with increasing  $\text{SO}_4^{2-}$  concentration. In the single-adsorbate system,  $\text{SO}_4^{2-}$  sorption is site-limited at  $\text{pH} \leq 6$  when  $(\text{SO}_4^{2-})_T \geq 10^{-3}\text{M}$  ( $\text{Fe}_T = 10^{-3}\text{M}$ ). Thus we may be able to test the prediction that the ratio  $(\Gamma_{\text{CrO}_4})/(\text{CrO}_4^{2-})$  is proportional to  $(\text{SO}_4^{2-})^{-1}$  under these conditions. Table 4-1 shows that at pH 5, an increase in  $(\text{SO}_4^{2-})^{-1}$  of an order of magnitude changes the ratio  $(\Gamma_{\text{CrO}_4})/(\text{CrO}_4^{2-})$  by less than an order of magnitude. The most likely explanation for this is that  $\text{CrO}_4^{2-}$  and  $\text{SO}_4^{2-}$  share many but not all of the same binding sites. Thus when  $\text{CrO}_4^{2-}$  is forced off sites by  $\text{SO}_4^{2-}$  in accordance with Eq. 4-21, some of the desorbed  $\text{CrO}_4^{2-}$  may bind to other sites unavailable to  $\text{SO}_4^{2-}$ . In such a case the desorption of  $\text{CrO}_4^{2-}$  would be less than expected for the case where  $\text{SO}_4^{2-}$  and  $\text{CrO}_4^{2-}$  compete for all sites. Consistent with other experiments which suggest that  $\text{SO}_4^{2-}$  and  $\text{SeO}_4^{2-}$  bind to the same group of sites with approximately equal strength, the effect of  $\text{SeO}_4^{2-}$  on the adsorption of  $\text{CrO}_4^{2-}$  is identical to that of  $\text{SO}_4^{2-}$  (Figure 4-10).

The results from competitive adsorption experiments indicate that removal of  $\text{SeO}_4^{2-}$  at any pH, and removal of  $\text{CrO}_4^{2-}$  at  $\text{pH} \lesssim 6.5$  may be difficult in the presence of large concentrations of  $\text{SO}_4^{2-}$ . Unless  $\text{SO}_4^{2-}$  is removed prior to adsorption or converted to a non-competing species (e.g., by complexation or precipitation), efficient removal of  $\text{CrO}_4^{2-}$  and  $\text{SeO}_4^{2-}$  will require addition of sufficient Fe to the system to ensure that availability of anion sorption sites is not a limiting factor.

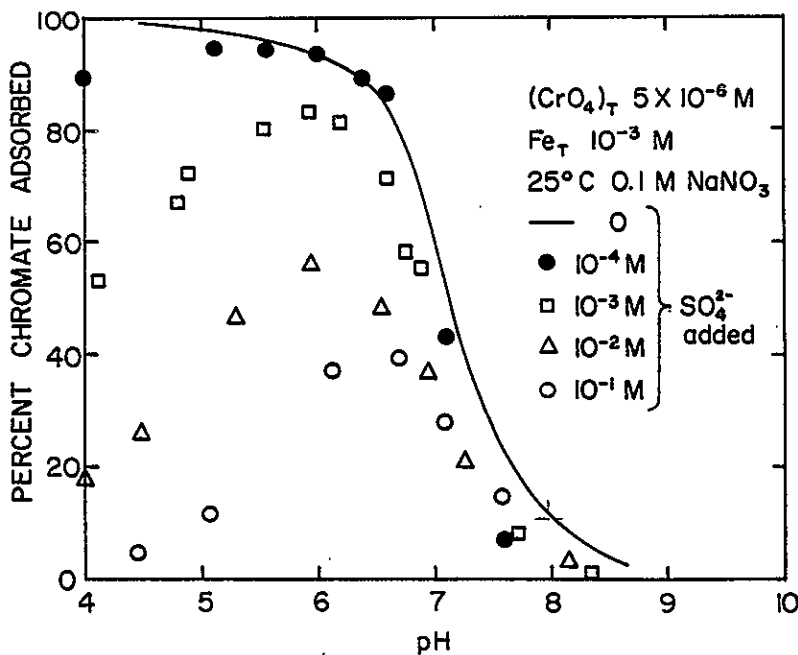


Figure 4-9. Effects of sulfate addition on chromate adsorption

Table 4-1

Competitive Adsorption Between  $\text{SO}_4^{2-}$  and  $\text{CrO}_4^{2-}$

$(\text{SO}_4^{2-}) \cong (\text{SO}_4^{2-})_T$	$(\text{SO}_4^{2-})^{-1}$	$\frac{\Gamma_{\text{CrO}_4^{2-}}}{\text{mole Fe}}$	$(\text{CrO}_4^{2-})$	$\frac{\Gamma_{\text{CrO}_4^{2-}}}{(\text{CrO}_4^{2-})}$
$10^{-3}$	$10^3$	$3.5 \times 10^{-3}$	$1.5 \times 10^{-6}$	$2.33 \times 10^3$
$10^{-2}$	$10^2$	$1.95 \times 10^{-3}$	$3.05 \times 10^{-6}$	$6.39 \times 10^2$
$10^{-1}$	10	$5 \times 10^{-4}$	$4.5 \times 10^{-6}$	$1.11 \times 10^2$

MODELING OF ANION ADSORPTION EXPERIMENTS BY THE SGMA MODEL

The results of computer modeling of the results from anion adsorption experiments are presented in Table 4-2. There are several points to note about the modeling results. First, the binding constants are generally weaker and the range of binding

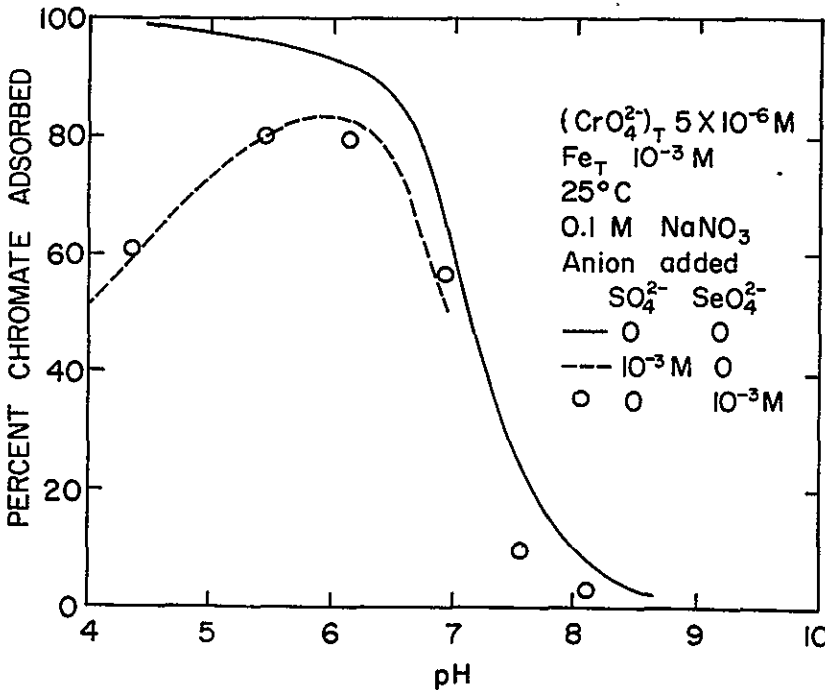


Figure 4-10. Comparison of the effects of sulfate and selenate addition on chromate adsorption

9 1 1 2 9 5 1 2 0 0

Table 4-2

Apparent Equilibrium Constants for Various Anions on am-Fe(OH)<sub>3</sub>

Surface Species <sup>a</sup>	-log (conc) (moles/l)	-log Fe <sub>T</sub>	log K	-log Γ at 50% Adsorbed (moles anion/mole Fe)
SOH <sub>2</sub> <sup>+</sup> -SO <sub>4</sub> <sup>2-</sup>	4.3	3	9.9	1.6
SOH <sub>2</sub> <sup>+</sup> -SO <sub>4</sub> H <sup>-</sup>	4.3	3	15.9	1.6
SOH <sub>2</sub> <sup>+</sup> -SeO <sub>4</sub> <sup>2-</sup>	4.3	3	9.9	1.6
SOH <sub>2</sub> <sup>+</sup> -SeOH <sub>4</sub> <sup>-</sup>	4.3	3	15.9	1.6
SOH <sub>2</sub> <sup>+</sup> -S <sub>2</sub> O <sub>3</sub> <sup>2-</sup>	4.3	3	10.0	1.6
SOH <sub>2</sub> <sup>+</sup> -CrO <sub>4</sub> <sup>2-</sup>	4.3	3	10.6	1.6
SOH <sub>2</sub> <sup>+</sup> -CrO <sub>4</sub> H <sup>-</sup>	4.3	3	18.1	1.6
SOH <sub>2</sub> <sup>+</sup> -SeO <sub>3</sub> <sup>2-</sup>	6.3 4.3	3 3.4	12.46 11.36	3.6 1.2
SOH <sub>2</sub> <sup>+</sup> -SeO <sub>3</sub> H <sup>-</sup>	6.3 4.3	3 3.4	18.94 18.34	3.6 1.2
SOH <sub>2</sub> <sup>+</sup> -AsO <sub>4</sub> H <sup>2-</sup>	6.3 4.3	3 3.3	25.90 25.00	3.6 1.3
SOH <sub>2</sub> <sup>+</sup> -AsO <sub>4</sub> H <sub>2</sub> <sup>-</sup>	4.3-6.3	3	31.08	1.6-3.6
<sup>a</sup> SOH + A <sup>m-</sup> + xH <sup>+</sup> $\overset{K}{\rightleftharpoons}$ SOH <sub>2</sub> <sup>+</sup> -AH <sub>x-1</sub> <sup>m-x</sup>				

constants is considerably smaller for anions than for cations (Table 3-4). This suggests that the binding mechanism is similar for many of the anions studied. Possibly the surface bond forms with an oxygen atom in the ligand molecule, and the strength of the bond is relatively insensitive to the remaining constituents of the anion. It is also likely that stereochemical factors often limit the closeness of approach of anions to the surface, and this may partially explain the

weakness of surface-anion bonds relative to those with cations. Contrary to the typical case for metals, the binding constants required to model anion adsorption are generally independent of adsorption density. This is a consequence of the observation that fractional sorption is independent of total adsorbate concentration at fixed pH and adsorbent concentration, as long as surface sites are in excess. Possible explanations for the difference between anions and cations in this respect have been discussed earlier.

In summary, adsorption of several anions on am-Fe(OH)<sub>3</sub> has been studied. Adsorption is rapid and usually completely reversible. Specific adsorption energies for anions are usually weaker and less variable than for metal ions. Adsorption of SeO<sub>4</sub><sup>2-</sup>, SO<sub>4</sub><sup>2-</sup>, CrO<sub>4</sub><sup>2-</sup>, and S<sub>2</sub>O<sub>3</sub><sup>2-</sup> can be accounted for by a single-site Langmuir model, but to explain adsorption of AsO<sub>4</sub><sup>3-</sup> and SeO<sub>3</sub><sup>2-</sup> a surface with non-homoe-energetic sites, similar to the model proposed for metal sorption, must be invoked. Experiments involving pairs of anions demonstrate some possible effects of anion/anion competition in systems where the anions have approximately equal adsorption energies and where one anion binds considerably more strongly than another.

#### REFERENCES

1. F. J. Hingston, A. M. Posner and J. P. Quirk. "Competitive Adsorption of Negatively Charged Ligands on Oxide Surfaces." Disc. Farad. Soc., 52, 334 (1972).
2. M. A. Anderson, J. F. Ferguson and J. Garvis. "Arsenate Adsorption on Amorphous Aluminum Hydroxide." J. Coll. Interface Sci., 54, 391 (1976).
3. K. C. Swallow. "Adsorption of Trace Metals by Hydrous Ferric Oxide in Seawater." Ph.D. Thesis, Massachusetts Institute of Technology, 1978.

## Section 5

### EFFECTS OF COMPLEXING LIGANDS ON METAL ION ADSORPTION: EXPERIMENTAL RESULTS AND A CONCEPTUAL MODEL

#### INTRODUCTION

As noted in Section 2, simple, soluble, inorganic complexing ligands generally decrease metal ion sorption. In the case of Hg sorption onto  $\alpha\text{-Fe(OH)}_3$ , the observed decrease in adsorption is consistent with the hypothesis that the free metal and hydroxo-complex can sorb but the chloro-complexes cannot (1). Since the interactions between ligands and metals can potentially alter the adsorptive behavior of metal ions (and ligands) it was necessary to investigate several metal-ligand types and the altered adsorptive behavior on several adsorbent types.

The effects of  $\text{Cl}^-$ ,  $\text{SO}_4^{2-}$ , and  $\text{S}_2\text{O}_3^{2-}$  on Cd sorption on  $\alpha\text{-Fe(OH)}_3$ ,  $\alpha\text{-SiO}_2$ , and  $\gamma\text{-Al}_2\text{O}_3$  were studied at ligand concentrations such that the activity ratio of the dissolved species (complexed Cd)/(free  $\text{Cd}^{2+}$ ) was in the range 1.0 to 100. The trend of decreasing metal adsorption with increasing ligand concentration was usually followed. However, in only one of the systems ( $\text{S}_2\text{O}_3/\alpha\text{-SiO}_2$ ) are the results consistent with the assumption of no adsorption of the complex. In fact, Cd and Ag adsorption onto  $\text{Fe(OH)}_3$  at low pH is enhanced by the addition of  $10^{-4}$  to  $10^{-2}\text{M}$   $\text{S}_2\text{O}_3^{2-}$  to the system and as little as  $4 \times 10^{-7}\text{M}$   $\text{S}_2\text{O}_3^{2-}$  increases sorption of Ag on  $\text{Fe(OH)}_3$ . The effects of  $\text{S}_2\text{O}_3^{2-}$  on Ag sorption are undoubtedly apparent at lower  $\text{S}_2\text{O}_3^{2-}$  concentrations than for Cd because the  $\text{Ag-S}_2\text{O}_3$  complex is much stronger than the  $\text{Cd-S}_2\text{O}_3$  complex.

In this section a conceptual and semi-quantitative model is developed for adsorption of metals in systems containing potentially sorbing ligands and metal-ligand complexes. Experimental results are then interpreted in terms of the model.

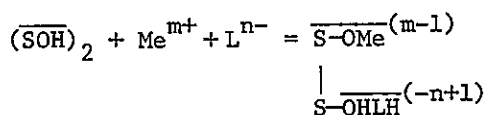
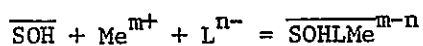
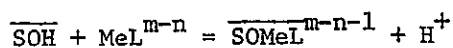
#### ARGUMENTS SUPPORTING ADSORPTION OF COMPLEXES

There are at least two ways in which the addition of complexing ligands to a system may increase metal sorption. The ligand may adsorb and change the electrostatic interaction between the solid and the metal; or a surface-metal-ligand complex may form.

In a system containing swamping electrolyte adsorption of a trace metal is expected to change negligibly in response to slight changes in surface electrical properties. If the ligands act only indifferently by changing the electrostatic interaction between the surface and the metal adsorbate, it is unreasonable that a ligand concentration as low as that used in the Ag-adsorption studies could cause the observed drastic increase in adsorption of the metal. Apparently species involving specific chemical interactions between a metal, a ligand, and the surface can exist.

Such surface species are entirely reasonable. For instance, if we consider adsorption of a free metal to be analogous to formation of a soluble metal-ligand complex, adsorption of a complex is analogous to formation of a soluble mixed-ligand complex. Such complexes are known to exist.

The formation of the surface complex may occur by sequential bonding of the ions, or by adsorption of the complex. Thermodynamically, these mechanisms are equivalent and equilibrium adsorption data provide no information with which to distinguish between them. In addition, complexes may adsorb in any of several different surface configurations or orientations. Discussion about which form is most likely is presented later. For the time being the phrase "adsorption of the metal-ligand complex" is meant to include any series of reactions which leads to a surface species in which adsorbent, metal, and ligand combine to form a single surface species. Some examples of such reactions are shown below:



The general adsorption patterns for uncomplexed metal ions and for simple inorganic anions have been reported and discussed in previous sections. In this section, the concepts developed earlier are expanded and used to help explain adsorptive interactions in more complex systems. Since only anionic ligands were investigated experimentally and since cationic metal-complexing ligands are extremely rare, in the following discussion the term "ligands" refers only to species for which the coulombic interaction with the surface becomes less attractive with increasing pH.

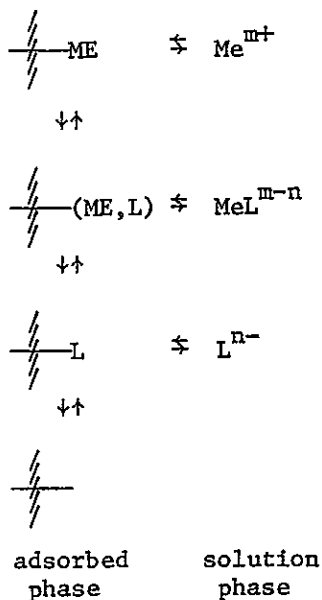
91120511274

In addition to anions, this group may include dipoles and zwitterions which carry no net charge, if the orientation of the adsorbed molecules is such that its anionic portion is closer to the surface than its cationic portion.

A SEMI-QUANTITATIVE MODEL OF METAL ADSORPTION IN SYSTEMS CONTAINING COMPLEXING LIGANDS

Conceptual Basis of the Model

Systems containing metal, ligand, and solid can be viewed as consisting of two phases with metal-ligand equilibria reactions governing speciation in each, as pictured below:



There are at least three possible ways in which the metal ligand complex may interact with the surface:

1. Adsorption of the complexed metal may be chemically analogous to and have similar pH dependence as that of the uncomplexed metal.
2. Adsorption of the complex may be similar to that of the free ligand.
3. The complex may not adsorb at all.

These are the extreme, and therefore simplest cases. Real systems may be represented by combinations of the limiting cases, and may behave differently under different environmental conditions.

9 1 1 2 7 1 1 6

In the first two situations, the complex may adsorb more or less strongly than uncomplexed species. Thus case (3) is a limiting case in which the complex is sorbed much less strongly than either uncomplexed species. Conceptually the effects of complexation can be classified as follows:

Relative magnitudes of terms contributing to total adsorption energy	pH-adsorption pattern of complex	Strength of MeL-surface bond		
Specific (chemical) $\gg$ non-specific (coulombic)	Similar to Me	Stronger than Me/S (A)	Weaker than Me/S (C)	Equal to Me/S (E)
Non-specific $\gg$ specific	Similar to L	Stronger than L/S (B)	Weaker than L/S (D)	Equal to L/S (F)

Chemical Reactions and Equilibria in Me/L/S Systems

Treating the surface analogous to a dissolved ligand, and surface reactions similar to hydrolysis reactions, the following adsorption-pH patterns for the complexes are expected (Figure 5-1).

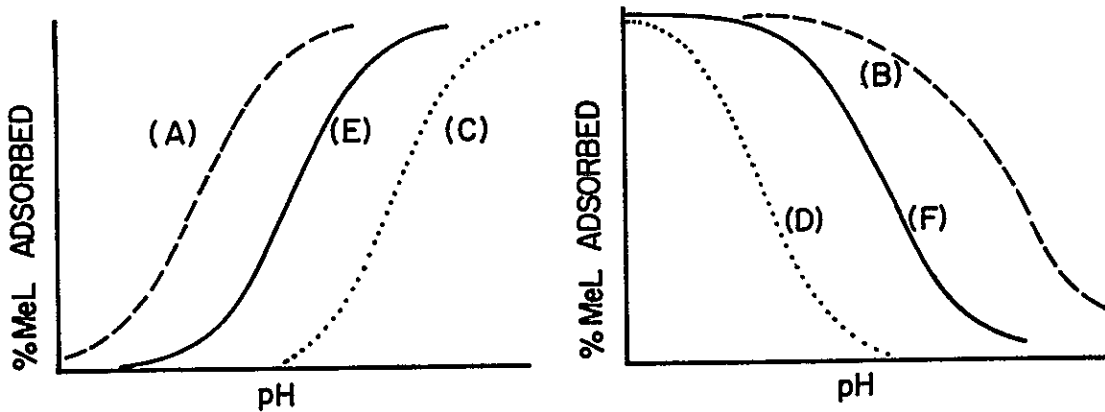


Figure 5-1. Possible pH-adsorption edges for different types of systems

9112051296

The total adsorption of metal in a system is the sum of adsorption of the free and complexed species. Consider the case where adsorption of the complex is similar to that of the free metal. We can write the following chemical equilibria for the adsorption reactions:



$$K_1 = \frac{\overline{(S^0 Me)} (H^+)^{x_0} (EDL_1)}{\overline{(S^0 H_{x_0})} (Me^{2+})}, \quad K_2 = \frac{\overline{(S^1 MeL)} (H^+)^{x_1} (EDL_2)}{\overline{(S^1 H_{x_1})} (MeL^{2-n})},$$

$$K_3 = \frac{\overline{(S^2 H_{x_2+x_3} L)} (EDL_3)}{\overline{(S^2 H_{x_2})} (H^+)^{x_3} (L)}, \quad K_4 = \frac{(MeL)}{(Me)(L)} \quad (5-5)$$

(Charge assignment to surface species is omitted in the equation for simplicity.)  $S^0$  and  $S^1$  are two different adsorption sites which may or may not be equivalent. Thus, a surface may be saturated with ligand molecules and still have excess metal-adsorbing sites available. Activities of bulk electrolyte at the surface and in solution are assumed to be constant. Since the three equilibria are coupled, adsorption may affect speciation in solution in addition to altering total dissolved concentrations of metal and ligand directly. For instance, if adsorption of the ligand is not site-limited, it is almost completely removed from solution at low pH, shifting the MeL/Me equilibrium toward the free metal. These equations include the tacit assumptions that free metal and a single complexed metal species are the only adsorbing species and that each can be treated as if it adsorbs onto only one

91143127

type of site by a single mechanism. It is further assumed that all protons released during the adsorption process originate at the surface. The validity of these assumptions and the expected results if they are violated are discussed later.

Some simple algebraic manipulations yield:

$$\frac{\overline{(S^1MeL)}}{\overline{(MeL)}} = K_2 \overline{(S^1H_{x_1})} (H^+)^{-x_1} (\overline{EDL_2})^{-1} \quad (5-6)$$

$$\frac{\overline{(S^0Me)}}{\overline{(MeL)}} = \frac{\overline{(S^0Me)}}{\overline{(Me)}} \frac{\overline{(Me)}}{\overline{(MeL)}} = K_1 \overline{(S^0H_{x_0})} (H^+)^{-x_0} \left[ \frac{1}{K_4(L)} \right] (\overline{EDL_1})^{-1} \quad (5-7)$$

$$\frac{\overline{(S^1MeL)} + \overline{(S^0Me)}}{\overline{(MeL)}} = \frac{K_2 \overline{(S^1H_{x_1})}}{(H^+)^{x_1} (\overline{EDL_2})} + \frac{K_1 \overline{(S^0H_{x_0})}}{(H^+)^{x_0} K_4(L) (\overline{EDL_1})} \quad (5-8)$$

The left-hand side can be converted to  $f$ , the ratio of adsorbed to dissolved metal, by multiplying by  $(1 + \overline{(Me)}/\overline{(MeL)})^{-1}$ . Thus,

$$f = \frac{\overline{(S^1MeL)} + \overline{(S^0Me)}}{\overline{(MeL)} + \overline{(Me)}} = \frac{\overline{(S^1MeL)} + \overline{(S^0Me)}}{\overline{(MeL)}} \cdot \frac{1}{1 + \frac{\overline{(Me)}}{\overline{(MeL)}}} \quad (5-9)$$

$$= \left[ \frac{K_2 \overline{(S^1H_{x_1})}}{(H^+)^{x_1} (\overline{EDL_2})} + \frac{K_1 \overline{(S^0H_{x_0})}}{(H^+)^{x_0} K_4(L) (\overline{EDL_1})} \right] \frac{1}{1 + \frac{1}{K_4(L)}}$$

$$= \left[ \frac{K_2 \overline{(S^1H_{x_1})}}{(H^+)^{x_1} (\overline{EDL_2})} + \frac{K_1 \overline{(S^0H_{x_0})}}{(H^+)^{x_0} K_4(L) (\overline{EDL_1})} \right] \frac{K_4(L)}{K_4(L) + 1}$$

$$= \frac{K_2 K_4(L) \overline{(S^1H_{x_1})}}{[K_4(L) + 1] (H^+)^{x_1} (\overline{EDL_2})} + \frac{K_1 \overline{(S^0H_{x_0})}}{[K_4(L) + 1] (H^+)^{x_0} (\overline{EDL_1})} \quad (5-10)$$

$$f = F_1 + F_2 \quad (5-11)$$

91120511209

The overall fractional adsorption is  $f/(f+1)$ . The first term in the above equation ( $F_1$ ) represents adsorption of the complex and the second ( $F_2$ ) represents sorption of the free metal. The four limiting situations of interest are outlined in Table 5-1(A).

Table 5-1  
Adsorption in Complex Systems

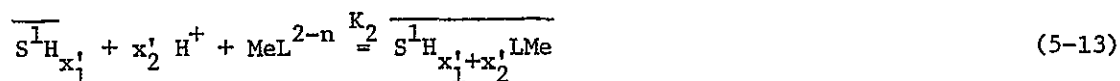
Case	Dominant Dissolved Metal Species	Dominant Adsorbed Metal Species	f
<b>A. Limiting Cases for Metal-Like Complexes</b>			
1	MeL, i.e. $K_4(L) \gg 1$	MeL, i.e. $F_1 \gg F_2$	$K_2(H^+)^{-x_1} \overline{(S^1H_{x_1})} (EDL_2)^{-1}$
2	MeL	Me, i.e. $F_1 \ll F_2$	$K_1 K_4^{-1} (H^+)^{-x_0} \overline{(S^0H_{x_0})} (L)^{-1} (EDL_1)^{-1}$
3	Me, i.e. $K_4(L) \ll 1$	MeL	$K_2 K_4 (H^+)^{-x_1} \overline{(S^1H_{x_1})} (L) (EDL_2)^{-1}$
4	Me	Me	$K_1 (H^+)^{-x_0} \overline{(S^0H_{x_0})} (EDL_1)^{-1}$
<b>B. Limiting Cases for Ligand-Like Complexes</b>			
5	MeL	MeL	$K_2' \overline{(S^1H_{x_2}')}) (H^+)^{x_2'} (EDL_2,)^{-1}$
6	MeL	Me	$K_1 K_4^{-1} (H^+)^{-x_0} \overline{(S^0H_{x_0})} (L)^{-1} (EDL_1)^{-1}$
7	Me	MeL	$K_2' K_4 (H^+)^{x_2'} \overline{(S^1H_{x_2}')}) (L) (EDL_2,)^{-1}$
8	Me	Me	$K_1 (H^+)^{-x_0} \overline{(S^0H_{x_0})} (EDL_1)^{-1}$

91120511209

In cases (1) and (4) one species dominates both dissolved and adsorbed phases, and fractional adsorption is independent of ligand concentration. In case (2), the metal-ligand complex adsorbs less strongly than free metal so increasing ligand concentration decreases overall metal adsorption. Case (3) is the opposite situation in which the complex is strongly adsorbed, so increasing the ligand concentration increases metal adsorption. Cases (1) and (3) are represented by curve (A) and cases (2) and (4) are represented by curve (B), where the ordinate is now overall fractional metal adsorption. The derivation is valid regardless of whether free and complexed metal species adsorb to the same group of sites.

The slope of curve (A) or (C) relative to that for the ligand-free system (curve (E)) is determined by the relative magnitudes of  $x_0$  and  $x_1$ , and the dependence of EDL on pH. Empirically the pH-percent adsorption curves in the presence and absence of ligand are often approximately parallel, so if each EDL term is constant  $x_0 \approx x_1$  for these systems. That is, the number of protons released is the same when the complex adsorbs as when the free metal adsorbs. Alternatively, it may be that  $x_0 \neq x_1$ , but that the difference between the two is offset by a change in the EDL term with pH. The magnitude of the EDL term is not well known (it depends on the model of the double layer chosen) and the proton release accompanying adsorption of complexed metal has not been measured unambiguously in any experimental system. Until the values of these parameters are definitely known, their relative importance in determining the slope of the adsorption edge is open to speculation. What can be stated is that if the adsorption edges for free and complexed metal are parallel, the net effect of the EDL and  $(H^+)^x$  terms is equivalent to a system in which EDL is constant and  $x_0 = x_1$ .

The analysis thus far is for the case where adsorption of complexes is similar to that of free metal. If complexes adsorb analogous to free ligands the expressions describing chemical equilibria and fractional adsorption are:





$$\frac{\overline{(\text{S}^{\text{I}}\text{H}_{x_1+x_2} \text{LMe})} + \overline{(\text{S}^{\text{O}}\text{Me})}}{\overline{(\text{MeL})} + \overline{(\text{Me})}} = \frac{K_1 \overline{(\text{S}^{\text{O}}\text{H}_{x_0})}}{(\text{H}^+)^{x_0} [\text{K}_4(\text{L}) + 1] (\text{EDL}_1)} + \frac{K_2 K_4 (\text{L}) \overline{(\text{S}^{\text{I}}\text{H}_{x_1})} (\text{H}^+)^{x_2}}{[\text{K}_4(\text{L}) + 1] (\text{EDL}_2)} \quad (5-16)$$

Limiting cases for adsorption in these systems are outlined in Table 5-1(B). If the complex is the dominant adsorbed species (cases (5) and (7)) the position of the pH-adsorption edge depends on whether it adsorbs more (curve (B)) or less (curve (D)) strongly than free ligand. If the free metal is the dominant sorbed species (cases (6) and (8)), the net adsorption is similar to curve (C), and the shift between curves (E) and (C) is related to the strength of the complex in solution.

#### Surface Speciation

It is instructive to consider the relative contributions to total metal adsorption of the free and complexed metal species for a constant ligand concentration as pH changes. Consider for example a situation in which dissolved ligand concentrations are such that  $\overline{(\text{MeL})} \gg \overline{(\text{Me})}$  and adsorption of the complex is metal-like. Comparing the values of  $f$  for cases (1) and (2) (see Table 5-1(A)),

$$f_1/f_2 = \frac{K_2 K_3}{K_1} (\text{H}^+)^{x_0-x_1} \frac{\overline{(\text{S}^{\text{O}}\text{H}_{x_0})}}{\overline{(\text{S}^{\text{I}}\text{H}_{x_1})}} (\text{L}) \cdot \frac{(\text{EDL}_1)}{(\text{EDL}_2)}$$

If there is no site limitation or if the same sites bind both Me and MeL, the ratio  $\overline{(\text{S}^{\text{O}}\text{H}_{x_0})}/\overline{(\text{S}^{\text{I}}\text{H}_{x_1})}$  is constant. The above equation can then be rewritten,

$$f_1/f_2 = K_0 (\text{H}^+)^{x_0-x_1} (\text{L}) \cdot \frac{(\text{EDL}_1)}{(\text{EDL}_2)}$$

where

$$K_0 = \frac{K_2 K_3}{K_1} \frac{\overline{(\text{S}^{\text{O}}\text{H}_{x_0})}}{\overline{(\text{S}^{\text{I}}\text{H}_{x_1})}}$$

If in addition  $x_0 \approx x_1$ , and  $(EDL_1)/(EDL_2)$  is constant, then  $f_1/f_2$  is constant over the entire pH range for a given dissolved ligand concentration. This result obtains when comparing any two limiting cases for metal-like complex adsorption (cases (1-4)). That is, surface speciation is independent of pH in metal-like systems if the concentration of dissolved ligand is invariant.

Adsorption of the ligand removes it from solution and in systems that are not site-limited, dissolved ligand concentration decreases significantly with decreasing pH. In such cases surface speciation varies in the pH range where ligand concentration does, with adsorption of the complex favored at lower pH and adsorption of the free metal favored at high pH. In most systems studies, ligand adsorption was site-limited so total soluble ligand concentration was approximately constant over the entire pH range.

If the complex adsorbs analogous to the free ligand, the ratio of adsorbed complex to adsorbed free metal is, for example,

$$f_5/f_6 = K'_o(H^+)^{x_2+x_0} (L) \cdot \frac{(EDL_1)}{(EDL_2)}$$

At constant dissolved ligand concentration, the surface speciation is highly pH-dependent, with the complex dominating at low pH and the free metal dominant at high pH. Depending on the concentration of ligand and the values of the equilibrium constants, several different pH-adsorption curves may obtain (Figure 5-2). A plot of fractional metal adsorption vs. pH may have four regions:

- Region I. At low pH, surface speciation is dominated by strongly sorbing complex species, and nearly all the metal is removed from solution if sufficient sites are available.
- Region II. At intermediate pH, the strength of the surface-complex bond and hence fractional adsorption of the complex decrease with increasing pH.
- Region III. Also at intermediate pH, the surface/free metal bond strength increases, and fractional adsorption of the free metal increases with increasing pH.
- Region IV. At still higher pH, adsorption of the free metal is so strong that nearly all of dissolved metal adsorbs, assuming once again that sites are in excess.

Thus, for a given ligand concentration if the regions of decreasing complexed metal adsorption (Region II) and increasing free metal adsorption (Region III) are widely

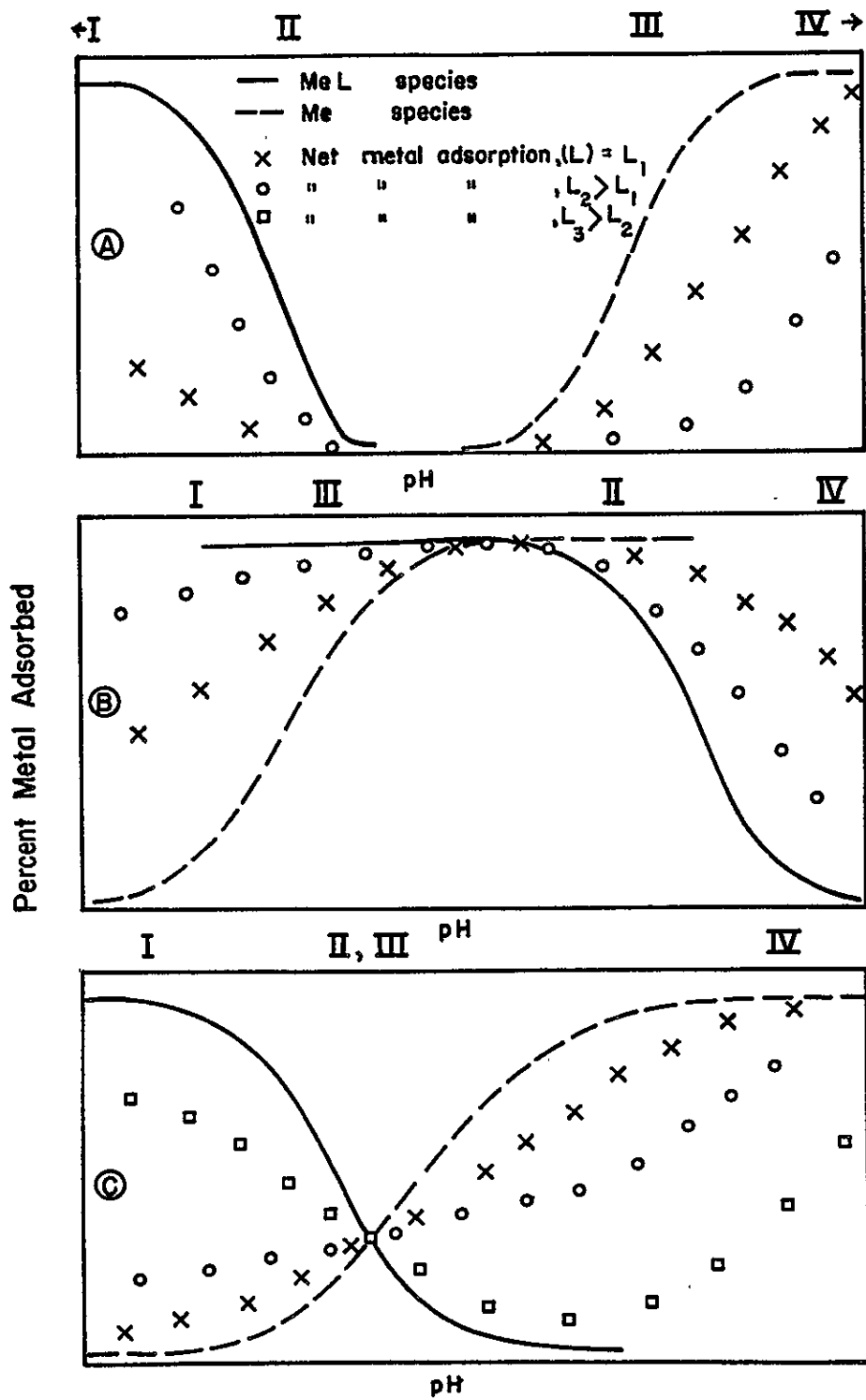


Figure 5-2. Effect of ligand concentration and equilibrium constants on pH-adsorption curves

91129511303

9 1 1 2 0 5 1 1 3 0 4

separated, the net adsorption curve is similar to Figure 5-2(A). If the pH range of Region II is higher than that of Region III, Regions I and IV overlap and the net curve is similar to Figure 5-2(B). Figure 5-2(C) represents the intermediate case, where Regions II and III overlap. It is interesting to note that increasing adsorbent concentration shifts the adsorption edge for anions to higher pH and that for cations to lower pH, other solution conditions being constant. Thus, the degree of overlap of the edges is theoretically arbitrary, and a system tends to shift from that represented by A to C to B as adsorbent concentration increases. Several important conclusions can be drawn from this qualitative analysis. If metal complex adsorption is analogous to that of the free ligand: 1) Assuming sufficient free-metal adsorbing and complex-adsorbing sites are available, fractional metal adsorption is near 100 percent at low and high pH, and decreases to a minimum at some intermediate pH, designated  $pH_m$ . 2) Depending on the magnitude of the minimum and the pH range under study, only a small portion of the adsorption curve may be evident from a single series of experiments. In addition, the decrease at the minimum may be undetectably small. 3) There exists a value of pH at which fractional adsorption of free metal equals that of complexed metal and total fractional adsorption is independent of ligand concentration ( $pH_c$ ). At  $pH < pH_c$ , increasing ligand concentration increases total metal adsorption. At  $pH > pH_c$ , increasing ligand concentration decreases ligand adsorption. Thus, at pH near  $pH_c$  a plot of fractional adsorption versus pH has decreasing slope with increasing ligand concentration.

#### Re-Evaluation of the Assumptions of the Model

At this point it is instructive to reconsider some of the assumptions of the derivation. The assumptions are:

1. Free metal and a single complexed metal species are the only adsorbing species, i.e., all complexes of a given metal-ligand pair adsorb equally.
2. Fractional adsorption of a species is a function of pH but not of its concentration.
3. Each species binds by a single mechanism, i.e., complexes are either "metal-like" or "ligand-like," but not both.
4. All protons released originate at the surface.

Each assumption will be analyzed individually with respect to its probable validity and the consequences if it is in error.

Assumption 1. Most ligands form multiple complexes of the form  $MeL_x$  with a given metal, where  $x$  is an integer varying between 1 and the coordination number of the metal ion. As the free ligand concentration in solution increases, the value of  $x$  of the dominant dissolved metal species also increases. The model for adsorption of metal-ligand complexes has been developed assuming that the adsorptive behavior of all complexes with a given ligand ( $x > 0$ ) is identical. While this assumption is probably an oversimplification, it should be noted that a) in most aqueous systems other than estuaries and rivers in arid regions ligand concentrations do not vary temporally or spatially by more than an order of magnitude, and b) for most metal-ligand pairs the average value of  $x$  changes by one unit for a change in free ligand concentration of  $1^{1/2}$  to 3 orders of magnitude.

Thus in most systems only one or two complexed metal species are of interest for a given ligand. The case of a single complex species being dominant has been modeled. The case for two-complex species can be developed in an exactly analogous way, by treating the cases where the second  $MeL$  complex adsorbs i) analogous to the free metal or the free ligand, ii) more or less strongly than the free metal, and iii) more or less strongly than the first complex. Clearly the number of situations to consider grows rapidly as the number of adsorbing species grows. However, only if the subsequent complexes adsorb in a manner that is qualitatively different from the first (i.e. free-metal-like vs. free-ligand-like) is a drastic change in adsorption behavior expected with increasing ligand concentration. Since the experimental data can be explained without invoking such an explanation, it is not developed further.

Assumption 2. The assumption that fractional adsorption of a species is independent of its concentration will be violated i) if multiple surface site-binding energies exist, ii) if sites are limiting, or iii) if adsorption significantly alters the electrical interaction between the surface and adsorbing ions.

i) The assumption of homeo-energetic surface sites is a contradiction of conclusions reached earlier. Fractional metal adsorption at constant pH in ligand-free systems often decreases with increasing total metal concentration. Generally no such trend occurs for adsorption of a large number of ligands in metal-free systems. Extending the analogy to adsorption of complexes, one expects fractional adsorption of metal-like complexes to decrease with increasing concentration. Fractional adsorption of ligand-like complexes is generally expected to be unaffected by changes in their concentration.

Graphically, the expected shifts in individual adsorption curves are shown in Figure 5-3. Consider first a complex that has free-metal-like adsorptive behavior. As metal concentration increases, fractional adsorption of both adsorbing species (free metal and complex) decreases at constant pH, and the net fractional adsorption curve shifts to higher pH. The shift may be expected, to a first approximation, to be equal to that for a similar increase in  $[Me_T]$  in ligand-free systems. If the ligand concentration is increased at constant pH while  $[Me_T]$  is constant, the free metal concentration decreases and the complexed metal concentration increases. The fractional adsorption of free metal increases, and that of complexed metal decreases. Depending on which species is dominant on the surface, total metal adsorption may increase or decrease slightly relative to that expected for the case of homeo-energetic surface sites. In any case, the effect of surface-site inhomogeneity is likely to be much smaller than that due to the difference in binding constants of the adsorbing species. Thus, the effect of surface-site inhomogeneity on metal adsorption in systems with metal-like complexes is to shift the fractional adsorption curve slightly, but probably not change its shape or its response to changes in other variables.

Fractional adsorption of ligand-like complexes is likely to be independent of their concentration. On multi-site surfaces fractional adsorption of uncomplexed metal decreases as metal concentration increases. Therefore, in a system consisting of

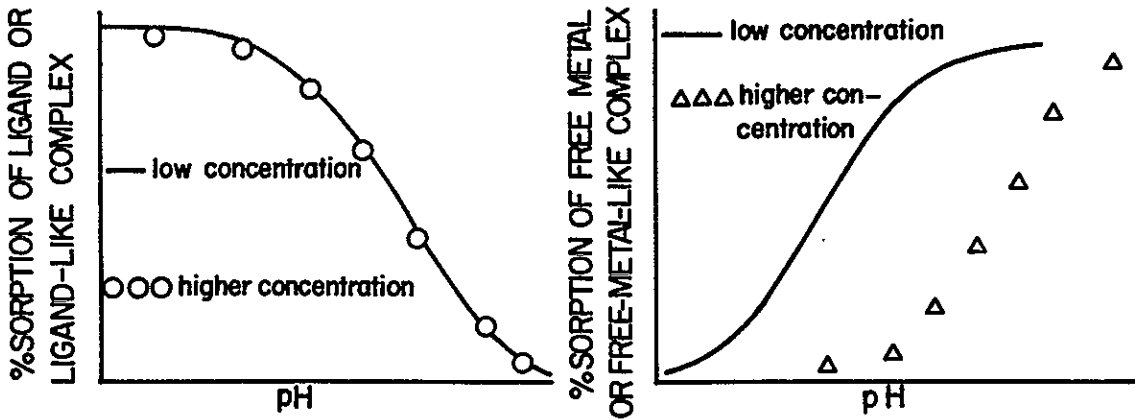


Figure 5-3. Expected dependence of adsorption edges for metals and ligands on total adsorbate concentration

9112051306

metal ions, ligand-like complexes, and an adsorbent with sites of non-uniform binding energies, fractional metal adsorption is dependent on total metal concentration only in the pH range where the uncomplexed metal is the dominant surface species (high pH). As a result, the pH at which fractional adsorption of uncomplexed metal equals that of complexed metal ( $pH_c$ ) is a function of total metal concentration. This can be demonstrated graphically (Figure 5-4). At  $pH = pH_c$  the curves of percent adsorbed vs. pH for the free and complexed species intersect. In Figure 5-4 this pH is labeled  $pH_{c,1}$  for the conditions  $(Me_T) = Me_1$ ,  $(L_T) = L_1$ . If free metal concentration is decreased either by decreasing total dissolved metal concentration or by adding a ligand, the curve for fractional adsorption of free metal shifts to lower pH but that for the complex is not affected. The intersection of the free metal and complexed metal adsorption curves ( $pH_{c,2}$ ) shifts to lower pH and greater fractional adsorption. Thus, the effect of surface-site inhomogeneities in systems with ligand-like complexes is that there no longer exists a pH at which fractional metal adsorption is independent of ligand concentration.

Typical plots of overall fractional metal adsorption vs. pH in systems with ligand-like complexes and non-homeoenergetic adsorbent surfaces can be generated based on the adsorption edges for the individual species, and are shown in Figure 5-5. The curves for total fractional metal adsorption do not intersect at a single point. The intersection of the curves for any two ligand concentrations is at a pH greater than  $pH_c$  for either of them. In addition, there is a region where total metal adsorption is not a monotonic function of ligand concentration. For instance, at the pH labeled  $pH^*$ , total metal adsorption increases as ligand concentration is increased from  $L_1$  to  $L_2$ , and then decreases as ligand concentration is further increased to  $L_3$ . The conclusion would be the same if ligand adsorption sites were not homeoenergetic.

Summarizing, surface-site inhomogeneity alters the quantitative aspects of the model somewhat, but most qualitative predictions are unaffected. For systems with ligand-like complexes, there exists a pH at which fractional metal adsorption is independent of ligand concentration only if metal-surface bond energies are approximately constant from site to site. For metal-like complexes, surface site inhomogeneity shifts the curve of fractional metal adsorption vs. pH to higher pH, but probably does not change its shape.

ii) The assumption that total available sites are not limiting is almost certainly valid for adsorption of the free metal or metal-like complexes. In all experiments

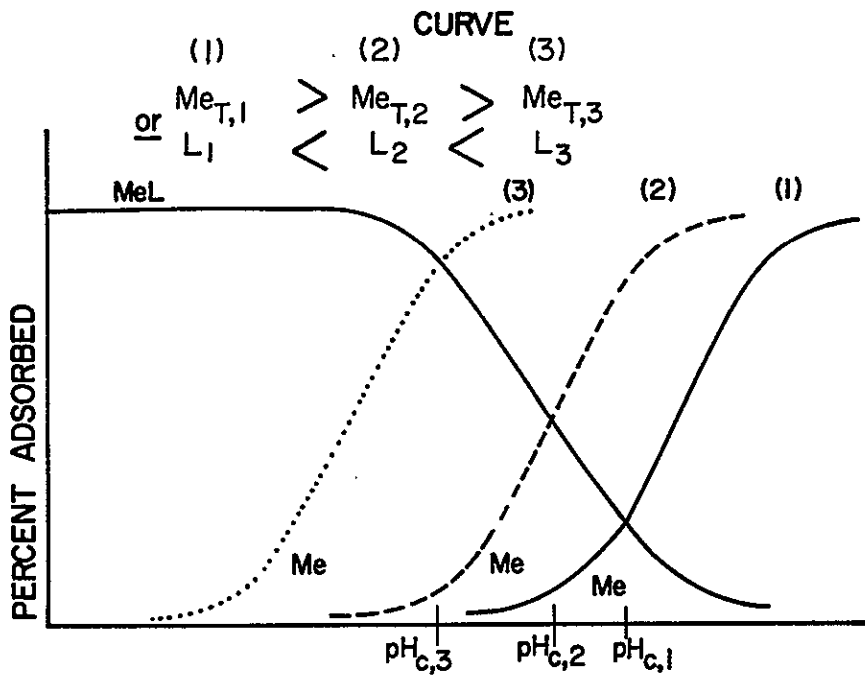


Figure 5-4. Effect of total metal concentration on pH

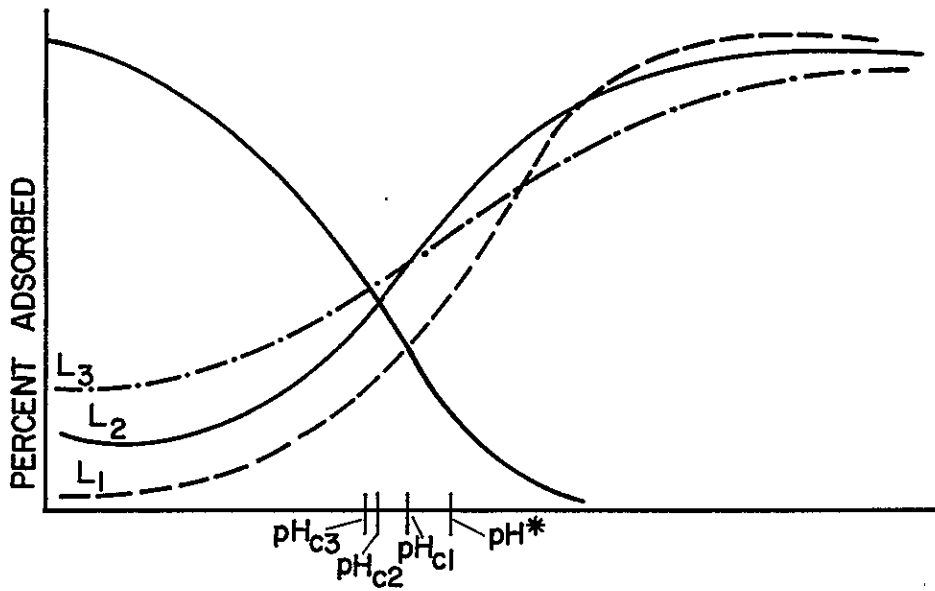


Figure 5-5. Total fractional metal sorption on non-homogeneous surfaces

91120511300

6  
0  
3  
1  
1  
5  
0  
2  
1  
1  
6

performed and in essentially all natural aquatic systems, the total trace metal concentration is much less than that of the total number of available adsorption sites. However in several experiments, free-ligand adsorption was probably site-limited. In particular, fractional adsorption of  $S_2O_3$  is significantly decreased at any pH in  $10^{-3}M$   $Fe(OH)_3$  suspensions if  $[S_2O_3]_T$  is greater than  $\sim 10^{-4}M$  (Figure 5-6). As noted earlier, site limitation generally decreases fractional ligand adsorption, even though absolute adsorption density increases. In such systems the availability of sites may limit adsorption of ligand-like complexes as well as that of free ligands. According to the model developed earlier, at low pH total fractional metal adsorption increases with decreasing pH due to adsorption of the complex. In a system which is site-limited for ligand and complex adsorption, the increase in metal adsorption at low pH is suppressed somewhat, and in extreme cases may not be evident at all. Other than this, site limitation does not alter the predicted adsorption behavior.

iii) If a charged species is specifically adsorbed the IEP of the solid shifts in a direction that opposes further adsorption (toward lower pH for an anion, higher pH for a cation). In the experimental systems, and most natural systems, trace metal concentrations are so low that their effect on the IEP of the solid is probably negligible. However, typical anionic ligand concentrations may significantly lower the pH of the IEP when they adsorb. For instance, Anderson et al. (2) found the IEP of amorphous aluminum hydroxide drops from pH 8.5 to pH 5.0 as  $\Gamma_{As}$  increases from  $8.9 \times 10^{-7}$  moles/m<sup>2</sup> to  $3.2 \times 10^{-6}$  moles/m<sup>2</sup> (assuming 500 m<sup>2</sup>/g am-Al(OH)<sub>3</sub>).

The effects of  $Cl^-$ ,  $SO_4^{2-}$ , and  $S_2O_3^{2-}$  on the IEP of oxides is expected to be much less severe than that of  $AsO_4^{3-}$ , since the specific adsorption energy of  $AsO_4^{3-}$  is much greater than that of the other ions (Table 4-2). Nevertheless, the anions were often present at relatively high concentrations and may have decreased the pH of the IEP significantly in the experimental systems. In such systems, the pH-adsorption edge for the ligand shifts to lower pH with increasing ligand concentration (Figure 5-7). This situation can be treated in an exactly analogous way to the decrease in fractional adsorption of metal with increasing metal concentration. If the fractional adsorption curve for the complex shifts significantly, fractional metal adsorption decreases with increasing ligand concentration at low pH. In addition, the pH of minimum adsorption decreases with increasing ligand concentration at low pH. In addition, the pH of minimum adsorption decreases and there is a region where fractional metal adsorption is not a monotonic function of ligand concentration. The potential effects of site limitation have already been discussed. Qualitative adsorption patterns are not altered.

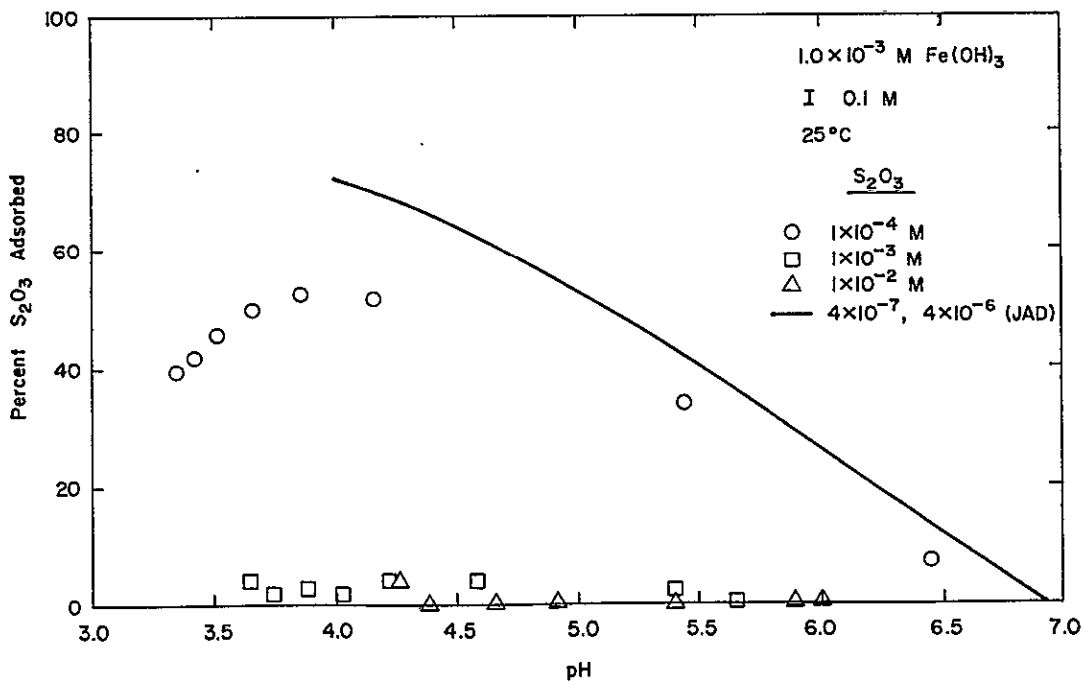


Figure 5-6. Effect of adsorbate concentration on adsorption edge in cases where site-limitation is suspected

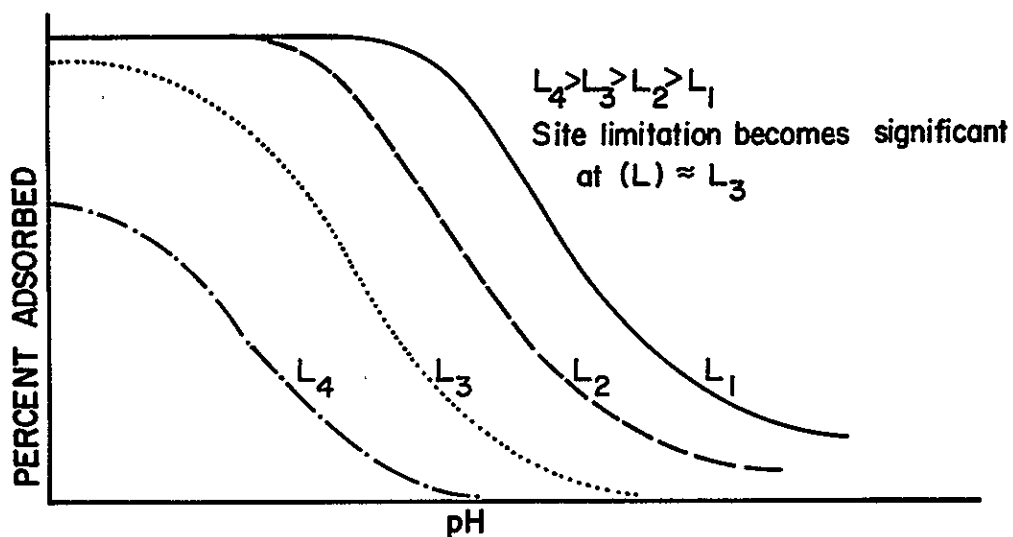


Figure 5-7. Effect of total adsorbate concentration on adsorption edge for ligands which significantly shift the IEP

91120511310

Assumption 3. The assumption that complexes adsorb by a single mechanism is a simplifying assumption that allows limiting cases to be analyzed more easily. Graphically, the assumption is that adsorption of the complex can be described by curve (A) or (B) below (Figure 5-8). If a complex can adsorb by either mechanism, curve (C) applies. In that case, total metal adsorption is that predicted by combining the two limiting cases of strictly ligand-like and strictly metal-like complex adsorption. Total metal adsorption is then the sum of the adsorption of the three surface species: free metal, ligand-like complex, and metal-like complex. The assumption that complexes adsorb by a single mechanism allows the more general case to be broken down into simpler, limiting cases for analysis. If this assumption is invalid, the analysis would be somewhat more complicated but the model would not require any major revision.

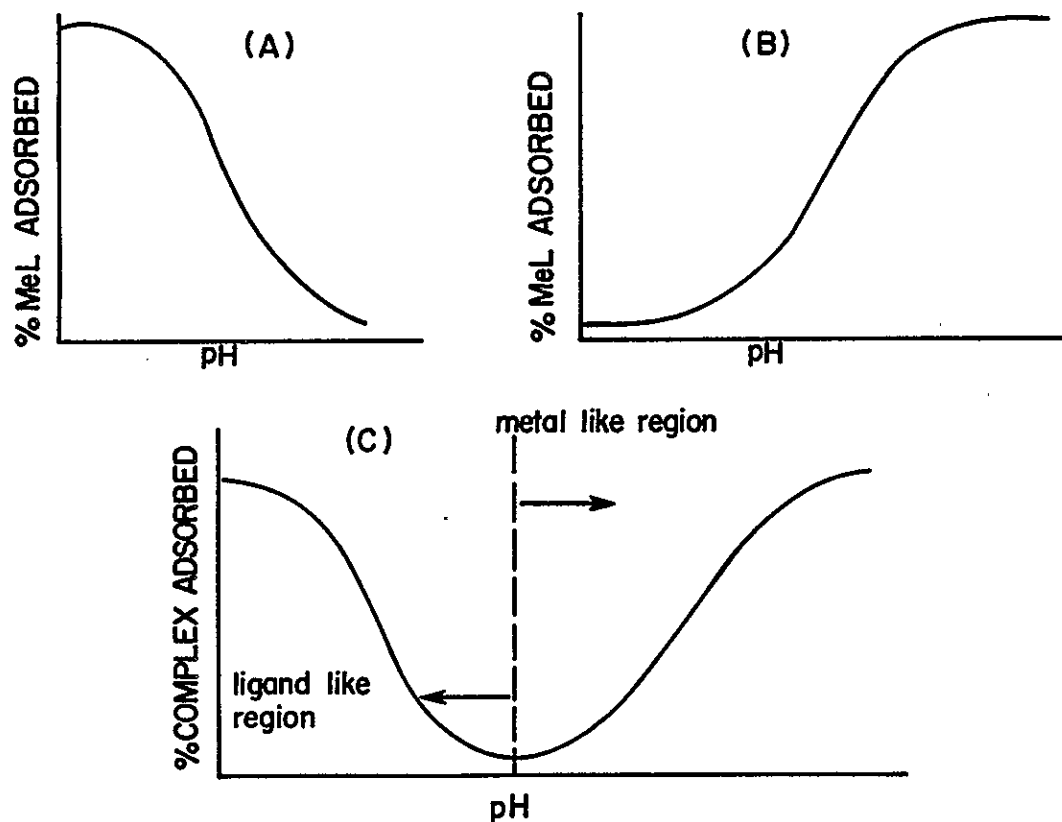


Figure 5-8. Adsorption edges for ligand-like, metal-like, and metal-or-ligand-like complexes

Assumption 4. Finally, the assumption that all protons originate at the surface is included strictly for mathematical simplicity. If metal ions hydrolyze in solution before adsorbing, the magnitude of the stability constants would change but neither the qualitative nor quantitative predictions of the model would be affected.

Table 5-2 summarizes the assumptions of the model, and their implications.

Table 5-2

Analysis of the Assumptions of the Proposed Model for Adsorption of Complexes

Assumption	Most Likely Deviation	Effects on Predicted Sorption Patterns
1. All $MeL_x$ complexes adsorb identically.	$MeL_1, MeL_2, \dots$ have different binding strengths to surface.	Analysis more complicated and quantitative predictions altered some; qualitative pattern probably not altered much.
2. Fractional sorption of a species independent of species concentration.	Surface site non-homogeneity.	For ligand-like complexes, $pH_m$ increased; region of non-monotonic relation between fractional metal sorption and ligand concentration appears; for metal-like complexes, adsorption edge shifts to higher pH with increasing metal concentration.
	Surface sites limiting.	Not likely to occur for metal-like complexes; decreases maximum sorption at low pH for ligand-like complexes.
	Shifting IEP with ligand concentrations.	Negligible effect on metal-like complexes; for ligand-like complexes, $pH_m$ decreases, metal sorption decreases some at low pH, but eventually attains 100% level; region of non-monotonic relation between metal sorption and ligand concentration appears.
3. Complexes sorb by only 1 mechanism.	Complexes can sorb in either metal-like or ligand-like fashion.	Analysis involves combining analysis for 2 limiting cases; no major effect.
4. Protons released all originate at surface.	Adsorption involves hydrolysis of metal.	Reaction equation changes somewhat; definition of equilibrium constant changes; no effect on adsorption patterns.

9112151312

### Summary of the Model

A model for the effects of ligands on metal adsorption has been developed. The assumptions used to derive it are reasonable, though somewhat oversimplified. The deviations from model behavior that would be expected if the assumptions are invalid have been discussed. The model can be summarized as follows:

1. Metal-ligand complexes have analogous pH dependence to either the free metal or the free ligand.
2. The magnitude of the adsorption equilibrium constant for the complex can be less than, equal to, or greater than that for the free metal or ligand. (The case of totally non-adsorbing complexes is a limiting case in which  $K_{MeL} = 0$ .)
3. If adsorption of the complex is similar to that of free metal:

- i) The percent adsorbed-pH curve is approximately parallel to that for the ligand-free system;
- ii) For a given ligand concentration, the ratio of adsorbed complex to adsorbed free metal is proportional to

$$(L)(H^+)^{x_0 - x_1} \frac{(EDL_1)}{(EDL_2)}$$

Thus, if  $x_0 \approx x_1$  and  $(L)$  and  $(EDL_1)/(EDL_2)$  are constant, the relative surface density of free and complexed metal is independent of pH. Based on experimental data  $x_0 = x_1$  for most of the systems studied. The condition that  $(L)$  is constant is met at pH more alkaline than the adsorption edge in systems that are not site-limited for ligands, and at any pH for systems in which ligand surface sites are nearly saturated. Most experimental systems fall in the latter category.

- iii) Increasing ligand concentration at a given pH has a monotonic effect on fractional adsorption until a maximum or minimum is reached, at which point increasing  $(L)$  further has no effect.
4. If adsorption of the complex is analogous to that of the free ligand:
    - i) The complex is the dominant surface species at low pH, and the free metal is dominant at high pH.
    - ii) There is a minimum in total fractional metal adsorption. Depending on solution conditions and surface-binding constants, the minimum may be anywhere from near zero to near 100 percent adsorbed.
    - iii) There is a pH ( $pH_c$ ) at which fractional adsorption of the complex and fractional adsorption of the free metal are equal. Near this pH, the slope of a plot of fractional metal adsorbed vs. pH decreases with increasing ligand concentration. At  $pH < pH_c$ , metal adsorption increases and at  $pH > pH_c$  metal

adsorption decreases as ligand concentration increases, if each species binds to a single site type. If surface-site inhomogeneity is significant or if ligand adsorption significantly shifts the IEP of the solid, there is a region where total metal adsorption is not a monotonic function of ligand concentration.

- iv) At very low and very high pH, nearly 100 percent of the metal is adsorbed, as complexed and free metal, respectively.

#### CORRELATION OF THE MODEL WITH EXPERIMENTAL RESULTS

The effects of  $\text{Cl}^-$ ,  $\text{SO}_4^{2-}$ , and  $\text{S}_2\text{O}_3^{2-}$  on cadmium and silver sorption on am- $\text{Fe}(\text{OH})_3$  are displayed in Figures 5-9 to 5-12. Similar plots for ligand effects in systems with other adsorbents are included in Appendix A. The results are summarized vis-à-vis the model in Table 5-3. In all systems containing  $\text{Cl}^-$  or  $\text{SO}_4^{2-}$  the pH adsorption edge for Cd or Ag is approximately parallel to that for the ligand-free system. Increasing ligand concentration monotonically decreases metal sorption. There is no evidence that the complex adsorbs in a ligand-like manner, but this may be due to the lack of experiments at sufficiently low pH.

Table 5-3

Characteristics of  $\text{CdL}_x$  and  $\text{AgL}_x$  Sorption on Various Adsorbents

Ligand Adsorbent	$\text{Cl}^-$		$\text{SO}_4^{2-}$		$\text{S}_2\text{O}_3^{2-}$	
	type <sup>a</sup>	strength <sup>b</sup>	type	strength	type	strength
$\alpha\text{-SiO}_2$	M	< Cd	M	< Cd	L	c
$\text{Fe}(\text{OH})_3$	M	< Cd	M	< Cd	L	> $\text{S}_2\text{O}_3$
$\alpha\text{-Al}_2\text{O}_3$	M	< Cd	M	< Cd	L	c
$\text{Fe}(\text{OH})_3$	M	< Ag	-	-	L	~ $\text{S}_2\text{O}_3$

<sup>a</sup>M = free metal-like, L = free ligand-like.  
<sup>b</sup>"< Cd" means complex sorbs, but less strongly than uncomplexed Cd.  
<sup>c</sup>Cannot be determined due to lack of information on sorption of free ligand.

The effect of thiosulfate on cadmium and silver adsorption is in all cases consistent with that predicted for ligand-like adsorption of the complex. Complexation

91120511314

of  $\text{Ag}^+$  with  $\text{S}_2\text{O}_3^{2-}$  in solution and at the surface is very strong. At low pH, when  $\text{S}_2\text{O}_3^{2-}$  does not adsorb, the dissolved ligand competes well with the surface for  $\text{Ag}^+$  ions, and overall Ag adsorption is consistent with the hypothesis that the complex does not adsorb in the high pH region. That is,  $\text{Ag}(\text{S}_2\text{O}_3)_x^{1-2x}$  complexes can strongly sorb in a ligand-like fashion, but cannot adsorb at all in a metal-like fashion.

Similarly,  $\text{Cd}(\text{S}_2\text{O}_3)_x^{2-2x}$  complexes can sorb only in a ligand-like manner. Complexation of Cd in solution and at the surface by  $\text{S}_2\text{O}_3^{2-}$  is much weaker compared to Ag. When  $\text{Fe}(\text{OH})_3$  is the adsorbent, pH regions where complex and free metal adsorption dominate are both evident. For each metal, in the lower pH range, total Me adsorption increases with increasing  $\text{S}_2\text{O}_3^{2-}$  concentration, while at higher pH it decreases. Consistent with the model for ligand-like complexes, plots of fractional Cd sorption vs. pH become progressively less steep as  $\text{S}_2\text{O}_3^{2-}$  is added to the system. The surface- $\text{Cd}(\text{S}_2\text{O}_3)_x$  bond is stronger than that of the surface-free ligand bond. This is evident from a comparison of the adsorption of the complex with that of the free ligand. In a metal-free system containing  $10^{-2}\text{M}$   $(\text{S}_2\text{O}_3)_T$  ( $\text{Fe}(\text{OH})_3 = 10^{-3}\text{M}$ ), less than 5 percent of the thiosulfate adsorbs at any pH (Figure 5-6). When  $5 \times 10^{-7}\text{M}$   $\text{Cd}_T$  is added, approximately 20 percent of the cadmium sorbs at  $\text{pH} = 5.5$  (Figure 5-10). Since under these conditions adsorption of free Cd is negligible, and essentially all of the dissolved Cd is complexed,  $\text{Cd}(\text{S}_2\text{O}_3)_x$  is presumably adsorbing. Since 20 percent of the ligand-like complex must be more strongly adsorbed, i.e., the complex has greater specific sorption energy, there is no pH at which fractional sorption is independent of ligand concentration, which is expected for inhomogeneous surfaces. Accordingly, there is a region ( $\text{pH} 6.0 \pm 0.3$ ) in which metal adsorption is not a monotonic function of ligand concentration. The predicted increase to near 100 percent metal adsorption at low pH is not evident. Possibly such a trend would be observed at  $\text{pH} < 5.0$ . However, it is more likely that adsorption of the complex is site-limited at low pH, in which case 100 percent metal removal is not expected. Adsorption of the free ligand is clearly site-limited under these conditions. Metal adsorption does increase to near 100 percent in analogous systems containing silver instead of cadmium, and in which free ligand adsorption is apparently not site-limited (Figure 5-11). On  $\alpha\text{-SiO}_2$ , which is strongly negatively charged in the pH range investigated ( $\text{pH} > \text{IEP} + 2$ ) the results are consistent with the prediction that only free Cd, and no complexed species adsorbs. (Recall that the relationship between the adsorption edge and the IEP is a controllable parameter and the presumption that anions do not adsorb at  $\text{pH} > (\text{IEP} + 2)$  is a rule-of-thumb for "typical" systems and is not a principle of anion adsorption.) On  $\gamma\text{-Al}_2\text{O}_3$ , (PZC  $\sim 8.0$  in pure systems)  $\text{Cd-S}_2\text{O}_3^{2-}$  complexes adsorb more

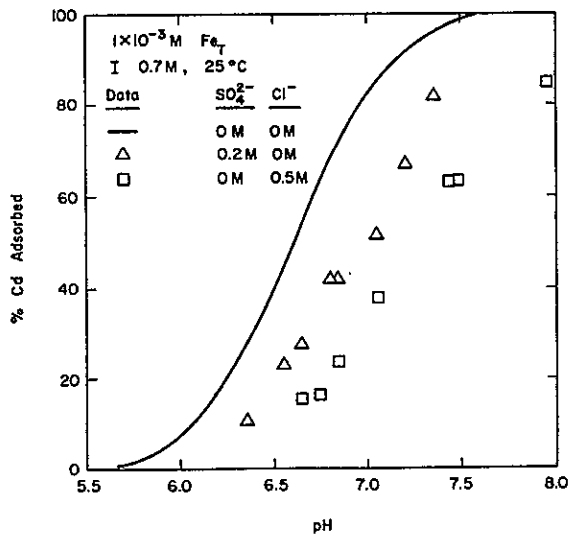


Figure 5-10a. Effects of  $\text{SO}_4^{2-}$  and  $\text{Cl}^-$  on Cd adsorption

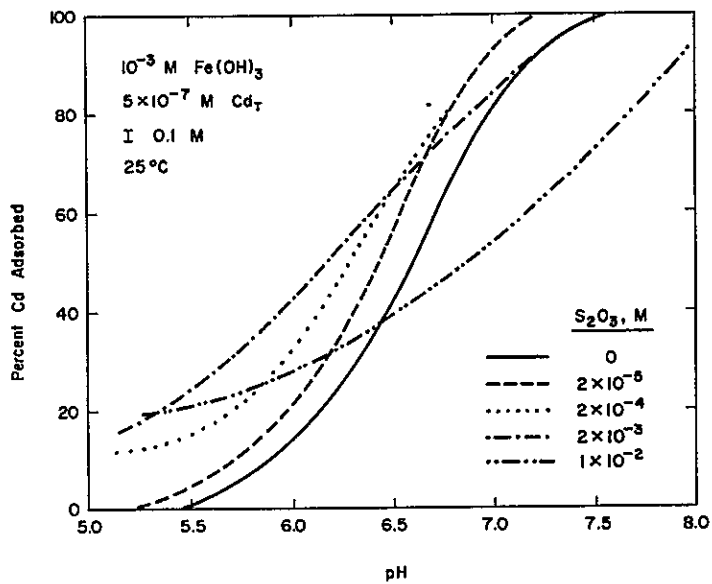


Figure 5-10b. Effects of  $\text{S}_2\text{O}_3^{2-}$  on Cd adsorption

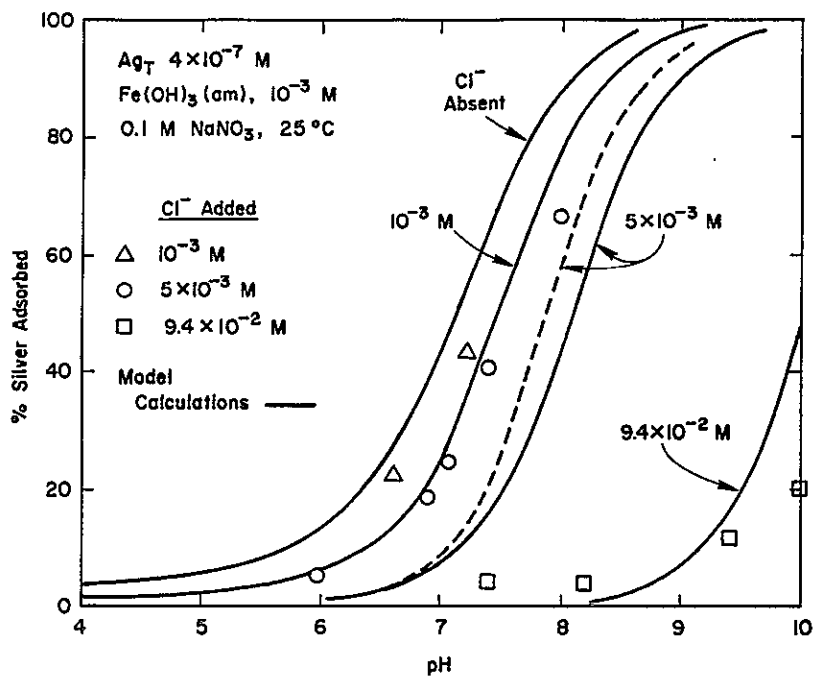


Figure 5-11. Effects of  $Cl^-$  on Ag adsorption

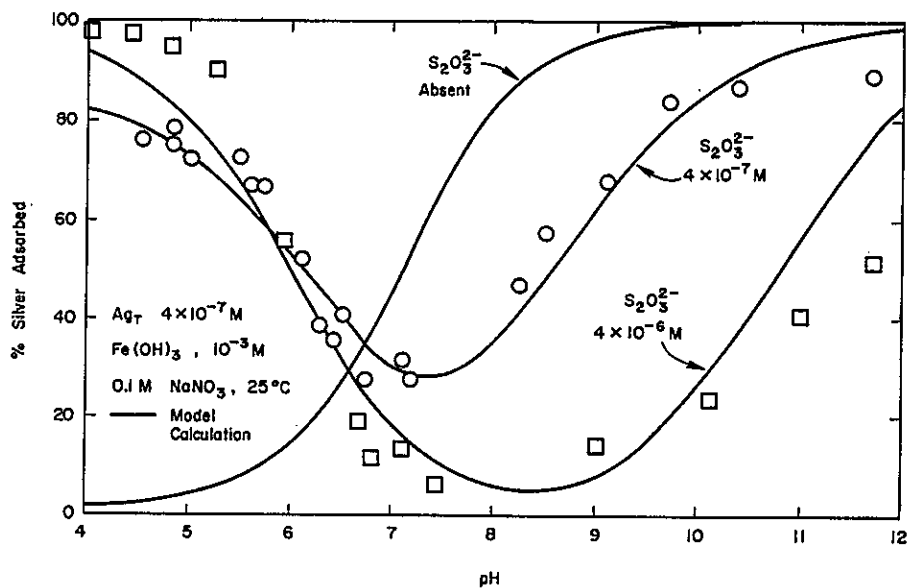


Figure 5-12. Effects of  $S_2O_3^{2-}$  on Ag adsorption

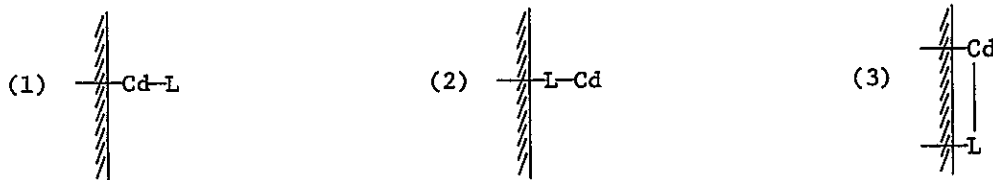
strongly than free Cd in the range  $5.5 \leq \text{pH} \leq 7.5$ . Adsorption of Cd at constant pH increases as  $[\text{S}_2\text{O}_3]_{\text{T}}$  increases from 0 to  $2 \times 10^{-3}\text{M}$  to  $1 \times 10^{-2}\text{M}$ . Adsorption of Cd at  $[\text{S}_2\text{O}_3]_{\text{T}} = 2 \times 10^{-4}$  is approximately equal to that at  $[\text{S}_2\text{O}_3]_{\text{T}} = 2 \times 10^{-3}\text{M}$ . This may be due to specific adsorption of free  $\text{S}_2\text{O}_3^{2-}$ . As  $\Gamma_{\text{S}_2\text{O}_3^{2-}}$  increases at constant pH, the IEP shifts to lower pH, partially counteracting the tendency for ligands and ligand-like complexes to adsorb.

Thus, all the results for the effects of  $\text{SO}_4^{2-}$ ,  $\text{Cl}^-$ , and  $\text{S}_2\text{O}_3^{2-}$  on Cd and Ag adsorption on the three adsorbents can be explained by the model described earlier.

#### STEREOCHEMISTRY OF ADSORBED COMPLEXES

An interesting conclusion to be drawn is that adsorptive behavior of a complex is apparently independent of the adsorbent. That is,  $\text{CdCl}_x$  and  $\text{Cd}(\text{SO}_4)_x$  complexes always adsorb in ligand-like fashion for the solids studied. In addition, the adsorptive behavior of chloro- and thiosulfato-complexes is the same when Cd is the metal as when Ag is. The difference between metal-like and ligand-like complexes may be attributable to different orientations of the complexes at the surface, which may in turn be partially explained by coordination chemistry.

There are at least three possible conformations for adsorbed complexes, pictured below:



(The following discussion describes adsorption of Cd complexes. It applies equally well to complexes of Ag or any other metal.) If net molecular charge were the dominant factor controlling sorption of the complex, one could explain the adsorptive behavior of a metal simply from its speciation in solution. For instance, one would then expect  $\text{CdCl}^+$  to be a metal-like and  $\text{CdCl}_3^-$  to be a ligand-like adsorbate. Table 5-4 shows dissolved speciation of cadmium in the systems studied; e.g.,  $\text{Cd}(\text{S}_2\text{O}_3)_x$ , adsorb similarly to anions even when the net charge on the dominant dissolved species is zero ( $\text{CdS}_2\text{O}_3^0$ ) and the average charge is positive. It is likely, therefore, that for these complexes direct surface-to-ligand bonds control adsorptive behavior. This eliminates configuration (1) as a probable orientation for ligand-like complexes. Similarly,  $\text{CdCl}_x$  and  $\text{Cd}(\text{SO}_4)_x$  exhibit metal-like adsorption

9112051513

Table 5-4

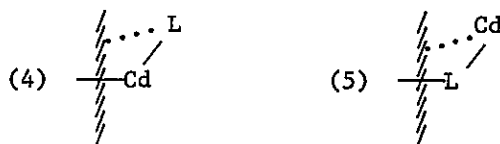
## Speciation of Dissolved Cadmium in Systems Containing Various Ligands

Ligand	Concentration	Percent Total Cadmium Activity As <sup>a</sup>					Average Charge per Cd ion
		Cd <sup>2+</sup>	CdL <sub>1</sub>	CdL <sub>2</sub>	CdL <sub>3</sub>	CdL <sub>4</sub>	
SO <sub>4</sub> <sup>2-</sup>	0.2M	4	49	47	0	0	-0.86
Cl <sup>-</sup>	0.1M	9	64	25	2	0	+0.78
Cl <sup>-</sup>	0.5M	1	29	50	17	3	+0.08
S <sub>2</sub> O <sub>3</sub> <sup>2-</sup>	3 x 10 <sup>-4</sup> M	51	48	1	0	0	+1.00
	1 x 10 <sup>-3</sup> M	24	71	5	0	0	+0.38
	3 x 10 <sup>-2</sup> M	8	74	18	0	0	-0.20
	1 x 10 <sup>-2</sup> M	2	56	42	0	0	-0.80
	0.3M	0	29	71	0	0	-1.42

<sup>a</sup>Hydroxo-complexes, which are unimportant at pH < 9, are excluded. Activity coefficients calculated from the Debye-Hückel Equation.

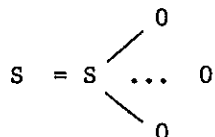
when the dominant dissolved species are uncharged or anionic. For these complexes, configuration (2) is highly improbable.

Complexes having orientation (3), by virtue of having two surface-to-complex bonds (i.e., forming a bi-dentate surface complex) probably adsorb more strongly than either free metal or free ligand. There also exist intermediate structures such as:



Structures (4) and (5) would have greater adsorptive strength than (1) and (2), respectively, but less than (3). Structure (3) or (5) may explain the extra specific adsorption energy of Cd(S<sub>2</sub>O<sub>3</sub>)<sub>x</sub> relative to free S<sub>2</sub>O<sub>3</sub><sup>2-</sup>. Since CdCl<sub>x</sub> and Cd(SO<sub>4</sub>)<sub>x</sub> complexes generally adsorb less strongly than free Cd, there is no evidence that these complexes are multidentate with the surface. However, orientations like (3) and (4) cannot be ruled out as possibilities for metal-like complexes.

The preferred conformation of an adsorbed molecule is related to the bond strengths of the constituent groups, i.e., the more energetic bond will form preferentially. The specific adsorption energy of most metals is greater than that of most ligands. However, if complexation decreases the driving force for forming a metal-surface bond much more than that for a ligand-surface bond, the adsorbed complex will orient with the ligand facing the surface. Thiosulfate ion can be thought of as a sulfate ion joined by a double bond:



When  $S_2O_3^{2-}$  adsorbs to an oxide, the most likely orientation is with the oxygen atom bonding to surface metal ions. However, metal ions generally bond to the sulfide end of the ligand:  $O_3S-S-Me$ . Thus, complexation of the metal has a relatively minor effect on the surface-active part of the  $S_2O_3^{2-}$  ion. The affinity of the Cd or Ag ion for the surface is decreased by complexation. Apparently, formation of the complex sufficiently destabilizes the surface bond that the free-energy change accompanying adsorption is greatest if the  $S_2O_3^{2-}$  group, rather than the metal, faces the surface. Thus, with sufficient information about the structural and coordination chemistry of a complex, it may be possible to predict which orientation it will prefer at an oxide/aqueous solution interface. Until such predictions are possible, a tentative generalization can be made that complexed metal-ion-adsorption patterns are independent of the identity of the oxide adsorbent. In addition there is at least preliminary evidence that the orientation of a complex depends primarily on the identity of the ligand and not on the metal. Such generalizations may be of great value in predicting metal adsorption in complex systems for which direct experimental information is limited or non-existent.

#### SUMMARY

In summary, it appears that complexed metal ions can adsorb to oxide surfaces with either the metal or the ligand bonding directly to the surface. The effect of a given ligand does not vary much from one adsorbent to the next.

If the ligand end of the complex is surface-bound, sorption of the complex can be modeled as a function of the speciation in solution, concentration and surface characteristics of the solid, and solution pH. As ligand concentration increases,



metal adsorption increases in one pH range and decreases in a higher pH range. A plot of fractional metal adsorption vs. pH has a region where the slope decreases with increasing ligand concentration. Outside this pH region, if there is no site-limitation fractional metal sorption is near 100 percent, and there is therefore a pH at which sorption attains a minimum. Surface speciation is highly pH-dependent.

If the metal end of the complex is surface-bound, the fractional sorption vs. pH curve is approximately parallel to that for the ligand-free system and is usually shifted to higher pH. Theoretically the pH-adsorption edge may shift to lower pH, but no such system has been found experimentally. In these systems, surface speciation is weakly pH-dependent, if at all.

Adsorption of chloro- and sulfato-complexes of cadmium and chloro-complexes of Ag is analogous to that of free metal, but adsorption of thiosulfato-complexes is more like that of free ligand. The differences among the complexes may be due to differences in the stereochemical arrangement at the surface. Specifically, it is proposed that  $\text{CdCl}_x$ ,  $\text{AgCl}_x$ , and  $\text{Cd}(\text{SO}_4)_x$  complexes bond with the metal closer to the surface, while  $\text{S}_2\text{O}_3^{2-}$  complexes generally bond with the ligand closer to the surface. The different orientations of various complexes can be explained by consideration of structural factors and coordination chemistry. Further experimentation and characterization of the surface will be required before the surface conformation of a given metal-like complex can be predicted a priori.

With the information provided by the studies of  $\text{SO}_4^{2-}$ ,  $\text{Cl}^-$ , and  $\text{S}_2\text{O}_3^{2-}$  effects on Me adsorption on several oxide surfaces, the basis for predicting which metal-ligand complexes will adsorb, and to what extent, has been established. After some more detailed studies of the surface-to-complex bonding mechanisms, it may be possible to predict surface orientation and pH-adsorption patterns for complexes a priori.

#### REFERENCES

1. P. V. Avotins. "Adsorption and Coprecipitation Studies of Mercury on Hydrrous Iron Oxides." Ph.D. Thesis, Stanford University, Stanford, Calif., 1975.
2. M. A. Anderson, J. F. Ferguson and J. Garvis. "Arsenate Adsorption on Amorphous Aluminum Hydroxide." J. Coll. Interface Sci., 54, 391 (1976).

## Section 6

### LABORATORY STUDIES WITH COAL-FIRED POWER PLANT WASTE STREAMS

#### GENERAL DISCUSSION OF POWER PLANT WASTES

##### Introduction

Steam-electric power plants, and coal-fired power plants in particular, produce many wastes. These wastes are contained in solid, liquid and gaseous forms. Trace elements can be found in almost all of these wastes; in some of the wastes the concentration levels of trace elements could cause harm to the environment if improperly released. As indicated in the previous sections, of particular interest is the removal of these trace elements when found in liquid wastes; specifically boiler-cleaning wastes and water which has been in contact with fly ash (fly-ash transport water).

While the previous sections have dealt with the removal of certain trace elements from clean, model systems using an adsorption process, this section will present and discuss the removal of trace elements from real wastes, that is boiler-cleaning wastes and fly-ash transport water. Because there are numerous other types of waste-water streams produced in coal-fired power plants, a literature review is presented first concerning the types of waste streams, their characteristics, and removal processes currently being applied. A comparison is drawn between literature information and the studies presented in this section. Brief mention is also made concerning the effectiveness and economics of the literature information in comparison to the adsorption coprecipitation processes evaluated in this study.

##### Review of Power Plant Wastes

Table 6-1 presents a list of estimated quantities associated with a number of waste-streams produced at coal-fired power plants: these include frequency, major pollutants, and typical treatment processes. A large range of values is associated with some of the quantity estimates. These large ranges occur because the data set from which they were derived included power plants of widely varying sizes and characteristics; the values without ranges are estimates associated with a typical 100 MW generating

Table 6-1

TYPICAL WASTE STREAMS FROM COAL-FIRED POWER PLANTS<sup>a</sup>

Waste Stream	Quantity	Frequency	Major Pollutants	Treatment Processes
Cooling tower blowdown.	20-7200 $\times 10^3$ GPD. <sup>1</sup>	Continuous.	Zinc, chromate, phosphate, organic biocides, copper, residual chlorine.	Chromate reduction to Cr(III). Precipitation for zinc(II), chromium(III), phosphate. Carbon adsorption for organics.
Recirculating ash-handling water. Blowdown (both bottom and fly ash).	300 GPD/ MW. <sup>2</sup>	Continuous.	Nickel, zinc, chromium, copper, lead, arsenic, cadmium, selenium.	Ponds for treatment through sedimentation, chemical precipitation and adsorption.
Boiler blowdown.	100 GPD/ MW. <sup>2</sup>	Continuous.	Possibly alkalinity TDS or EDTA, but overall quality is high.	Generally does not require treatment, may be discharged to ponds or mixed with miscellaneous wastes.
Evaporator blowdown.	0.1-1060 $\times 10^3$ GPD. <sup>1</sup>	300-365 cycles <sup>2</sup> per year.	High in TDS.	Reuse within plant for applications not requiring low TDS water.
Ion-exchange regeneration wastes.	88 GPD/ MW. <sup>2</sup>	52-365 cycles <sup>1</sup> per year.	Usually very low (H <sub>2</sub> SO <sub>4</sub> ) or very high (NaOH) pH; also very high in TDS and 20-200 ppm of Cu, Fe, and Zn.	Neutralization to 6.0-9.0 and use throughout plant or use as low-grade acid or caustic.
Boiler cleaning	3-5 boiler volumes. <sup>1</sup> 4 GPD/ MW. <sup>2</sup>	Once/7 mos. <sup>1</sup> to Once/100 mos.	Copper, ammonia, EDTA, zinc, chromium, selenium, nickel, iron.	Ammonia oxidation followed by heavy metal precipitation.  Treatment in ash ponds. Incineration, especially for EDTA containing waste. Disposal by chemical cleaning contractor.

Table 6-1 cont.

Table 6-1 continued

Waste Stream	Quantity	Frequency	Major Pollutants	Typical Treatment Processes
Fireside cleaning.	24-270 x 10 <sup>3</sup> gal. <sup>1</sup> 5 GPD/ MW. <sup>2</sup>	2-8/year. <sup>1</sup>	Alkaline solutions containing containing high TDS, TSS, zinc, iron, nickel, chromium.	Usual procedure is to discharge to ash ponds.  Sometimes coagulation, settling and filtration is done with low-TDS water returned for in-plant use.
Air-preheater cleaning.	43-600 x 10 <sup>3</sup> gal. <sup>1</sup> 100 GPD/ MW. <sup>2</sup>	4-12/year. <sup>1</sup>	Essentially same metals as boiler cleaning except more iron, copper, nickel, chromium; also oily wastes and polynuclear hydrocarbons, alkaline detergents.	Same treatment method as for boiler tube and fireside cleaning.
Coal-pile runoff.	17-27 x 10 <sup>6</sup> gal/ year.	Dependent on rainfall.	Acidic wastes containing sulfates, aluminium, zinc, copper, cadmium, beryllium, nickel, chromium, silver, uranium, and lead.	Sedimentation. Neutralization, coagulation, settling and filtration before discharge or plant use.
Floor and yard drains.	-- 30 GPD/ MW. <sup>2</sup>	Dependent on cleaning and rainfall.	Phosphates, oil, and phenols.	Ash ponds.
Miscellaneous waste including sanitary wastes.	3.22 GPD/ MW. <sup>2</sup>	Continuous.	BOD/COD, pathogens.	Sewage treatment plant and then to ash ponds.

<sup>a</sup>Data derived from References 1 and 2, as indicated by superscript number.

unit, which may or may not actually represent a real plant, because of the great variety of operating modes possible. Given this background it is apparent that some wastes are produced in much greater quantities than others. For instance, the production of cooling-tower blowdown waste may be as much as six orders of magnitude greater than that of boiler cleaning wastes and the production of recirculating ash-handling water blowdown is probably about one hundred times greater than the waste volume produced during boiler cleaning.

Of major importance is the large variation in frequency of waste production. Some wastes are produced continuously, others almost daily, in a batch mode. The wastes in boiler-cleaning operations may be produced as infrequently as once every 2-3 years. In general, the larger volume wastes are produced continuously while the smaller volume wastes are produced infrequently. This enables plant operators to store such wastes as those from waterside and fireside boiler-cleaning for later treatment.

Another aspect of the data in Table 6-1 is the absence of numerical data on the constituents present in these wastes. This absence is primarily due to the difficulty in obtaining data on many of these wastes in the open literature, as very little recent work has been done on these types of waste. Also the variations in waste constituents caused by different operating procedures, different coals, different cleaning compounds, etc., make general analysis less meaningful. In general, it appears that trace elements are found in almost all of the effluents to some degree. Table 6-2 lists the possible concentrations of selected constituents found in typical cooling-tower inhibitor systems. Table 6-3 gives a list of the concentrations of some constituents found in the fly-ash handling water (non-recirculating system) at one plant site.

Again, as far as treatment of these wastes is concerned, it is very difficult to identify the best treatment process for a particular waste because the quality and quantity of the waste and the end use of the treated water vary from plant to plant. However, it can be said that precipitation is the favored method for removing trace elements that are highly insoluble at higher pHs and that efforts are usually made to 1) eliminate compounds that form soluble complexes and 2) reduce the concentrations of interfering ions that increase pollutant solubilities. Other considerations (3) appear to be to 1) omit flows with pollutant concentrations lower than the concentration in equilibrium with the precipitate formed; 2) reduce the waste water volumes requiring treatment; 3) control conditions to

Table 6-2

## WASTE DISPOSAL CHARACTERISTICS OF TYPICAL COOLING TOWER INHIBITOR SYSTEMS

Inhibitor System	Concentration in Recirculating Water, mg/l
Chromate only	200-500 as $\text{CrO}_4$
Zinc	8-35 as Zn
Chromate	17-65 as $\text{CrO}_4$
Chromate	10-15 as $\text{CrO}_4$
Phosphate	30-45 as $\text{PO}_4$
Zinc	8-35 as Zn
Phosphate	15-60 as $\text{PO}_4$
Zinc	8-35 as Zn
Phosphate	15-60 as $\text{PO}_4$
Organic	3-10 as organic
Organic only	100-200 as organic 10 est. as BOD 100 est. as COD 50 est. as $\text{CCl}_4$ extract 5 est. as MBAS
Organic Biocide	30 as chlorophenol 5 as sulfone 1 as thiocyanate
Source: (1).	

Table 6-3

CHARACTERISTICS OF ONCE-THROUGH ASH POND DISCHARGES<sup>a</sup>

	Fly-Ash Pond			Bottom Ash Pond		
	Min.	Ave.	Max.	Min.	Ave.	Max.
Flow (gpm) <sup>b</sup>	3100	6212.5	8800	4500	16152	23000
Total alkalinity (as CaCO <sub>3</sub> )	-	-	-	30	85	160
Phen. alkalinity (as CaCO <sub>3</sub> )	0	0	0	0	0	0
Conductivity (umhos/cm)	615	810	1125	210	322	910
Total hardness (as CaCO <sub>3</sub> )	185	260.5	520	76	141.5	394
pH	3.6	4.4	6.3	4.1	7.2	7.9
Dissolved solids	141	508	820	69	167	404
Suspended solids	2	62.5	256	5	60	657
Aluminum	3.6	7.19	8.8	0.5	3.49	8.0
Ammonia (as N)	0.02	0.43	1.4	0.04	0.12	0.34
Arsenic	<0.005	0.010	0.023	0.002	0.006	0.015
Barium	0.2	0.25	0.4	<0.10	0.15	0.30
Baryllium	<0.01	0.011	0.02	<0.01	<0.01	<0.01
Cadmium	0.023	0.037	0.052	<0.001	0.0011	0.002
Calcium	94	136	180	23	40.12	67
Chloride	5	7.12	14	5	8.38	15
Chromium	0.012	0.067	0.17	<0.005	0.009	0.023
Copper	0.16	0.31	0.45	<0.01	0.065	0.14
Cyanide	<0.01	<0.01	<0.01	<0.01	<0.01	<0.01
Iron	0.33	1.44	6.6	1.7	5.29	0.11
Lead	<0.01	0.058	0.2	<0.01	0.016	0.031
Magnesium	9.4	13.99	20	0.3	5.85	9.3
Manganese	0.29	0.48	0.63	0.07	0.16	0.26
Mercury	<0.0002	0.0003	0.0006	<0.0002	0.0007	0.0026
Nickel	0.06	1.1	0.13	0.05	<0.059	0.12
Total phosphate (as P)	<0.01	0.021	0.06	<0.01	0.081	0.23
Selenium	<0.001	0.0019	0.004	<0.001	0.002	0.004
Silica	10	12.57	15	6.1	7.4	8.6
Silver	<0.01	<0.01	<0.01	<0.01	<0.01	<0.01
Sulfate	240	357.5	440	41	48.75	80
Zinc	1.1	1.51	2.7	0.02	0.09	0.16

<sup>a</sup>Source: (2).<sup>b</sup>Units are mg/liter unless otherwise indicated.7  
6  
3  
1  
1  
5  
0  
7  
1  
1  
6

increase the proportion of the pollutants in the ionic form required for the precipitation reactions; 4) avoid conditions that will produce harmful amounts of gases; 5) select a process that will give the lowest practicable or economically achievable amounts of pollutants in the effluent, up to and including no discharge of pollutants; and 6) select a process that will produce a sludge that can be disposed of in accordance with environmental considerations. As Table 6-1 suggests, adsorption/coprecipitation processes of the type examined in this work do not appear to be in use for trace element removal.

## WASTES AND WASTE CHARACTERISTICS

### Characterization of the Fly Ashes

Three different fly-ash materials were used to prepare synthetic fly-ash slurry waters for experimental purposes. Table 6-4 presents the chemical composition of the fly ashes used in this study. The analysis (by emission spectrograph) indicates a close correspondence between fly ashes 1 and 2, both from the same Eastern coal source. Fly ash 3 is derived from a Western coal source and has important composition differences from fly ashes 1 and 2 in some of the minor and trace elements (Ba, Co, Cr, Cu, Mo, Sr, and V). In addition, there are undoubtedly differences between these fly ashes in particle size distribution, surface area, morphology, and chemical reactivity. These aspects have not been considered in this study.

### Preparation and Handling of Fly-Ash Solutions

The fly-ash-derived solutions used in this study were prepared by mixing the appropriate fly ash with deionized water in 5-gal plastic containers such that a 100-g/l fly-ash solution was produced. These solutions were then mixed for four days and then allowed to settle for two days; at all times the containers were open to the atmosphere. After settling, the supernatant was siphoned off into 18-liter carboys and stored for later analysis and experimental use. The slurry concentration of 100 g/l was chosen to represent average concentrations expected in fly-ash-handling operations (4).

### Preparation and Handling of Power Plant Wastes

The three power plant wastes, acid-iron, bromate, and vertan, were produced at and collected from the Marshall Power Station of Duke Power Company, Charlotte, North Carolina, in March 1978. After arrival at Stanford, these wastes were stored undiluted, at room temperature, in the original 5-gal plastic containers until samples were needed for analysis or other experimental work. At that time, the required aliquots of waste were drawn directly from the original containers.

Table 6-4

## CHEMICAL COMPOSITION OF FLY ASHES USED IN STUDY

Elemental Composition (Dry, whole ash basis)	Fly Ashes <sup>a</sup>		
	1.	2.	3.
<u>Major Elements (%)</u>			
Si	30	31	30
Al	12	12	10
Fe	4.2	4.2	1.7
Ca	1.1	1.1	2.9
Mg	0.56	0.57	0.77
Na	0.43	0.44	0.70
K	2.4	2.5	0.73
Ti	0.96	1.0	0.41
P	0.24	0.20	0.45
<u>Minor and Trace Elements (ppm)</u>			
Ag	0.79	0.81	0.3
As	<100	<100	<100
Au	1.2	0.50	<0.5
[REDACTED]	213	208	>214
[REDACTED]	790	765	2350
Be	18	17	4.6
Bi	<10	<10	5.9
Cd	<2	<2	<2
[REDACTED]	180	186	122
Co	62	61	5.6
[REDACTED]	166	161	21
[REDACTED]	185	185	46
Ga	50	48	16
Hg	<500	<500	<500
La	98	100	73
Li	285	286	84
Mn	236	258	<200
Mo	22	21	4.8
Nb	38	39	19
[REDACTED]	132	126	14
Pb	73	86	25
Re	<50	<50	<50
Sb	<100	<100	<100
Sc	44	43	12
[REDACTED]	210	208	200
Sn	4.5	3.9	5.9
Sr	665	563	1300
Te	<50	<50	<50
Tl	<10	<10	<10
[REDACTED]	324	318	53
W	<100	<100	<100
Y	90	88	40
Zn	39	49	<10
[REDACTED]	402	405	500

<sup>a</sup>Fly ashes 1 and 2 from Duke Power Company, Charlotte, North Carolina; fly ash 3 from Public Service Company of Colorado, Arapahoe Station.

### Analysis of Selected Constituents in Power Plant Wastes

The analysis for sulfate, alkalinity, chloride, sodium, potassium, magnesium, and calcium followed the procedures outlined in Standard Methods (5) for those constituents. Analysis for the trace elements [REDACTED] and [REDACTED] was done by atomic absorption spectrophotometry. A Sargeant-Welch pH meter was used to measure pH. Ammonia was measured with an ammonia probe and an Orion Research No. 901 microprocessor analyzer. A Beckman portable conductivity meter was used to measure conductivity. Determination of ferrous and ferric iron concentrations was accomplished with a modification of the ferrozine spectrophotometric method.

### Characteristics of the Fly Ash, Bromate, Vertan, and Acid-Iron Wastes

As noted previously, the power plant wastes chosen for this study included wastes from the waterside boiler-cleaning and fly-ash-handling operations. Although a general characterization of these wastes was presented above, a more detailed characterization of these wastes is necessary to understand and interpret the experiments discussed below. Table 6-5 lists values of the selected major and trace elements measured in these wastes. There is a considerable difference in constituent make-up between the fly ashes and the boiler-cleaning wastes, as well as substantial differences within these two groups.

A characteristic of the boiler-cleaning wastes is the relatively high pH of the vertan and bromate solutions compared to the acid-iron waste solution. The acid-iron waste has relatively high levels of chloride, iron, copper, zinc, chromium, and nickel, while the bromate and vertan wastes both have high concentrations of alkalinity, ammonia, selenium, and nickel. The bromate solution has a high copper concentration and a low zinc concentration while the vertan solution has copper and zinc concentrations present in the opposite order. Cadmium, chromium, and arsenic levels are low in both bromate and vertan solutions. If one compares the data in Table 6-5 for the bromate and acid-iron solutions with the concentration data for trace elements in boiler-cleaning wastes (from Allen Steam Station as reported in Table 6-6) it is apparent that great differences in concentration exist. For the bromate waste, the copper concentrations at the two plants were similar, but the zinc, nickel, and arsenic concentrations at the Allen Station were at least two orders of magnitude greater than the values reported for the bromate waste collected from the Marshall Station. For the acid-iron waste, both the iron and copper concentrations in the Marshall Station waste are somewhat less than those reported for the Allen Station acid-iron waste. In general, the trace element content at the

Table 6-5

CHARACTERIZATION OF FLY-ASH TRANSPORT WATER AND BOILER-CLEANING WASTES  
FROM A COAL-FIRED POWER PLANT

Constituent	Fly-Ash Solutions <sup>a</sup>			Boiler-Cleaning Wastes		
	1. <sup>b</sup>	2. <sup>c</sup>	3. <sup>d</sup>	Bromate <sup>e</sup>	Vertan <sup>e</sup>	Acid-Iron <sup>e</sup>
pH	6.6	9.0	11.9	10.4	9.3	0.7
Conductivity	1740	1180	4000	5250	22,050	nm
Alk., mg/l	22.8	73.0	878	18,700	10,600	0
Cl <sup>-</sup> , mg/l	1.9	3.1	2.5	1100	2300	40,000
SO <sub>4</sub> <sup>-</sup> , mg/l	nm	nm	nm	nd	550	130
Na, mg/l	9.35	9.26	5.34	215	85.2	43.2
K, mg/l	16.2	15.0	1.4	0.7	1.4	0.31
Mg, mg/l	14.5	0.12	0.61	0.43	1.10	3.74
Ca, mg/l	34.6	262	99.4	0.87	0.62	3.34
Fe, mg/l	nd	nd	nd	nm	nm	5130
Cu	4.6 µg/l	1.48 µg/l	0.4 µg/l	683 mg/l	1.1 mg/l	159.4 mg/l
Zn	2.87 mg/l	39.7 µg/l	2.0 µg/l	0.8 µg/l	6.63 mg/l	15.89 mg/l
Cd, µg/l	0.24	nd	nd	<0.5	<0.5	22
Cu, µg/l	230.5	512.4	119	3.8	4.6	1620.1
Se, µg/l	390	511.7	nm	151.4	86.7	<5.0
As, µg/l	49	57	0.1	nd	20	7
Pb, µg/l	nd	nd	nd	nd	111	20.5
Ni, µg/l	<4	<2	<5	123	739	7910
NH <sub>3</sub> , mg/l	nm	nm	nm	4250	3520	nm

nd = not detectable ; nm = not measured.

<sup>a</sup>Data for fly ash: water ratio of 100 (W/W) and 6-day contact period.

<sup>b</sup>Marshall Steam Station, Unit #1, Duke Power Company.

<sup>c</sup>Marshall Steam Station, Unit #2, Duke Power Company.

<sup>d</sup>Arapahoe Station, Public Service, Colorado.

<sup>e</sup>Marshall Steam Station, Unit #2, Duke Power Company

Marshall Station acid-iron waste is consistently less than those for the Allen Station (except for nickel). Although little data is available in the literature on the trace element content of these wastes, recently reported data (7) for bromate wastes from TVA power plants indicate a range of copper and ammonia concentrations from 100-790 mg/l and 850-5700 mg/l, respectively, and average values of 440 mg/l and 2930 mg/l, respectively. The data for the Marshall Station fall within these ranges.

Because both the bromate and vertan wastes contain large amounts of ammonia (the ingredients forming the bromate solution include sodium bromate, ammonium carbonate

Table 6-6

COMPARISON BETWEEN TYPICAL TRACE METALS IN AMMONIACAL BROMATE AND HYDROCHLORIC ACID WASTES PRODUCED AT ALLEN STEAM STATION VS. THOSE PRODUCED AT MARSHALL STEAM STATION

Element	Ammoniacal Bromate		Hydrochloric Acid		Vertan
	Allen <sup>a</sup>	Marshall	Allen <sup>a</sup>	Marshall	Marshall
Cu, mg/l	409.0	683	318.0	159.4	1.1
Fe, mg/l	1.92	nm	8330.0	513.0	nm
Ni, mg/l	255	0.123	1.74	7.91	0.74
Zn, mg/l	1.03	0.83 ppb	166.0	15.9	6.63
Cd, mg/l	<0.02	<0.5 ppb	0.154	0.022	<0.5 ppb
Cr, mg/l	<0.05	0.004	4.4	1.62	0.005
Pb, mg/l	0.1	nd	4.79	0.021	0.111
Hg, µg/l	14.9	nm	54.5	nm	nm
As, µg/l	307	nd	9.6	7	20
Se, µg/l	23.6	151.4	<5	<5	87

nd = not detectable ; nm = not measured.

<sup>a</sup>Source: (6).

and ammonium hydroxide), many trace metals are probably present as complexes. At the high pH values of the wastes most trace metals such as copper, zinc, nickel, and cadmium would have low solubilities controlled by the appropriate hydroxide or oxide. In order to evaluate the extent of complexation present an experiment was performed in which increasing volumes of bromate waste were added to a known volume of deionized water containing copper at a known concentration. The results of this experiment at pH 6.0 are shown in Figure 6-1. Results indicate that complexation begins to occur when the bromate concentration in the solution reaches about 5 percent by volume and that the free copper concentration is reduced by almost 3 orders of magnitude in a 27.5 percent (by volume) bromate solution. Results of a similar experiment with the vertan waste are shown in Figure 6-2. Apparently the vertan waste complexes copper much more intensely as evidenced by the immediate drop in free metal concentrations upon vertan addition and the 3-order-of-magnitude reduction at a concentration level of only 0.063 percent by volume. This observation is consistent with the fact that the vertan waste probably contains an EDTA concentration of 5-10 percent by weight (1).

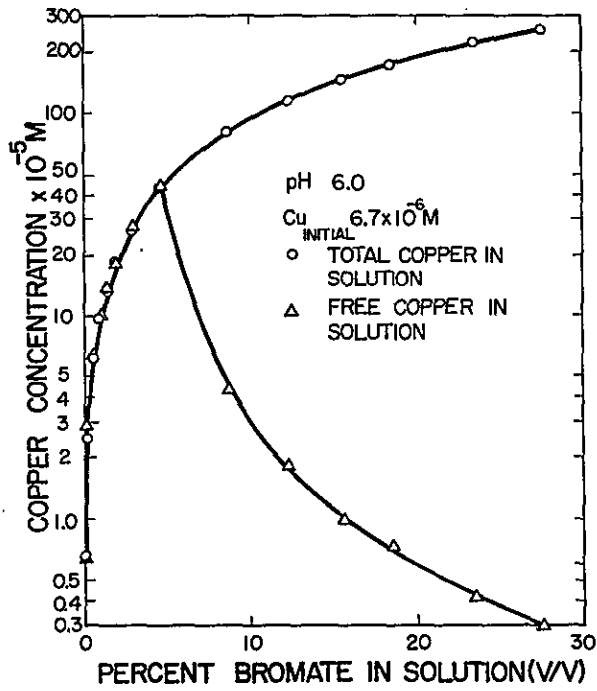


Figure 6-1. Complexation of copper ion in solution as a function of bromate addition

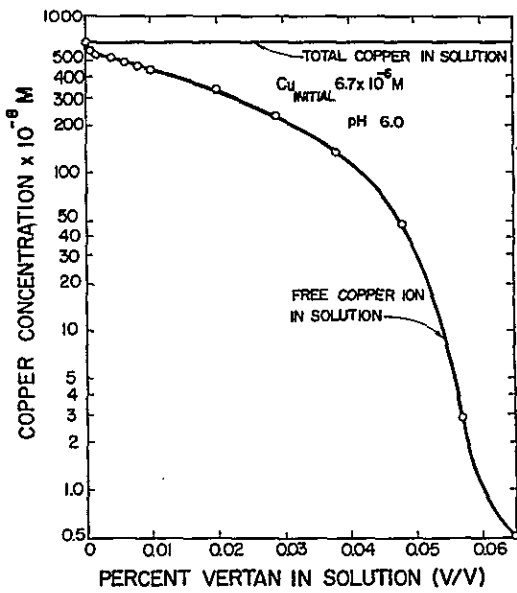


Figure 6-2. Complexation of copper ion in solution as a function of vertan addition

91143511773

As previously noted, there are considerable differences in the qualities of the waters held in contact with the fly ashes studied. Major differences occur in the pH and conductivity measurements. Fly ash 3 has a very high pH, while fly ash 1 has a much lower pH.

In order to investigate these results another set of experiments were conducted in which the concentration of fly ash was varied, and pH and conductivity measurements were taken immediately after four days of mixing and centrifugation for solids separation. These results are shown in Figures 6-3 and 6-4. As expected, both pH and conductivity decreased with decreasing concentrations of fly ash. Similar results for four lignite fly ashes, diluted in deionized water to different concentrations, have been reported elsewhere (8). An anomaly exists, however, between the pH of the fly ashes reported in Table 6-5 and the pH of the fly ashes with a water:ash ratio of 10 reported in Figure 6-3. For instance, the pH of the fly ash 1 solution decreased from 8.9 to 6.6, the pH of the fly ash 2 solution decreased from 11.3 to 9.0 and the pH of the 3 solution decreased from 12.4 to 11.9. This difference is probably due to carbon dioxide absorption, causing the pH to drop with exposure to air. The pH values in Table 6-5 were measured just before constituent analysis and several weeks after the ash-transport water was prepared.

With regard to the trace element content of these fly-ash waters, the greatest differences seem to be in the zinc and arsenic concentrations. The two and three order-of-magnitude difference in zinc concentration between fly ash 2 and fly ash 3 solutions, respectively, and fly ash 1 solution can probably be attributed to its pH value of 8.9 during contact versus the pH value of 11.3 for fly ash 2 and a pH value of 12.4 for fly ash 3. Accordingly, zinc concentration differences between fly ash 2 and fly ash 3 solutions may also be caused by pH differences. Other workers (4,9,10) have also reported decreasing zinc concentrations with increasing pH for fly ashes having different solution pH values and one fly ash at different pH values. It should be pointed out that zinc differences could be due to differing zinc concentrations in the fly ashes. However, the chemical composition data shown in Table 6-4 indicate that fly ash 1 and 2 have similar chemical compositions. The information listed in Table 6-4, of course, does not tell anything about surface concentration.

The differences in arsenic concentrations are somewhat harder to explain as other work seems to both support and contradict the trend presented here. Dreesen (9) found that during trace element extraction from one fly ash, arsenic extractability decreased with increasing pH, although not as dramatically as reported here. Theis and Wirth (10), on the other hand, reported seeing greater average arsenic availability as the pH increased from 9 to 12, a result not in line with the analysis

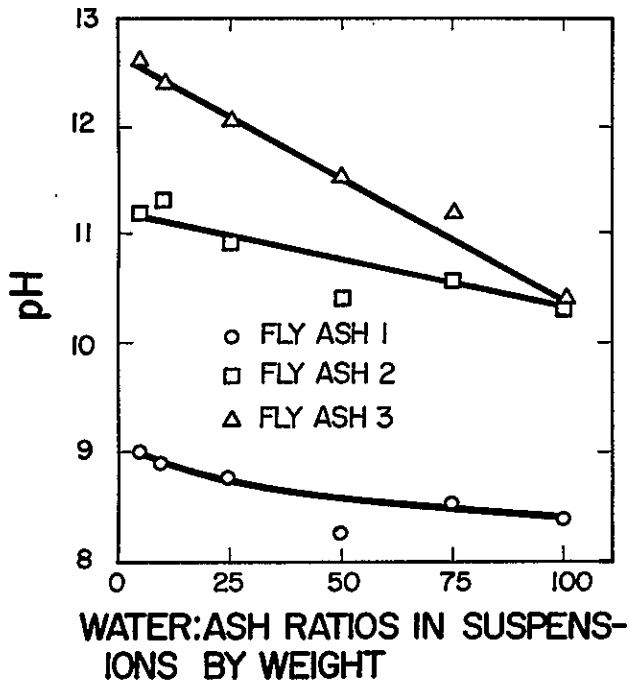


Figure 6-3. Variation in the pH of various fly-ash solutions as a function of water:ash ratios. 4 days contact

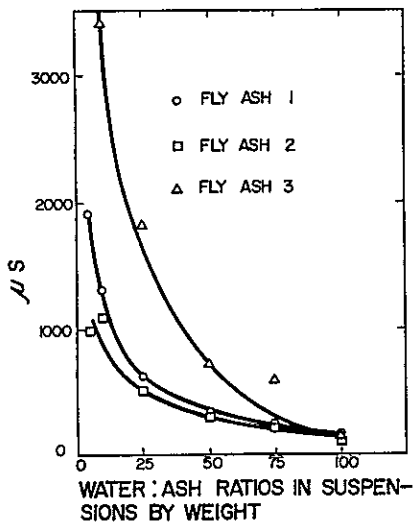


Figure 6-4. Variation of the conductivity of various fly-ash solutions as a function of water:ash ratios

reported here. The differences may again be due to the arsenic content of the fly ashes.

Tables 6-3, 6-5, and 6-7 can be used to compare the trace element content of fly-ash solutions in this study with those reported in other investigations. In reviewing these data it is difficult to draw conclusions because of the differing initial fly-ash concentrations, as well as the differing characteristics of the parent fly ash. However, it does appear to be generally true that solution concentrations of such metals as cadmium, copper, lead, nickel, and zinc decrease as the pH is raised up to pH values near 12. Neither the selenium nor the chromium concentration seems to follow any particular trend.

Table 6-7

TRACE ELEMENT CONTENT OF VARIOUS FLY ASHES AND WATER SOLUTIONS

Constituent	Fruitland, N.M., Power Plant <sup>a</sup>			Illinois Fly Ash and Distilled H <sub>2</sub> O <sup>b</sup>		Average Values for Eleven Different Fly Ashes <sup>c</sup>			
	Fly ash and Re- distilled H <sub>2</sub> O	Intake Water	Ash Pond Effluent						
pH	11.9	-	-	~11	~4	3	6	9	12
Cu	<1.0	3	3	30	300	164	72	1180	
Zn	<11	590	440	60	590	1660	52	340	
Cd	<0.1	1	1	35	50	82	30	36	
Cr	25	<1	2	210	40	380	400	480	
Se	92	<1	57	-	-	-	-	-	
As	3	2.6	27	200	500	200	160	8580	
Pb	-	-	-	750	250	280	146	182	
Ni	-	-	-	-	-	720	100	122	

<sup>a</sup>Fly-ash concentration in redistilled H<sub>2</sub>O is about 225 g/l. Mixture agitated for 3 hours and then filtered and prepared for analysis (9).

<sup>b</sup>Fly-ash concentration in distilled H<sub>2</sub>O is 200 g/l. Mixture was shaken for 3 days, filtered and analyzed (4).

<sup>c</sup>Fly-ash concentration is 200 g/l. Mixture was shaken for 24 hours, filtered and analyzed (10).

## COPRECIPITATION OF TRACE ELEMENTS USING WASTE MATERIALS

The adsorption of selected cations in the waste solutions onto amorphous iron oxyhydroxide surfaces is examined below. The results of the adsorption experiments for each cation in the various waste solutions are presented together, so that the differences imposed on metal removal by the different solution characteristics can be fully appreciated. Experimental work on Zn, Cu, and Cd is presented here. The adsorption of Pb and Ag, although investigated in the model systems described in Section 3, was not investigated in these preliminary studies. Future experimental work should include lead for those wastes containing high levels of Pb.

### Zinc Adsorption

As mentioned previously in Section 3 and detailed in Appendix A, the pH-adsorption edge for zinc in clean systems is very steep, with percent adsorption varying from 0 to 100 percent in a pH range of about 2 units (5.5-7.5 for  $2 \times 10^{-6} \text{M Zn}_T$  with  $1 \times 10^{-3} \text{M Fe}_T$  at 0.1M I). When the waste acid-iron solution, containing among other things an inhibitor (a proprietary coal-tar derivative), is used to provide the solid surface, the pH-adsorption edge (Figure 6-5) is quite different compared to a clean system; adsorption is greater at low pH values and lower at high pH values. These results conform quite well with the concept of ligand-like adsorption postulated in Section 5 and demonstrated there for Cd in the presence of  $\text{S}_2\text{O}_3^{2-}$  anions.

The increased adsorption in the low pH range is then probably due to the binding of the negatively charged metal-ligand complexes to the surface because of the higher positive charge of the surface at lower pH values. At higher pH values, the reduced adsorption could be due to the existence of ligand-metal complexes which do not bind strongly to the solid surface. An alternative explanation is that site-limitation is occurring resulting in competition of several metal ions for the same adsorption sites. Considering that the molar copper concentration is five times that of zinc it is possible such a competition with copper exists. However, as noted in Section 3, competition studies in clean systems indicated that high Cu concentrations have little, if any, effect on zinc adsorption.

Zinc pH adsorption edges in waste-iron solutions with different solid concentrations are shown in Figure 6-6. These results show some shift of the higher iron curves toward lower pH values but are somewhat difficult to interpret because of the varying zinc concentrations. Varying zinc concentrations were caused by the large zinc concentration in the acid-iron solution and the different acid-iron

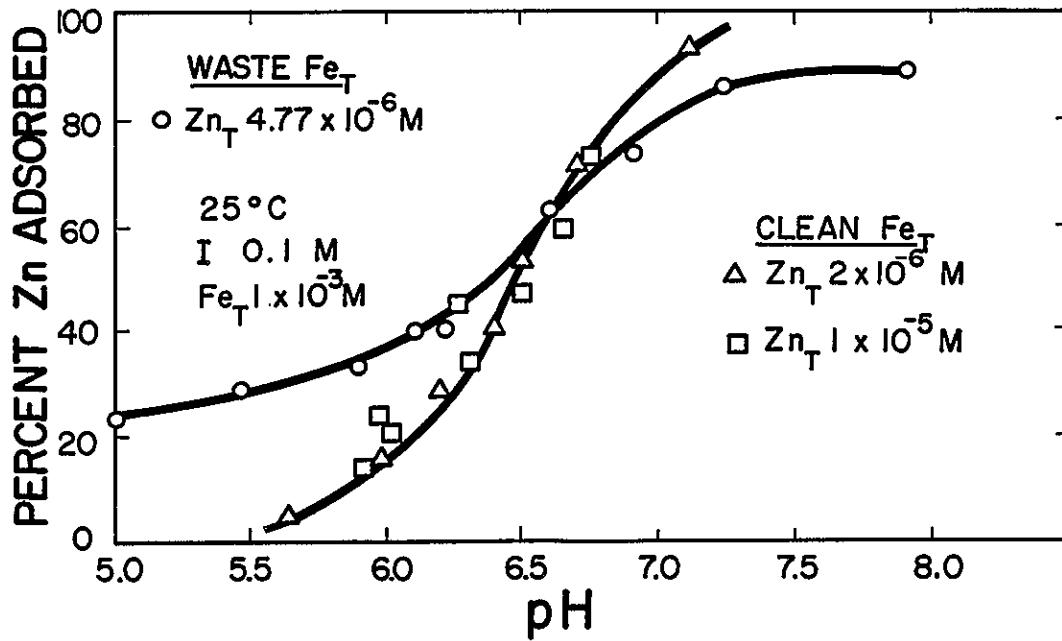


Figure 6-5. Percent adsorption of zinc onto waste am- $Fe(OH)_3$  as a function of pH in a coprecipitating system

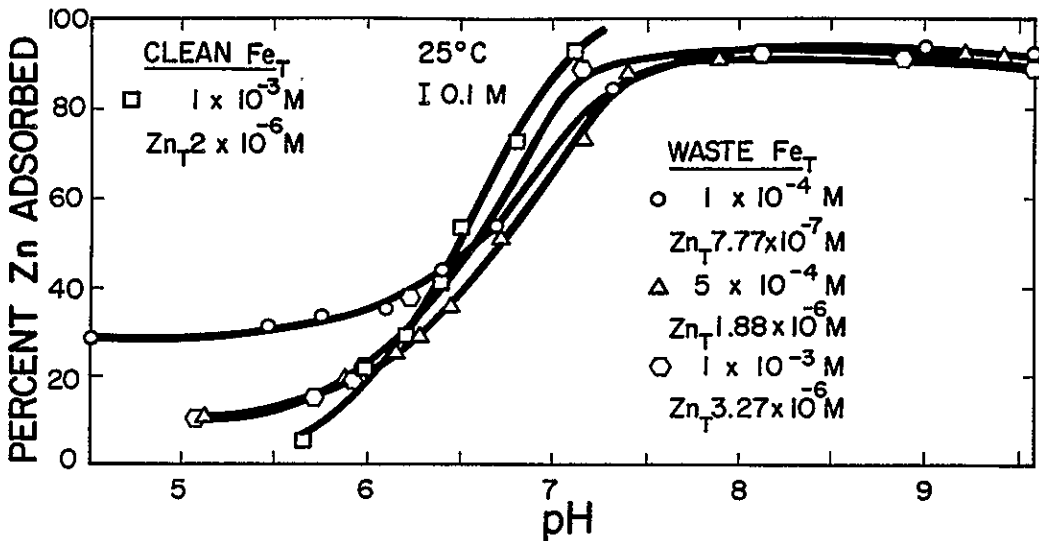


Figure 6-6. Percent zinc adsorbed onto waste am- $Fe(OH)_3$  as a function of pH and iron dose

6  
3  
1  
5  
0  
3  
1  
6

doses required. The lack of significant shift is probably due to the molar Zn/Fe ratios being less than  $10^{-2}$ . Comparing Figures 6-5 and 6-6, it is interesting to note the great similarity between the  $5 \times 10^{-4}$  and  $1 \times 10^{-3}$  M  $Fe_T$  curves in Figure 6-6 and the large difference in the  $1 \times 10^{-3}$  M  $Fe_T$  waste-iron curves in the two figures. Similar results are observed when the waste-iron solutions are added to the fly-ash solutions.

This is evident in Figure 6-7, which compares the results for each fly-ash solutions and the clean systems at an iron dose of  $1 \times 10^{-3}$  M  $Fe_T$ . Apparently the effect of ligands in fly-ash solution 1 is slightly greater than that in fly-ash solution 2 or fly-ash solution 3. Interestingly, the zinc pH adsorption edge for the waste-iron surface alone, in 0.1M electrolyte, is nearly identical to that found for fly-ashes 2 and 3 solutions. This observation would seem to indicate that ionic strength has very little effect on zinc adsorption in these solutions as there exists little difference in the general metal content of fly-ash 2 and 3 solutions and the zinc content specifically in all three after addition of the acid-iron waste. Because the concentration of zinc in fly-ash 1 solution is at least an order of magnitude greater than that found in fly-ash 2 and 3 solutions, and the overall characteristics of the three wastes are not that different, the difference in pH adsorption edges may be due to the high zinc concentration in fly-ash 1 solution. This result contrasts with that found for the clean system, viz., that variations in zinc concentrations have little effect on adsorption curves.

A possible explanation of this phenomenon can be found in the ligand-like behavior of zinc adsorption in these systems. Because the concentration of zinc is much greater in fly ash 1 solution and the concentration of ligands contributed to the various fly-ash solutions from the waste iron solution is the same, the concentration of the metal-ligand complex in solution should be greater. The greater concentration of metal-ligand complex presumably leads to greater adsorption at low pH because of the ligand-like behavior of the metal-ligand complex.

Another interesting result for zinc shows up in Figures 6-8, 6-9, and 6-10, which show pH adsorption edges developed from the three fly-ash solutions as a function of waste-iron dose ( $1 \times 10^{-4}$  M,  $5 \times 10^{-4}$  M, and  $1 \times 10^{-3}$  M  $Fe_T$ ). The distinct shift observed in Figure 6-8 for fly-ash 1 solution is expected as the molar Zn/Fe ratio is much greater than  $10^{-2}$ . The absence of any shift in Figure 6-9 for fly-ash 2 solutions also follows expectations, as the molar Zn/Fe ratio is less than  $10^{-2}$ . In the fly-ash 3 solution the results are somewhat mixed. Although the molar Zn/Fe ratio is greater than  $10^{-2}$  in all cases, a large shift was observed in the  $1 \times 10^{-4}$  M  $Fe_T$  solution.

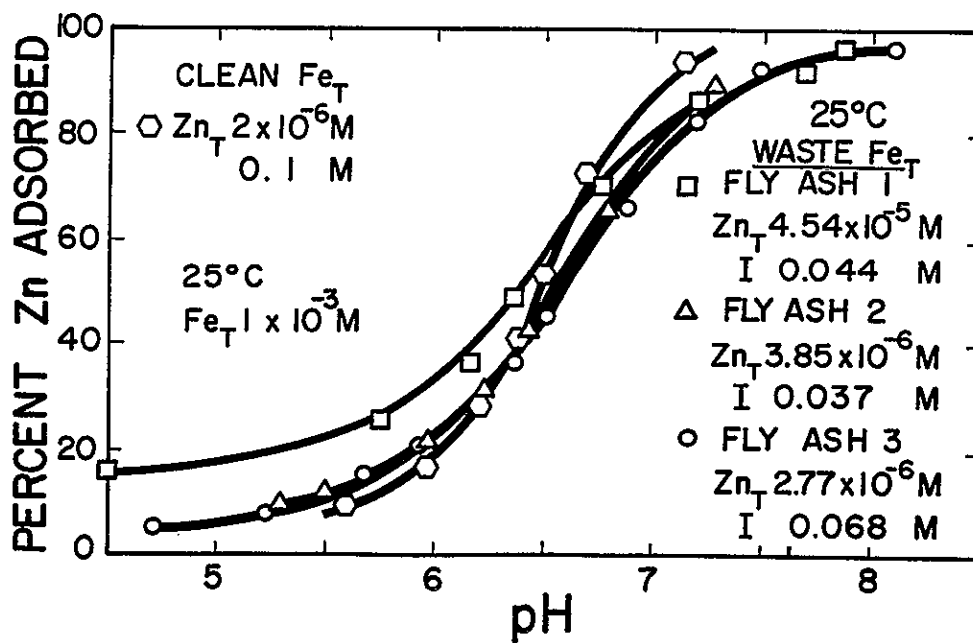


Figure 6-7. Percent zinc adsorbed onto waste am-Fe(OH)<sub>3</sub> as a function of pH and fly-ash leachate

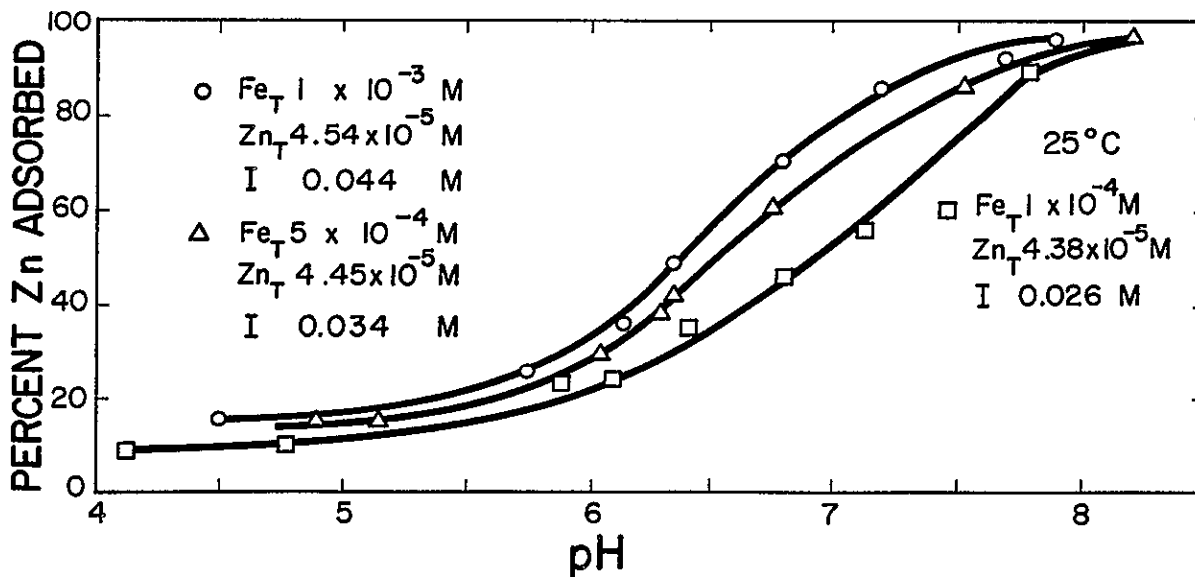


Figure 6-8. Percent zinc adsorbed onto waste am-Fe(OH)<sub>3</sub> in fly-ash 1 leachate as a function of pH and iron dose

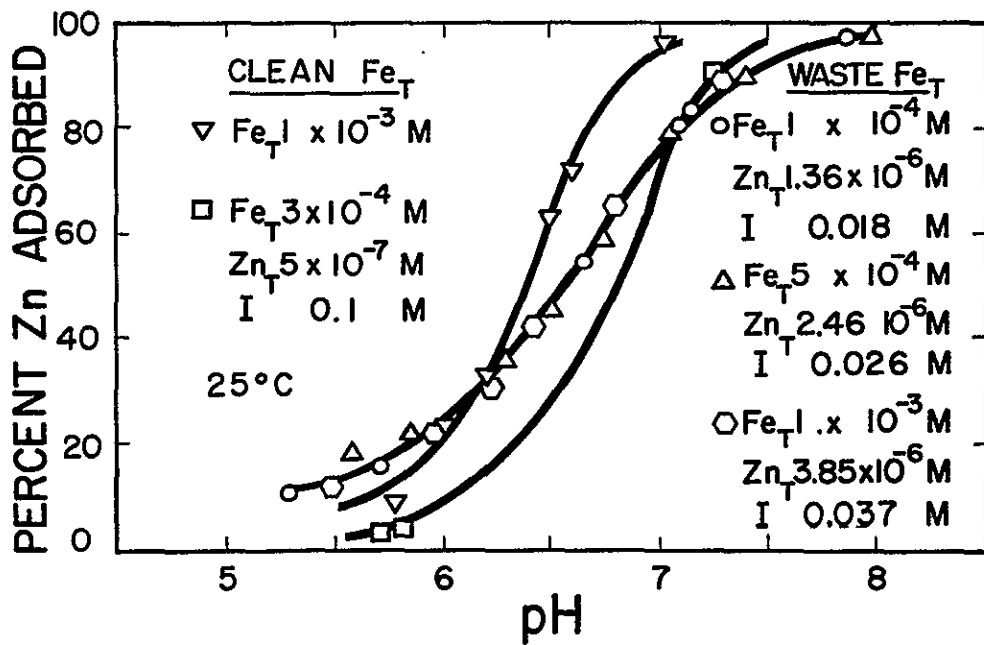


Figure 6-9. Percent zinc adsorbed onto waste am- $Fe(OH)_3$  in fly ash 2 as a function of pH and iron dose

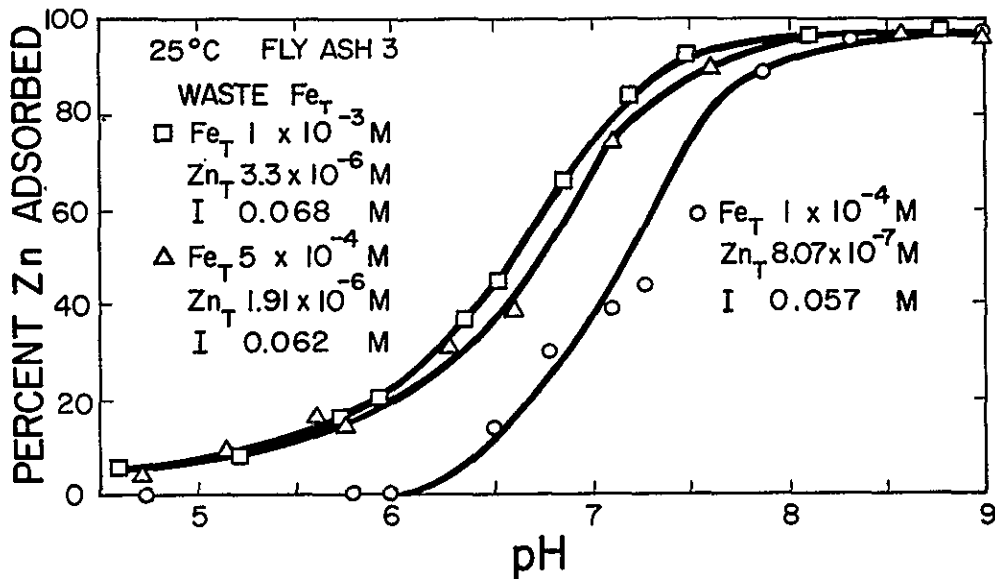


Figure 6-10. Percent zinc adsorbed onto waste am- $Fe(OH)_3$  in fly ash 3 as a function of pH and iron dose

A typical plot of the kinetics of zinc adsorption onto the iron surface is shown in Figure 6-11 for fly-ash 1 solution. In this experiment adsorption was almost instantaneous. The change in percent adsorption is apparently due to the change in pH during the experiment. Results for fly-ash 2 and 3 solutions are similar.

The pH adsorption edges for zinc in the bromate solution are quite different from results seen previously. Presumably, previously the complexing ability of ligands in the waste-iron solution determined the ligand-like behavior of the metal-ligand complex in the adsorption experiments. As seen in Figure 6-12, ligand-like behavior is only evident when the bromate concentration is very low (1%). At higher bromate concentrations the dominant metal-ligand complex is one of the zinc-ammonia complexes. These complexes exhibit metal-like behavior as shown by the shifting of the curves toward higher pH as the bromate (or ammonia) concentration increases. It is also interesting to note that at high pH values and high ammonia concentrations, where complex formation increases, that the percent adsorption begins to decrease.

As mentioned previously, the vertan solution, because of its high EDTA concentration, has a higher capacity for forming complexes than the bromate waste. It was observed that no zinc was adsorbed onto the waste iron surface ( $1 \times 10^{-4}M$ ,  $5 \times 10^{-4}M$ , and  $1 \times 10^{-3}M$   $Fe_T$ ) in a 20% vertan solution. The effects of a considerably more dilute vertan solution on zinc adsorption can be seen in a 0.2% vertan solution (see Figure 6-13) with varying amounts of waste iron surface available. In the low pH range, there appears to be competition between the metal-ligand complex formed from the acid iron waste and the zinc-EDTA complex. The complexing ability of EDTA increases over six orders of magnitude as the pH is increased from 5 to 9. As the pH is increased, the metal-like behavior of the zinc-EDTA complex begins to dominate. Zinc adsorption decreases at very high pH as the strength of the zinc-EDTA bond becomes stronger than that between the metal and waste iron surface.

#### Cadmium Adsorption

The pH adsorption edges for cadmium with waste iron in a swamping electrolyte solution are shown in Figure 6-14. These results were similar to those observed for zinc, in that the greatest shift (from the  $1 \times 10^{-3}M$   $Fe_T$  curve) was observed for the  $1 \times 10^{-4}M$   $Fe_T$  waste iron surface between fly ash 3 solution and a clean system of 0.1M I as is shown in Figure 6-15. The pH adsorption curves for the  $1 \times 10^{-3}M$   $Fe_T$  solutions indicate very little difference between fly-ash 3 solution and the clean system at these low concentrations of cadmium. For the  $1 \times 10^{-4}M$   $Fe_T$  solutions,

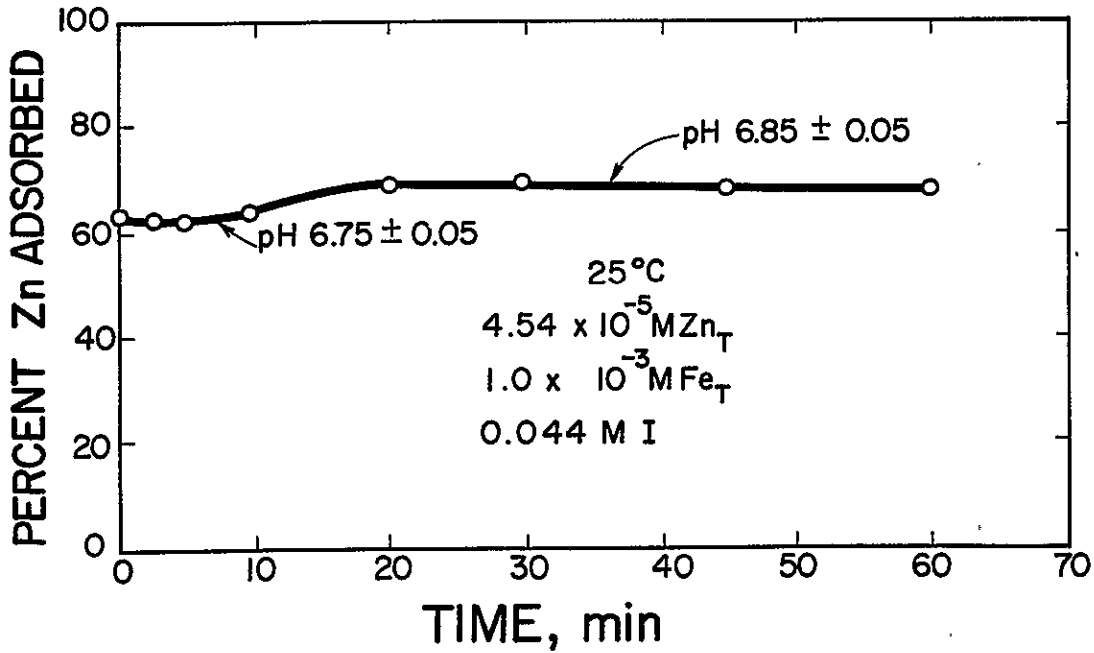


Figure 6-11. Percent zinc adsorption on waste am-Fe(OH)<sub>3</sub> in fly ash 1 as a function of time at constant pH

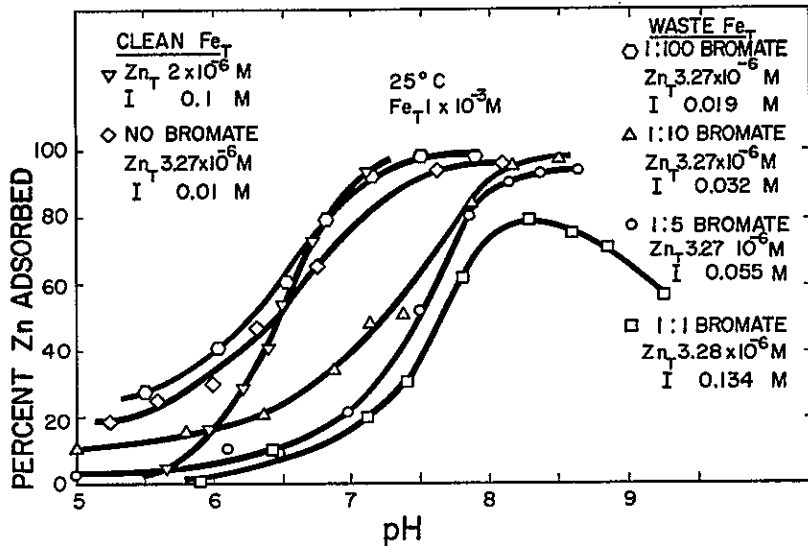


Figure 6-12. Percent zinc adsorption onto am-Fe(OH)<sub>3</sub> as a function of pH and bromate waste addition

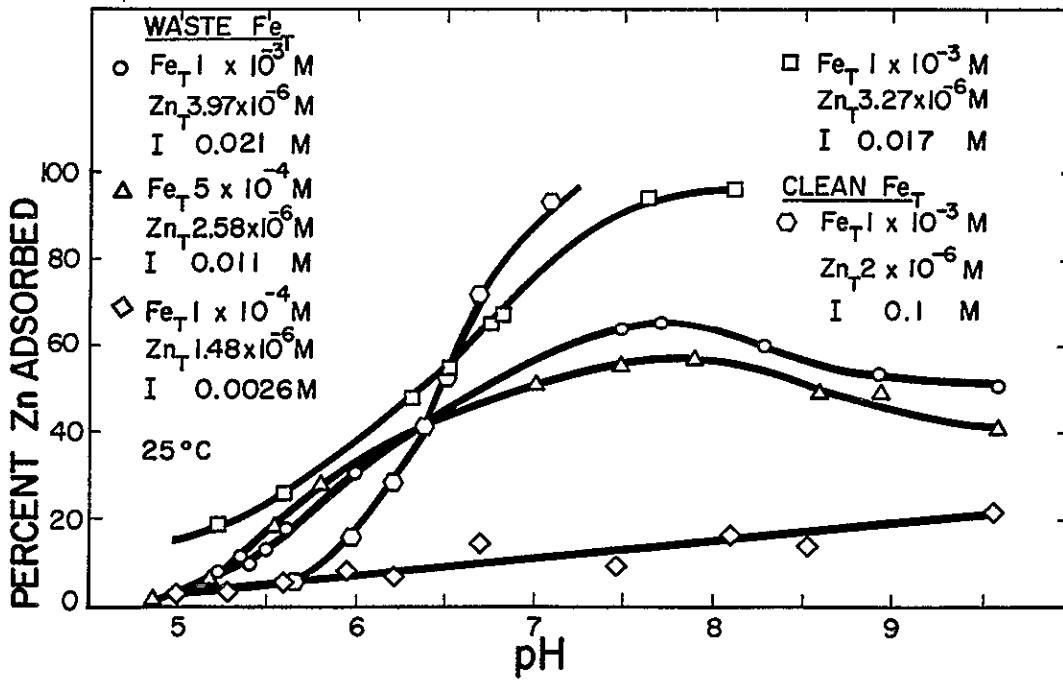


Figure 6-13. Percent zinc adsorbed onto waste am- $Fe(OH)_3$  from a vertan waste diluted 1:500

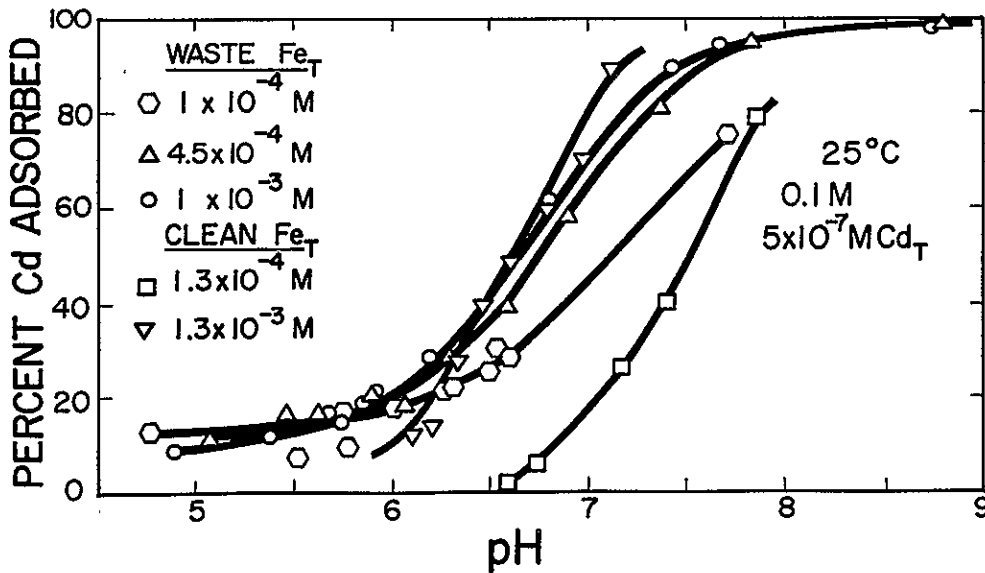


Figure 6-14. Percent cadmium adsorbed onto waste am- $Fe(OH)_3$  as a function of pH and iron dose

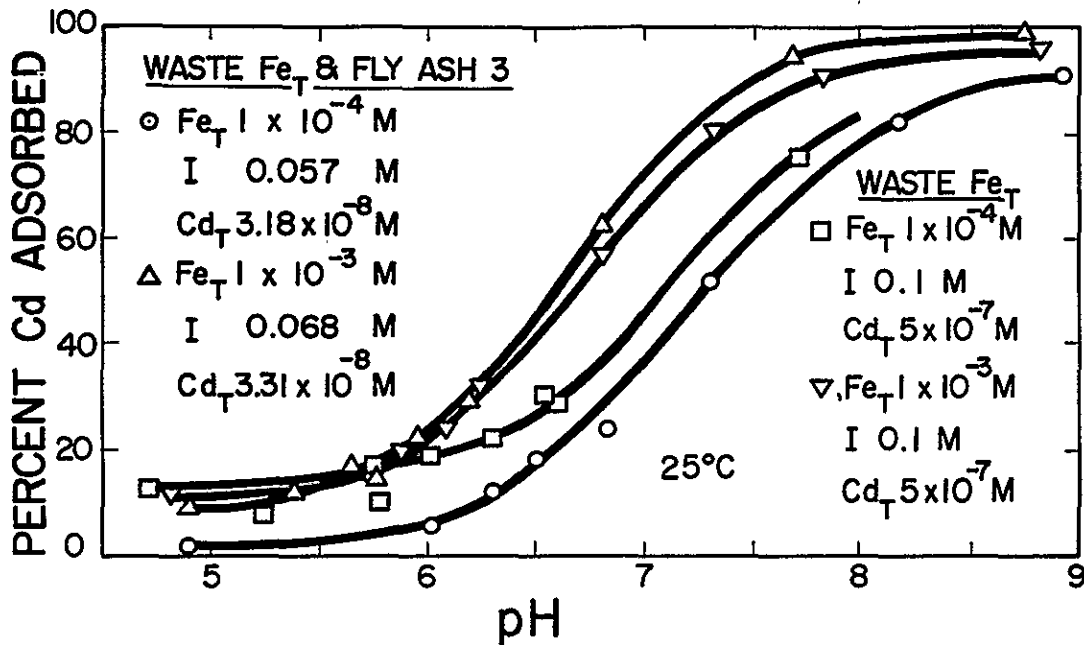


Figure 6-15. Comparison of cadmium adsorption onto waste am-Fe(OH)<sub>3</sub> from fly-ash waste and distilled water

expected patterns were not followed. The fly-ash 3 solution, which contains less cadmium, is shifted toward higher pH values, rather than lower as one would expect. The curve enhanced ligand-like adsorption at lower pH values. Although it is difficult to interpret the pH shift, the second difference may be attributable to binding of other cations in the fly-ash solution to the ligands in the acid iron waste, thus leading to a reduced ligand effect. This reduced ligand effect is not observed in the 1 x 10<sup>-3</sup> M Fe<sub>T</sub> solution presumably because the ten-fold increase in ligand concentration is more than sufficient to bind significant concentrations of cations in the fly-ash solutions. A complete and fundamental interpretation requires a more detailed characterization of the various waste solutions and, in some instances, additional experimental work in well-defined model systems.

#### Copper Adsorption

The results for copper have similarities to those observed for zinc, but there are also dramatic differences. For instance, the pH adsorption edge for copper in fly-ash 1 solutions (with various amounts of waste iron solid surface) showed the characteristic pH shift to higher pH values when the amount of solid surface decreased

(see Figure 6-16). On the other hand, the maximum adsorption (~80%) was much less than that observed for zinc (>95%) and the pH adsorption edges showed enhanced adsorption at low pH (Figure 6-16). One possible explanation for the rather low maximum value of adsorption is competition between other metals in solution. As the zinc concentration is over an order of magnitude greater than the copper concentration in the solution, it may be that zinc is competing for the same sites as copper. However, clean-system data reported earlier in Section 3 indicates that copper and zinc adsorb at different sites, i.e., no competitive effects between the two metals should be expected. Another possibility is that a ligand in solution is more strongly bound to copper than to zinc and exhibits constant acid/base behavior in the pH range from 6.5 to 9.5.

Enhanced copper adsorption at low pH values with decreasing solid surface is consistent with the formation of a strong complex which adsorbs in a ligand-like manner. With the ligand coming from the waste iron solution there should be a linear correspondence between iron dose and ligand effect. Thus increased adsorption with increased iron dose at low pH is consistent with this hypothesis.

Copper adsorption in the presence of the bromate solution was somewhat different from the corresponding zinc system. For instance, the pH adsorption edge for copper in a 1% bromate solution (Figure 6-17) is shifted to lower pH values rather than higher pH values. Considering that the major complexing ligand in the bromate forms a metal-like adsorbing complex with copper, it is possible that the enhanced adsorption at low pH is due to a ligand-like complex formed between the copper-complexing material in the acid iron waste. The results for copper and zinc were very similar for the 10% bromate solution as the pH adsorption edge was displaced toward higher pH values and began decreasing at still higher pH as the amount of ammonia in solution increased. Figure 6-18 shows the much larger displacement between adsorption edges at different waste iron surface coverages than was observed for zinc. This larger shift is probably due to the extremely high concentration of copper in the bromate which resulted in an inordinately large value for the molar ratio of metal to iron.

The results observed for copper adsorption in 0.2% vertan solution are somewhat anomalous when compared to zinc adsorption in a similar vertan solution (Figure 6-19). For zinc, it was possible to identify competition between the ligand-like behavior of the acid-iron-zinc complex and the metal-like behavior of the zinc-EDTA complex. However, it is difficult to attribute any metal-like behavior in the data

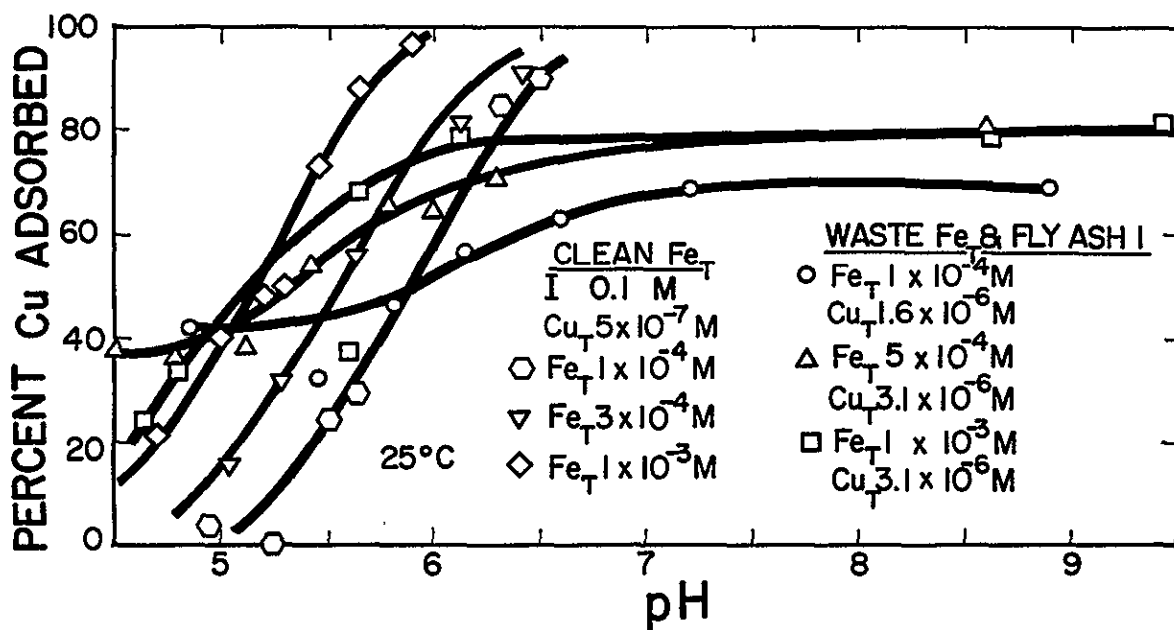


Figure 6-16. Percent Cu adsorbed onto waste am-Fe(OH)<sub>3</sub> in fly-ash 1 solution as a function of pH and iron dose.

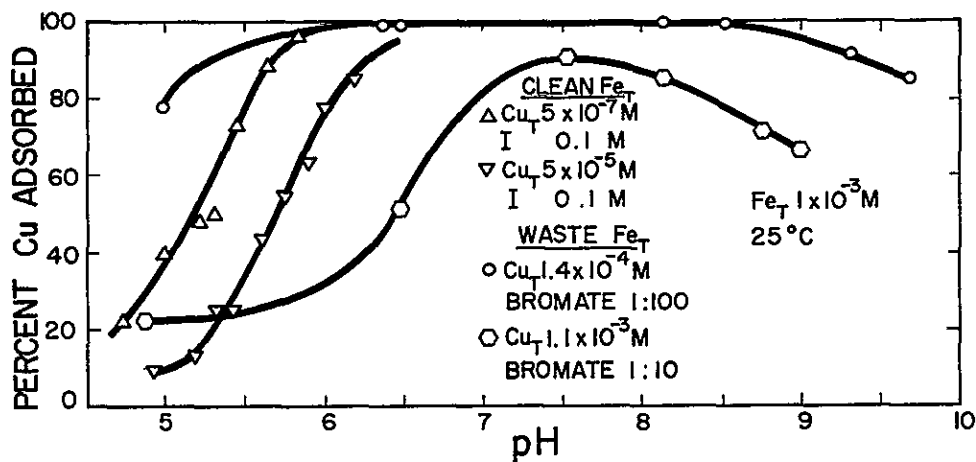


Figure 6-17. Percent Cu adsorbed onto waste am-Fe(OH)<sub>3</sub> as a function of pH and bromate concentration (dilution ratio given as volume bromate waste per volume distilled water).

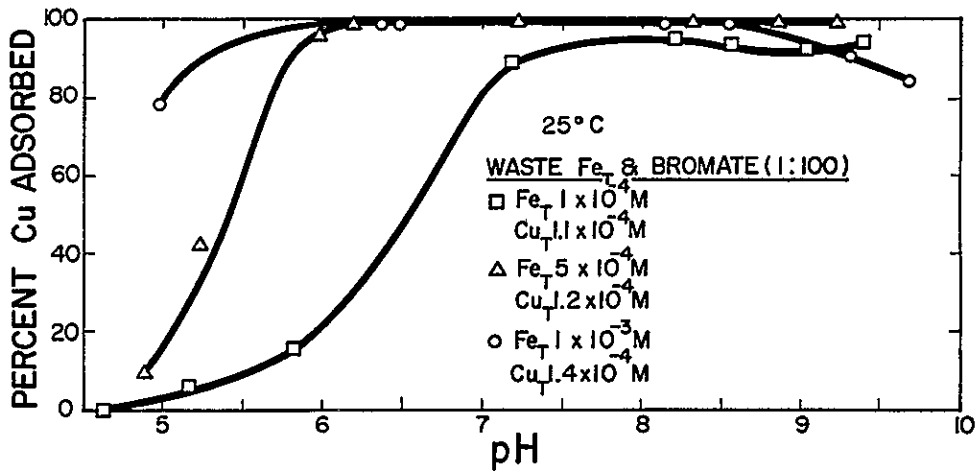


Figure 6-18. Percent Cu adsorbed onto waste am-Fe(OH)<sub>3</sub> as a function of pH and iron dose

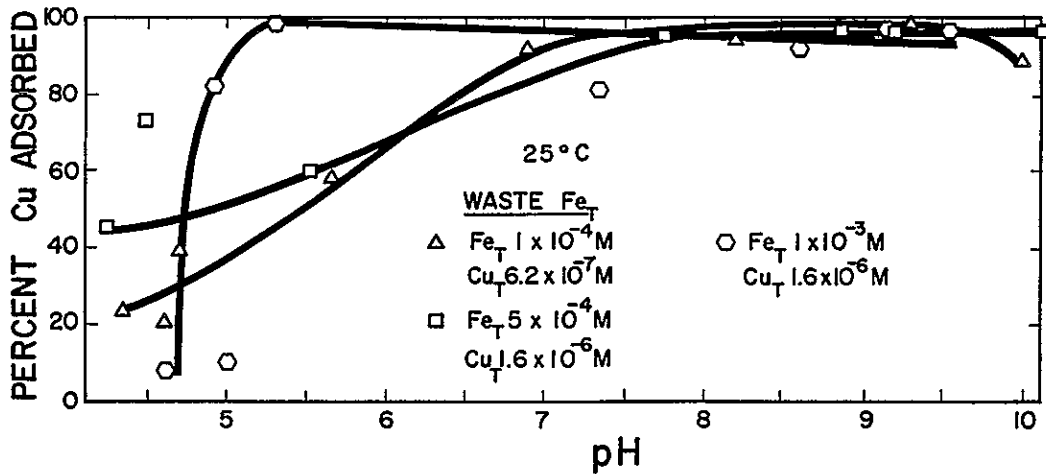


Figure 6-19. Percent Cu adsorbed onto waste am-Fe(OH)<sub>3</sub> in 0.2% vertran as a function of pH and iron dose

for  $1 \times 10^{-4} \text{M Fe}_T$  and  $5 \times 10^{-4} \text{M Fe}_T$  waste iron surface, as the  $5 \times 10^{-4} \text{M Fe}_T$  solution (which has five times as much ligand from the acid-iron waste as does the  $1 \times 10^{-4} \text{M Fe}_T$ ) showed enhanced adsorption at lower pH and decreased adsorption at higher pH. Also, adsorption did not decrease at high pH, even though the complexing power of EDTA increases at high pH and the stability constant for the copper-EDTA complex is greater than that for the zinc-EDTA complex. In the  $1 \times 10^{-3} \text{M Fe}_T$  solution, the adsorption edge is shifted toward lower pH values and is steeper than that observed in a comparable clean system.

#### ANION REMOVAL

The adsorption of selected anions, present in waste solutions, onto the surface of amorphous iron hydroxide was investigated. The potential of an acid-iron waste solution as an iron source for removing anions is also reported here. The results of adsorption experiments for each waste are presented under the respective heading of each anion: arsenate, chromate, and selenite. Since selenium was present in the waste solution as the selenite species only, the removal of selenate was not studied in the waste solutions.

#### Selenite Adsorption

The adsorption of selenite onto amorphous iron hydroxide in model systems was presented in Section 4. As shown in Figure 4-2, the pH adsorption edge for selenite in the model systems is quite steep, covering a pH range of roughly two units (pH 8-10) as the percent-selenite adsorption goes from near zero to 80 percent. (Model systems refers to those systems in which all reactants are prepared from reagent-grade chemicals.)

A preliminary experiment, using acid-iron waste as the iron adsorbent source and sodium selenite ( $\text{Na}_2\text{SeO}_3$ ) as the adsorbate source, was conducted and compared to the model system. The pH adsorption edges for the acid-iron waste/ $\text{Na}_2\text{SeO}_3$  system and the corresponding model system are shown in Figure 6-20. There are two striking differences between the two systems: 1) adsorption above pH-10 occurs only in the acid-iron waste system, and 2) there is less adsorption below pH-8 in the acid-iron system, compared to the model system. Analogous differences were observed for zinc (see, e.g., Figure 6-5).

The concentration of the major inorganic constituents in the acid-iron waste (under the experimental conditions described in Appendix B) are shown in Table 6-8. The acid-iron waste provides a variety of counter ions which may bind selenite. The

Table 6-8

ACID-IRON WASTE CONSTITUENT CONCENTRATION IN EXPERIMENTAL SYSTEM

	Acid-Iron Waste $Fe_T = 1.0 \times 10^{-3} M$		Acid-Iron Waste $Fe_T = 1.0 \times 10^{-3} M$
Cl	$6.7 \times 10^{-3} M$	Zn	$2.6 \times 10^{-6} M$
SO <sub>4</sub>	$1.5 \times 10^{-5} M$	Cd	$1.5 \times 10^{-9} M$
Na	$2.0 \times 10^{-5} M$	Cr	$3.4 \times 10^{-7} M$
K	$8.6 \times 10^{-8} M$	Se	$6.9 \times 10^{-10} M$ ( $5.0 \times 10^{-6} M$ )*
Mg	$1.7 \times 10^{-6} M$	As	$1.0 \times 10^{-9} M$
Ca	$9.1 \times 10^{-7} M$	Pb	$3.8 \times 10^{-10} M$
Fe	$1.0 \times 10^{-3} M$	Ni	$1.5 \times 10^{-6} M$
Cu	$2.7 \times 10^{-5} M$	NH <sub>3</sub>	nm
nm = not measured.		*Se: $5.0 \times 10^{-6} M$ selenite added.	

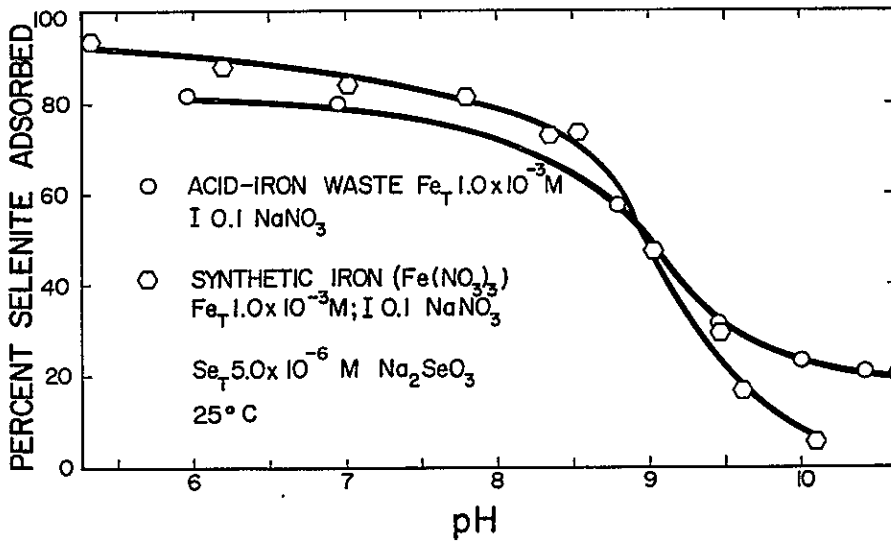


Figure 6-20. Percent adsorption of selenite onto am-Fe(OH)<sub>3</sub> as a function of pH in a coprecipitating system

adsorption of selenite above pH 10 is probably due to metal-like adsorption of a metal/selenite complex or ion pair; i.e., at pH values above the adsorption edge, selenite adsorption is made possible by a bonding interaction of the anion with an adsorbing metal. A modified solid surface may also be the cause of the adsorption of selenite above pH 10. At pH values below pH 8, the reduced adsorption of selenite may be due to the formation of metal-selenite complexes. Below the pH of the pzc (e.g., 7.9 for Fe(OH)<sub>3</sub>-am), the electrostatic attraction of the free anion is decreased by complex formation. An alternate explanation for the lower adsorption of selenite below pH 8 is that there is competition for anion surface sites. Relatively high concentrations of sulfate (1.5 x 10<sup>-5</sup>M) and chromate (3.4 x 10<sup>-7</sup>M) are present in the acid-iron waste system; thus competition for anion surface sites is possible.

The pH range investigated in the acid-iron waste system was pH 5 to 10. Competition between chromate and selenite is expected (if it occurs) in the pH range of 6 to 8, i.e., the pH range where chromate adsorption occurs in the model system. Sulfate competition is expected in the pH range of 4 to 6. As shown in Figure 6-20, neither chromate nor sulfate appear to compete with selenite in the acid-iron waste system (see, e.g. Figure 4-9 for the shape of the pH adsorption edge in systems where competition is occurring). Apparently, under the experimental conditions, the ratio of total anion concentration to total iron concentration ( $A_T:Fe_T$ ) is sufficiently small so that site-limitation is not occurring ( $Cr_T:Fe_T = 3.4 \times 10^{-4}M$ ,  $SO_4^{2-}:Fe_T = 1.5 \times 10^{-5}M$ ,  $Se_T:Fe_T = 5.0 \times 10^{-3}M$ ). As subsequent data on the fly-ash solutions will show, when the  $A_T:Fe_T$  ratio becomes large enough, site-limitation does occur, and changes in the adsorption edge, characteristic of surface-site competition, are observed.

#### Selenite Adsorption: Fly-Ash Waste

The results of using acid-iron waste for the removal of selenite from three different fly-ash solutions are shown in Figures 6-21, 6-22, and 6-23. The characteristics of these fly ashes have been described earlier (see, e.g. Table 6-4 and Table 6-5). The concentrations of the major inorganic constituents of the fly-ash solutions under the experimental condition are given in Tables 6-9a, 6-9b, 6-9c, and 6-9d. The results of selenite adsorption in the model system, the acid-iron waste/ $Na_2SeO_3$  system, and the acid-iron waste/fly-ash system are shown together in Figure 6-24. The characteristics noted above for the acid-iron waste/ $Na_2SeO_3$  system are also present in the acid-iron waste/fly-ash systems. There are, however, several additional interesting features: 1) there is higher percent adsorption above

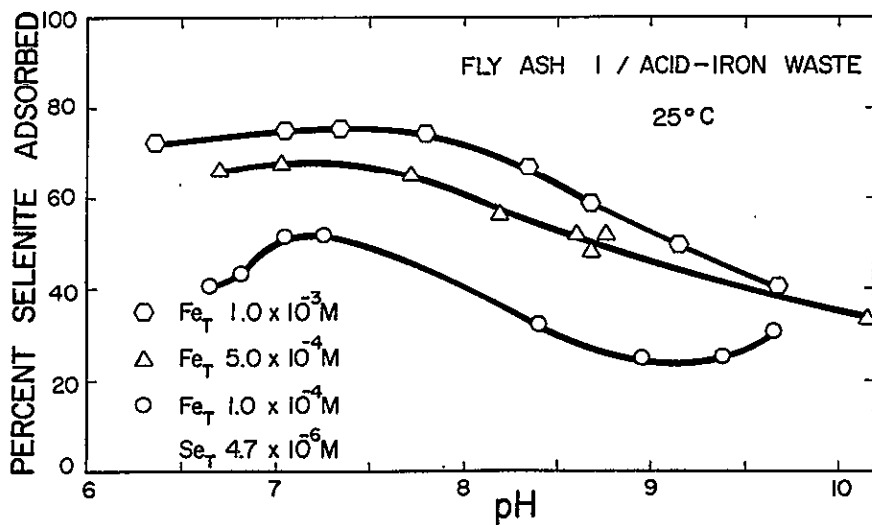


Figure 6-21. Adsorption of selenite onto waste am-Fe(OH)<sub>3</sub> from fly-ash 1 waste solution

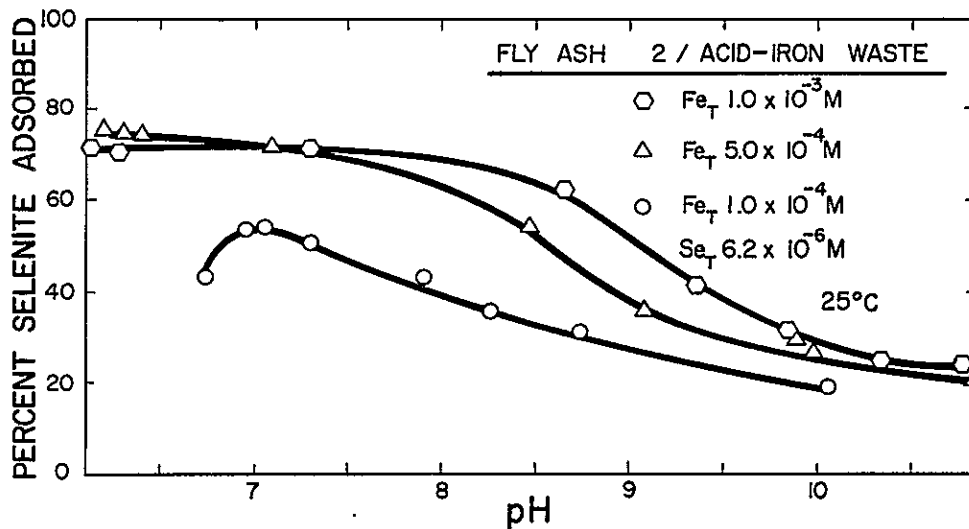


Figure 6-22. Adsorption of selenite onto waste am-Fe(OH)<sub>3</sub> from fly-ash 2 waste solution

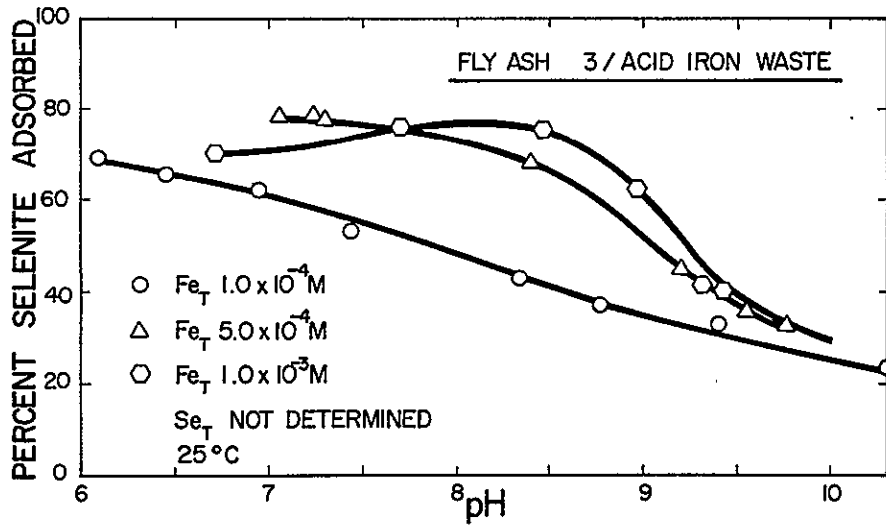


Figure 6-23. Adsorption of selenite onto waste am- $Fe(OH)_3$  from fly-ash 3 waste solution

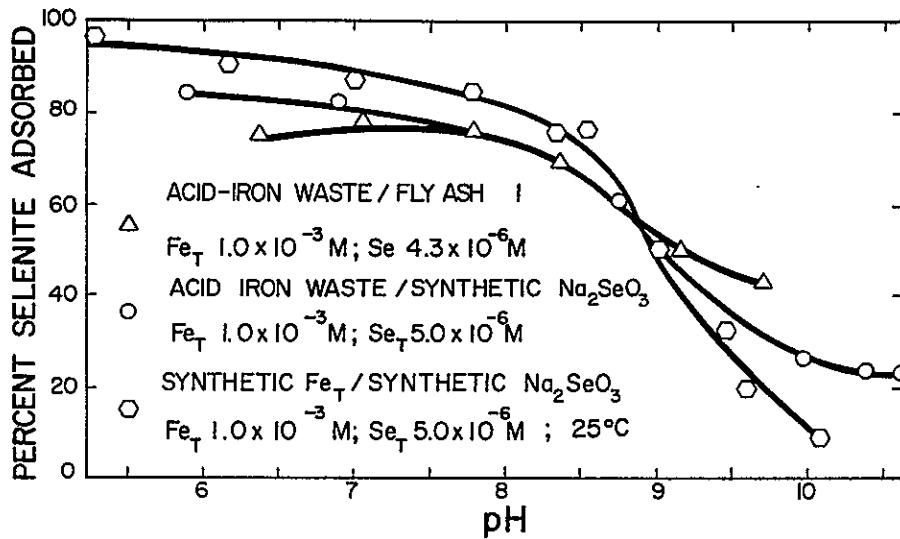


Figure 6-24. Selenite adsorption onto am- $Fe(OH)_3$  from various sources

Table 6-9

CONSTITUENT CONCENTRATIONS UNDER GIVEN EXPERIMENTAL CONDITIONS  
(filtered fly-ash solution supernatant)

## a. Fly-Ash 1/Acid-Iron Waste System

## b. Fly-Ash 2/Acid-Iron Waste System

	$Fe_T = 1.0 \times 10^{-4}*$	$Fe_T = 5.0 \times 10^{-4}*$	$Fe_T = 1.0 \times 10^{-3}*$		$Fe_T = 1.0 \times 10^{-4}*$	$Fe_T = 5.0 \times 10^{-4}*$	$Fe_T = 1.0 \times 10^{-3}*$
Cl	$1.3 \times 10^{-3}$	$6.2 \times 10^{-3}$	$1.2 \times 10^{-2}$	Cl	$1.3 \times 10^{-3}$	$6.2 \times 10^{-3}$	$1.2 \times 10^{-2}$
SO <sub>4</sub>	$>1.5 \times 10^{-6}$	$>1.5 \times 10^{-6}$	$>1.5 \times 10^{-6}$	SO <sub>4</sub>	$>1.5 \times 10^{-6}$	$>7.4 \times 10^{-6}$	$>1.5 \times 10^{-5}$
Na	$3.9 \times 10^{-4}$	$4.0 \times 10^{-4}$	$4.1 \times 10^{-4}$	Na	$3.9 \times 10^{-4}$	$4.0 \times 10^{-4}$	$4.1 \times 10^{-4}$
K	$4.0 \times 10^{-4}$	$4.0 \times 10^{-4}$	$4.0 \times 10^{-4}$	K	$3.7 \times 10^{-4}$	$3.7 \times 10^{-4}$	$3.7 \times 10^{-4}$
Mg	$5.7 \times 10^{-4}$	$5.7 \times 10^{-4}$	$5.7 \times 10^{-4}$	Mg	$4.6 \times 10^{-6}$	$4.6 \times 10^{-6}$	$4.6 \times 10^{-6}$
Ca	$8.3 \times 10^{-4}$	$8.3 \times 10^{-4}$	$8.3 \times 10^{-4}$	Ca	$6.3 \times 10^{-3}$	$6.3 \times 10^{-3}$	$6.3 \times 10^{-3}$
Fe	$1.0 \times 10^{-4}$	$5.0 \times 10^{-4}$	$1.0 \times 10^{-3}$	Fe	$1.0 \times 10^{-4}$	$5.0 \times 10^{-4}$	$1.0 \times 10^{-3}$
Cu	$2.6 \times 10^{-6}$	$1.3 \times 10^{-5}$	$2.6 \times 10^{-5}$	Cu	$2.6 \times 10^{-6}$	$1.3 \times 10^{-5}$	$2.6 \times 10^{-5}$
Zn	$4.2 \times 10^{-5}$	$4.4 \times 10^{-5}$	$4.5 \times 10^{-5}$	Zn	$8.5 \times 10^{-7}$	$1.9 \times 10^{-6}$	$3.2 \times 10^{-6}$
Cd	$2.2 \times 10^{-9}$	$2.3 \times 10^{-9}$	$3.6 \times 10^{-9}$	Cd	$7.7 \times 10^{-10}$	$7.7 \times 10^{-10}$	$7.7 \times 10^{-10}$
Cr	$4.3 \times 10^{-6}$	$4.4 \times 10^{-6}$	$4.6 \times 10^{-6}$	Cr	$9.5 \times 10^{-6}$	$9.6 \times 10^{-6}$	$9.8 \times 10^{-6}$
Se	$4.3 \times 10^{-6}$	$4.3 \times 10^{-6}$	$4.3 \times 10^{-6}$	Se	$4.3 \times 10^{-6}$	$4.3 \times 10^{-6}$	$6.5 \times 10^{-6}$
As	$6.5 \times 10^{-7}$	$6.5 \times 10^{-7}$	$6.5 \times 10^{-7}$	As	$6.5 \times 10^{-7}$	$6.5 \times 10^{-7}$	$6.5 \times 10^{-7}$
Pb	nd	nd	nd	Pb	nd	nd	nd
Ni	$1.5 \times 10^{-7}$	$7.3 \times 10^{-7}$	$1.5 \times 10^{-6}$	Ni	$1.5 \times 10^{-7}$	$7.3 \times 10^{-7}$	$1.5 \times 10^{-6}$
NH <sub>3</sub>	nm	nm	nm	NH <sub>3</sub>	nm	nm	nm

c. Fly-Ash 3/Acid-Iron Waste System				d. Comparison of Fly Ash 1, Fly Ash 2, and Fly-Ash 3/Acid-Iron Waste Systems			
	$Fe_T = 1.0 \times 10^{-4}*$	$Fe_T = 5.0 \times 10^{-4}*$	$Fe_T = 1.0 \times 10^{-3}*$		Fly Ash 1	Fly Ash 2	Fly Ash 3
Cl	$1.3 \times 10^{-3}$	$6.2 \times 10^{-3}$	$1.2 \times 10^{-2}$	Cl	$1.3 \times 10^{-3}$ *	$1.3 \times 10^{-3}$	$1.3 \times 10^{-3}$
SO <sub>4</sub>	$>1.5 \times 10^{-6}$	$>7.4 \times 10^{-6}$	$>1.5 \times 10^{-5}$	SO <sub>4</sub>	$>1.5 \times 10^{-6}$	$>1.5 \times 10^{-6}$	$>1.5 \times 10^{-6}$
Na	$2.3 \times 10^{-4}$	$2.3 \times 10^{-4}$	$2.4 \times 10^{-4}$	Na	$3.9 \times 10^{-4}$	$3.9 \times 10^{-4}$	$2.3 \times 10^{-4}$
K	$3.4 \times 10^{-5}$	$3.4 \times 10^{-5}$	$3.4 \times 10^{-5}$	K	$4.0 \times 10^{-4}$	$3.7 \times 10^{-4}$	$3.4 \times 10^{-5}$
Mg	$2.4 \times 10^{-5}$	$2.4 \times 10^{-5}$	$2.4 \times 10^{-5}$	Mg	$5.7 \times 10^{-4}$	$4.6 \times 10^{-6}$	$2.4 \times 10^{-5}$
Ca	$2.4 \times 10^{-3}$	$2.4 \times 10^{-3}$	$2.4 \times 10^{-3}$	Ca	$8.3 \times 10^{-4}$	$6.3 \times 10^{-3}$	$2.4 \times 10^{-3}$
Fe	$1.0 \times 10^{-4}$	$5.0 \times 10^{-4}$	$1.0 \times 10^{-3}$	Fe	$1.0 \times 10^{-4}$	$1.0 \times 10^{-4}$	$1.0 \times 10^{-4}$
Cu	$2.6 \times 10^{-6}$	$1.3 \times 10^{-5}$	$2.6 \times 10^{-5}$	Cu	$2.6 \times 10^{-6}$	$2.6 \times 10^{-6}$	$2.6 \times 10^{-6}$
Zn	$2.1 \times 10^{-7}$	$1.3 \times 10^{-6}$	$2.7 \times 10^{-6}$	Zn	$4.2 \times 10^{-5}$	$8.5 \times 10^{-7}$	$2.1 \times 10^{-7}$
Cd	$1.5 \times 10^{-9}$	$1.5 \times 10^{-9}$	$1.5 \times 10^{-9}$	Cd	$2.2 \times 10^{-9}$	$7.7 \times 10^{-10}$	$1.5 \times 10^{-9}$
Cr	$2.3 \times 10^{-6}$	$2.4 \times 10^{-6}$	$2.5 \times 10^{-6}$	Cr	$4.3 \times 10^{-6}$	$9.5 \times 10^{-6}$	$2.2 \times 10^{-6}$
Se	nm	nm	nm	Se	$4.3 \times 10^{-6}$	$4.3 \times 10^{-6}$	nm
As	$1.3 \times 10^{-9}$	$1.3 \times 10^{-9}$	$1.3 \times 10^{-9}$	As	$6.5 \times 10^{-7}$	$6.5 \times 10^{-7}$	$1.3 \times 10^{-9}$
Pb	nd	nd	nd	Pb	nd	nd	nd
Ni	$1.5 \times 10^{-7}$	$7.3 \times 10^{-7}$	$1.5 \times 10^{-6}$	Ni	$1.5 \times 10^{-7}$	$1.5 \times 10^{-7}$	$1.5 \times 10^{-7}$
NH <sub>3</sub>	nm	nm	nm	NH <sub>3</sub>	nm	nm	nm

nd = not detectable; nm = not measured.  
\* All concentrations expressed as moles/l (M).

pH 10 in the fly-ash systems compared to the acid-iron waste/ $\text{Na}_2\text{SeO}_3$  system;  
 2) at pH values below 8, the selenite adsorption of the fly-ash systems is lower than the acid-iron waste/ $\text{Na}_2\text{SeO}_3$  system; 3) there is a slight curvature toward lower selenite adsorption in the acid-iron waste fly-ash systems at  $\text{pH} < 8$ .

The general shape of the fly-ash adsorption edge is quite similar to that observed for the acid-iron waste/ $\text{Na}_2\text{SeO}_3$  system. The adsorption of selenite above pH 10 is most likely due to the adsorption of metal-like selenite complexes. The lower selenite adsorption and slight curvature below pH 8 are possibly due to the effects of complex formation and surface-site competition. The relative changes in the acid-iron waste/fly-ash system compared to the acid-iron waste/ $\text{Na}_2\text{SeO}_3$  system are probably due to the relative increase in the concentration of competing ligands and complexing metals in the acid-iron waste/fly-ash system. Table 6-10 gives the constituent concentrations of three acid-iron waste/fly-ash systems and the corresponding acid-iron waste/ $\text{Na}_2\text{SeO}_3$  system. The substantial difference in  $\text{K}^+$  and  $\text{Ca}^{2+}$  concentrations between the acid-iron waste/fly-ash systems and the acid-iron waste/ $\text{Na}_2\text{SeO}_3$  system may very well account for the observed differences. The existence of adsorbing  $\text{CaSeO}_3$  and  $\text{KHSeO}_3$  ion pairs is quite reasonable (11,12). A general discussion of the possible complexes and ion pairs in the waste systems is given on page 6-45.

Table 6-10

COMPARISON OF THE CONSTITUENT CONCENTRATIONS OF ACID-IRON WASTE/FLY-ASH SYSTEMS AND ACID-IRON WASTE/ $\text{Na}_2\text{SeO}_3$  SYSTEM

	Acid Iron + Fly Ash 1	Acid Iron + Fly Ash 2	Acid Iron + Fly Ash 3	Acid Iron + Reagent Se
Cl	$1.2 \times 10^{-2*}$	$1.2 \times 10^{-2}$	$1.2 \times 10^{-2}$	$6.7 \times 10^{-3}$
$\text{SO}_4$	$\geq 1.5 \times 10^{-6}$	$\geq 1.5 \times 10^{-5}$	$\geq 1.5 \times 10^{-5}$	$1.5 \times 10^{-5}$
Na	$4.1 \times 10^{-4}$	$4.1 \times 10^{-4}$	$2.4 \times 10^{-4}$	$2.0 \times 10^{-5}$
K	$4.0 \times 10^{-4}$	$3.7 \times 10^{-4}$	$3.4 \times 10^{-5}$	$8.6 \times 10^{-8}$
Mg	$5.7 \times 10^{-4}$	$4.6 \times 10^{-6}$	$2.4 \times 10^{-5}$	$1.7 \times 10^{-6}$
Ca	$8.3 \times 10^{-4}$	$6.3 \times 10^{-3}$	$2.4 \times 10^{-3}$	$9.1 \times 10^{-7}$
Fe	$1.0 \times 10^{-3}$	$1.0 \times 10^{-3}$	$1.0 \times 10^{-3}$	$1.0 \times 10^{-3}$
Cu	$2.6 \times 10^{-5}$	$2.6 \times 10^{-5}$	$2.6 \times 10^{-5}$	$2.7 \times 10^{-5}$
Zn	$4.5 \times 10^{-5}$	$3.2 \times 10^{-6}$	$2.7 \times 10^{-6}$	$2.6 \times 10^{-6}$
Cd	$3.6 \times 10^{-9}$	$7.7 \times 10^{-10}$	$1.5 \times 10^{-9}$	$1.5 \times 10^{-9}$
Cr	$4.6 \times 10^{-6}$	$9.8 \times 10^{-6}$	$2.5 \times 10^{-6}$	$3.4 \times 10^{-7}$
Se	$4.3 \times 10^{-6}$	$6.5 \times 10^{-6}$	nm	$5.0 \times 10^{-6}$
As	$6.5 \times 10^{-7}$	$6.5 \times 10^{-7}$	$1.3 \times 10^{-9}$	$1.0 \times 10^{-9}$
Pb	nd	nd	nd	$3.8 \times 10^{-10}$
Ni	$1.5 \times 10^{-6}$	$1.5 \times 10^{-6}$	$1.5 \times 10^{-6}$	$1.5 \times 10^{-6}$
$\text{NH}_3$	nm	nm	nm	nm

nd = not detectable; nm = not measured.  
 \* All concentrations expressed as moles/l (M).

Selenite Adsorption: Bromate Waste

Results of using acid-iron waste for the removal of selenite from a bromate waste (diluted 1:5) are shown in Figure 6-25. Concentrations of the major inorganic constituents (under the experimental conditions) are given in Table 6-11. The pH adsorption edge for the acid-iron waste/bromate system is very similar to that described previously for acid-iron waste/ $\text{Na}_2\text{SeO}_3$  system and acid-iron waste/fly-ash systems, with one exception: adsorption of a metal-like complex above pH 10 is absent in the bromate-waste system.

The apparent absence of metal-like adsorption in the bromate-waste system can be explained. Two major differences exist between the acid-iron waste/bromate-waste system and the acid-iron waste/ $\text{Na}_2\text{SeO}_3$  and acid-iron waste/fly-ash systems: 1) the total selenite concentration ( $\text{Se}_T$ ) in the bromate-waste system ( $3.8 \times 10^{-7}\text{M}$ ) is an order of magnitude lower than the selenite concentration in the  $\text{Na}_2\text{SeO}_3$  system ( $5.0 \times 10^{-6}\text{M}$ ) and the fly-ash systems ( $\sim 5.0 \times 10^{-6}\text{M}$ ); and 2) the bromate-waste system has a significantly higher copper concentration ( $2.2 \times 10^{-3}\text{M}$ ) compared to the  $\text{Na}_2\text{SeO}_3$  and fly-ash systems ( $2.6 \times 10^{-6}\text{M}$ ). The concentration of the major inorganic constituents of the bromate and fly-ash wastes are compared in Table 6-12.

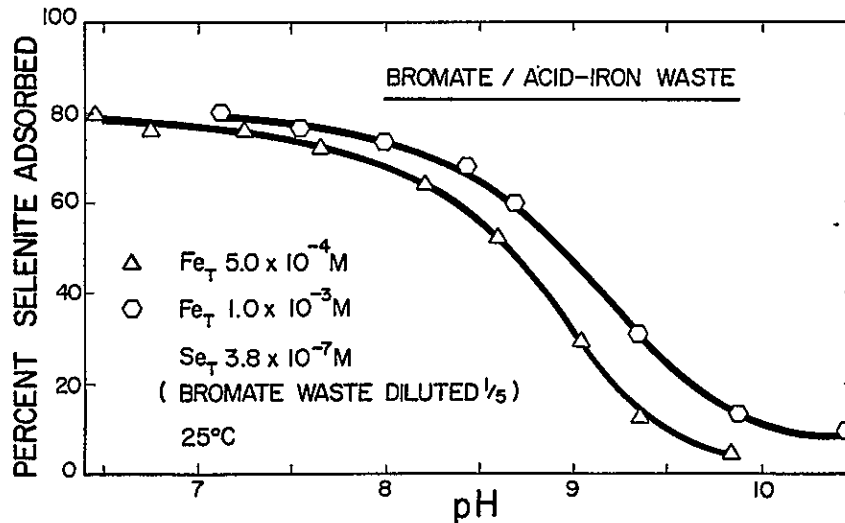


Figure 6-25. Adsorption of selenite onto waste am- $\text{Fe}(\text{OH})_3$  from a bromate waste solution

Table 6-11

CONSTITUENT CONCENTRATIONS OF BROMATE ACID-IRON WASTE SYSTEM  
UNDER EXPERIMENTAL CONDITIONS

		$Fe_T = 5.0 \times 10^{-4}$	$Fe_T = 1.0 \times 10^{-3}$
Cl	$7.4 \times 10^{-3}$ *	$1.2 \times 10^{-2}$	$1.8 \times 10^{-2}$
SO <sub>4</sub>	$\geq 1.5 \times 10^{-6}$	$\geq 7.4 \times 10^{-6}$	$\geq 1.5 \times 10^{-5}$
Na	$1.9 \times 10^{-3}$	$1.9 \times 10^{-3}$	$1.9 \times 10^{-3}$
K	$3.4 \times 10^{-3}$	$3.4 \times 10^{-6}$	$3.4 \times 10^{-6}$
Mg	$1.7 \times 10^{-5}$	$1.7 \times 10^{-5}$	$1.7 \times 10^{-5}$
Ca	$4.3 \times 10^{-6}$	$4.3 \times 10^{-6}$	$4.3 \times 10^{-6}$
Fe	$\geq 1.0 \times 10^{-4}$	$\geq 5.0 \times 10^{-4}$	$\geq 1.0 \times 10^{-3}$
Cu	$2.2 \times 10^{-3}$	$2.2 \times 10^{-3}$	$2.2 \times 10^{-3}$
Zn	$2.1 \times 10^{-7}$	$1.3 \times 10^{-6}$	$2.7 \times 10^{-6}$
Cd	$< 1.0 \times 10^{-9}$	$< 1.7 \times 10^{-9}$	$< 2.4 \times 10^{-9}$
Cr	$4.8 \times 10^{-8}$	$1.7 \times 10^{-7}$	$3.5 \times 10^{-6}$
Se	$3.8 \times 10^{-7}$	$3.8 \times 10^{-7}$	$3.8 \times 10^{-7}$
As	nd	nd	nd
Pb	$> 1.1 \times 10^{-10}$	$> 1.1 \times 10^{-10}$	$> 1.1 \times 10^{-10}$
Ni	$5.7 \times 10^{-7}$	$1.2 \times 10^{-6}$	$1.9 \times 10^{-6}$
NH <sub>3</sub>	$\geq 2.5 \times 10^{-4}$	$\geq 2.5 \times 10^{-4}$	$\geq 2.5 \times 10^{-4}$

nd = not detectable.  
\*All concentrations expressed in moles/l (M).

Table 6-12

COMPARISON OF CONSTITUENT CONCENTRATIONS ( $Fe_T 5.0 \times 10^{-4}M$ )

	Bromate	Fly Ash 1	Fly Ash 2	Fly Ash 3
Cl	$1.2 \times 10^{-2}$ *	$6.2 \times 10^{-3}$	$6.2 \times 10^{-3}$	$6.2 \times 10^{-3}$
SO <sub>4</sub>	$\geq 7.4 \times 10^{-6}$	$\geq 1.5 \times 10^{-6}$	$\geq 7.4 \times 10^{-6}$	$\geq 7.4 \times 10^{-6}$
Na	$1.9 \times 10^{-3}$	$4.0 \times 10^{-4}$	$4.0 \times 10^{-4}$	$2.3 \times 10^{-4}$
K	$3.4 \times 10^{-6}$	$4.0 \times 10^{-4}$	$3.7 \times 10^{-4}$	$3.4 \times 10^{-5}$
Mg	$1.7 \times 10^{-5}$	$5.7 \times 10^{-4}$	$4.6 \times 10^{-6}$	$2.4 \times 10^{-5}$
Ca	$4.3 \times 10^{-6}$	$8.3 \times 10^{-4}$	$6.3 \times 10^{-3}$	$2.4 \times 10^{-3}$
Fe	$\geq 5.0 \times 10^{-4}$	$5.0 \times 10^{-4}$	$5.0 \times 10^{-4}$	$5.0 \times 10^{-4}$
Cu	$2.2 \times 10^{-3}$	$1.3 \times 10^{-5}$	$1.3 \times 10^{-5}$	$1.3 \times 10^{-5}$
Zn	$1.3 \times 10^{-6}$	$4.4 \times 10^{-5}$	$1.9 \times 10^{-6}$	$1.3 \times 10^{-6}$
Cd	$< 1.7 \times 10^{-9}$	$2.3 \times 10^{-9}$	$7.7 \times 10^{-10}$	$1.5 \times 10^{-9}$
Cr	$1.7 \times 10^{-7}$	$4.4 \times 10^{-6}$	$9.6 \times 10^{-6}$	$2.4 \times 10^{-6}$
Se	$3.8 \times 10^{-7}$	$4.3 \times 10^{-6}$	$4.3 \times 10^{-6}$	nm
As	nd	$6.5 \times 10^{-7}$	$6.5 \times 10^{-7}$	$1.3 \times 10^{-9}$
Pb	$> 1.1 \times 10^{-10}$	nd	nd	nd
Ni	$1.2 \times 10^{-6}$	$7.3 \times 10^{-7}$	$7.3 \times 10^{-7}$	$7.3 \times 10^{-7}$
NH <sub>3</sub>	$\geq 2.5 \times 10^{-4}$	nm	nm	nm

nd = not detectable; nm = not measured.  
\*All concentrations expressed as moles/l (M).

It was suggested previously that the adsorption of the ion pairs,  $\text{KHSeO}_3$  and  $\text{CaSeO}_3$ , may explain the observed adsorption of selenite at pH values above pH 10 in the  $\text{Na}_2\text{SeO}_3$  and fly-ash systems. If these ion pairs are important to the observed adsorption, then the amount of selenite available for ion-pair formation will be important. When the selenite concentration is not in excess with respect to ion-pair formation, then the concentration of ion pairs will diminish. In this respect, lower selenite concentrations will lead to decreased adsorption of metal-selenite ion pairs above pH 10.

Similarly, the formation of non-adsorbing complexes could also cause a decrease in adsorption above pH 10. It is likely that copper is forming non-adsorbing, copper-selenite complexes in the bromate waste; the relatively high concentration of copper and low concentration of selenite probably result in most selenite being bound as a copper selenite complex, and subsequently selenite is not available to form adsorbing complexes or ion pairs.

#### Selenite Adsorption: Vertan Waste

Results of using acid-iron waste for the removal of selenite from the vertan waste (dilution by 1/2) are shown in Figure 6-26. The concentrations of the major inorganic constituents under the experimental conditions are given in Table 6-13. In addition to the inorganic ions present in the waste, EDTA is also present at a concentration of about 0.2-0.3M.

As Figure 6-26 shows, selenite adsorption is substantially reduced over the entire pH range investigated. Comparison of the fly-ash, bromate, and vertan systems shows that there are only slight differences in concentration of the major inorganic ions. The major noticeable differences are the high concentration of  $\text{SO}_4^{=}$  ( $2.9 \times 10^{-7}\text{M}$ ) and the relatively high concentration of Pb ( $2.7 \times 10^{-7}\text{M}$ ) in the vertan waste. These differences alone certainly cannot account for the striking change in selenite adsorption. Perhaps the single-most important factor is the presence of EDTA. The ability of organic molecules to adsorb to oxide surfaces is well known (13). The EDTA molecule is probably effectively coating the oxide surface causing substantially reduced adsorption of selenite.

#### Chromate Adsorption

The adsorption of chromate onto amorphous iron hydroxide in model systems was discussed in Section 4. As shown in Figure 6-27, the pH adsorption edge for chromate

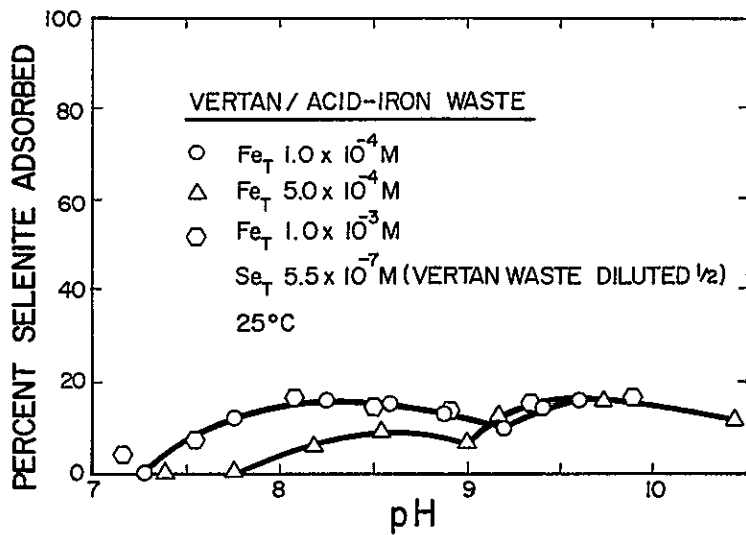


Figure 6-26. Adsorption of selenite onto am-Fe(OH)<sub>3</sub> from vertan waste solution

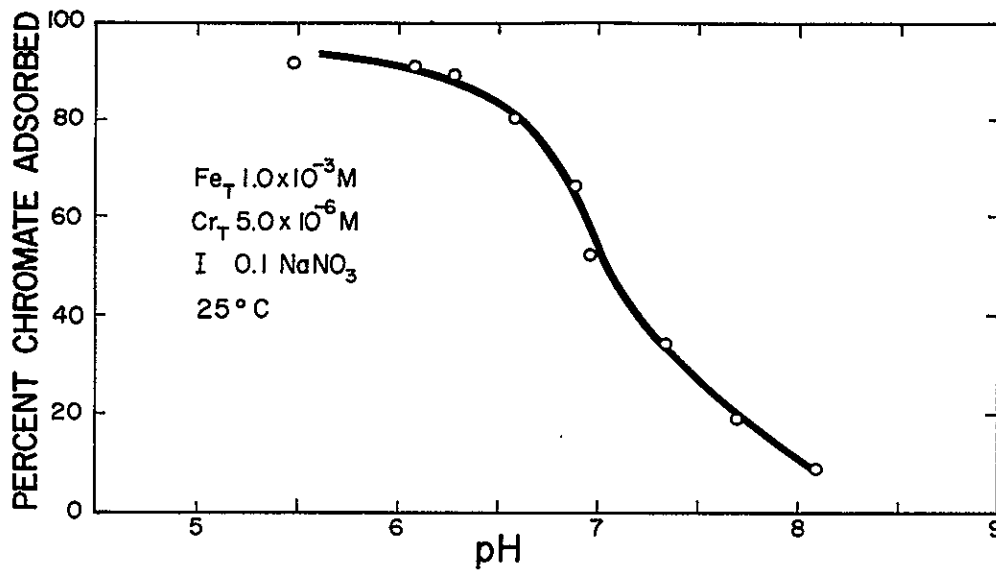


Figure 6-27. Percent chromate adsorbed onto am-Fe(OH)<sub>3</sub> as a function of pH

Table 6-13

CONSTITUENT CONCENTRATIONS OF VERTAN WASTE/ACID-IRON WASTE SYSTEM  
UNDER GIVEN EXPERIMENTAL CONDITIONS

	$Fe_T = 1.0 \times 10^{-4*}$	$Fe_T = 5 \times 10^{-4}$	$Fe_T = 1.0 \times 10^{-3}$
Cl	$3.4 \times 10^{-2}$	$3.9 \times 10^{-2}$	$4.5 \times 10^{-2}$
SO <sub>4</sub>	$2.9 \times 10^{-3}$	$2.9 \times 10^{-3}$	$2.9 \times 10^{-3}$
Na	$1.9 \times 10^{-3}$	$1.9 \times 10^{-3}$	$1.9 \times 10^{-3}$
K	$3.4 \times 10^{-5}$	$3.4 \times 10^{-5}$	$3.4 \times 10^{-5}$
Mg	$4.3 \times 10^{-5}$	$4.3 \times 10^{-5}$	$4.3 \times 10^{-5}$
Ca	$7.7 \times 10^{-6}$	$7.7 \times 10^{-6}$	$7.7 \times 10^{-6}$
Fe	$\geq 1.0 \times 10^{-4}$	$\geq 5.0 \times 10^{-4}$	$\geq 1.0 \times 10^{-3}$
Cu	$1.1 \times 10^{-5}$	$2.2 \times 10^{-5}$	$3.5 \times 10^{-5}$
Zn	$5.1 \times 10^{-5}$	$5.2 \times 10^{-4}$	$5.3 \times 10^{-5}$
Cd	$< 1.0 \times 10^{-9}$	$< 1.7 \times 10^{-9}$	$< 2.4 \times 10^{-9}$
Cr	$7.8 \times 10^{-8}$	$1.7 \times 10^{-7}$	$3.5 \times 10^{-7}$
Se	$5.5 \times 10^{-7}$	$5.5 \times 10^{-7}$	$5.5 \times 10^{-7}$
As	$2.7 \times 10^{-7}$	$2.7 \times 10^{-7}$	$2.7 \times 10^{-7}$
Pb	$2.7 \times 10^{-7}$	$2.7 \times 10^{-7}$	$2.7 \times 10^{-7}$
Ni	$6.4 \times 10^{-6}$	$7.0 \times 10^{-6}$	$7.8 \times 10^{-6}$
NH <sub>3</sub>	$1.0 \times 10^{-4}$	$1.0 \times 10^{-4}$	$1.0 \times 10^{-4}$

\*All concentrations expressed as moles/l (M).

in the model systems is quite steep, covering a pH range of roughly 2 units (pH 6-8) as the percent-chromate adsorption goes from near zero to > 90% adsorption.

#### Chromate Adsorption: Fly-Ash Waste

The results of using acid-iron waste for the removal of chromate from fly ash 1 and 2 solutions are shown in Figures 6-28 and 6-29, respectively. (The concentration of the major inorganic constituents of the fly-ash solutions have been given previously; see Tables 6-9a and 6-9b.) As shown in Figures 6-28 and 6-29, there is > 90% adsorption of chromate over the entire pH range investigated (pH 5.5-9.5). (This contrasts sharply with the adsorption behavior of chromate in the model systems shown in Figures 6-28 and 6-29 for comparison.) These results are quite different from those observed for selenite; however, the cause of the observed > 90% adsorption over the entire pH range studied may be due to the same types of reactions as were postulated for the selenite system. The adsorption of chromate above pH 8 may be due to the formation of metal-like, adsorbing ion pairs or complexes of chromate. (Like  $CaSeO_3$  and  $KHSeO_3$  in the selenite systems,  $CaCrO_4$  and  $KHCrO_4$  are possible adsorbing ion pairs here.) An alternate explanation is that chromate is

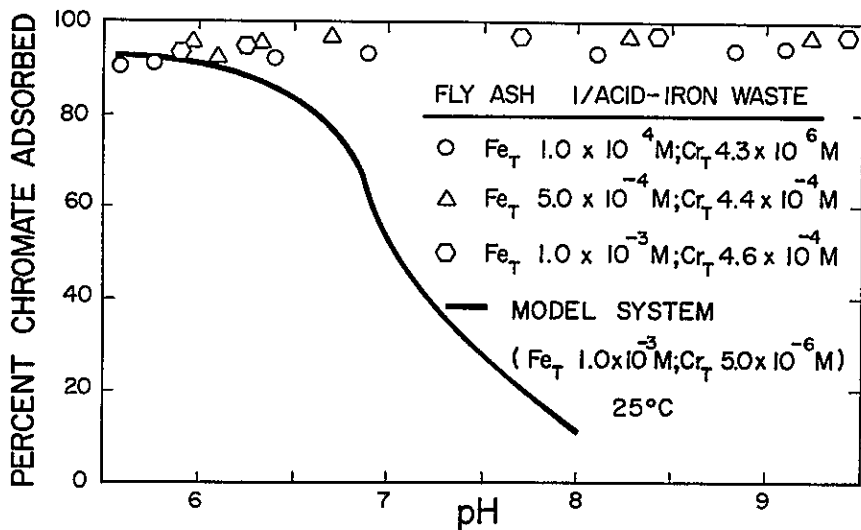


Figure 6-28. Chromate adsorption onto waste am- $Fe(OH)_3$  from fly ash 1 and in a model system

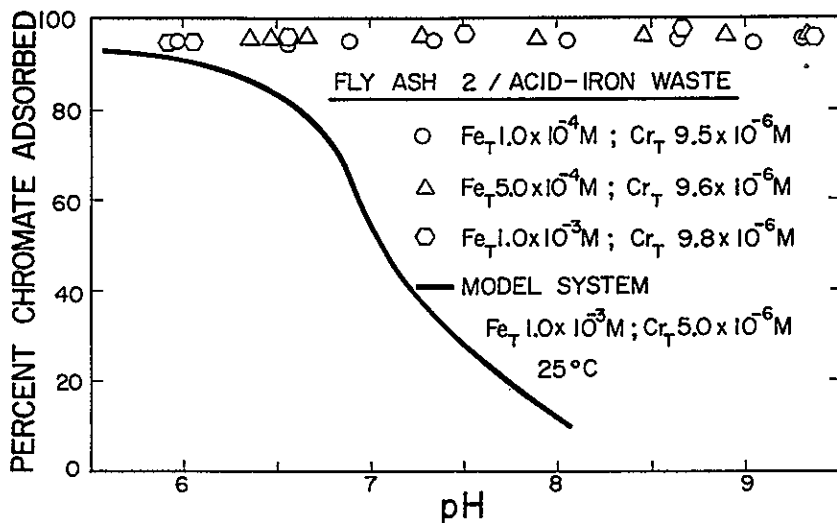


Figure 6-29. Chromate adsorption onto waste am- $Fe(OH)_3$  from fly ash 2 and in a model system

undergoing a precipitation reaction. With the present data the two phenomena cannot be distinguished one from the other. By changing solution conditions and checking reversibility of adsorption, the cause of the removal of chromate from the fly-ash systems might be determined.

#### Chromate Adsorption: Bromate Waste

The results of using acid-iron waste for the removal of chromate from a bromate waste are given in Figure 6-30. (The concentration of the major inorganic constituents have been given previously, see Table 6-11.) These results differ slightly from the results shown in Figures 6-28 and 6-29 for chromate removal from fly ashes 1 and 2. At pH 9, a decrease in chromate adsorption, typical of the beginning of an adsorption edge, is noticeable. As stated before, the only major difference in the concentration of inorganic ions between the fly-ash systems and bromate systems is the rather high concentration of Cu in the bromate system ( $\text{Cu}_T$   $2.2 \times 10^{-3}\text{M}$ ). The decrease in chromate adsorption at pH > 9 may be due to the formation of soluble, non-adsorbing  $\text{CuCrO}_4$  complexes. The  $\text{pK}_{a2}$  for chromic acid is 9.4 so the observed decrease in adsorption at pH  $\geq$  9 is consistent with the formation of non-adsorbing divalent metal/chromate complexes.

#### Chromate Adsorption: Vertan Waste

The results of using acid-iron waste for the removal of chromate from the vertan waste are given in Figure 6-31. The concentration of the major inorganic constituents in the vertan waste under experimental conditions have been given previously; see Table 6-13. As noted in the discussion of selenite adsorption, the vertan-waste system has a rather high concentration of EDTA (~0.2-0.3M). The general low percent adsorption of chromate is likely due to the adsorption of EDTA onto the oxide surface.

#### Arsenate Adsorption

The adsorption of arsenate onto amorphous iron hydroxide in model systems was discussed in Section 4. As shown in Figure 6-32, the pH adsorption edge for arsenate in the model systems is quite steep, covering a pH range of roughly 2 units (pH 9.5 to 11.5) as the percent adsorption goes from near zero to > 95% adsorption.

#### Arsenate Adsorption: Fly-Ash Waste

The results of using acid-iron waste for the removal of arsenate from fly ashes 1 and 2 are shown in Figures 6-33 and 6-34, respectively. The concentration of the

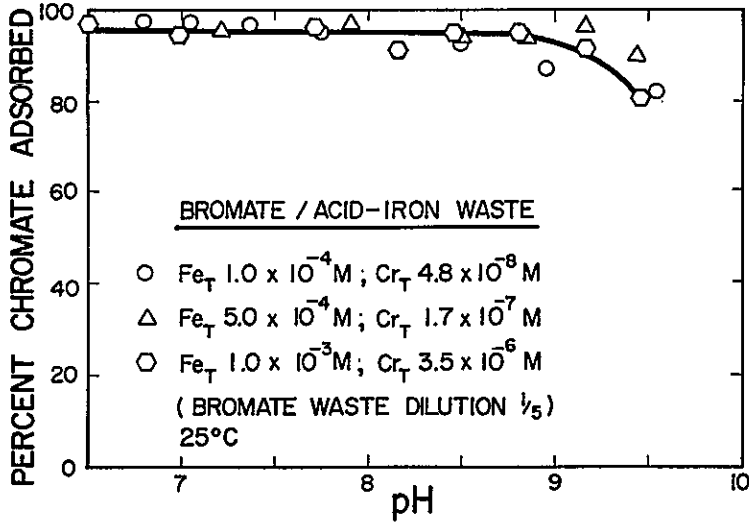


Figure 6-30. Chromate adsorption onto waste am- $Fe(OH)_3$  from bromate waste

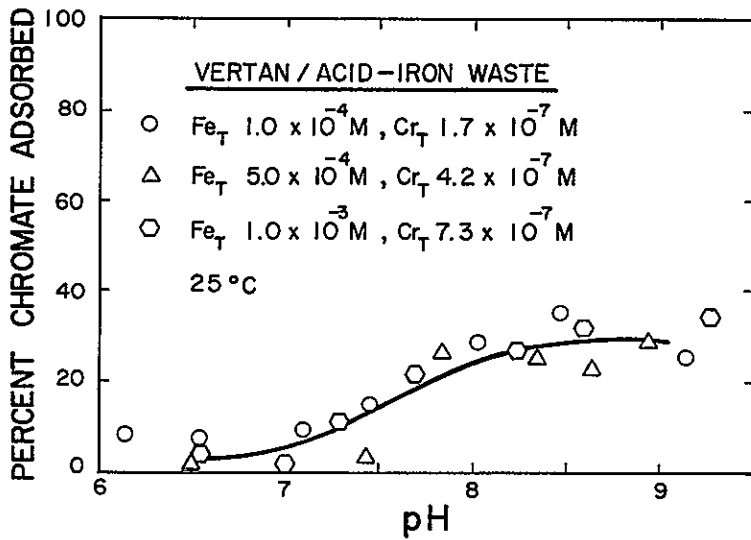


Figure 6-31. Chromate adsorption onto waste am- $Fe(OH)_3$  from a vertan waste solution

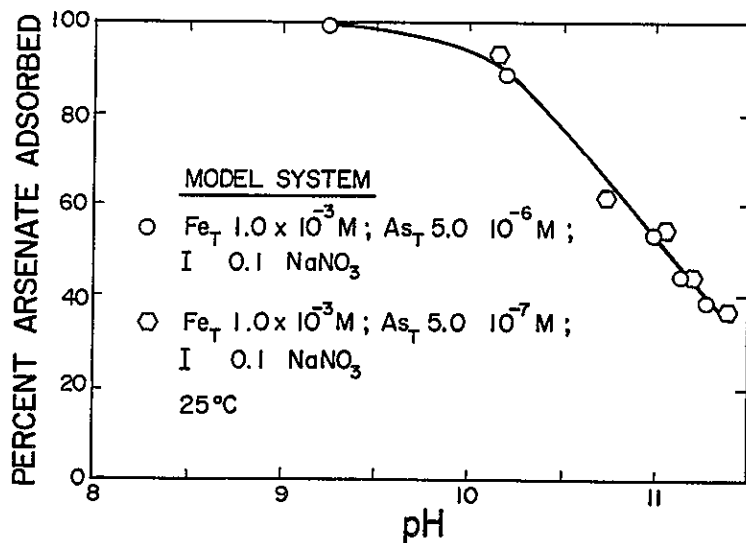


Figure 6-32. Arsenate adsorption onto am-Fe(OH)<sub>3</sub> in a model system

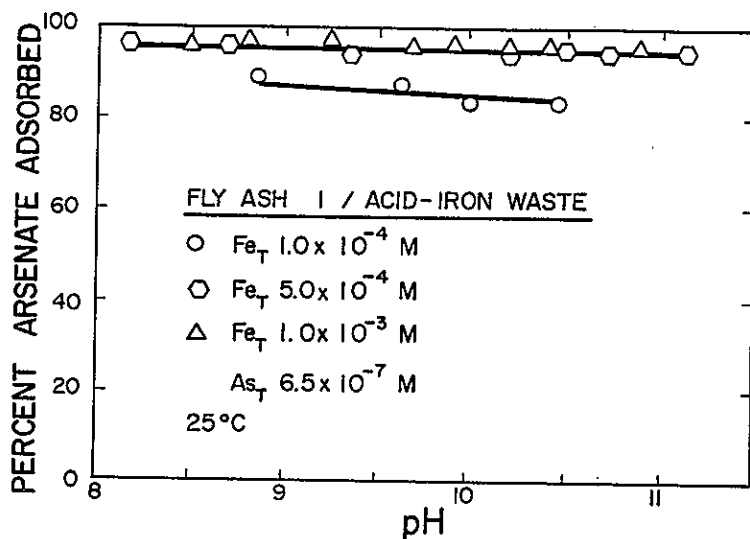


Figure 6-33. Adsorption of arsenate onto am-Fe(OH)<sub>3</sub> as a function of pH

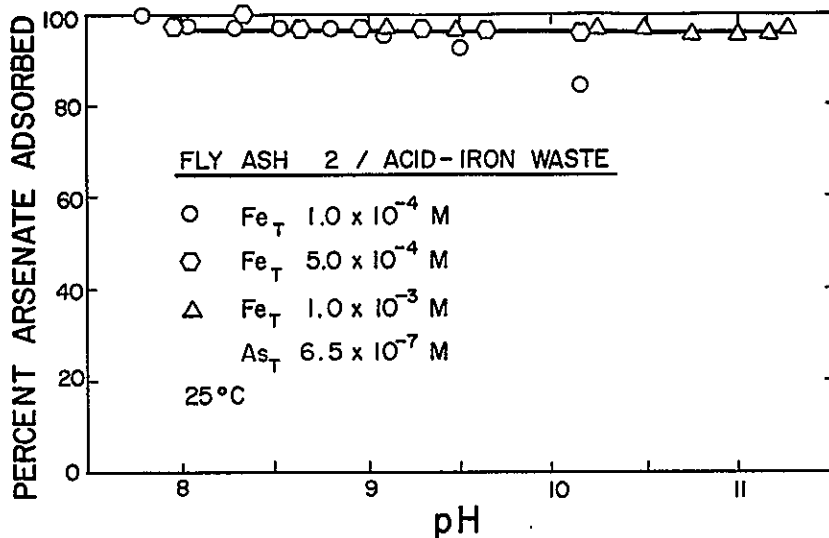


Figure 6-34. Arsenate adsorption onto waste am- $Fe(OH)_3$  from fly-ash 2 waste solution

major inorganic constituents of the fly ashes are given in Tables 6-9a and 6-9b. The same trends noted for chromate adsorption in the fly-ash systems are also present for arsenate adsorption; for  $As_T:Fe_T$  ratios  $< 1.3 \times 10^{-3}$  the observed adsorption is  $> 90\%$  over the entire pH range investigated (pH 8-11). The adsorption of arsenate above pH 9.5 is probably due to metal-like adsorption of arsenate complexes or ion pairs. Alternatively, there may be a precipitation reaction occurring in the system. The decrease in adsorption of arsenate when the  $As_T:Fe_T$  ratio  $\geq 6.5 \times 10^{-3}$  may be due to site limitation, i.e., perhaps there is surface competition between metal/ligand complexes as the number of available surface sites becomes limiting. Further work on arsenate is warranted.

#### Arsenate Adsorption: Bromate and Vertan Wastes

No experiments were run to determine the potential of acid-iron waste for the removal of arsenate from bromate and vertan wastes.

ANIONS: ION-PAIR AND COMPLEX FORMATION

It has been suggested that the formation of ion pairs and complexes may significantly alter the adsorption behavior of the anions. Ideally, it would be desirable to have experimentally determined association and stability constants for every possible ion pair or complex. Unfortunately, the association and stability constants of the ion pairs and complexes postulated for some arsenate, chromate, and selenite either have not been experimentally determined or are not available in the readily accessible literature. The ion pairs and complexes thought significant are shown in Table 6-14. Even though association constants are not available for the ion pairs shown in Table 6-14, it is reasonable that a significant concentration of the ion-pair species may exist. For example, an association constant of the order of 100, a typical value for a moderate association constant, would give a concentration of  $\text{CaSeO}_3$  of  $10^{-7}\text{M}$  (given  $\text{SeO}_3^{2-} = 10^{-6}\text{M}$  and  $\text{Ca}^{2+} = 10^{-3}\text{M}$ ). Likewise, provided a moderate stability constant exists, e.g.  $10^4$ , it is reasonable that significant concentration of complexes like  $\text{CuSeO}_3$ ,  $\text{CuCrO}_4$ , and  $\text{CuHAsO}_4$  would be present; a waste solution with a  $\text{Cu}^{2+}$  concentration of  $10^{-5}\text{M}$ , a  $\text{SeO}_3^{2-}$  concentration of  $10^{-6}\text{M}$ , and a stability constant for the complex formation of  $10^4$ , would give an equilibrium concentration of  $\text{CuSeO}_3$  of  $10^{-7}\text{M}$ . Hence, by assuming moderate association and stability constants, the concentration of the ion pairs and complexes shown in Table 6-14 are of the right order of magnitude to justify the explanations presented earlier.

Table 6-14

POSSIBLE ION PAIRS AND COMPLEXES  
FOR ARSENATE, CHROMATE, AND SELENITE

Ion Pairs	Complexes
$\text{CaSeO}_3$	$\text{CuSeO}_3$
$\text{CaCrO}_4$	$\text{CuCrO}_4$
$\text{CaHAsO}_4$	$\text{CuHAsO}_4$
$\text{KHSeO}_3$	
$\text{KHCrO}_4$	
$\text{KH}_2\text{AsO}_4$	

### Summary: Anion Removal from Wastes

The removal of arsenate, chromate, and selenite from several fly-ash wastes, using an acid-iron waste as the iron source for producing am-Fe(OH)<sub>3</sub> has been described in this section. The removal of selenite and chromate from a vertan waste and a bromate waste has also been described. In general, it appears the presence of EDTA in the vertan waste make treatment with coprecipitating iron hydroxide unfeasible. The results of selenite and chromate removal from the bromate and fly-ash waste indicate that acid-iron waste treatment of these wastes is feasible.

Several general remarks on acid-iron waste treatment of a given waste are appropriate here. For proper treatment design, a complete characterization of the waste must be made. As shown in this study, a knowledge of important adsorbing and non-adsorbing complexes or ion pairs may be necessary for design consideration. Possible precipitation reactions might be important. The existence of these types of complexes and reactions may cause considerable variation from model system behavior. Further work on real waste systems in conjunction with fundamental studies on complex, well-defined systems is required at this point.

Finally, an important consequence of this study is that the pH adsorption edge in a complex waste is obviously the result of adsorption of all adsorbing species. Any analysis of data should account for all such species in order to obtain predictable results.

### MIXING STUDIES

Preliminary studies of the effect of the mode of mixing of the iron solution with a simulated waste stream were undertaken to evaluate the degree to which trace element removal is affected by mixing conditions. Adsorption of cadmium under specified conditions was selected as the diagnostic tool to evaluate altered characteristics due to the mode of mixing. A well-characterized mixing chamber with an impellar was designed (Appendix B) to give a range of mixing conditions (i.e., residence time, rpm, etc.). A series of residence time distribution studies were conducted to determine changes in quality of mixing with variations in impellar speed and residence time. Two mixing conditions were selected as characteristic of fast and slow mixing rates. Variation in the adsorption characteristics (both equilibrium and kinetic) of cadmium was the criteria selected to indicate altered physical/chemical characteristics of the precipitated iron oxyhydroxide. Because details of the formation of the amorphous iron oxyhydroxide are relevant to the physical/chemical characteristics of the end product, they are summarized prior to discussion of the mixing studies themselves.

### Characteristics of Amorphous Iron Oxyhydroxide

Recent studies of hydrolysis and precipitation in ferric nitrate solutions provide information that is useful for the characterization of the amorphous iron oxyhydroxide produced for this study. Dousma and de Bruyn (14) presented evidence that the rate of formation of monomers and dimers of Fe(III) are fast and reversible reactions. However, above a critical pH (dependent on solution conditions) higher polymers were formed which resulted in increased optical density in solution. The formation of these higher polymers was slower but increased with increasing ionic strength and temperature.

Murphy et al. (15) characterized the ferric oxyhydroxide polycations formed in a range of ferric nitrate solutions by electron microscopy and density gradient ultra-centrifugation. The variables of interest were iron concentration, OH/Fe molar ratio, and aging time. In all solutions studied the ferric oxyhydroxy polycations were spherical and in the same size range (15-30 Å in diameter) after 3-4 hours of aging. A larger OH/Fe ratio generally increased the modal distribution of particle sizes at any given time of aging; however, after 3-4 hours of aging there was little difference in particle sizes as a function of OH/Fe ratio. Longer aging resulted in the formation of short rods consisting of 2-5 polycation spheres which then formed raftlike structures composed of rods. With further aging the spheres comprising the rods became indistinct and coalesced. The individual spheres and rods gave no electron diffraction pattern but goethite was identified in rafts where coalescence occurred.

Avotins (16) examined the effect of solution conditions and aging periods on iron oxyhydroxide precipitation. Ferric iron, precipitated from solution by dropwise addition of base to pH values between 6 and 9, formed an x-ray amorphous iron oxyhydroxide. Dousma and DeBruyn's (14) data indicate that the rapid dropwise addition of sodium hydroxide resulted in the rapid formation of the higher polymers followed by a slow oxolation process during a four-hour aging period. The dropwise addition technique may produce a wide range of particle sizes. The decrease in pH observed during the four-hour aging period is a result of protons produced by the slow oxolation reaction. The higher polymers correspond to the 15-30 Å diameter polycation spheres observed by Murphy et al. (15), who also showed that decreasing iron concentration lowers the average particle size within this range (15-30 Å diameter). Since the iron concentrations used in this study were generally an order of magnitude lower than the lowest concentration (0.0165M Fe) studied by Murphy et al. (15), one can conclude that the diameter of the iron oxyhydroxide

polycations in approximately 20 Å diameter (or less) at the end of four hours aging. Also, since precipitation always occurred at relatively high ionic strength (~0.1M) it is likely that the formation of rods was suppressed. The OH/Fe ratio was generally higher in this study (2-30), but a range of OH/Fe ratio values (0.95-2.37) in the solutions of Murphy et al. (15) had little discernible effect in the first four hours of aging on the formation of rods and coalescence reactions which introduce short-range order into the rods.

To summarize, it is believed that the amorphous iron oxyhydroxide produced in these adsorption/coprecipitation studies was composed of flocculated aggregates of spherical polycations about 20 Å in diameter, and rafts of these particles, similar to the structures observed by other workers (14).

### Results of Mixing Experiments

The results of the mixing study are in two parts: 1) evaluation of the mixing characteristics of the experimental mixing chamber, and 2) evaluation of the characteristics of the solid iron oxyhydroxide formed under different mixing conditions. Details of the experimental apparatus and protocol are given in Appendix B.

Characteristics of Mixing Chamber. Comparisons between residence time distribution (RTD) curves for ideal mixing conditions and the experimental cases studied was used as a measure of the performance of the mixing vessel under experimental conditions (17).

In the ideal case the pulse of tracer instantaneously forms a homogeneous solution of concentration  $C_0$ . The concentration of tracer in the outflow,  $C$ , changes with time and is characteristic of mean residence time  $\bar{t}$ . This relationship is given as (18,19)

$$C = C_0 \exp(-t/\bar{t}) \quad (6-1)$$

where  $C_0$ ,  $C$  are initial and instantaneous concentrations of tracer, and  $t$ ,  $\bar{t}$  are real time and mean residence time, respectively. The theoretical residence time,  $\bar{t}$ , is defined as the ratio of the vessel volume,  $V$ , to the fluid flowrate,  $Q$ ,

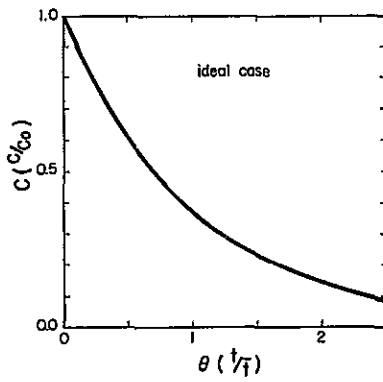
$$\bar{t} = V/Q \quad (6-2)$$

A dimensionless measure of the change in tracer concentration can be obtained by dividing both sides of Eq. 6-1 by  $C_0$  and defining the time ratio  $\theta = (t/\bar{t})$ . Thus a plot of  $C/C_0$  vs  $\theta$  is known as a C-curve. The value of C-curves is ease of analysis and comparison among RTD data for several different residence times. Differences among peak heights, shape of curves and other characteristics can be readily analyzed. Figure 6-35a depicts the C-curve for the ideal mixing case. C-curves for each of the several cases studied are shown in Figures 6-35b through 6-35e for conditions of  $\bar{t}$  5 sec, 500 RPM;  $\bar{t}$  5 sec, 3000 RPM;  $\bar{t}$  30 sec, 500 RPM; and  $\bar{t}$  30 sec, 3000 RPM.

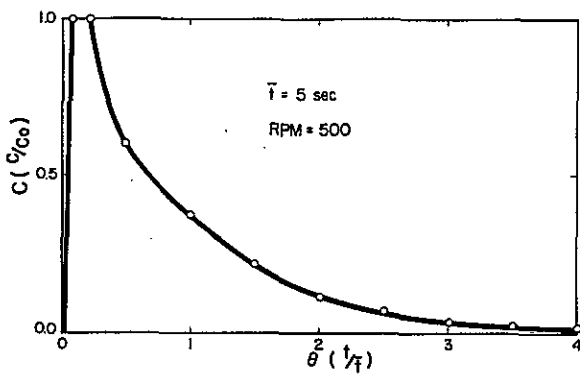
In the ideal case  $C/C_0$  decreases to  $e^{-1}(0.367)$  at  $\theta = 1$ . Figure 6-36 presents a plot of  $\bar{t}$  against  $t$  (elapsed time) at  $C/C_0$  of 0.367 for a range of mixing rates. The cases for  $\bar{t} \leq 20$  sec at all RPM values are very close to the ideal case while there is a slight decrease in elapsed time compared to residence time for a  $\bar{t}$  of 30 sec. Major deviations occurred for RPM of zero.

A comparison of peak heights in Figure 6-35 shows that at 500 RPM ( $\bar{t}$  5 sec),  $C/C_0$  exceeds a value of 1.0. This can be viewed as indicative of short circuiting in the mixing vessel. Based on tracer studies the conditions chosen for evaluating the effect of mixing rate (mean residence time,  $\bar{t}$ ) on solid characteristics were  $\bar{t}$  of 5 sec, 3000 RPM, and  $\bar{t}$  of 30 sec, 3000 RPM. Mixing conditions differed by a factor of six with the slow rate ( $\bar{t}$  30 sec) indicative of large-scale mixing operations.

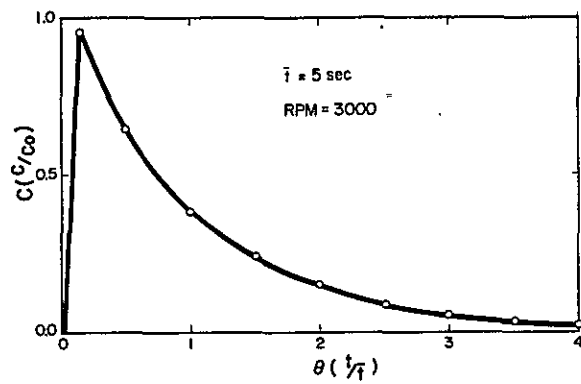
Evaluation of Solid Characteristics. Kinetic and equilibrium experiments were designed to indirectly evaluate any changes in the physical/chemical characteristics of the iron oxyhydroxide formed under different mixing conditions. The adsorption behavior of cadmium was used as a diagnostic tool. Any changes in either the kinetic or equilibrium adsorptive behavior of cadmium is assumed reflective of changes in the physical/chemical nature of the iron oxyhydroxide solid. Figures 6-37a and 6-37b present kinetic data for cadmium removal under conditions of coprecipitation. No significant differences are seen between rapid (5 sec) and slow (30 sec) mixing conditions. In addition, the kinetics of cadmium removal are indistinguishable from kinetics of adsorption on preformed iron oxyhydroxide (Appendix B). Results for the equilibrium studies on solids formed under different mixing conditions are given in Figure 6-38. Figures 6-38a and 6-38b give equilibrium data for coprecipitation of cadmium under two different mixing conditions. Comparison is made at 50 percent removal; in both cases this occurs at pH 6.8.



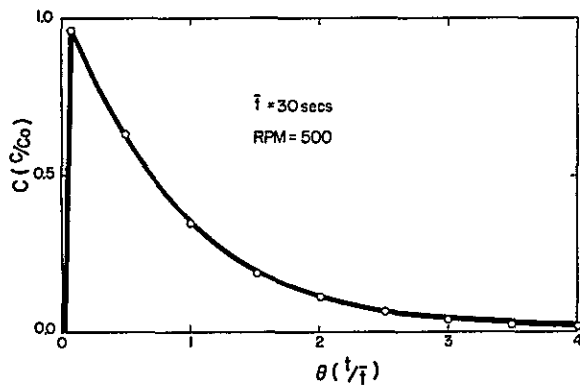
(a)



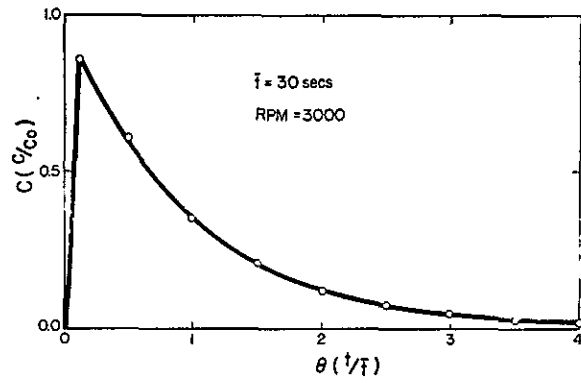
(b)



(c)



(d)



(e)

Figure 6-35. Mixing characteristic curves for ideal case and four experimental systems

142115, 2116

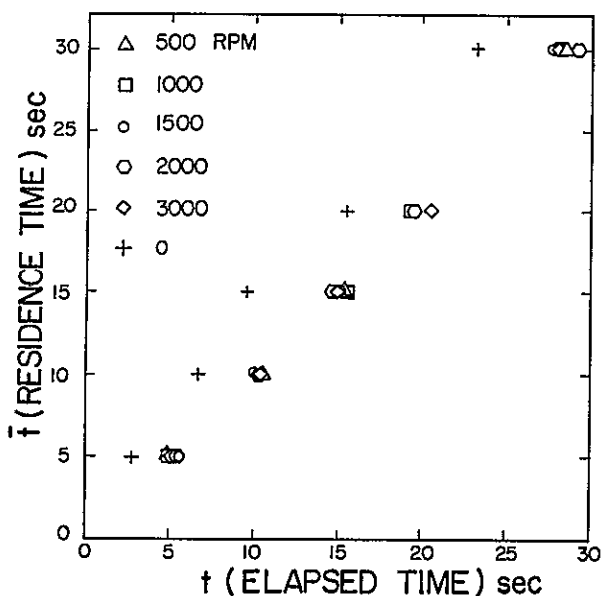


Figure 6-36. Elapsed time versus residence time at constant  $C/C_0$  (0.367) for various experimental mixing rates

To evaluate the characteristics of the solid one hour after formation (all other conditions the same), the solid was aged one hour and then cadmium was added. These experimental data are given in Figures 6-38c and 6-38d for the two different mixing conditions. Again, no perceptible differences are noted, either between mixing conditions or time of contact with cadmium (e.g., Figure 6-38a vs 6-38c). Thus the conclusion that for reasonable mixing operations (complete mixing within 30 sec) the resultant solids show no difference as is measured by the removal of cadmium. On this basis additional mixing studies were precluded. Since most engineering processes (e.g., coagulation, sedimentation) require typical contact times on the order of 30 to 90 minutes it is concluded that mixing conditions are of minor importance so long as complete dispersion of the iron reagent occurs within the first minute. This is achievable with currently available commercial mixing devices.

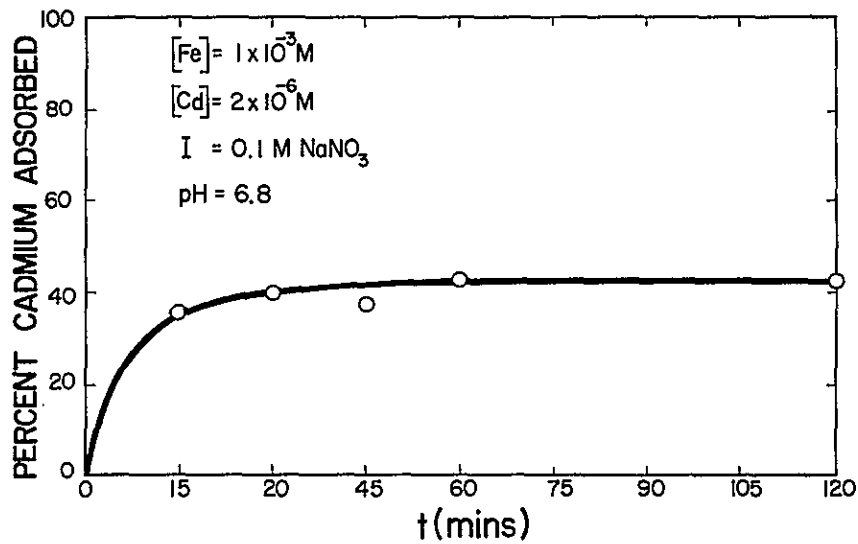


Figure 6-37a. Kinetics of Cd adsorption on am-Fe(OH)<sub>3</sub> formed in mixing chamber with  $\bar{t} = 5$  sec

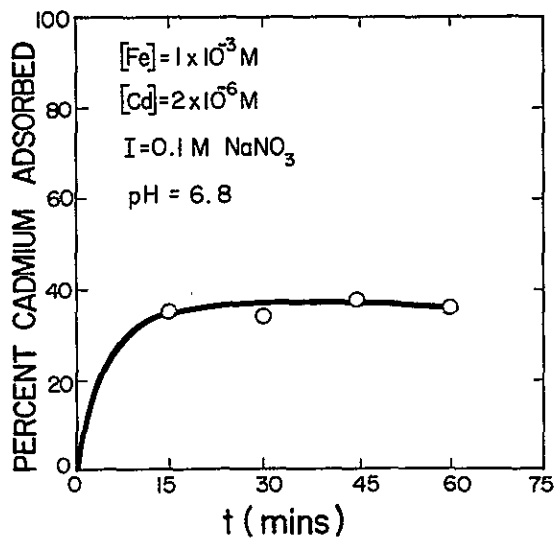
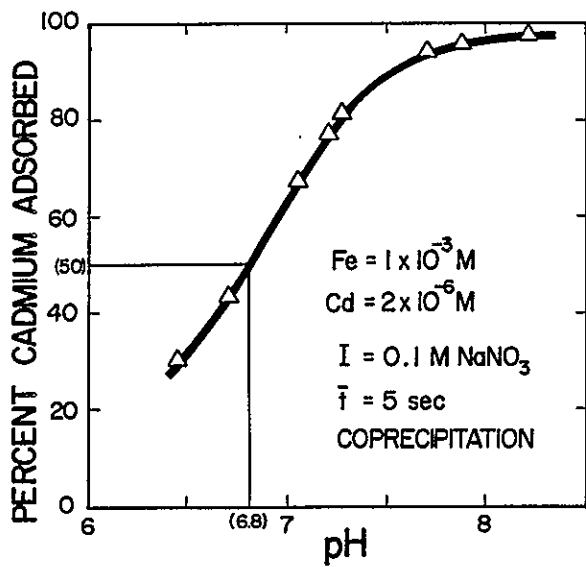
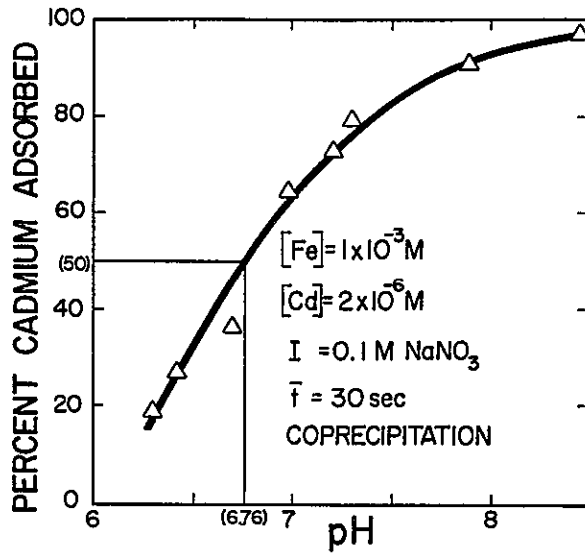


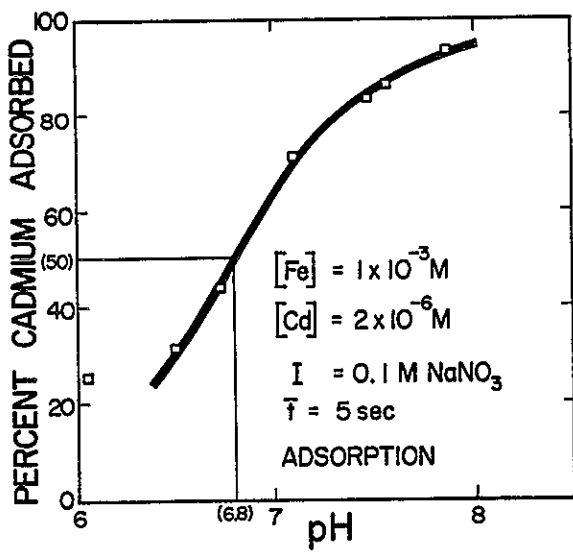
Figure 6-37b. Kinetics of Cd adsorption on am-Fe(OH)<sub>3</sub> formed in mixing chamber with  $\bar{t} = 30$  sec



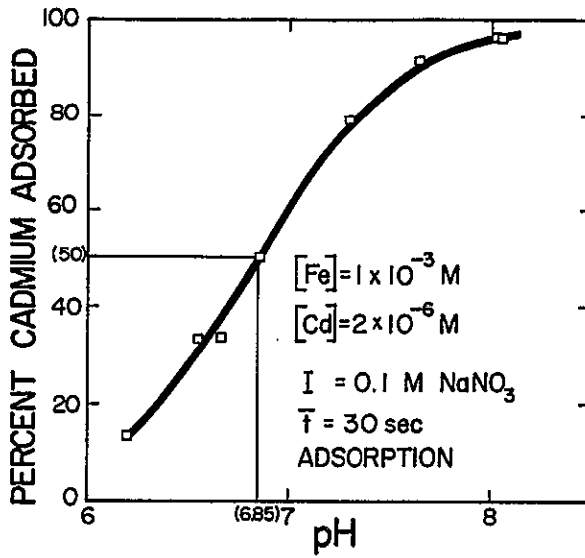
(a)



(b)



(c)



(d)

Figure 6-38. pH-adsorption and pH-coprecipitation edges for Cd on am-Fe(OH)<sub>3</sub> formed under varying mixing regimes

## COAGULATION AND SETTLING STUDIES

Coagulation and settling studies were conducted in order to help assess the technical and economic feasibility of using waste-iron solutions for trace metal removal from certain power-plant effluents. The technical feasibility assessment for this study is based on residual turbidity after prescribed periods of mixing, flocculation, and settling. The economic feasibility is assessed in terms of the doses of iron and polymer (Primaflor) required, as well as the required mixing, flocculation, and settling times.

This information was developed through a phased program of experimentation in which the important variables affecting residual turbidity measurements were varied sequentially so that in each step one variable was optimized. The variables which were examined included iron dose, polymer dose (Primaflor), pH, waste dilution, and settling time. A standard set of mixing, flocculation, and settling conditions were used for all experiments except, of course, settling time. These conditions, as well as the other methods used in this study, are included in Appendix B.

### Technical Feasibility

The first parameter to be investigated was iron dose. The wastes studied included fly-ash 1 and 3 solutions, as well as 1:10 diluted bromate solution and 1:100 diluted vertan solution. A range of iron doses of from  $1.0 \times 10^{-4}M$  to  $2.5 \times 10^{-3}M$ , at pH 7.0, and a polymer dose of 1.0 mg/l, was examined. Results for the bromate and vertan solutions are shown in Figure 6-39. On the basis of these results an iron dose of  $1.0 \times 10^{-3}M$  was selected as optimum for both the 1:10 bromate and the 1:100 vertan solutions. Similar data were generated for fly-ash 1 and 3 solutions; these results indicated that an iron dose of  $3.0 \times 10^{-4}M$  would provide for optimal removal efficiency, based on residual turbidity measurements.

In the next set of experiments, the polymer dose was varied from 0.5 to 5.0 mg/l, with the pH again held constant at 7.0 and the iron dose at  $3 \times 10^{-4}M$  for the fly ashes and  $1.0 \times 10^{-3}M$  for the boiler-cleaning wastes. The results of this experiment on the boiler-cleaning wastes are shown in Figure 6-40. From these experiments an optimal polymer dose of 3.0 mg/l was chosen. Similar experiments on the fly-ash solutions also indicated that a 3.0 mg/l dose would be optimal for maximum residual turbidity reduction.

The next parameter to be varied was pH. The results of these experiments (for all wastes except the 1:100 vertan) are shown in Figure 6-41. Combining these

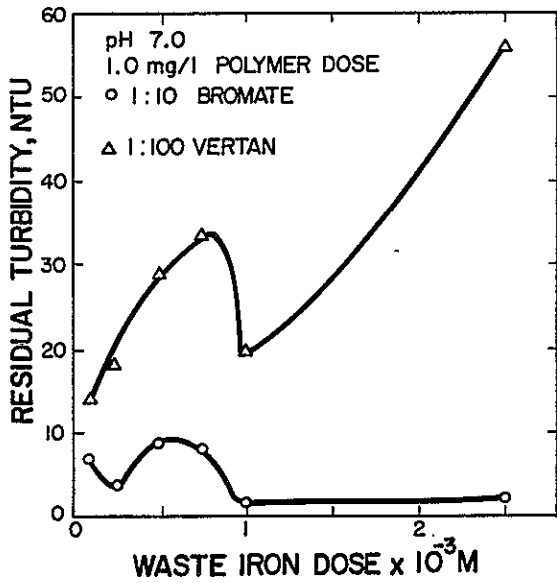


Figure 6-39. Variation of residual turbidity with iron dose for 1:10 bromate and 1:100 vertan solutions

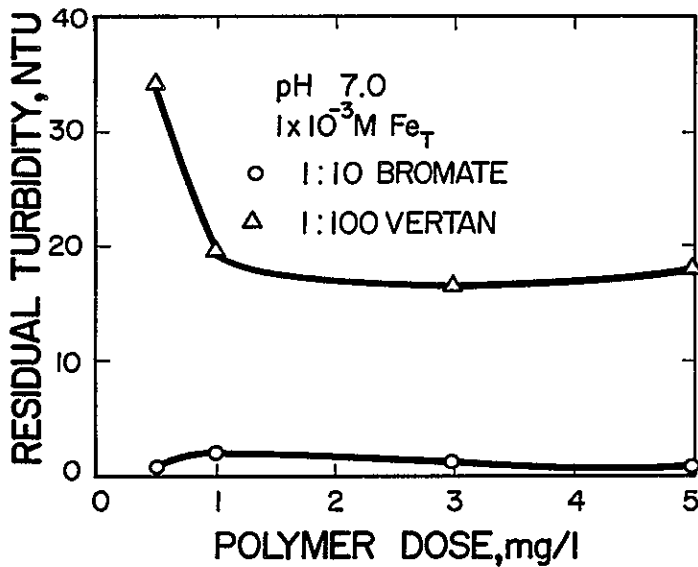


Figure 6-40. Variation of residual turbidity as a function of polymer dose for 1:10 bromate and 1:100 vertan solutions

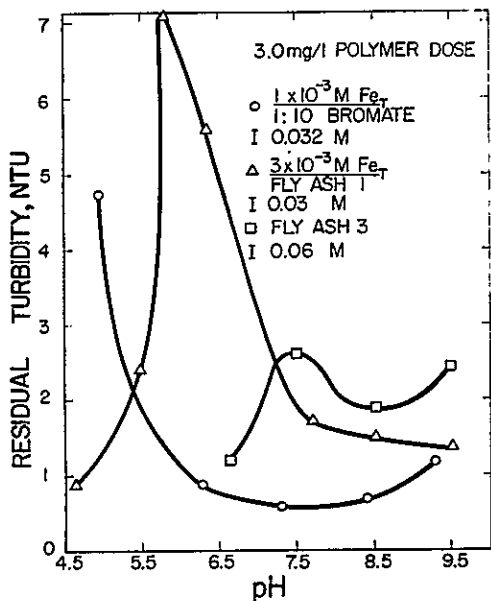


Figure 6-41. Variation of residual turbidity as a function of pH for 1:10 bromate and fly-ash solutions

observations with the results of the adsorption experiments reported previously, an optimum pH was chosen for the fly-ash solutions and the 1:10 bromate solution. An optimum pH of 8.5 was chosen for the fly-ash solutions while a pH of 8.25 was chosen for the 1:10 bromate. The results of the experiments on the 1:100 vertan dilution indicated that optimum coagulation and settling occurred around pH 5.5; however, very little adsorption occurs at that pH, and hence the vertan solution was essentially untreatable by this process. Thus, no further coagulation tests were run on the vertan solution.

Because the bromate solution was diluted, a series of experiments were run to see how residual turbidity was affected by bromate waste concentration. The results of these tests are shown in Figure 6-42. As can be seen from the data, the magnitude of the dilution factor has very little effect on residual turbidity, except at the lowest dilution factor of two.

Lastly, the rate of settling in the fly-ash solutions and 1:10 bromate solutions was investigated. The results of these studies are shown in Figure 6-43. As the data indicate, settling occurs rapidly and is relatively unchanged after 10-15 min. It is apparent from Figure 6-43 that the bromate solution under the conditions

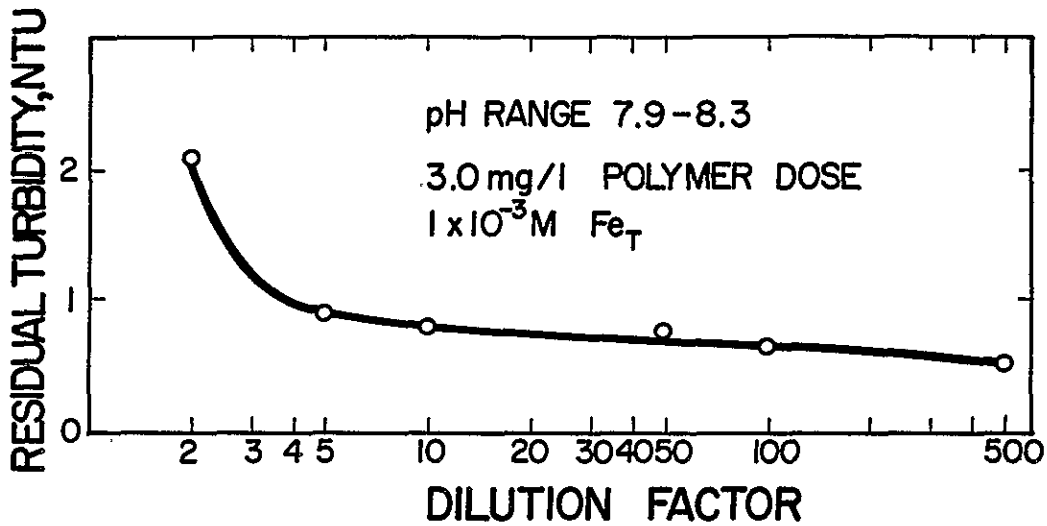


Figure 6-42. Variation of residual turbidity as a function of bromate dilution

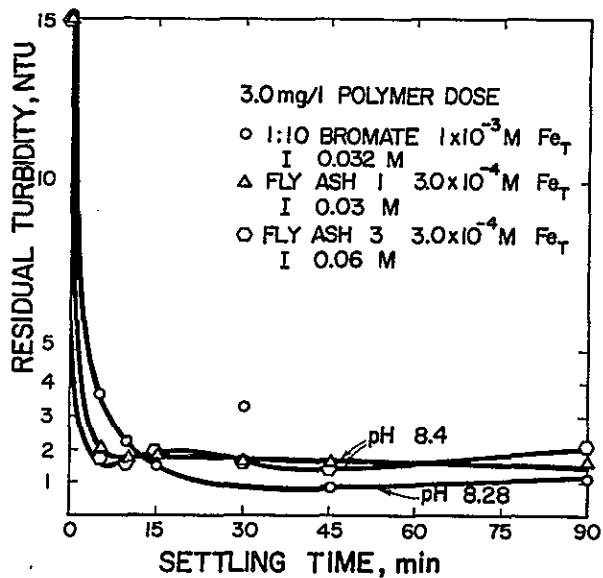


Figure 6-43. Residual turbidity as a function of settling time for 1:10 bromate and fly-ash solutions

chosen, is most amenable to effective settling, while there seems to be little difference in settling characteristics between the fly-ash solutions.

### Economic Feasibility

As discussed previously, under appropriate conditions it is possible to substantially remove trace elements from ash-transport water and waterside boiler-cleaning wastes by adsorption of the elements onto waste-iron oxyhydroxide particles. The adsorption work indicates that greater than 90 percent removal of some of the elements from solution can be achieved with an iron dose as low as  $1 \times 10^{-4} \text{M Fe}_T$  at a pH greater than 8.0 for the wastes considered. Experiments conducted to determine the settling characteristics indicated that optimal settling of the waste iron oxyhydroxide particles occurred in the pH range of 8.0-8.5 and at a polymer dose of 3.0 mg/l. Considering the above information one can calculate the comparative costs of using the acid-iron waste versus purchasing the iron needed. Either ferrous sulfate or ferric chloride would be acceptable synthetic iron sources. Because the cost of using ferrous sulfate is about one-half of the unit cost of using ferric chloride, ferrous sulfate is the synthetic iron source used in the cost calculations. However, use of ferrous sulfate may be complicated in some situations by consumption of oxygen required for the oxidation of ferrous iron. If the dissolved oxygen level of the waste is low (below 1.0 mg/l, as oxidation of a  $1 \times 10^{-4} \text{M Fe}^{+2}$  solution requires somewhat less than 1.0 mg/l of  $\text{O}_2$ ), ferric chloride would probably be a better choice. The cost per million gallons of waste solution for ferric chloride is about \$8.20 compared to about \$3.80 for  $\text{FeSO}_4$ . Substitution of  $\text{FeCl}_3$  would have little effect on total chemical costs.

As can be seen from Table 6-15 the chemical costs per million gallons of solution treated vary according to the waste treated. For fly-ash 1 and 2 solutions it appears to be less expensive to use a synthetic iron source rather than the acid-iron, while for fly-ash 3 solution and the bromate waste, the chemical costs associated with the use of the acid-iron waste appear to be somewhat less. Several remarks should be made regarding this analysis. First, the data presented include only the cost of chemicals and does not include either capital or operating costs of tanks, piping, metering equipment, and other appurtenances that would be needed to make the process work. With respect to the apparent reduced costs of using a synthetic iron source for fly-ash 1 and 2 solutions, it should be noted that the acid-iron waste would still need treatment. Also it should be noted that very acidic and basic solutions are produced elsewhere in a coal-fired power plant so that it might be possible to reduce or eliminate the costs associated with acid or base addition through the use of these waste materials.

Table 6-15

COMPARATIVE COSTS OF USING ACID-IRON WASTE VS.  
FERROUS SULFATE FOR TRACE ELEMENT REMOVAL  
(Costs \$/MG of Waste Solution)

Chemicals <sup>a</sup>	Fly-Ash 1 Solution		Fly-Ash 2 Solution		Fly-Ash 3 Solution		Bromate Solution	
	Acid-Iron	FeSO <sub>4</sub>	Acid-Iron	FeSO <sub>4</sub>	Acid-Iron	FeSO <sub>4</sub>	Acid-Iron	FeSO <sub>4</sub>
FeSO <sub>4</sub>	-	3.8	-	3.8	-	3.8	-	3.8
Polymer	25.1	25.1	25.1	25.1	25.1	25.1	25.1	25.1
NaOH	240	49.6	187	23.0	-	-	-	-
H <sub>2</sub> SO <sub>4</sub>	-	-	-	-	140.3	167.0	300	307
	265.1	78.5	212.1	51.9	165.4	195.9	325.1	335.9

<sup>a</sup>The following unit costs were assumed:

Chemical	Unit Cost
FeSO <sub>4</sub>	\$ 60/ton (20)
Polymer	\$ 1/lb (21)
NaOH	\$340/ton (20)
H <sub>2</sub> SO <sub>4</sub>	\$ 60/ton (20)

To get some idea of the relative magnitude of the other cost items associated with a treatment plant, it is instructive to look at Table 6-16 which lists the projected annual costs of a central treatment plant for both a 100- and 1000-MW plant. This facility would handle such wastes as from a waterside and fireside boiler tube, an air preheater, ion exchange, a laboratory, cooling-tower-basin washing, boiler and scrubber blowdown as well as floor-drain. Costs for chemicals and power for a 1000-MW plant require about 12 percent of the annual expenditure. If one were to calculate the annual chemical costs of the adsorption process discussed in this report for a 1000-MW plant, they would range from \$7600 to \$35,000 depending on the waste and the source of iron. This calculation also assumes a blowdown of 400 gpd/MW from the ash-transport water system and mixing of the bromate waste with the fly-ash transport water.

The last item which should be mentioned is the ability of the adsorption process to meet the waste discharge limitations imposed on the effluents from coal-fired

Table 6-16

ESTIMATED ANNUAL COSTS--CENTRAL TREATMENT PLANT FOR COAL-FIRED POWER PLANTS<sup>a</sup>  
 (Based on Flow of 220 GPD/MW)

Item	100 MW		1000 MW	
	Retrofit \$ (1000)	New Sources \$ (1000)	Retrofit \$ (1000)	New Sources \$ (1000)
Construction Cost (CC)	178.9	138.3	582.3	450.0
Total Capital Cost (TCC)	232.5	179.9	756.9	585.0
Maintenance (at 3% of CC)	5.4	4.1	17.5	13.5
Fixed Charges (at 15% of TCC)	34.9	27.0	113.5	87.7
Chemicals and Power	4.2	4.2	38.0	38.0
Labor	100.0	100.0	190.0	190.0
Total Annual Cost	144.5	135.3	359.0	329.2
Unit Cost, mills/kwh:				
Base-load (0.77 capacity factor) <sup>b</sup>	0.214	0.201	0.055	0.049
Cyclic (0.44 capacity factor) <sup>b</sup>	0.375	0.353	0.096	0.086
Peaking (0.09 capacity factor) <sup>b</sup>	1.84	1.72	0.467	0.422
<sup>a</sup> Source: (1).				
<sup>b</sup> Note: Assumes full costs of maintenance, chemicals, power, and labor. These costs would actually be less than shown and would reflect the extent of utilization of the plant.				

power plants. Presently, limitations have only been imposed on the iron and copper content of the effluents from the boiler-cleaning operations; no trace-metal-effluent limitations have yet been placed on the effluent from fly-ash ponds. The cost estimates developed previously assume that the waste streams are treated separately. For the fly-ash solutions, using a synthetic iron source, both the iron and copper limitations would be met as iron and copper content of the fly-ash solutions are at least two orders of magnitude below the limit of 1.0 mg/l. When the waste-iron solution is used the limitations would also be met as the oxidation of ferrous ion to ferric ion and its subsequent precipitation as amorphous iron oxyhydroxide reduced the soluble iron to below 1.0 mg/l. As for the copper, its concentration of 160 mg/l in the acid-iron is reduced to about 1.74 when mixed with any of the three fly-ash solutions studied when the waste-iron dose is  $1 \times 10^{-4} \text{M Fe}_T$

Ninety percent copper adsorption onto the amorphous iron oxyhydroxide would reduce the copper concentration to well below the 1.0-mg/l level.

For the bromate solution on the other hand, copper effluent limitations could not be reached with either ferrous sulfate or acid-iron waste without some dilution of the bromate waste. For instance, it was found in the experimental section that about a one-hundred-fold dilution was needed for a 90-percent adsorption of copper at iron levels of  $1 \times 10^{-4} \text{M Fe}_T$ . At such a dilution the copper concentration of the waste would be about 7.2 mg/l, so that 90-percent adsorption would leave about 0.7 mg/l copper in solution. Such a large dilution is easily obtained by mixing the fly-ash transport waters with the bromate. For example, data presented in the EPA Effluent Limitation Document (1) indicate that for a 1000-MW power plant about 400,000 GPD of fly-ash transport blowdown waste are produced while the bromate waste would be about 100 GPD, indicating that an average dilution of 4000:1 is possible. Of course, if the bromate waste was mixed with such volumes of fly-ash transport water the costs of treating the additional bromate solution would become quite small and therefore the cost of treatment would be almost equivalent to the cost of treating the fly-ash transport water separately.

#### REFERENCES

1. EPA Development Document for Effluent Limitations and Source Performance Standards for the Steam Electric Generating Point Source Category. EPA 440/1-74-029-9 (1974).
2. J. K. Rice and S. D. Strauss. "Water-Pollution Control in Steam Plants." Power, 120(4), S1-S20 (1977).
3. N. A. Curry. "Philosophy and Methodology of Metallic Waste Treatment." Paper presented at the 27th Industrial Waste Conference, Purdue University, May 1972.
4. T. L. Theis. "The Potential Trace Metal Contamination of Water Resources Through the Disposal of Fly Ash." 2nd National Conference on Complete Water Reuse, Proc., 219-224 (1975).
5. Standard Methods for the Examination of Water and Wastewater, 14th ed. American Public Health Association, Washington, D.C., 1976.
6. Duke Power Company. "Ash Basin Equivalency Demonstration for Metal-Cleaning Wastes." Duke Power, Charlotte, North Carolina, 1976.
7. T.-Y. J. Chu, G. R. Steiner and C. L. McEntyre. "Removal of Complex Copper-Ammonia Ions from Aqueous Wastes with Fly-Ash." J. Water Poll. Cont. Fed., 50, 2157-2174 (1978).
8. D. G. Shannon and L. O. Fine. "Cation Solubilities of Lignite Fly Ashes." Environ. Sci. Tech., 8(12), 1026-1028 (1974).

9. D. R. Dreesen, G. S. Gladney, J. W. Owens, B. L. Parlang, C. L. Wienke and L. G. Wangen. "Comparison of Levels of Trace Elements Extracted from Fly Ash and Levels Found in Effluent Waters from a Coal-Fired Power Plant." Environ. Sci. Tech., 11, 1017-1018 (1977).
10. T. L. Theis and J. L. Wirth. "Sorptive Behavior of Trace Metals on Fly Ash in Aqueous Systems." Environ. Sci. Tech., 11, 1096-1100 (1977).
11. C. W. Davis. Ion Association. London: Butterworth, 1962.
12. G. H. Nancollas. Interactions in Electrolyte Solutions. New York: Elsevier Publishing Company, 1966.
13. B. K. G. Teng. The Chemistry of Clay-Organic Reactions. New York: Halsted Press, 1974.
14. J. Dousma and P. L. DeBruyn. "Hydrolysis-Precipitation Studies of Iron Solutions. I. Model for Hydrolysis and Precipitation from Fe(III) Nitrate Solutions." J. Coll. Interface Sci., 56, 527 (1976).
15. P. J. Murphy, A. M. Posner and J. P. Quirk. "Characterization of Partially Neutralized Ferric Nitrate Solutions." J. Coll. Interface Sci., 56, 270 (1976).
16. P. V. Avotins. "Adsorption and Coprecipitation Studies of Mercury on Hydrous Iron Oxides." Ph.D. Thesis, Stanford University, Stanford, Calif., 1975.
17. J. B. Gray. "Flow Patterns, Fluid Velocities, and Mixing in Agitated Vessels," Mixing: Theory and Practice, Vol. 1. New York: Academic Press, 1966.
18. F. A. Holland and F. S. Chapman. Liquid Mixing and Processing in Stirred Tanks. New York: Reinhold Publishing Corp., 1966.
19. O. Levenspiel and K. B. Bischoff. "Patterns of Flow in Chemical Process Vessels," Adv. in Chemical Engineering, Vol. 4. New York: Academic Press, 1963.
20. Chemical Marketing Reporter, 214(12), September 18 (1978).
21. R. L. Culp, G. M. Wesner and G. L. Culp. Handbook of Advanced Wastewater Treatment, 2nd ed. New York: Van Nostrand Reinhold Company, 1978.

## Section 7

### SUMMARY, CONCLUSIONS, AND SUGGESTIONS FOR FUTURE WORK

This study has examined the adsorptive/coprecipitation behavior of several inorganic cations and anions in systems containing x-ray amorphous iron oxyhydroxide. The project examined experimentally several simple, well-characterized model systems to establish type behavior in sufficient detail to allow interpretation of subsequent experimental work on less well-characterized waste materials. A prominent feature of this project was evaluation of the feasibility of utilizing iron-bearing waste liquids as source materials for the precipitation of amorphous iron oxyhydroxide in trace element removal processes. Although much of the experimental work was conducted in clean-model systems, it is now possible to characterize the roles of certain types of complexing ligands and competing metals and ligands, and their significance in controlling the distribution of trace elements at the solution/oxide interface.

#### SUMMARY

The terms adsorption and coprecipitation are used interchangeably. No significant difference was noted in the rate and equilibrium data for removal of trace elements on preformed iron oxyhydroxide (adsorption) and simultaneous precipitation (coprecipitation). Reversibility was achieved in both adsorption and coprecipitation systems with the contact time studied (4-6 hours). Thus, trace element adsorption onto and coprecipitation with amorphous iron oxyhydroxide are considered to be operationally the same.

Adsorption of cadmium, zinc, copper, lead, silver, arsenic, selenium, and chromium onto amorphous iron oxyhydroxide and  $\gamma$ -alumina was studied as a function of adsorbent and adsorbate concentrations, solution composition, and pH. All systems were studied under well-controlled conditions.

Fractional adsorption of dissolved metal increases abruptly in a narrow pH range. The pH of abrupt adsorption increases in the order  $Pb < Cu < Zn < Cd \approx Ag$  and  $SeO_4 < CrO_4 < SeO_3 < AsO_4$  under otherwise identical conditions. At extremely low

surface coverage, for a given adsorbent concentration, fractional adsorption is independent of total metal concentration. However, at greater adsorption densities, fractional sorption decreases with increasing adsorbate concentration. The Langmuir isotherm cannot model the data.

The adsorption density at which fractional sorption first becomes dependent on total adsorbate concentration varies over several orders of magnitude for different metals on the same adsorbent. The behavior can be modeled by postulating that the surface consists of a wide distribution of surface-site types. Competitive adsorption experiments indicate that in many cases different metal ions preferentially adsorb to different groups of sites. Therefore, adsorption of one metal often may have only a small effect on adsorption of a second ion.

Ligands which form dissolved complexes with metal ions can either increase or decrease metal adsorption. Chloride, sulfate, and ammonia generally decrease fractional adsorption of cadmium at a given pH. The decrease is consistent with the hypothesis that the complexed metal adsorbs somewhat less strongly than the uncomplexed metal. For example, cadmium thiosulfate complexes adsorb in a qualitatively different manner and, on oxides with sufficiently positive surface charge, they can adsorb more strongly than free aquo cadmium. On highly negative surfaces there is negligible adsorption of these complexes. On the other hand, sulfato and chloro complexes of cadmium always adsorbed more weakly than aquo cadmium.

The James-Healy, surface-complexation, and SGMA (Stanford General Model for Adsorption) adsorption models all assume that oxide surfaces are composed of only one type of site. They fail to totally predict the observed variations in adsorption with changing adsorbate concentration. The SGMA adsorption model has been used to model adsorption in this study.

Experimental work to evaluate removal of trace elements from typical waste streams indicated feasibility for removal of trace anions and cations from power-plant fly-ash transport water as well as an ammonia bromate cleaning waste. Results indicated that the adsorption/coprecipitation process would not be feasible for treating trace elements contained in an EDTA vertan cleaning waste. Experimental results from studies using real power-plant waste materials have been interpreted in terms of the general behavior characteristics of well-characterized model systems. Complete verification of the behavior of trace element removal in complex real wastes was not achieved.

## CONCLUSIONS

Based on work presented in this report the following major conclusions are drawn:

1. Trace elements, in both anionic and cationic form can potentially be removed from very dilute solutions utilizing either a preformed solid ( $\text{Fe}(\text{OH})_3$ ) or by precipitating the solid in situ. The removal behavior of the trace elements studied appeared to be identical regardless of the mode of preparation of the freshly precipitated amorphous iron oxyhydroxide.
2. The presence or absence of competing ligands for trace metal cations can have a dramatic effect on the removal of the trace metals. This effect is directly correlated to the chemical behavior of the solution complex of the trace metal, where the complex may adsorb or not adsorb, altering the adsorption behavior of the trace metal accordingly. Similar behavior is expected but not confirmed for trace metal anions and major electrolyte cation (e.g.,  $\text{AsO}_4^{2-}$  and  $\text{Ca}^{2+}$  or  $\text{Mg}^{2+}$ ). Thus, solution species which compete for coordination with the trace element species may enhance or retard removal of the trace element on  $\text{Fe}(\text{OH})_3$ .
3. The presence or absence of major or minor solute species which compete for surface sites can displace the equilibrium concentration of the adsorbing trace element. For example, sulfate competes for the same sites as selenate and chromate causing a decrease in the amount of Se or Cr adsorbed under specific conditions. The presence of a second strongly adsorbing trace metal appears not to strongly influence the adsorption characteristics of a trace metal at very dilute concentrations (e.g., simultaneous adsorption of Pb and Cd).
4. The rate at which iron reagents are mixed does not appear to affect the partitioning of trace metals after one-hour contact time.
5. Feasibility of using an acid-metal cleaning waste containing high concentrations of dissolved iron as the iron source for coprecipitation of trace elements has been confirmed.
6. The adsorptive removal of trace elements from real waste streams in complex systems using either reagent iron sources or acid-metal cleaning waste can be interpreted in terms of the generalized behavior of model systems.
7. The adsorptive removal characteristics of each trace element of concern must be experimentally verified. Thus, each trace element must be tested experimentally to understand both the qualitative and quantitative aspects of removal by amorphous ferric hydroxide.
8. Because the removal characteristics of each trace element is a function of the speciation of the trace element and the degree of competition for surface sites on the solid, rather complete chemical characterization of waste streams is required before quantitative prediction will be possible.
9. Basic work on clean model systems has led to important information concerning the process mechanisms:
  - a. Oxide surfaces consist of sites of varying energy. The variation may be estimated as at least  $\pm 1$  to  $\pm 5$  Kcal/mole, depending on which model of the interface is used. Metals adsorb preferentially to the high-energy sites.

- b. The density of high-energy sites varies from solid to solid, and from trace element to trace element for a given oxide.
- c. The high-energy sites represent a small fraction, often less than 0.1 percent, of the total number of surface sites available for trace element adsorption.
- d. Adsorption of metal ions often has a very small effect on adsorption of other cations, suggesting that high-energy sites can be metal-specific. On the other hand, adsorption of anions can have major effects on adsorption of other anions indicating a more general overlap of site occupancy for anions than cations.
- e. Complex metal-ligand moieties can adsorb to amorphous iron oxyhydroxide. Under some circumstances the complex can adsorb more strongly than the free metal ion.
- f. Adsorption of metal-ligand complexes can be analogous to that of either free ligand or free metal. The distinction between the two may be related to the stereochemical orientation of the adsorbed complex.
- g. All systems were reversible in the contact times studied.

#### SUGGESTIONS FOR FURTHER WORK

The need for further study in several areas has been realized during the conduct of this research. In some cases, an interpretation of the results of this study awaits clarification by further experimental work. Some suggested research topics expected to yield important information follow.

Additional experimental and field work needs to be done to determine why trace element concentrations in power plant wastes vary as much as they do. Especially important, considering the great volume of fly ash produced, is a better understanding of the mechanisms controlling the dissolution of trace elements from fly ash in aqueous systems.

Experimental adsorption/coprecipitation studies are needed with a wider range of power plant waste streams. This should then allow a more comprehensive, comparative study investigating the technical and economic feasibility of trace element removal using conventional treatment processes such as precipitation, coagulation, and sedimentation versus adsorption, coagulation, and sedimentation.

Several model studies investigating the effects of metal/ligand and ion-pair formation, as well as anion competition, would be useful. These experiments should study the following:

- The effect of such anions as selenite, arsenate, and chromate on trace metal adsorption.

- The effect of such metals as zinc, copper, cadmium, and lead on trace anion adsorption.
- The effect of competing anions such as sulfate, arsenate, and chromate on selenite adsorption.
- The effect of such potential ion-pair formers as calcium and magnesium on arsenate, selenite, and chromate adsorption.
- The possibility that chromate and arsenate removal at high pH values is due to a precipitation reaction rather than an adsorption reaction.
- Basic adsorption studies to evaluate adsorption removal characteristics of vanadate, molybdate, and borate.

From this research, a new semi-quantitative model of oxide surfaces has been proposed, as well as a model to describe adsorption of various metal-ligand complexes. The research suggested several lines of investigation which may help elucidate the adsorption process using amorphous iron oxyhydroxide.

To improve our capability to model reactions at oxide surfaces, there is a critical need to establish the causes for the variations among surface oxide sites. Research in this area should emphasize analysis of well-characterized pure solids both in the presence and absence of adsorbate. Spectroscopic studies of surfaces should be valuable both in terms of establishing what types of sites are available to a given metal and why certain sites are specific for certain trace elements. Studies of adsorption stoichiometry will be valuable in this area.

From an engineering point of view, it would be useful to study the distribution of surface-site energies for several metals on various model adsorbents, including amorphous iron oxyhydroxide. Such studies may establish some general empirical patterns which could be used to predict metal partitioning in engineering processes, even in the absence of a complete physical-chemical characterization of the adsorbent.

The adsorption of ligands and complexes which have two or more potential surface-bonding sites should be studied so that predictions of adsorption stereochemistry and energy can be attempted solely from information about the coordination chemistry of the dissolved species and the surface characteristics of the adsorbent.

Finally, additional studies on well-characterized types of wastes from coal-fired power plants would be useful to give empirical data on the range of adsorptive behavior of selected trace elements in real complex solutions. The combination of basic research and applied experimental work should yield very useful information, both theoretical and practical.

REFERENCES

1. M. G. MacNaughton. "Adsorption of Mercury(II) at the Solid-Water Interface." Ph.D. Thesis, Stanford University, Stanford, Calif., 1973.
2. J. Vuceta. "Adsorption of Pb(II) and Cu(II) on  $\alpha$ -Quartz from Aqueous Solutions: Influence of pH, Ionic Strength, and Complexing Ligands." Ph.D. Thesis, California Institute of Technology, Pasadena, Calif., 1976.
3. D. E. Yates. "The Structure of the Oxide/Aqueous Electrolyte Interface." Ph.D. Thesis, University of Melbourne, Australia, 1975.
4. P. V. Avotins. "Adsorption and Coprecipitation Studies of Mercury on Hydrous Iron Oxides." Ph.D. Thesis, Stanford University, Stanford, Calif., 1975.
5. J. A. Davis. "Adsorption of Trace Metals and Complexing Ligands at the Oxide/Water Interface." Ph.D. Thesis, Stanford University, Stanford, Calif., 1977.
6. H. J. van den Hull and J. Lyklema. "Determination of Specific Surface Areas of Dispersed Materials. Comparison of the Negative Adsorption Method with Some Other Methods." J. Amer. Chem. Soc., 90, 3010 (1968).
7. P. J. Murphy, A. M. Posner and J. P. Quirk. "Characterization of Partially Neutralized Ferric Nitrate Solutions." J. Coll. Interface Sci., 56, 270 (1976).
8. G. A. Parks. "The Isoelectric Points of Solid Oxides, Solid Hydroxides, and Aqueous Hydroxo Complex Systems." Chem. Rev., 65, 177 (1965).
9. G. A. Parks and P. L. DeBruyn. "The Zero Point of Charge of Oxides." J. Phys. Chem., 66, 967-976 (1962).
10. W. Stumm, C. P. Huang and S. R. Jenkins. "Specific Chemical Interaction Affecting the Stability of Dispersed Systems." Croat. Chem. Acta, 42, 223-245 (1970).
11. E. A. Jenné. "Controls on Mn, Fe, Co, Ni, Cu, and Zn Concentrations in Soils and Water: The Significant Role of Hydrous Mn and Fe Oxides." Adv. in Chem. Series, No. 73, 337-387 (1968).
12. M. G. MacNaughton and R. O. James. "Adsorption of Aqueous Mercury(II) Complexes at the Oxide/Water Interface." J. Coll. Interface Sci., 47, 431-440 (1974).
13. C. G. Armistead, A. J. Tyler, F. H. Hambleton, S. A. Mitchell, and J. A. Hockey. "Surface Hydroxylation of Silica." J. Phys. Chem., 73, 3947 (1969).
14. C. P. Huang and W. Stumm. "Specific Adsorption of Cations on Hydrous  $\gamma$ -Al<sub>2</sub>O<sub>3</sub>." J. Coll. Interface Sci., 43, 409 (1973).
15. H. Hohl and W. Stumm. "Interaction of Pb<sup>2+</sup> with Hydrous  $\gamma$ -Al<sub>2</sub>O<sub>3</sub>." J. Coll. Interface Sci., 55, 281-288 (1976).
16. C. P. Huang, H. A. Elliott and R. M. Ashmead. "Interfacial Reactions and the Fate of Heavy Metals in Soil-Water Systems." J. Water Poll. Cont. Fed., 49, 745-756 (1977).



17. J. B. Peri. "Infrared and Gravimetric Study of the Surface Hydration of  $\gamma$ -Alumina." J. Phys. Chem., 69, 211 (1965).
18. J. W. Murray. "The Interactions of Metal Ions at the Manganese Dioxide-Solution Interface." Geochim. Cosmochim. Acta, 39, 505-519 (1975).
19. P. Loganathan and R. Burau. "Sorption of Heavy Metal Ions by a Hydrous Manganese Oxide." Geochim. Cosmochim. Acta, 37, 1277-1293 (1973).
20. M. A. Anderson, J. F. Ferguson and J. Gavis. "Arsenate Adsorption on Amorphous Aluminum Hydroxide." J. Coll. Interface Sci., 54, 391-399 (1976).
21. Y. G. Bérubé and P. L. DeBruyn. "Adsorption at the Rutile-Solution Interface." J. Coll. Interface Sci., 27(2), 305-318 (1968).
22. J. B. Gray. "Flow Patterns, Fluid Velocities, and Mixing in Agitated Vessels," Mixing: Theory and Practice, Vol. 1. New York: Academic Press, 1966.
23. O. Levenspiel and K. B. Bischoff. "Patterns of Flow in Chemical Process Vessels," Adv. in Chemical Engineering, Vol. 4. New York: Academic Press, 1963.

## Appendix A

## EXPERIMENTAL DATA

Figures A-1 through A-28: Single Cation Adsorbate, Ligand-Free System

Figure No.	Adsorbent	Adsorbate	Abscissa	Ordinate	Other Parameters	Description	
A-1	am-Fe(OH) <sub>3</sub>	Cd	pH	PA <sup>a</sup>	Fe <sub>T</sub>	Edge <sup>b</sup>	
A-2			pH	PA	Cd <sub>T</sub>	Edge	
A-3			log[Cd]	log Γ	pH	Isotherm	
A-4			log[Fe]	log[Cd]	pH	Dose <sup>c</sup>	
A-5			pH	PA	Cd <sub>T</sub>	Edge (low Γ)	
A-6			log[Cd]	log Γ		Isotherm (low Γ)	
A-7		Cu	pH	PA	Cu <sub>T</sub>	Edge	
A-8			pH	PA	Fe <sub>T</sub>	Edge	
A-9			log[Cu]	log Γ	pH	Isotherm	
A-10			log[Fe]	log[Cu]	pH	Dose	
A-11		Zn	pH	PA	Zn <sub>T</sub>	Edge	
A-12			pH	PA	Zn <sub>T</sub>	Edge	
A-13			pH	PA	Fe <sub>T</sub>	Edge	
A-14			log[Zn]	log Γ		Isotherm	
A-15			Pb	pH	PA	Pb <sub>T</sub>	Edge
A-16				pH	PA	Fe <sub>T</sub>	Edge
A-17				log[Pb]	log Γ		Isotherm
A-18	γ-Al <sub>2</sub> O <sub>3</sub>	Cd	pH	PA	Cd <sub>T</sub>	Edge	
A-19			pH	PA	Cd <sub>T</sub>	Edge (low Γ)	
A-20			Cu	pH	PA	Cu <sub>T</sub>	Edge
A-21	α-SiO <sub>2</sub>	Zn	pH	PA	Zn <sub>T</sub>	Edge	
A-22		Pb	pH	PA	Pb <sub>T</sub>	Edge	
A-23		Cd	pH	PA	Cd <sub>T</sub>	Edge	
A-24			pH	PA	Si <sub>T</sub> , Cd <sub>T</sub>	Edge	
A-25			log[Cd]	log Γ	pH	Isotherm	
A-26		Cu	pH	PA	Cu <sub>T</sub>	Edge	

continued

Figure No.	Adsorbent	Adsorbate	Abscissa	Ordinate	Other Parameters	Description
A-27	$\alpha\text{-SiO}_2$	Zn	pH	PA	$\text{Zn}_T$	Edge
A-28		Pb	pH	PA	$\text{Pb}_T$	Edge

Figures A-29 through A-37: Single Anion Adsorbate Systems

Figure No.	Adsorbent	Adsorbate	Abscissa	Ordinate	Other Parameters	Description	
A-29	am-Fe(OH) <sub>3</sub>	AsO <sub>4</sub>	pH	PA	As <sub>T</sub>	Edge	
A-30			log[As]	log $\Gamma$	pH	Isotherm	
A-31			log[Fe]	log[As]	pH	Dose	
A-32		CrO <sub>4</sub>		pH	PA		Edge
A-33				pH	PA		Edge
A-34		SeO <sub>4</sub>		pH	PA	Se <sub>T</sub>	Edge
A-35				log[Se]	log $\Gamma$	pH	Isotherm
A-36				log[Fe]	log[Se]	pH	Dose
A-37	SeO <sub>3</sub>		pH	PA	Se <sub>T</sub>	Edge	

Figures A-38 through A-43: Coprecipitation Systems with Complexing Ligands

(All plots are percent adsorption vs pH)

Figure No.	Adsorbent	Adsorbate	Ligand
A-38	am-Fe(OH) <sub>3</sub>	Cd	Cl
A-39			SO <sub>4</sub>
A-40		Cu	Cl
A-41			NH <sub>3</sub>
A-42		Zn	Cl
A-43			SO <sub>4</sub>

Figures A-44 through A-46: Adsorption in Systems with Complexing Ligands

(All plots are percent adsorption vs pH)

Figure No.	Adsorbent	Adsorbate	Ligand
A-44	am-Fe(OH) <sub>3</sub>	Cd	Cl, SO <sub>4</sub>

continued

Figure No.	Adsorbent	Adsorbate	Ligand
A-45	am-Fe(OH) <sub>3</sub>	Cd	S <sub>2</sub> O <sub>3</sub>
A-46			S <sub>2</sub> O <sub>3</sub>

Figures A-47 through A-52: Adsorption in Systems with Competing Metal Adsorbates

(All plots are percent "primary" metal adsorbed vs pH)

Figure No.	Adsorbent	Primary Metal (low concentration)	Competing Metal (high concentration)
A-47	am-Fe(OH) <sub>3</sub>	Cd	Cu
A-48			Zn
A-49			Pb
A-50		Zn	Cd
A-51			Pb
A-52			Cu

<sup>a</sup>PA = percent adsorbed.  
<sup>b</sup>Edge = adsorption edge.  
<sup>c</sup>Dose = iron dose curve.

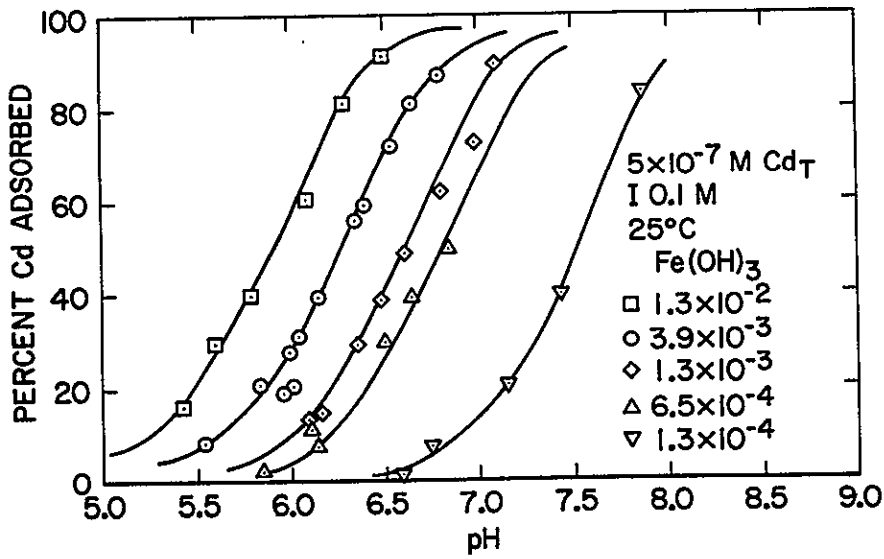


Figure A-1. pH-adsorption edge for Cd on am-Fe(OH)<sub>3</sub>: Effect of total iron

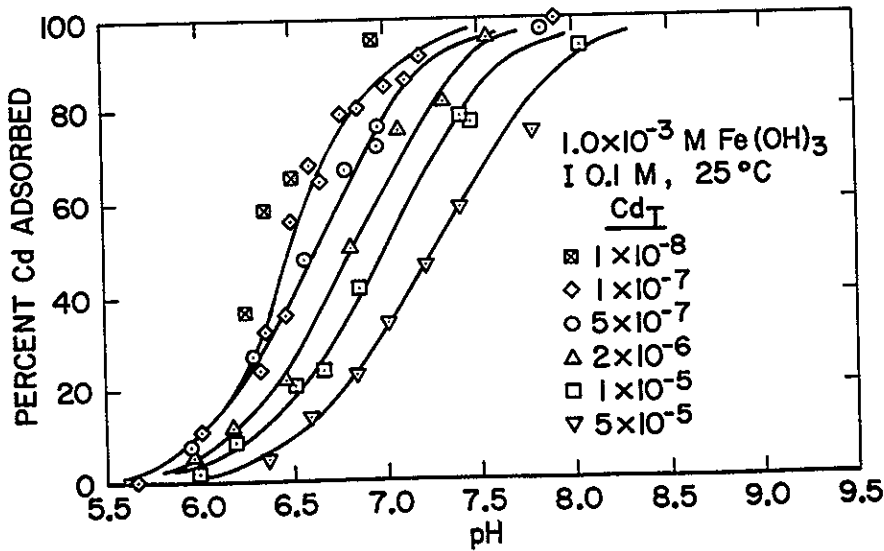


Figure A-2. pH-adsorption edge for Cd on am-Fe(OH)<sub>3</sub>: Effect of total Cd

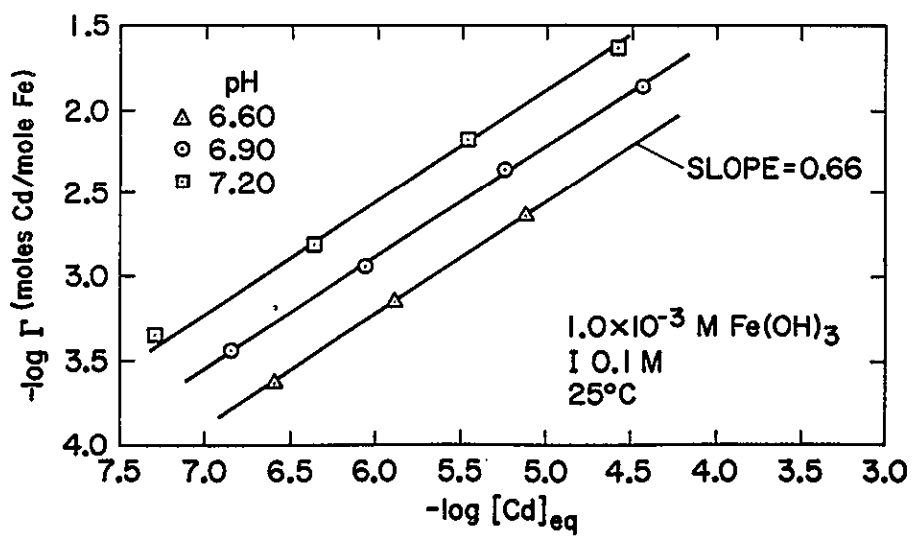


Figure A-3. Adsorption isotherm for Cd on am-Fe(OH)<sub>3</sub>

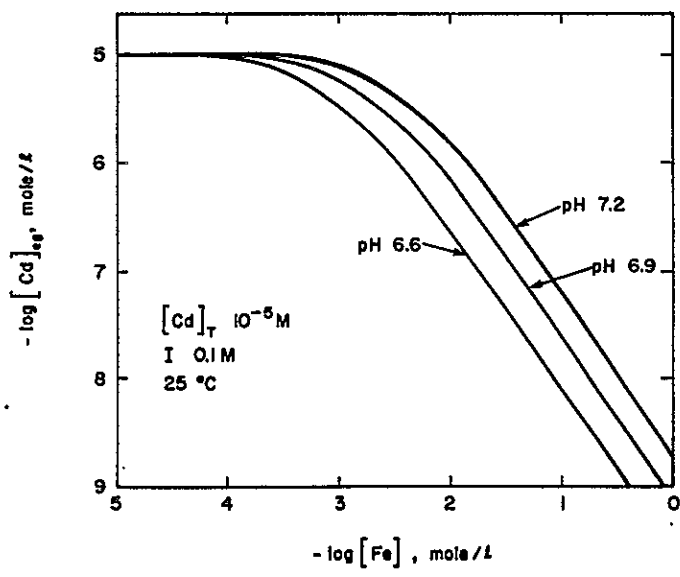


Figure A-4. Cadmium removal as a function of am-Fe(OH)<sub>3</sub> dosage at varying pH



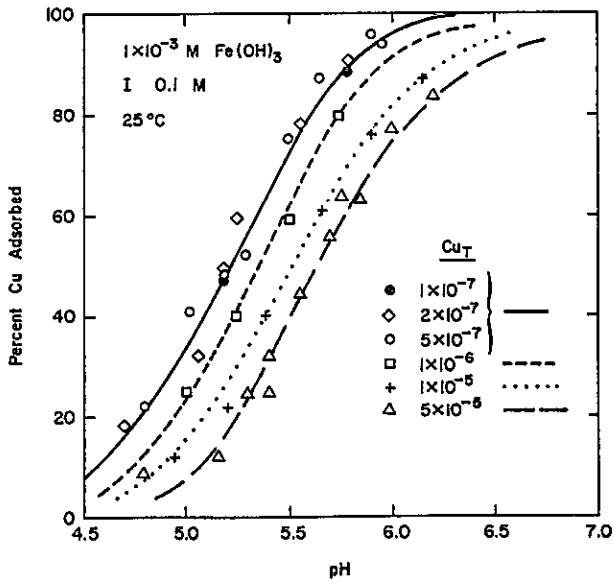


Figure A-7. pH-adsorption edge for Cu on am-Fe(OH)<sub>3</sub>: Effect of total Cu

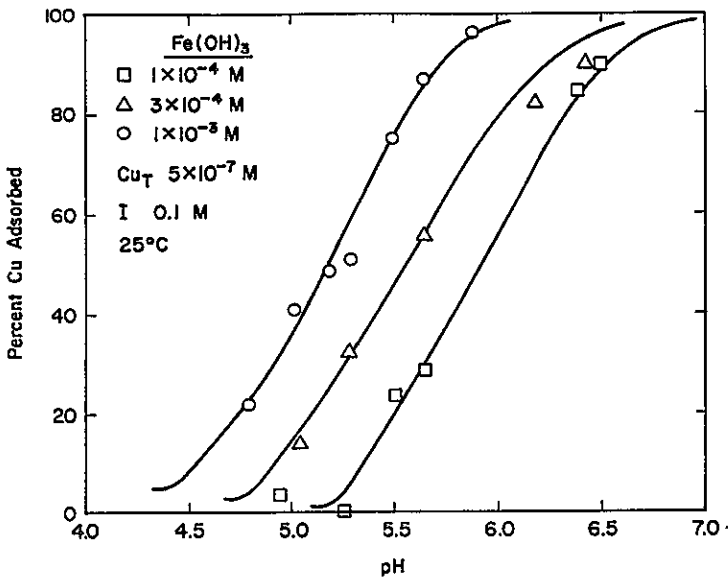


Figure A-8. pH-adsorption edge for Cu on am-Fe(OH)<sub>3</sub>: Effect of total iron

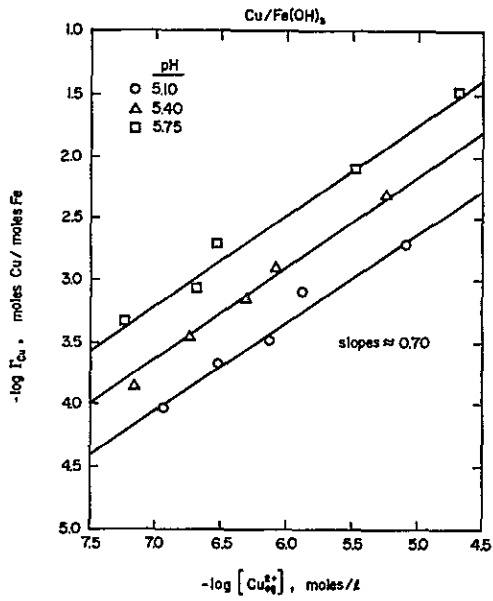
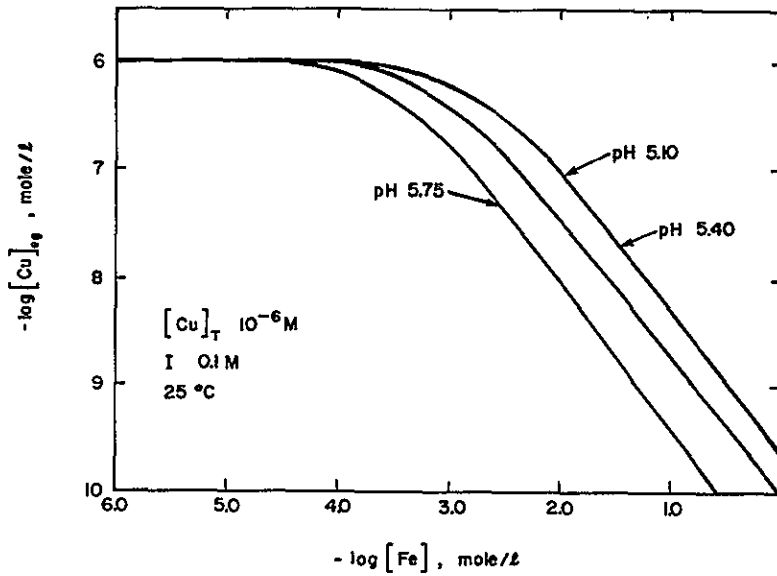


Figure A-9. Adsorption isotherm for Cu on am-Fe(OH)<sub>3</sub>



A-10. Copper removal as a function of am-Fe(OH)<sub>3</sub> dosage at varying pH

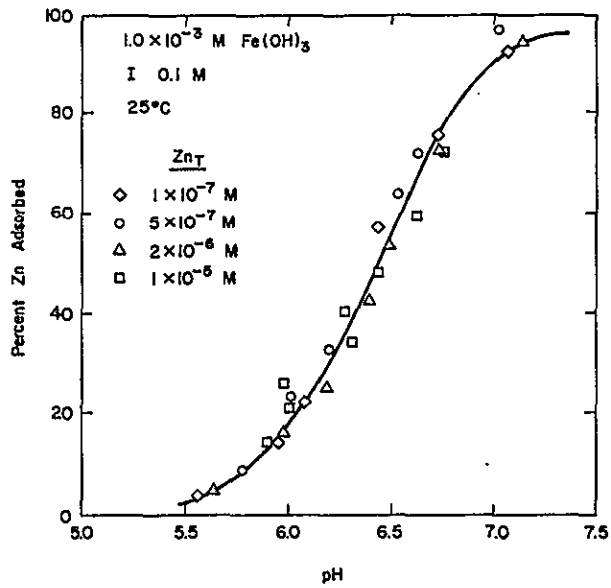


Figure A-11. pH-adsorption edge for Zn on am-Fe(OH)<sub>3</sub>: Effect of total Zn

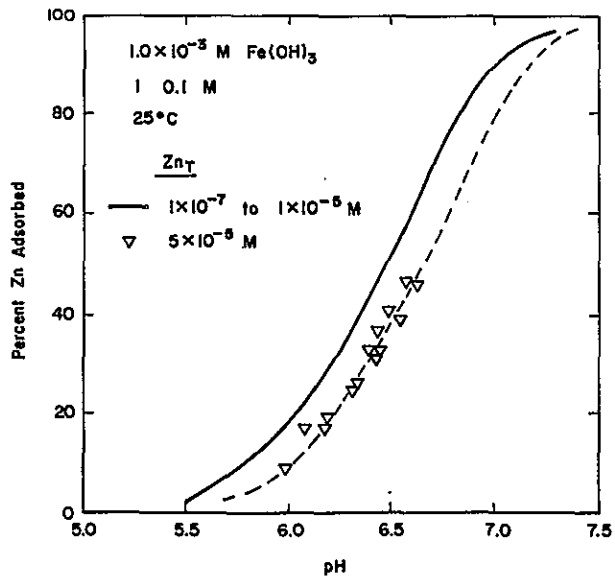


Figure A-12. pH-adsorption edge for Zn on am-Fe(OH)<sub>3</sub>: Effect of total Zn

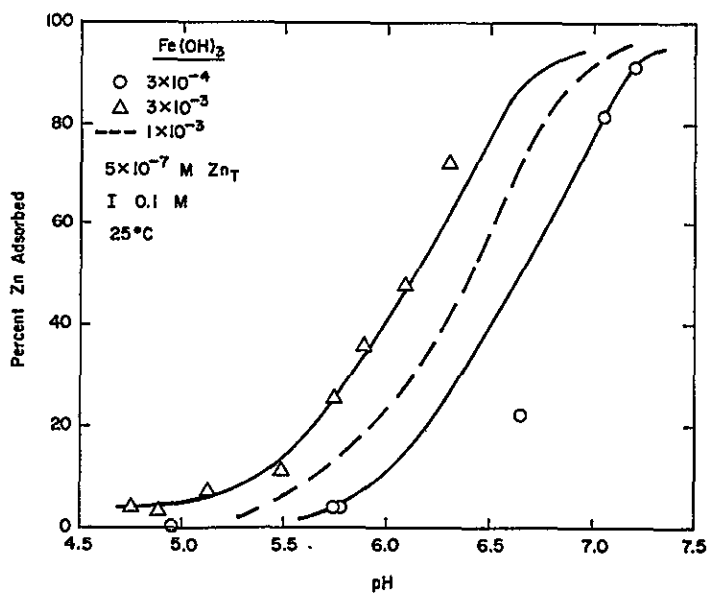


Figure A-13. pH-adsorption edge for Zn on am-Fe(OH)<sub>3</sub>: Effect of total iron

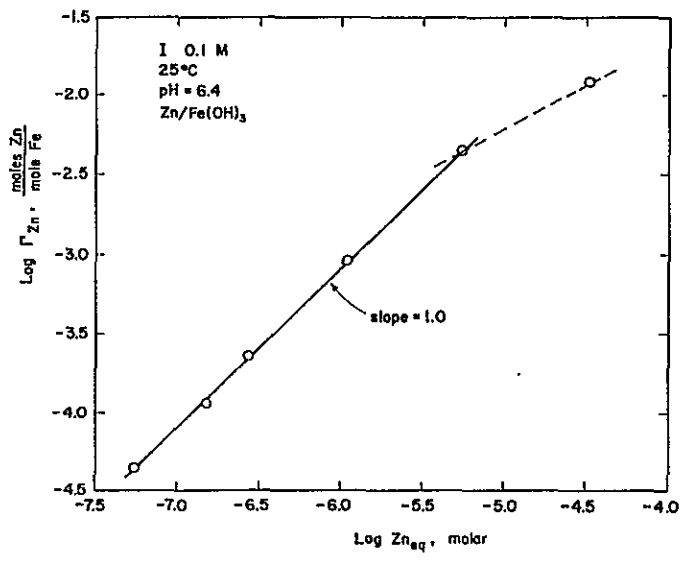


Figure A-14. Adsorption isotherm for Zn on am-Fe(OH)<sub>3</sub>

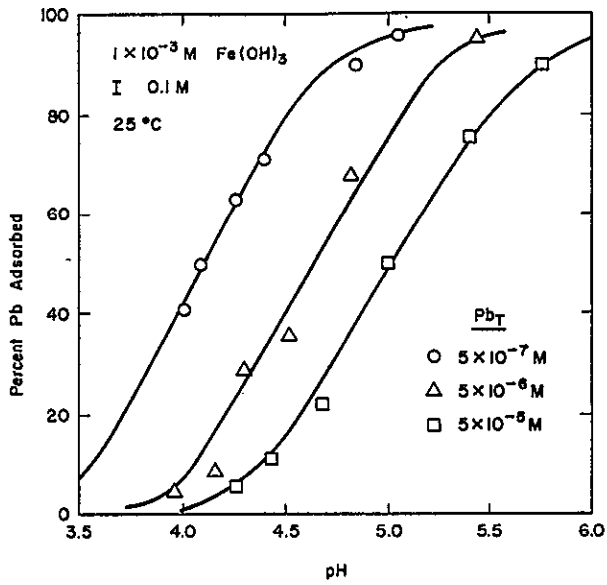


Figure A-15. pH-adsorption edge for Pb on am-Fe(OH)<sub>3</sub>: Effect of total Pb

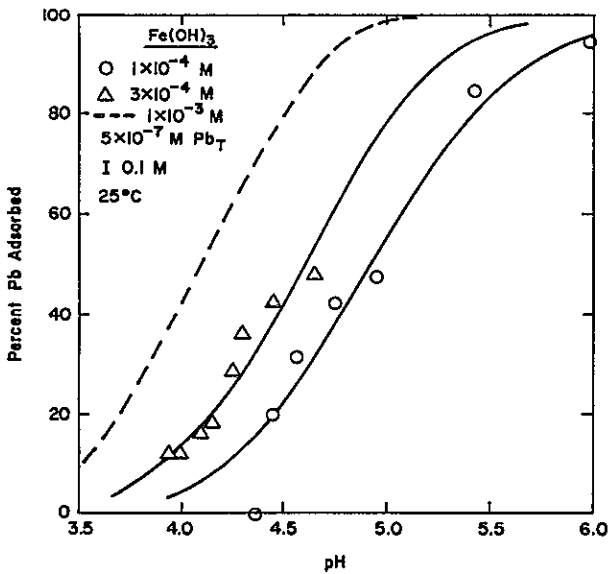


Figure A-16. pH-adsorption edge for Pb on am-Fe(OH)<sub>3</sub>: Effect of total iron

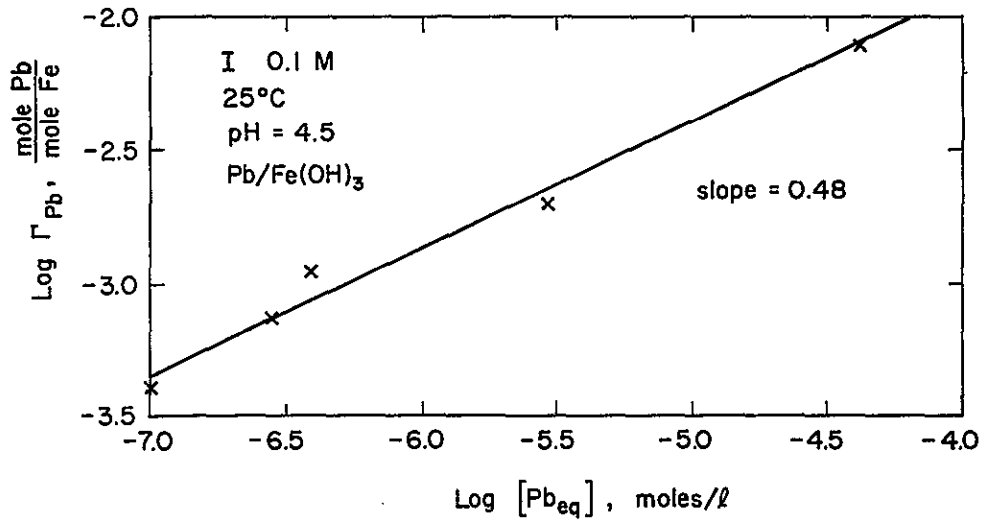


Figure A-17. Adsorption isotherm for Pb on am-Fe(OH)<sub>3</sub>

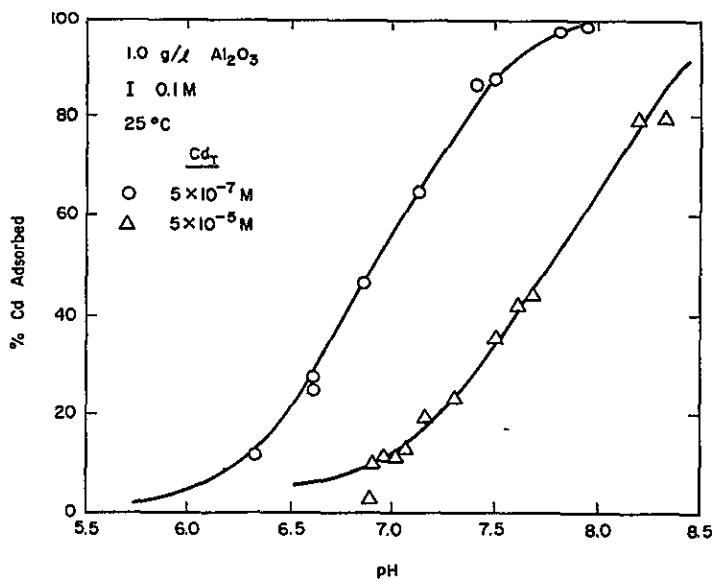


Figure A-18. pH-adsorption edge for Cd on γ-Al<sub>2</sub>O<sub>3</sub>:  
Effect of total Cd

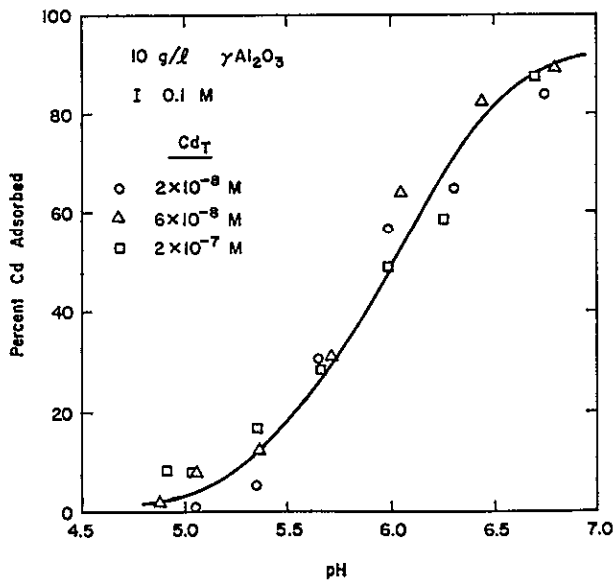


Figure A-19. pH-adsorption edge for Cd on  $\gamma\text{-Al}_2\text{O}_3$ : Effect of total Cd at very low adsorption density

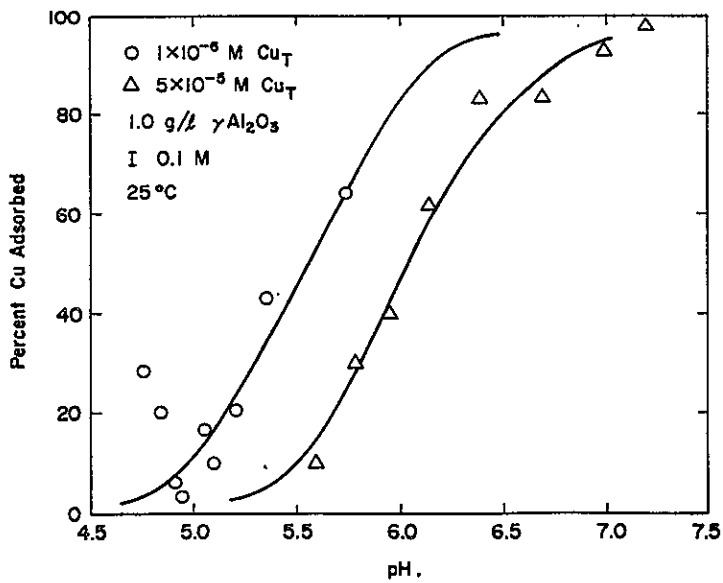


Figure A-20. pH-adsorption edge for Cu on  $\gamma\text{-Al}_2\text{O}_3$ : Effect of total Cu

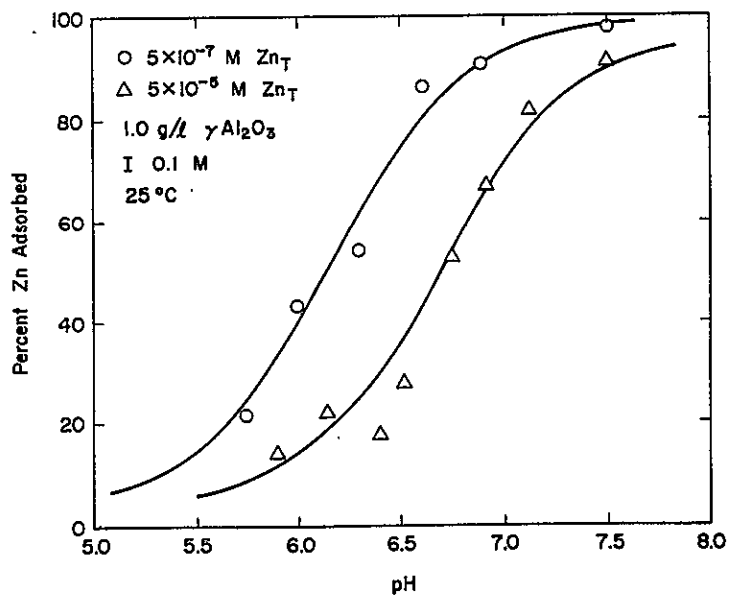


Figure A-21. pH-adsorption edge for Zn on  $\gamma\text{-Al}_2\text{O}_3$ :  
Effect of total Zn

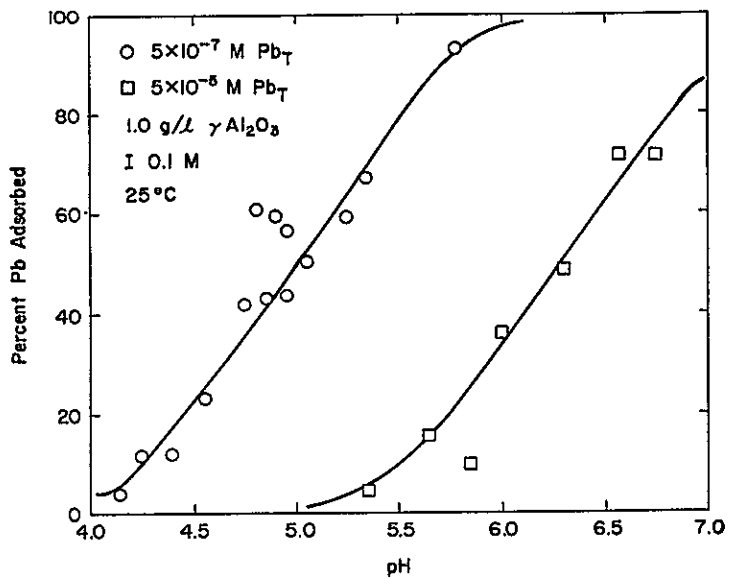


Figure A-22. pH-adsorption edge for Pb on  $\gamma\text{-Al}_2\text{O}_3$ :  
Effect of total Pb

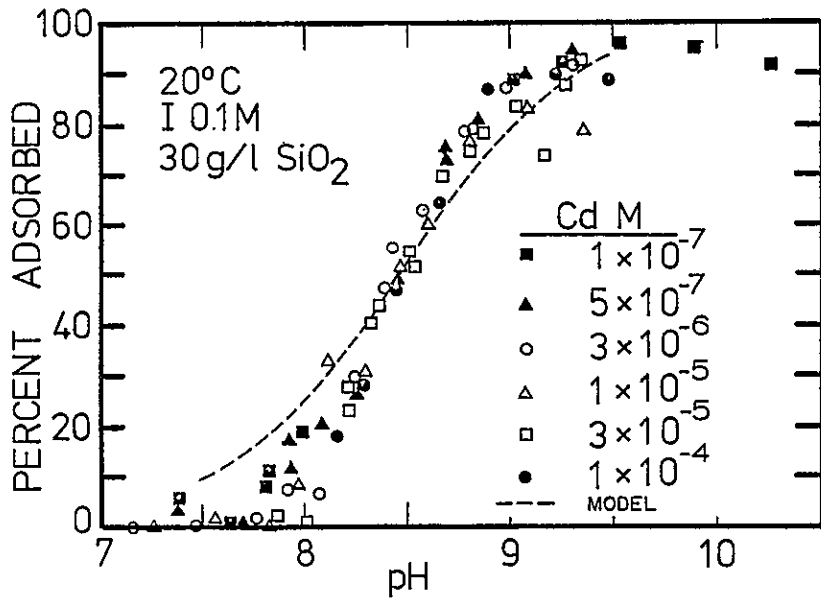


Figure A-23. pH-adsorption edge for Cd on  $\alpha$ -SiO<sub>2</sub>:  
Effect of total Cd

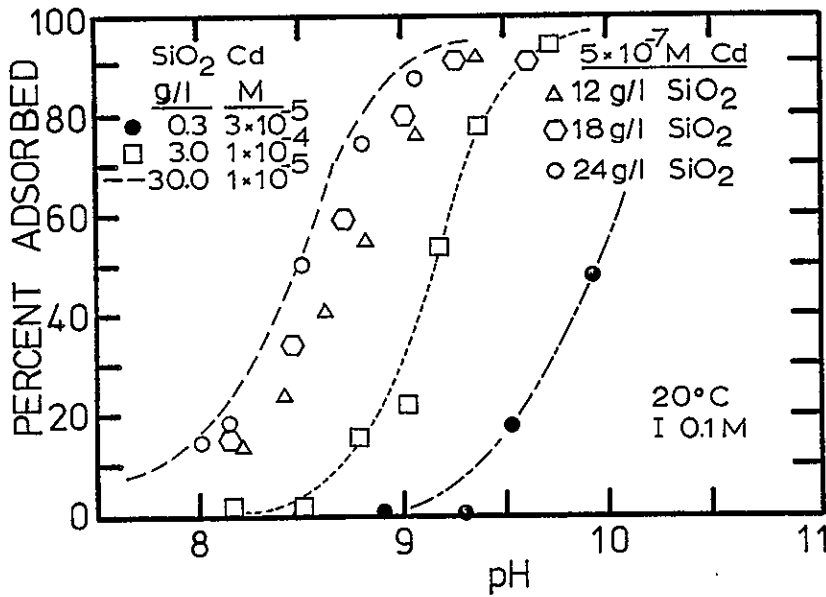


Figure A-24. pH-adsorption edge for Cd on  $\alpha$ -SiO<sub>2</sub>:  
Effect of total SiO<sub>2</sub> and total Cd

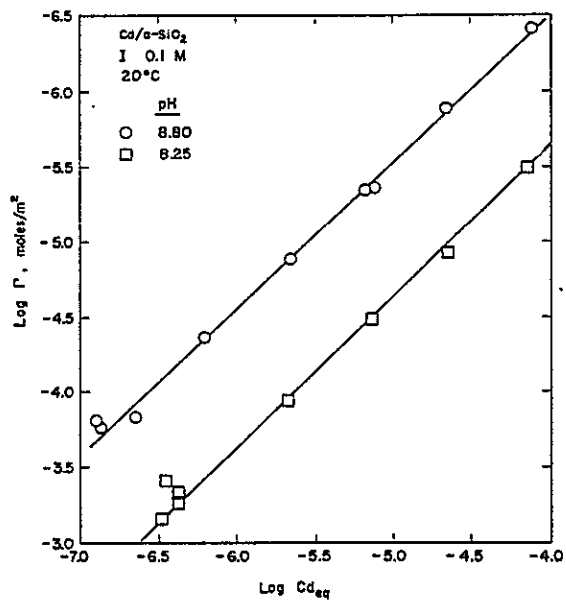


Figure A-25. Adsorption isotherm for Cd on  $\alpha$ -SiO<sub>2</sub>: Effect of pH

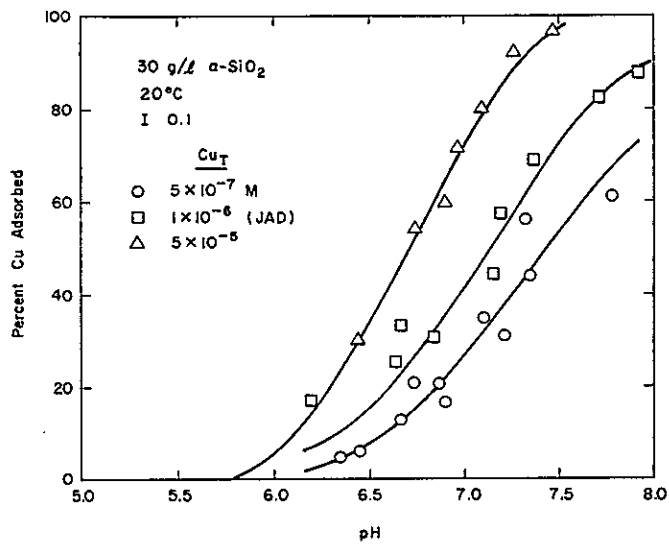


Figure A-26. pH-adsorption edge for Cu on  $\alpha$ -SiO<sub>2</sub>: Effect of total Cu

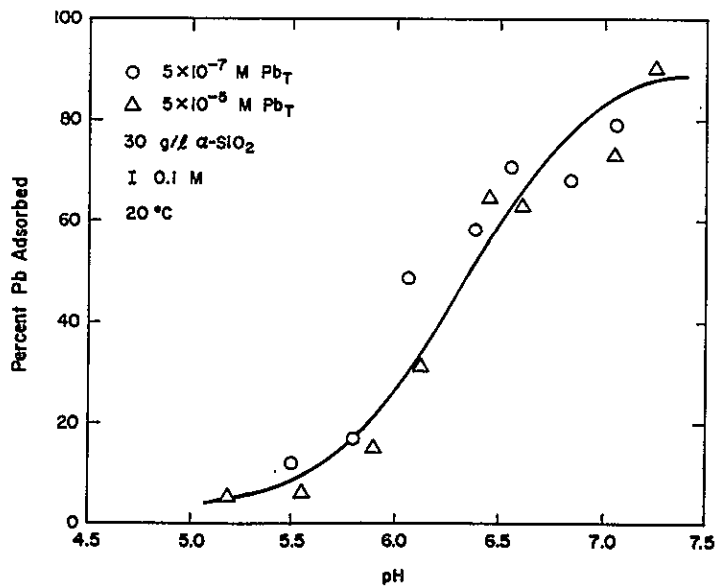


Figure A-27. pH-adsorption edge for Pb on  $\alpha$ -SiO<sub>2</sub>:  
Effect of total Pb

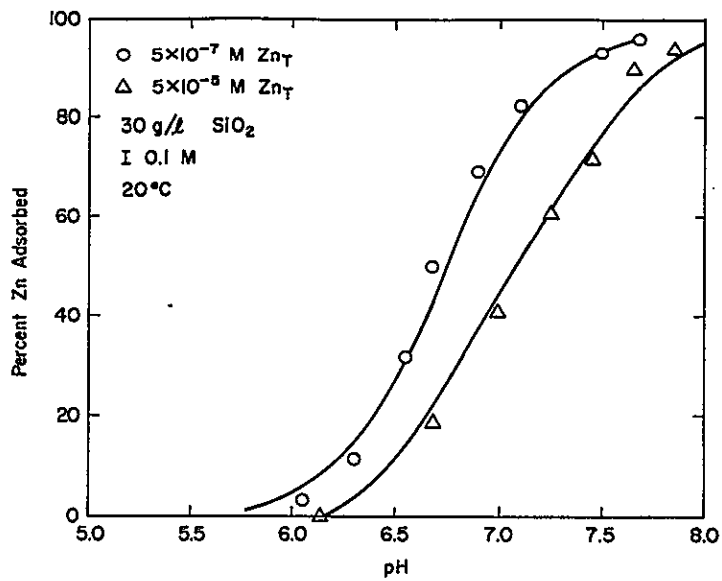


Figure A-28. pH-adsorption edge for Zn on  $\alpha$ -SiO<sub>2</sub>:  
Effect of total Zn

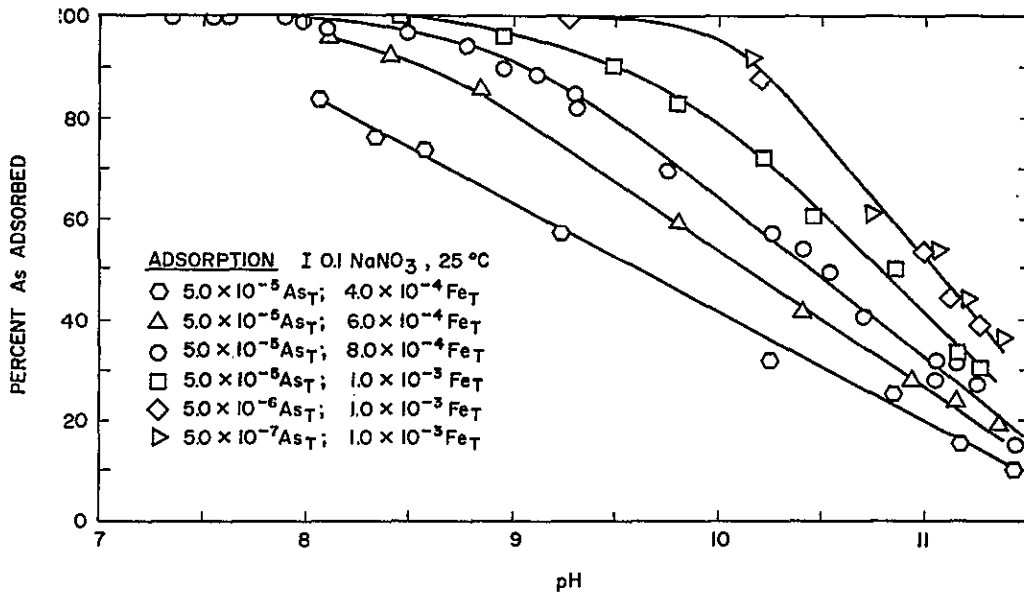


Figure A-29. pH-adsorption edge for arsenate on am-Fe(OH)<sub>3</sub>: Effects of total iron and total arsenate

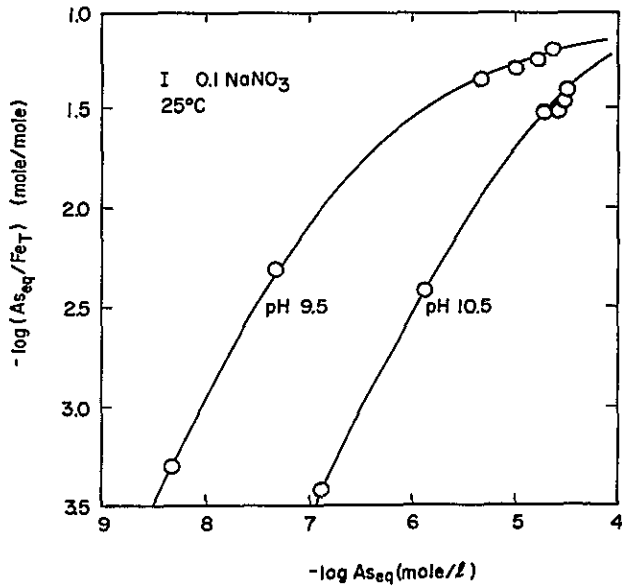


Figure A-30. Adsorption isotherm for arsenate on am-Fe(OH)<sub>3</sub>: Effect of pH

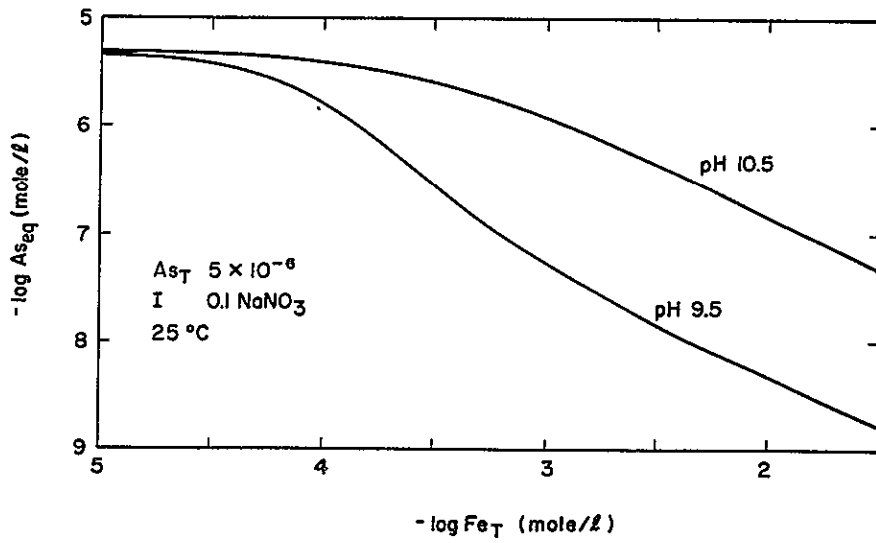


Figure A-31. Arsenate removal as a function of am- $Fe(OH)_3$  dosage at pH = 9.5 and pH = 10.5

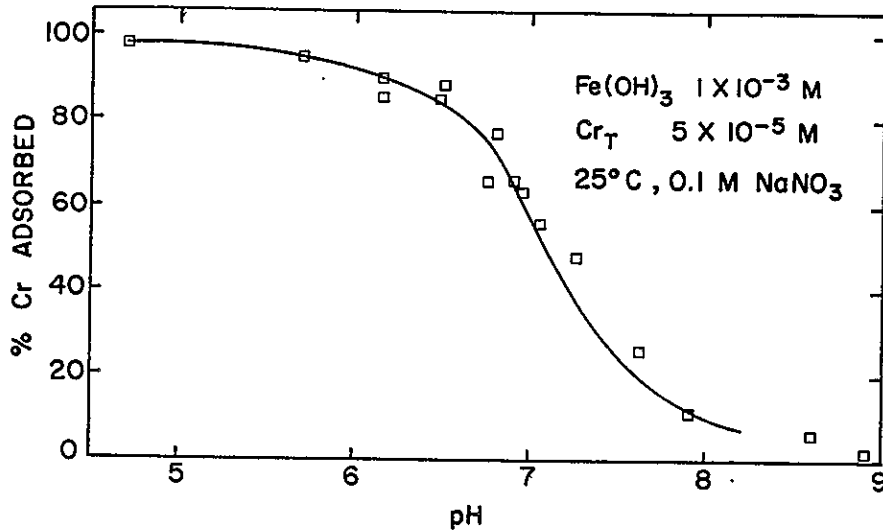


Figure A-32. pH-adsorption edge for chromate on am- $Fe(OH)_3$

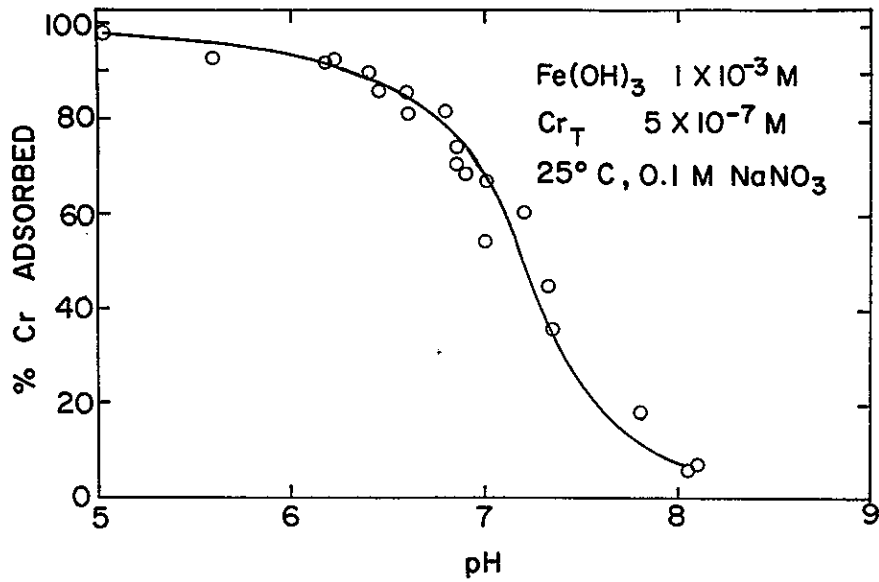


Figure A-33. pH-adsorption edge for chromate on am- $\text{Fe(OH)}_3$

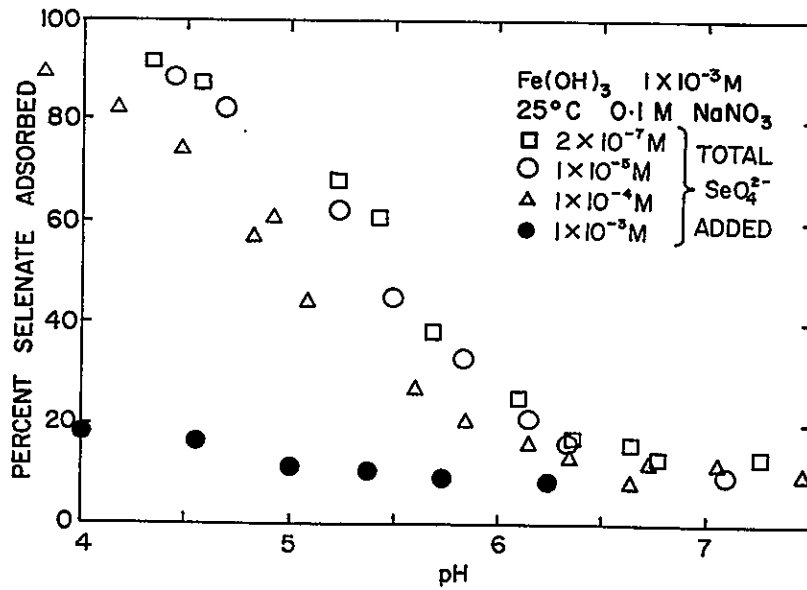


Figure A-34. pH-adsorption edge for selenate on am- $\text{Fe(OH)}_3$ : Effect of total  $\text{SeO}_4^{2-}$

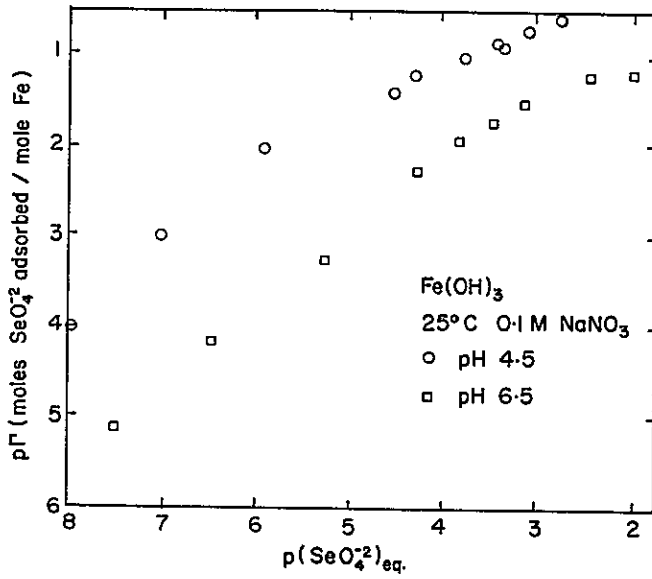


Figure A-35. Adsorption isotherm of selenate on am- $\text{Fe(OH)}_3$ : Effect of pH

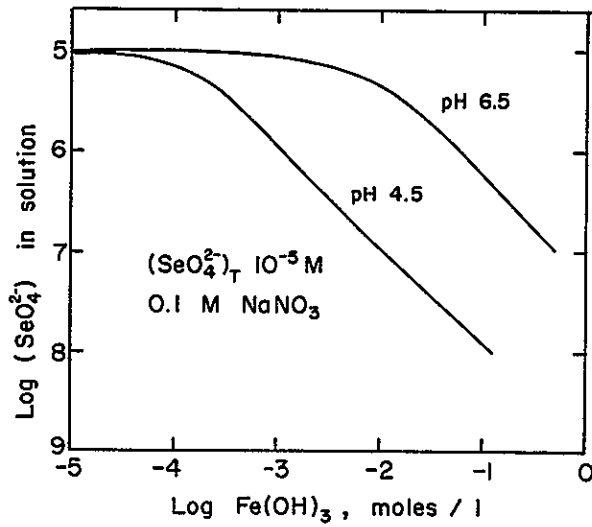


Figure A-36. Selenate removal as a function of am- $\text{Fe(OH)}_3$  dosage at pH = 4.5 and pH = 6.5

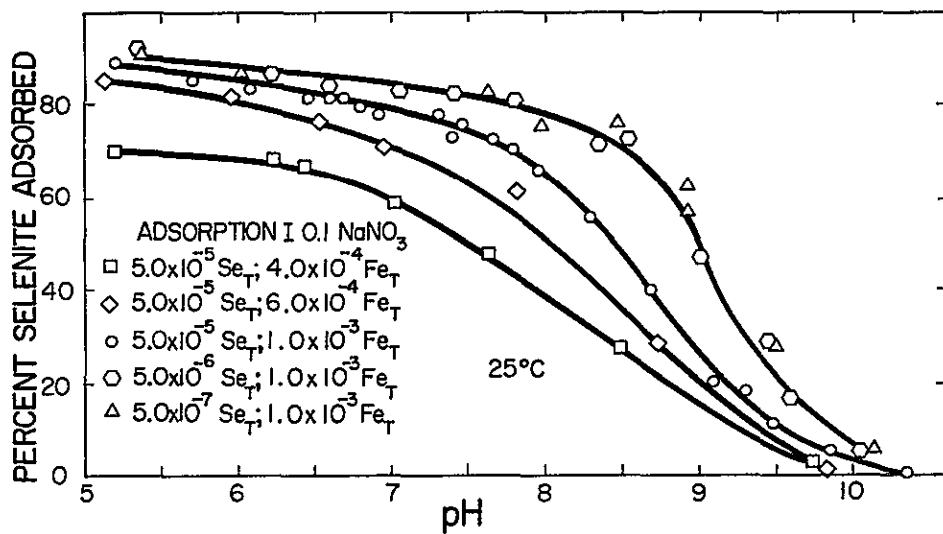


Figure A-37. pH-adsorption edge for selenite on am-Fe(OH)<sub>3</sub>: Effect of total iron and total SeO<sub>3</sub><sup>2-</sup>

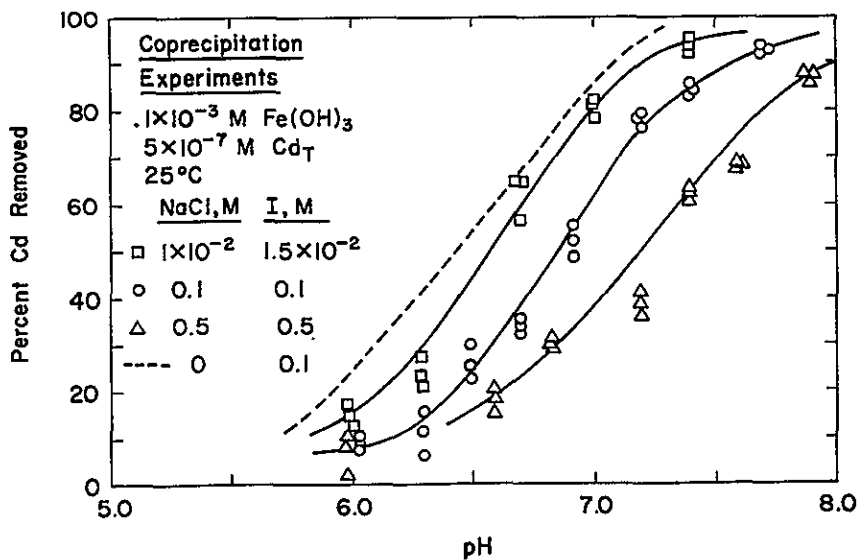


Figure A-38. pH-adsorption edges for Cd on am-Fe(OH)<sub>3</sub>: Effect of NaCl concentration

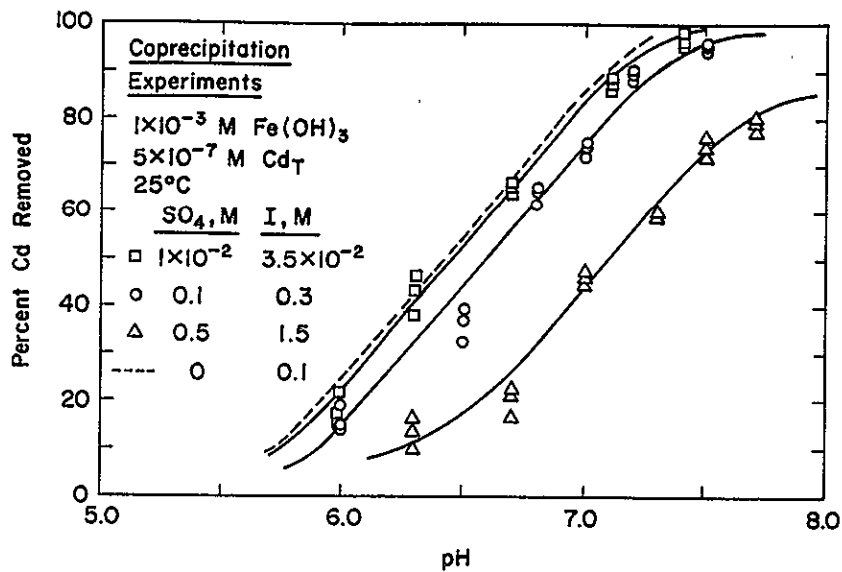


Figure A-39. pH-adsorption edge for Cd on am- $\text{Fe}(\text{OH})_3$ :  
 Effect of  $\text{SO}_4^{2-}$  concentration

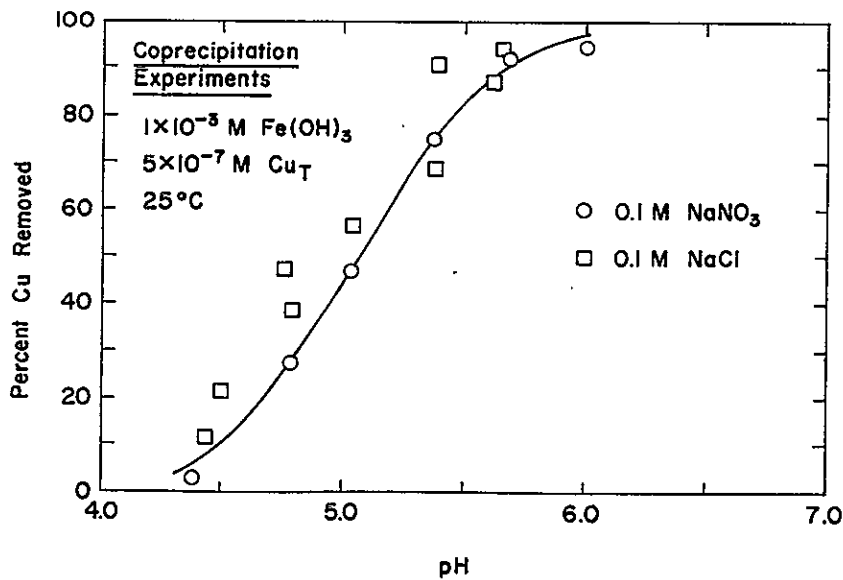


Figure A-40. pH-adsorption edge for Cu on am- $\text{Fe}(\text{OH})_3$ :  
 Effect of swamping media anion ( $\text{Cl}^-$  on  $\text{NO}_3^-$ )

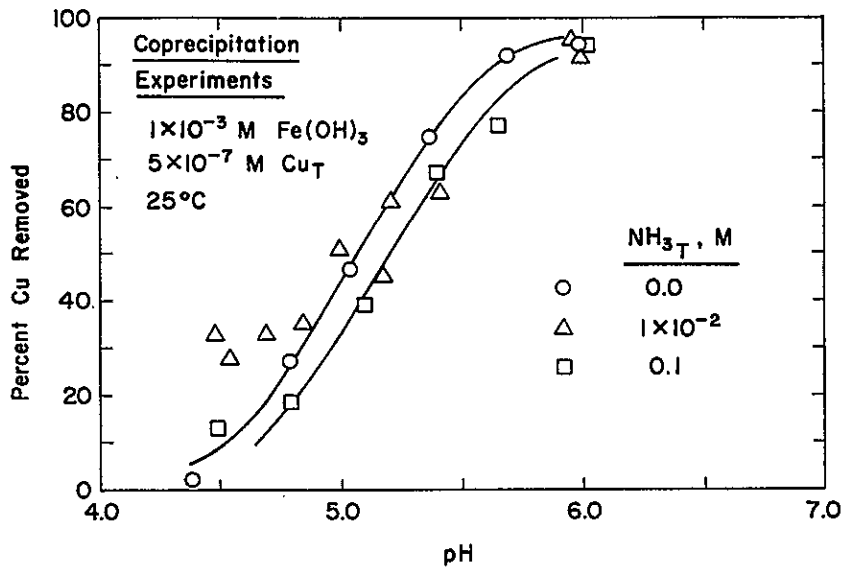


Figure A-41. pH-coprecipitation edge for Cu on am- $\text{Fe}(\text{OH})_3$ : Effect of  $\text{NH}_3$  concentration

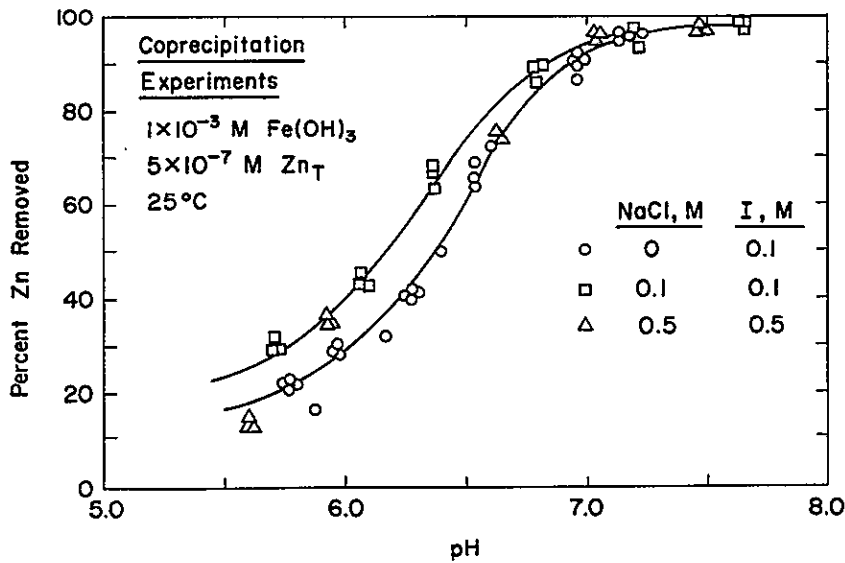


Figure A-42. pH-coprecipitation edge for Zn on am- $\text{Fe}(\text{OH})_3$ : Effect of NaCl concentration

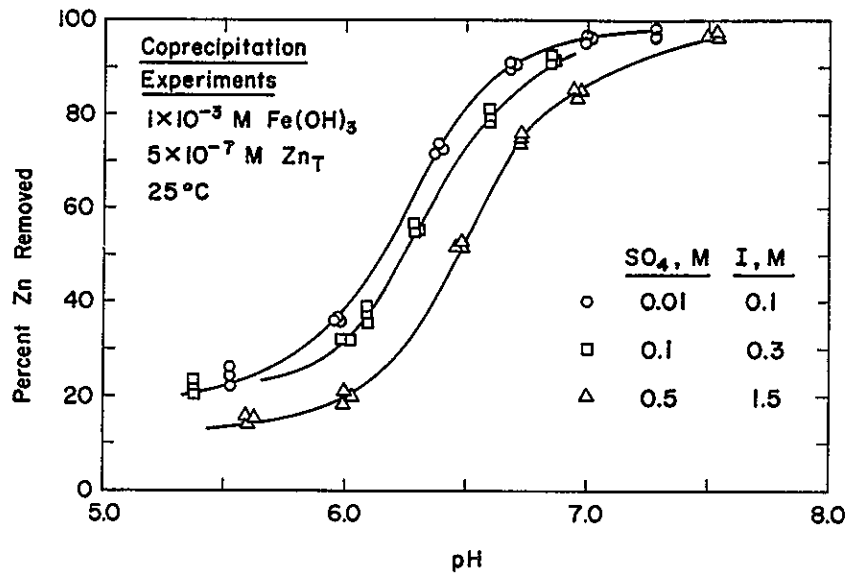


Figure A-43. pH-coprecipitation edge for Zn on am- $\text{Fe}(\text{OH})_3$ : Effect of  $\text{SO}_4^{2-}$  concentration

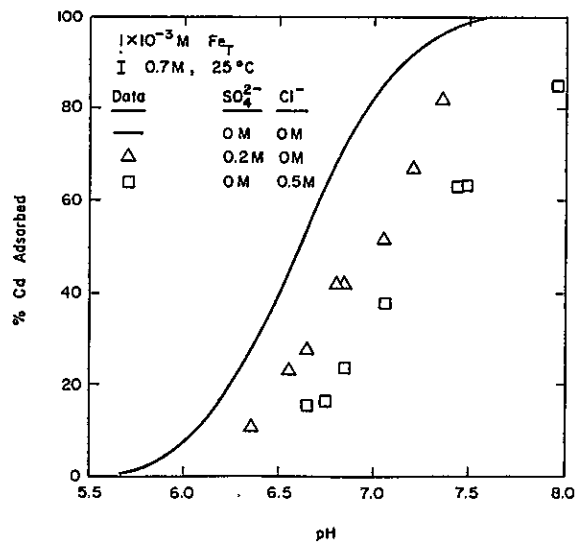


Figure A-44. pH-adsorption edge for Cd on am- $\text{Fe}(\text{OH})_3$ : Effect of  $\text{SO}_4^{2-}$ ,  $\text{Cl}^-$  concentration

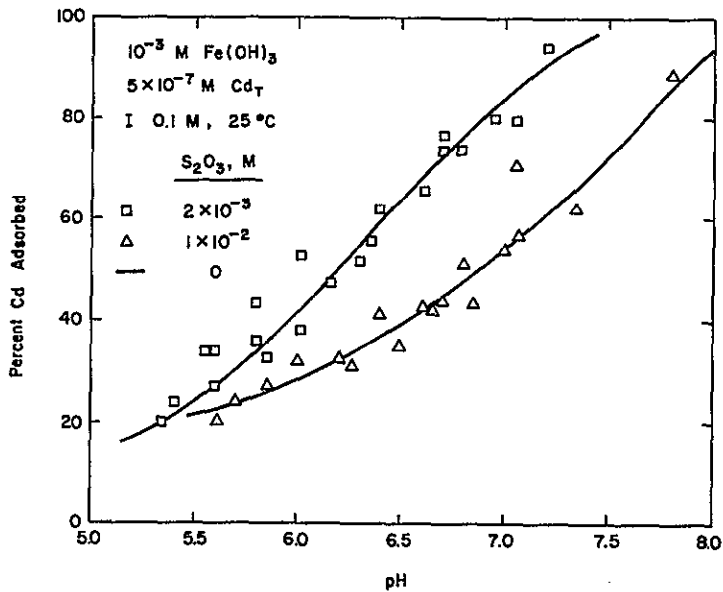


Figure A-45. pH-adsorption edge for Cd on am- $\text{Fe}(\text{OH})_3$ : Effect of  $\text{S}_2\text{O}_3$  concentration

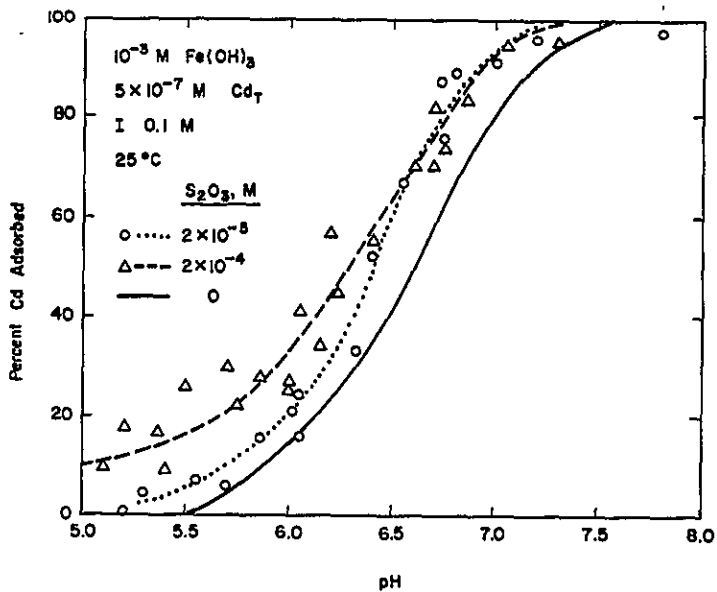


Figure A-46. pH-adsorption edge for Cd on am- $\text{Fe}(\text{OH})_3$ : Effect of  $\text{S}_2\text{O}_3$  concentration

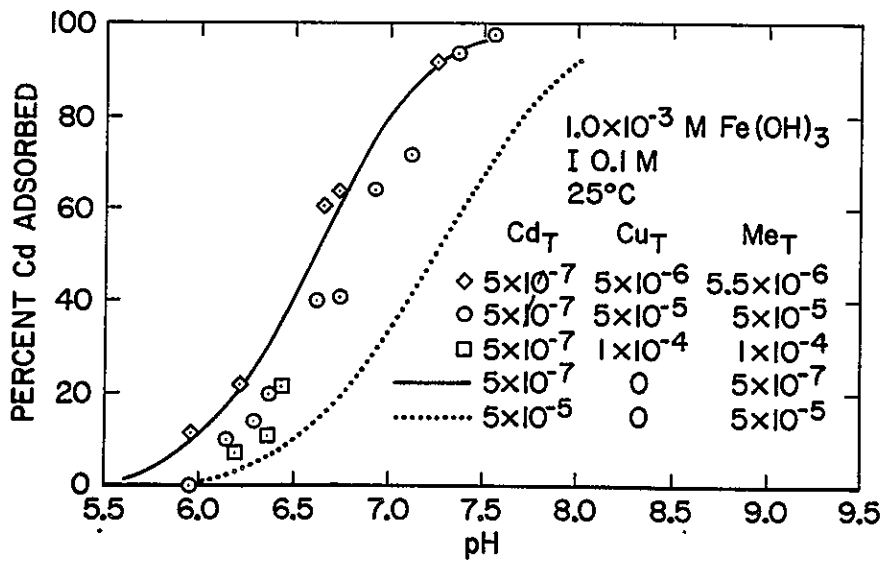


Figure A-47. pH-adsorption edge for Cd on am-Fe(OH)<sub>3</sub> in presence of Cu

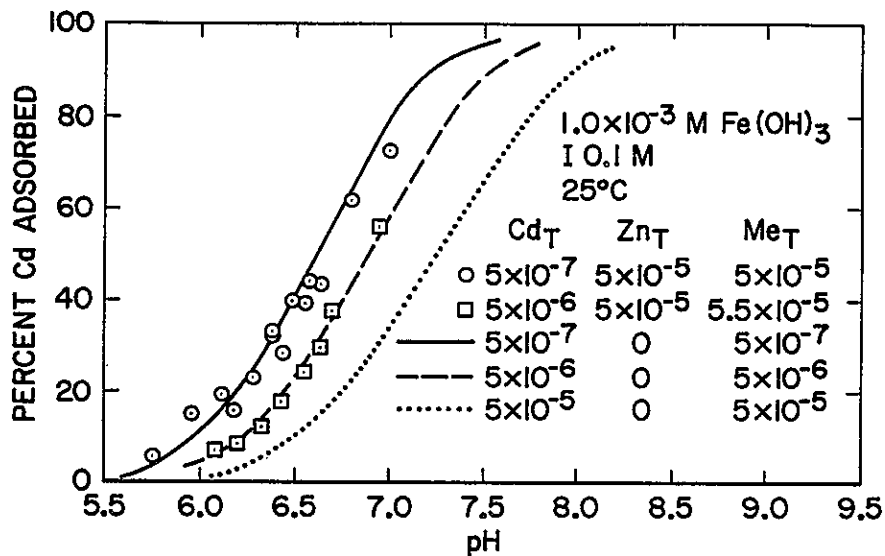


Figure A-48. pH-adsorption edge for Cd on am-Fe(OH)<sub>3</sub> in presence of Zn

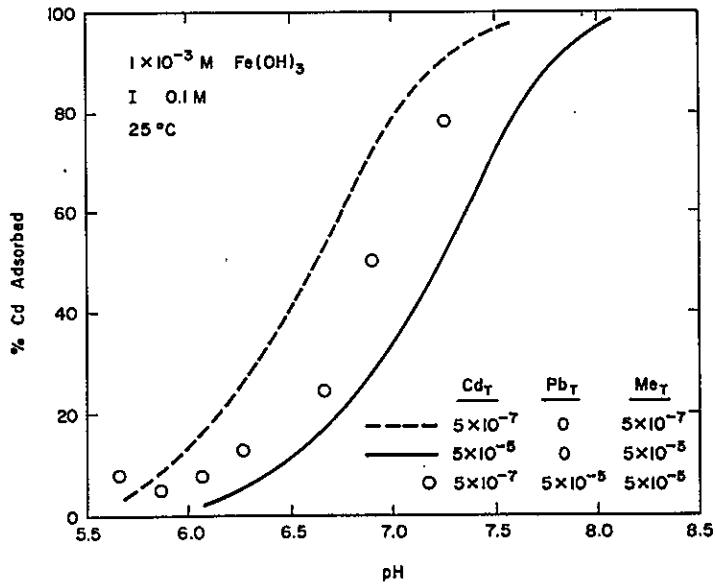


Figure A-49. pH-adsorption edge for Cd on am- $\text{Fe(OH)}_3$  in presence of Pb

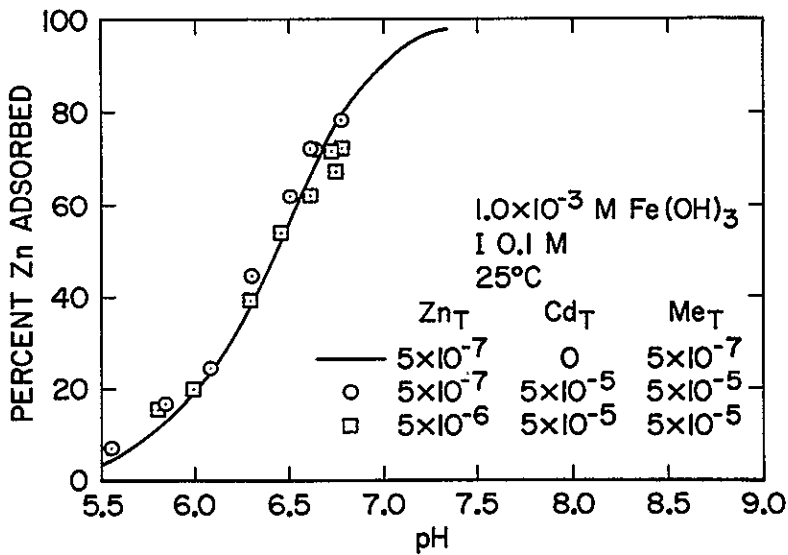


Figure A-50. pH-adsorption edge for Zn on am- $\text{Fe(OH)}_3$  in presence of Cd



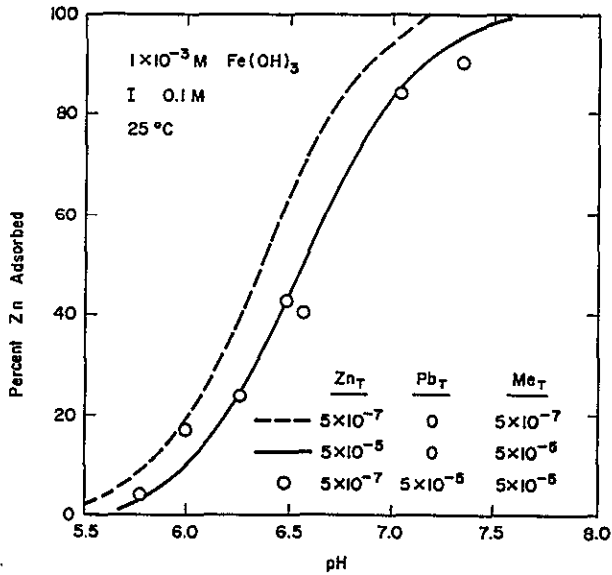


Figure A-51. pH-adsorption edge for Zn on am-Fe(OH)<sub>3</sub> in presence of Pb

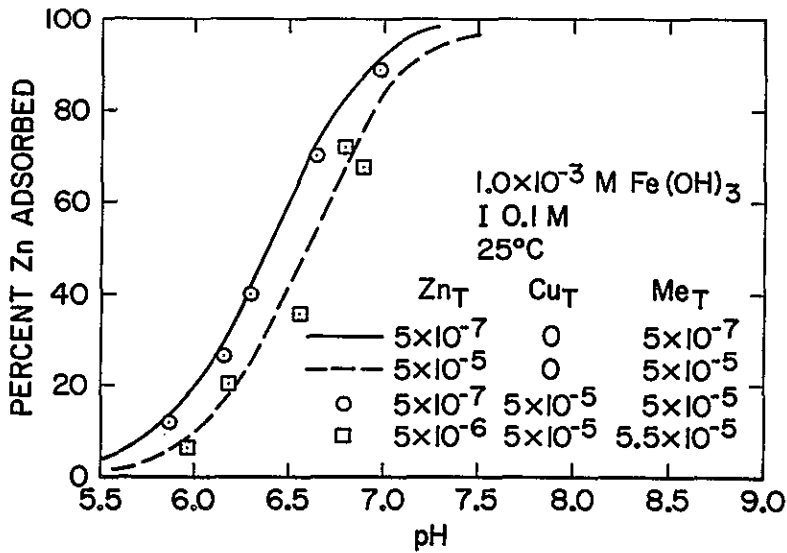


Figure A-52. pH-adsorption edge for Zn on am-Fe(OH)<sub>3</sub> in presence of Cu

## Appendix B

### EXPERIMENTAL METHODS AND MATERIALS

#### REAGENTS AND INSTRUMENTATION

All reagents used in this study were analytical grade or better. Water was deionized, conductivity grade. Approximately 1.0M and 0.1M nitric acid were prepared by diluting concentrated redistilled nitric acid. When a solution of nitric acid or sodium hydroxide of exact molarity was required, Dilut-it (VWR Corp., San Francisco, Calif.) reagents were used. Carbonate-free sodium hydroxide was stored in a rubber-capped serum bottle under nitrogen. Stock 0.1M and 1.0M ferric nitrate solutions were prepared in approximately 0.7M nitric acid and standardized by the ferrozine method. Stock solutions of adsorbate metals were made by dissolving the pure metal or the metal nitrate in 0.1M nitric acid. Stock solutions of anions were prepared by dissolving the sodium anion salt into dissolved water.

Arsenic-74, Silver-110m, Chromium-51, Selenium-75, Cadmium-109, and Zinc-65 were obtained from New England Nuclear Corp. (Boston, Mass.). Radioactive counting was performed using a Baird Atomic Model 810c well counter, with a 1 $\frac{3}{4}$ " dia x 2" thick NaI(Tl) crystal. Carrier-free thiosulfate tagged with S-35 was also purchased from New England Nuclear. Radioactive counting of this isotope was performed on a Packard Tri-Carb liquid scintillation counter with quenching correction by automatic external standardization.

Electrophoretic mobility measurements were made with a Zeta meter (Zeta Meter, Inc., New York, N. Y.).

pH was measured with a Radiometer Model 22 pH meter using a Model GK2301C combination electrode. For measurements of copper-ion activity the potential of an Orion ion-selective electrode versus an Orion double junction calomel reference electrode was measured using a precision dc voltmeter which could be read to within  $\pm 10 \mu\text{V}$ .

All experimental vessels and storage containers were Pyrex glass or Nalgene.

## EXPERIMENTAL PROCEDURES

### Preparation of the Adsorbents

am-Fe(OH)<sub>3</sub>. Amorphous hydrous iron oxyhydroxide was precipitated in situ. An appropriate amount of 0.1M Fe(NO<sub>3</sub>)<sub>3</sub> stock solution was pipeted into a 500-ml double-walled Pyrex reaction flask maintained at 20°C by a circulating water bath. One-tenth molar NaNO<sub>3</sub> and deionized water were added to attain the total volume and ionic strength desired. The solution was stirred with a teflon-coated magnetic spin bar and was purged with water-saturated CO<sub>3</sub>-free nitrogen gas continuously. After 10 minutes the solution was adjusted to pH 7.5 ± 0.5 by dropwise addition of 1.0M CO<sub>3</sub>-free NaOH, precipitating the iron. The suspension was aged under these conditions for 3 hours, with dropwise addition of 0.1M CO<sub>3</sub>-free NaOH as needed to maintain near-neutral pH. The pH was then adjusted to the lowest pH at which adsorption was to be studied and was maintained for one hour before addition of the adsorbate.

α-SiO<sub>2</sub>. α-quartz was purchased from Pennsylvania Glass Sand Corp. (Pittsburgh, Penn.) under the brand name Min-U-Sil 5. It consists of particles of 5-μm median diameter which have a slightly reddish tint due to iron oxide impurities.

The cleaning procedure used to prepare the silica was similar to that of MacNaughton (1). A batch of the solid was heated to 550°C for 48 hours to oxidize organic contaminants. It was then refluxed in 4M HNO<sub>3</sub> for 4 hours and rinsed continuously with deionized water until the pH of the rinse water was approximately 4.5. The refluxing and rinsing steps were repeated, following which the solid was rinsed with deionized water adjusted to pH 10 with NaOH. It was then rinsed repeatedly with deionized water until the pH of the rinse water was approximately 7. After drying at 125°C the solid was a milky-white powder which released no detectable iron when soaked overnight in 0.1M HNO<sub>3</sub>. X-ray diffraction analyses by MacNaughton (1) and Vuceta (2) confirm the crystal structure as that of α-quartz. The prepared silica was used in adsorption experiments without further pretreatment.

γ-Al<sub>2</sub>O<sub>3</sub>. The γ-alumina (γ-Al<sub>2</sub>O<sub>3</sub>) was provided by Cabot Co. (Boston, Mass.). Since a 1.0-g/l slurry released no detectable copper or lead to solution at pH 3.5, the solid was used in adsorption experiments without pretreatment.

### Characterization of the Adsorbents

The adsorbents were characterized with respect to their bulk and surface properties. All three adsorbents had been carefully characterized by other workers for

use in adsorption experiments. Since this information is used only for qualitative comparisons among adsorbents, literature values were not experimentally verified. The properties of interest are bulk crystal structure, particle size and shape, the point of zero charge, iso-electric point, and specific surface area.

Amorphous Iron Oxyhydroxide

Specific Surface Area. Freeze-dried amorphous iron oxyhydroxide had a surface area of 182 m<sup>2</sup>/g as measured by BET nitrogen adsorption with 48 hours of outgassing at room temperature (Table B-1). Yates (3) and Avotins (4) measured the BET surface area of amorphous iron oxides prepared in a similar manner from ferric nitrate solution and obtained values of 257 and 159 m<sup>2</sup>/g, respectively. Yates estimated the chemical composition thermogravimetrically as Fe<sub>2</sub>O<sub>3</sub> · H<sub>2</sub>O. The water content was approximately 10 percent as determined by weight loss on heating at 980°C in air after outgassing to constant weight at room temperature (3).

The BET nitrogen surface-area measurement must be used with some caution. Yates (3) studied weight loss of amorphous iron oxyhydroxide as a function of time and temperature of outgassing. As the temperature of outgassing was increased, more chemisorbed water was released. Surface structure is probably altered by the evolution of chemisorbed water (3). Yates presented evidence that outgassing of amorphous iron oxyhydroxide even at room temperature caused some surface decomposition. The result is probably an underestimate of the actual specific surface area.

Table B-1

SPECIFIC SURFACE AREA OF am-Fe(OH)<sub>3</sub>

Method	Specific Surface Area (m <sup>2</sup> /g)	Reference
BET	254 159 182	Yates (3) Avotins (4) Davis (5)
Negative adsorption-Mg <sup>2+</sup>	700 (pH 5)	Avotins (4)
Negative adsorption-Na <sup>+</sup>	270-335 (pH 4)	Davis (5)

The results of sodium-negative adsorption experiments at pH 4 in this study indicated a surface area in the range 270-335 m<sup>2</sup>/g for amorphous iron oxyhydroxide. Avotins (4) reported a surface area of 700 m<sup>2</sup>/g, measured by negative adsorption of Mg(II) at pH 5. However, a gel layer porous to water but not to Na<sup>+</sup> or Mg<sup>2+</sup> could result in an erroneously low value for surface area measured by this technique. Van den Hull and Lyklema (6) have shown that the method applies only to smooth, non-porous surfaces. Irregularities in surface structure and pores smaller than the double layer thickness are not observed.

Both negative adsorption and BET measurement techniques may provide low estimates of surface area for amorphous iron oxyhydroxide because of porosity and surface decomposition, respectively. Assuming spherical particles of 20 Å diameter and the density (3.57 g/cm<sup>3</sup>) given by Murphy et al. (7), a specific surface area of 840 m<sup>2</sup>/g is estimated for amorphous iron oxyhydroxide. The actual specific surface area is probably less than 840 m<sup>2</sup>/g but more than that determined by negative adsorption (~300 m<sup>2</sup>/g). All figures in this study are based on the BET measurement of 182 m<sup>2</sup>/g unless otherwise stated.

Surface Charge and pHPZC. The surface charge density ( $\sigma_o$ ) on hydrous oxides is defined by the net uptake of protons by the surface and is determined by potentiometric titration, i.e.,

$$\sigma_o = F(\Gamma_{H^+} - \Gamma_{OH^-}) = F(C_A - C_B + [OH^-] - [H^+])/A \quad (B-1)$$

where  $\sigma_o$  has the units of coulombs/cm<sup>2</sup> and A is the surface area in suspension in cm<sup>2</sup>/l. Unfortunately, experimental difficulties were encountered in acid-base titrations of amorphous iron oxyhydroxide. Hysteresis problems were serious. In the pH region 6-9 an acid titration curve was sometimes separated by as much as 0.4 pH units from a base titration curve. Similar problems were reported by Yates (3). As a result there were difficulties in the determination of pHPZC by potentiometric titration. Batch acid titrations at different ionic strengths indicated that pHPZC was in the pH region 7.5-8.5. The pHPZC of most iron oxides are in this region (3,8). Yates (3) stated that pHPZC of amorphous iron oxyhydroxide in KNO<sub>3</sub> was 8.0 but did not show the titration data at different ionic strengths.

A salt titration method was preferable for determination of the pHPZC of amorphous iron oxyhydroxide. The salt titration was accomplished simply by observing the change in pH upon addition of electrolyte to batches of iron oxide suspensions.

A large batch of iron oxyhydroxide ( $10^{-3}\text{M Fe}$ ) was prepared by the normal preparation procedure in deaerated double-distilled water in a flowing nitrogen atmosphere. After one hour of aging the iron oxide batch was washed with deaerated water until the ionic strength was lowered to  $\sim 10^{-3}\text{M}$  and then the iron oxyhydroxide suspension was concentrated by an order of magnitude ( $10^{-2}\text{M Fe}$ ). This concentrated suspension was divided into several smaller batches, each kept under a flowing nitrogen atmosphere. pH adjustments were made during the final (fourth) hour of aging so that the batch suspensions had a series of pH values within the pH region 6.5-9.5. Sodium nitrate was then added to increase the ionic strength. The addition of salt moves the pH toward  $\text{pH}_{\text{PZC}}$  by increasing surface charge. At the  $\text{pH}_{\text{PZC}}$  there should be no change in pH upon addition of salt. Figure B-1 displays  $\Delta\text{pH}$ , the change in pH upon addition of salt, versus the pH of the low ionic strength batches. A  $\text{pH}_{\text{PZC}}$  near 7.9 is indicated which is in good agreement with the  $\text{pH}_{\text{PZC}}$  (8.0) determined by Yates (3) and others (8).

Figure B-2 shows surface charge density ( $\sigma_0$ ) on amorphous iron oxyhydroxide as a function of pH at various ionic strengths. Surface charge was determined by potentiometric titration of amorphous iron oxyhydroxide and comparison with titrations of the ionic medium (9). A surface area of  $182\text{ m}^2/\text{g}$  (BET) and  $\text{pH}_{\text{PZC}}$  of 7.9 were used for the surface charge density calculation. Figure B-3 displays the results of Yates (3) for three different iron oxides. Yates proposed that the higher surface charge density and differential capacity observed for amorphous iron oxyhydroxide are indications that a porous double layer or gel layer exists at the surface. A comparison of the results of potentiometric titrations (Fig. B-2) with Yates' amorphous iron oxyhydroxide data (Fig. B-3) shows that significantly larger surface charge density and differential capacity were observed for the iron oxyhydroxide used in this study. The surface charge density of the iron oxyhydroxide used in this study was  $\sim 65\text{-}70\ \mu\text{C}/\text{cm}^2$  at pH 4 in  $0.1\text{M NaNO}_3$ . This surface charge density is larger than has been reported for most oxides (3,10). The surface charge density of goethite (Fig. B-3) is similar to that of most crystalline oxides reported in the literature. It is very likely that the specific surface areas reported for amorphous iron oxyhydroxide that were measured by BET gas adsorption were underestimated due to surface decomposition during outgassing. Thus, the surface charge densities of amorphous iron oxyhydroxide calculated by Yates (3) and in this study (Fig. B-2) may be too large. A larger specific surface area would decrease the derived surface charge density and differential capacitance.

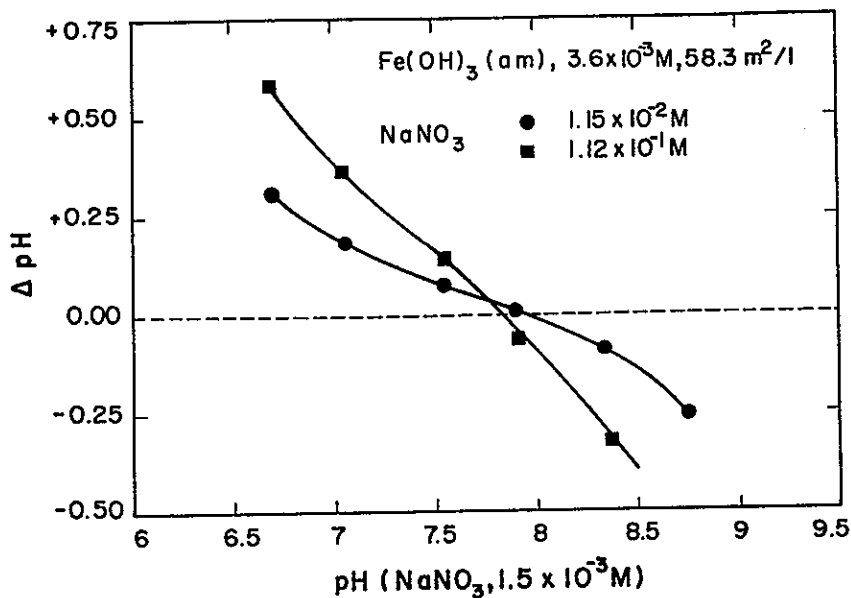


Figure B-1. Change in pH ( $\Delta$ pH) upon addition of sodium nitrate to amorphous iron oxide suspensions as a function of pH measured in low ionic strength medium ( $1.5 \times 10^{-3}$  M NaNO<sub>3</sub>).  $pH_{pZC}$  is  $\sim 7.9$

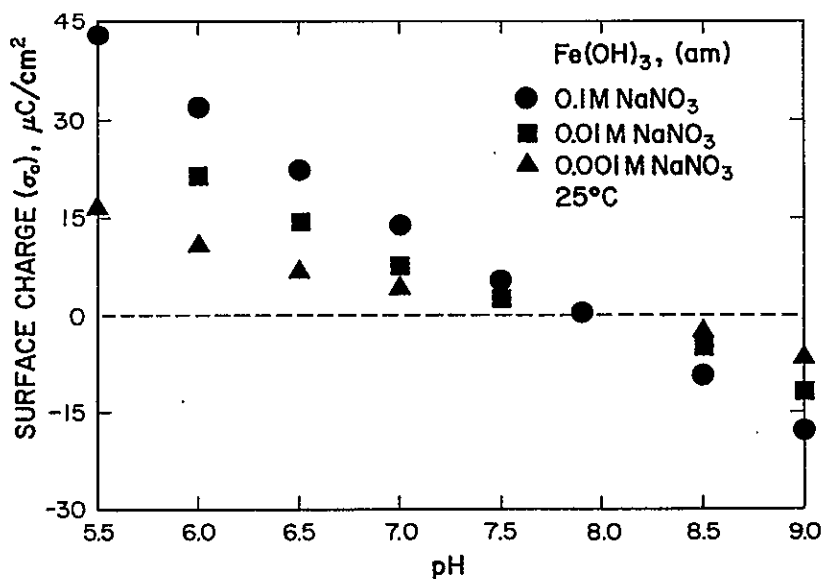


Figure B-2. Surface charge density ( $\sigma_0$ ) of amorphous iron oxide as a function of pH at various ionic strengths. BET surface area of 182 m<sup>2</sup>/g and  $pH_{pZC}$  of 7.9 used in the calculation of surface charge density

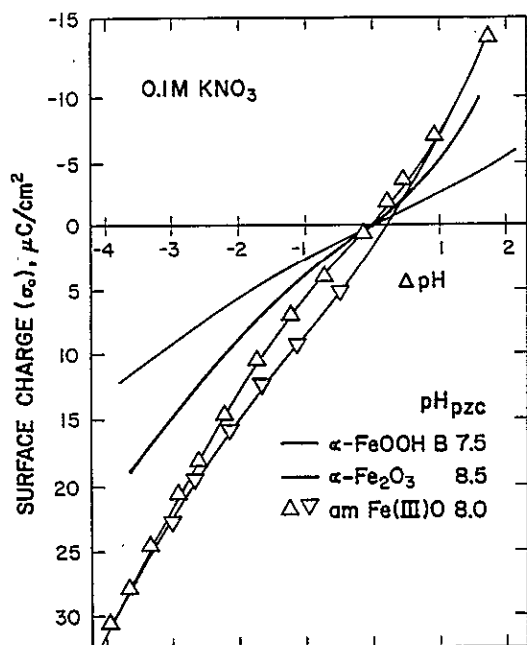


Figure B-3. Surface charge density curves for goethite, hematite, and amorphous iron oxide in 0.1M KNO<sub>3</sub>. After Yates (3)

The emphasis of this study has been on the distribution of solutes between solution and solid phases. The solid substrates have not been well characterized and uncertainty remains about the properties of amorphous iron oxyhydroxide. The incomplete characterization resulted partly because amorphous iron oxyhydroxide is not a model colloid and a complete understanding of its physical and chemical properties is difficult, even with the many advanced techniques available. A complete characterization of amorphous iron oxyhydroxide would constitute a full research problem in itself and is recommended for future investigations. In addition to the techniques already mentioned in this section, other experimental information would be useful, e.g.

1. Rate of dissolution in acid, oxalate solution, complexing agents, etc. (3).
2. Determination of rapidly and/or slowly exchangeable OH surface groups by tritium exchange (3).
3. Reversibility of nitrogen gas adsorption.

4. Electron Microscopy and ultracentrifugation techniques (7).
5. Potentiometric titrations in various ionic media.
6. A determination of "ion porosity," i.e., if a porous or gel layer exists, which ions may enter the pores?

Despite the fact that a complete characterization of amorphous iron oxyhydroxide was not made, this study has great practical value in that amorphous iron oxyhydroxide is used in engineering processes and is frequently found in natural aquatic systems as surface coatings and as a discrete mineral phase (11). It is important that an examination of these complex systems is made, even if a full interpretation of the results awaits further experimental work.

$\alpha$ -SiO<sub>2</sub>. The BET surface area of the  $\alpha$ -SiO<sub>2</sub> as determined by N<sub>2</sub>-adsorption is 3.3 m<sup>2</sup>/g. This value, which was confirmed by independent analysis (Department of Mineral Science and Engineering, University of California, Berkeley, Calif.), is somewhat lower than the values of 4 to 5 m<sup>2</sup>/g reported by MacNaughton (1) and Vuceta (2) for Min-U-Sil 5. The mildly alkaline rinse may have partially coated the particles with a layer of amorphous silica. Since MacNaughton did not specify the pH of his alkaline rinse and Vuceta used 4M NH<sub>4</sub>OH, it is possible that the thickness of the amorphous silica layer was different in the three studies, leading to the variation in specific surface areas.

The crystal structure of Min-U-Sil 5 treated in this way is that of  $\alpha$ -SiO<sub>2</sub> ( $\alpha$ -quartz) (12). The PZC of non-porous silica depends on how it is formed, but is generally in the range 2.0 to 3.0 (8). Literature values for the surface site density are generally in the range 3 to 6 sites per nm<sup>2</sup> (13).

$\gamma$ -Al<sub>2</sub>O<sub>3</sub>. The  $\gamma$ -alumina was provided by Cabot Co. (Boston, Mass.) under the trade name ALON and was from the same batch characterized by Huang and Stumm (14) and used in adsorption studies by Hohl and Stumm (15) and Huang et al. (16). The material consists of low-density particles of 0.3  $\mu$ m average diameter. The PZC as determined by acid-base titration is 8.3 (15). Huang and Stumm (14) reported the specific surface area to be 125  $\pm$  10 m<sup>2</sup>/g as determined by BET, negative adsorption, and differential capacity of the double layer (Table B-2). They claim the similarity of the results measured by the three techniques indicates that the oxide surface structure is relatively smooth and nonporous and is not altered by washing in 10<sup>-2</sup>M NaOH. The total concentration of surface hydroxyls was estimated from titration data to be 0.25 mole/kg or 1.3-OH groups per nm<sup>2</sup> by Hohl and

Table B-2

SPECIFIC SURFACE AREA OF  $\gamma\text{-Al}_2\text{O}_3$  MEASURED BY 3 DIFFERENT METHODS

Method	Specific Surface Area ( $\text{m}^2/\text{g}$ )	State of Adsorbent	State of Adsorbate
BET	129	Dry, untreated	$\text{N}_2$ -gas
t-plot	128	Dry, untreated	$\text{N}_2$ -gas
Negative adsorption	118	Wet, treated with NaOH	NaCl $2.5 \times 10^{-6}$ - $1.5 \times 10^{-5}\text{M}$
Capacity	117	Wet, treated with NaOH	NaCl ( $10^{-3}\text{M}$ )
From Huang and Stumm (14).			

Stumm (15). As pointed out by Yates (3), an acid-base titration may seriously underestimate the surface-site density. Peri (17) estimated the surface-site density to be  $8/\text{nm}^2$  from spectroscopic evidence.

A summary of the bulk and surface properties of  $\alpha\text{-SiO}_2$ ,  $\gamma\text{-Al}_2\text{O}_3$ , and  $\text{am-Fe}(\text{OH})_3$  is provided in Table B-3.

Table B-3

## SUMMARY OF SURFACE PROPERTIES OF THE ADSORBENTS

	$\text{Fe}(\text{OH})_3$	$\alpha\text{-SiO}_2$	$\gamma\text{-Al}_2\text{O}_3$
PZC	$7.9^a$	$2.5^b$	$8.3^c$
IEP	$7.9^a$	$2.5^b$	$8.3^c$
BET area	$182 \text{ m}^2/\text{g}^d$	$3.3 \text{ m}^2/\text{g}^d$	$125 \text{ m}^2/\text{g}^c$
Negative adsorption area	$300 \text{ m}^2/\text{g}^a$ $700 \text{ m}^2/\text{g}^e$	not done	$125 \text{ m}^2/\text{g}^c$
Oxide sited/ $\text{nm}^2$	$9.8^d$	3 to $6^g$	$8^h$
<sup>a</sup> Davis (5).		<sup>e</sup> Avotins (4)	
<sup>b</sup> Parks (8).		<sup>g</sup> Armistead et al. (13).	
<sup>c</sup> Huang and Stumm (14).		<sup>h</sup> Peri (17).	
<sup>d</sup> This work.			

### Adsorption Kinetics

Most studies of adsorption onto oxides or clays have been characterized either by rapid attainment of equilibrium or by two-step kinetics. In the latter case the first step is rapid, being complete within a few minutes, and is attributed to adsorption onto easily accessible surface sites (3). The second step is much slower, often continuing for days, and is related to solid-state diffusion of the adsorbate into the bulk adsorbent, sometimes accompanied by release of substrate metal ion to the solution (18).

Diffusion of adsorbate into the solid matrix can sometimes alter the bulk solid characteristics. Yates (3) showed that the PZC of oxides changes during the course of long-term experiments and that therefore certain types of data derived from such experiments are ambiguous.

Two-step kinetics have been reported for adsorption onto manganese dioxide (19), amorphous aluminum hydroxide (20), titanium dioxide (21), and amorphous iron hydroxide (5).

The goal of this work was to study adsorption under conditions that may be typical of engineering processes. For such conditions, only the rapid adsorption step is expected to be important. Reaction times were chosen to assure completion of this step and minimize the effect of the diffusion step. Based on preliminary experiments and results reported in the literature, an equilibrium time of four hours after addition of the adsorbate was chosen for experiments using  $\gamma\text{-Al}_2\text{O}_3$  and am- $\text{Fe}(\text{OH})_3$ . For experiments using  $\alpha\text{-SiO}_2$ , a one-hour equilibration period was used. The only deviation from this procedure was that a one-hour reaction period was used for the study of thiosulfate adsorption onto am- $\text{Fe}(\text{OH})_3$ .

### Procedures for Equilibrium Adsorption and Coprecipitation Experiments

Adsorption of Cd, Zn, Cu, Pb, As, Se, and Cr. The desired weight of  $\alpha\text{-SiO}_2$  or  $\gamma\text{-Al}_2\text{O}_3$  was ultrasonically dispersed in approximately 100 ml 0.1M  $\text{NaNO}_3$  and added to a 600-ml double-walled Pyrex beaker. The suspension which was continuously stirred by a teflon-coated magnetic spin bar and purged with nitrogen gas, was made up to the desired volume and ionic strength (typically 500 ml and 0.1M), and the pH was adjusted to near 4.5 with 0.1M  $\text{HNO}_3$ . After about 10 minutes the pH was adjusted to the lowest pH at which significant adsorption was expected for cations and highest pH for anions. One hour later the adsorbate ions were added

From their stock solutions along with sufficient 1.0M CO<sub>3</sub>-free NaOH to maintain the desired pH. In no case was the volume of (metal + base) added greater than 0.6 percent of the total suspension volume.

Adsorption onto silica. The slurry was stirred under nitrogen for one hour, at which time the pH was recorded and 15 ml of the slurry was transferred to a Pyrex centrifuge tube using a teflon-tipped glass syringe. The slurry was centrifuged in a clinical centrifuge for 10 minutes. A 4-ml sample of the clear supernatant was pipeted into a glass counting vial and acidified with 10  $\mu$ l concentrated, redistilled HNO<sub>3</sub>. The pH of the slurry remaining in the 600-ml flask was adjusted upward by approximately 0.3 units by addition of CO<sub>3</sub>-free NaOH and was re-equilibrated for one hour, at which time another sample was taken. This process was repeated until a pH was attained at which near 100-percent adsorption was expected.

Adsorption onto am-Fe(OH)<sub>3</sub> or  $\gamma$ -Al<sub>2</sub>O<sub>3</sub>. As described earlier, the am-Fe(OH)<sub>3</sub> was precipitated and aged four hours before addition of the adsorbate. Thereafter, the expected procedure was identical to that for  $\gamma$ -Al<sub>2</sub>O<sub>3</sub>. Approximately one minute after addition of the adsorbate, a 15-ml slurry sample was transferred into a nitrogen-purged Pyrex centrifuge tube, and the tube was tightly recapped. A small volume of CO<sub>3</sub>-free NaOH (< 100  $\mu$ l) was added to the bulk slurry and another sample was transferred into a centrifuge tube. This process was repeated until 8 to 12 15-ml slurry samples had been taken. The centrifuge tubes were placed on an end-over-end roller for 4 hours at ambient temperature. The pH in each centrifuge tube was measured in the magnetically stirred slurry using a combination pH electrode. The electrode was fitted with a Nalgene cup which made a tight fit with the mouth of the centrifuge tube, preventing entry of CO<sub>2</sub> during pH measurement. After the pH was recorded, the tubes were recapped and centrifuged on a clinical centrifuge for 10 minutes. A 4-ml sample of the clear supernatant was pipeted into a glass counting vial, acidified with 10  $\mu$ l concentrated HNO<sub>3</sub>, and stored for subsequent analysis. At pH less than approximately 7.0 the  $\gamma$ -Al<sub>2</sub>O<sub>3</sub> could not be completely separated from the solution phase by centrifugation. For these samples, solid/liquid separation was by vacuum filtration through a 0.45- $\mu$ m Millipore filter supported in a plastic filter holder. Analysis of adsorbent-free standard solutions of Cd, Cu, and Pb before and after filtering showed that the metals were neither lost to nor leached from the filter and/or holder.

Adsorption of Se, As, Cr. The adsorption of anions onto  $\alpha\text{-SiO}_2$  and  $\gamma\text{-Al}_2\text{O}_3$  was not studied. The experimental procedures described for adsorption of cations onto  $\text{am-Fe(OH)}_3$  were also used to study the adsorption of chromate, selenite, selenate, and arsenate onto  $\text{am-Fe(OH)}_3$ .

Systems Containing Complexing Ligands. Adsorption of cadmium on each adsorbent was studied in the presence of  $\text{Cl}^-$ ,  $\text{SO}_4^{2-}$ , or  $\text{S}_2\text{O}_3^{2-}$ . When the adsorbent was  $\alpha\text{-SiO}_2$  or  $\gamma\text{-Al}_2\text{O}_3$ , the sodium salt of the ligand was added from a stock solution before the solid was dispersed. The  $\text{S}_2\text{O}_3^{2-}$  stock solution was stored at pH 12 to prevent reduction of the sulfur. In experiments using  $\text{am-Fe(OH)}_3$ , the ligand was added approximately 30 minutes after the solid was precipitated, so the precipitation was always from a solution containing only  $\text{Fe(NO}_3)_3$ ,  $\text{NaNO}_3$ ,  $\text{HNO}_3$ , and deionized water.

Adsorption of thiosulfate. Experimental details for the adsorption of thiosulfate onto  $\text{am-Fe(OH)}_3$  were the same as for metal adsorption studies, except that the pH was adjusted downward instead of upward between slurry samples using 0.1M  $\text{HNO}_3$ . In addition, since  $\text{S}_2\text{O}_3^{2-}$  analysis was done by liquid scintillation counting of  $\text{S}^{35}$ , 10 ml of the supernatant from each tube was pipeted into a plastic counting vial containing 10 ml Insta-Gel Liquid Scintillation cocktail. The solution was swirled and stored for subsequent analysis.

Coprecipitation experiments-- $\text{am-Fe(OH)}_3$ . The only difference between adsorption and coprecipitation experiments was the addition of adsorbate prior to precipitation in the coprecipitation system.

## ANALYTICAL PROCEDURES

### Radioisotopes

Chromium-51, Selenium-75, Arsenic-74, Zinc-65, and Cadmium-109 were added to their respective stock solutions and used as tracers of adsorbate concentration. Fractional adsorption was computed by comparing the background-corrected activity of the 4-ml supernatant sample with that of a 4-ml sample of slurry taken shortly after addition of the metal to the bulk suspension. At least 5000 counts above background were collected for each sample. The instrumental settings were

	<u>Cadmium</u>	<u>Zinc</u>	<u>Selenium</u>	<u>Arsenic</u>	<u>Chromium</u>
Voltage	1200	1400	900	950	900
Lower level	0.4 V	10.0 V	2.0 V	1.0 V	2.1 V
Window	1.0 V	2.0 V	1.8 V	7.0 V	0.8 V
Coarse grain	1/8	1/4	1/4	1/4	1/4
Fine grain	0.75	0	0	0	0

#### Copper and Lead

Copper and lead were analyzed by flameless atomic absorption spectrophotometry. Total copper or lead in  $\text{Fe}(\text{OH})_3$  systems was measured by adding 20  $\mu\text{l}$  concentrated  $\text{HNO}_3$  to a 4-ml slurry sample to dissolve the  $\text{Fe}(\text{OH})_3$  and analyzing the resulting solution. Since  $\alpha\text{-SiO}_2$  and  $\gamma\text{-Al}_2\text{O}_3$  cannot be dissolved easily and the solids interfere with AA analysis, the following procedure was adopted. Shortly after the adsorbate was added to the system, a 15-ml slurry sample was transferred to a centrifuge tube and enough 1.0M  $\text{HNO}_3$  was added to adjust the sample pH to between 3.0 and 3.5. The tube was placed on an end-over-end roller for 30 minutes, after which solid separation was accomplished by centrifugation or filtration. The amount of metal in solution was taken to be the total exchangeable metal in the system. Tests showed that the amount of metal lost to or leached from the solid and/or container walls at pH between 3.0 and 3.5 was small compared to the amount added.

#### pH Measurement

Measurement of pH in a slurry can be complicated because the motion of charged particles near the electrode surface can change the electrode response characteristics. Deviations from normal electrode behavior can include a shift in the potential vs. pH curve or a slow approach to the equilibrium pH value. Davis (5) and Avotins (personal communication) found that in am- $\text{Fe}(\text{OH})_3$  slurries the pH reading drifted slowly and continuously with time, and chose to record the measured pH after the electrode had been immersed in the unstirred slurry a specified length of time as the "equilibrium" pH. In stirred slurries of  $\alpha\text{-SiO}_2$  or  $\gamma\text{-Al}_2\text{O}_3$ , no pH drift was observable shortly after the electrode was immersed.

The pH drift of stirred  $\text{Fe}(\text{OH})_3$  slurries was also very slight after 1 minute of immersion. Therefore, the pH recorded as the equilibrium value in all experiments was that of the stirred slurry 30 seconds to 3 minutes after immersion of the combination electrode, at which time electrode drift appeared negligible

(< 0.02 units/min). This technique gave approximately the same pH-adsorption relationship for copper adsorbing onto am-Fe(OH)<sub>3</sub> as the method of Davis (5).

### Mixing Studies

The residence time distribution (RTD) studies were conducted using a plexiglass tank (volume of 109.4 ml) with a six-blade turbine impeller (Figure B-4). The distribution of residence times in the mixing tank was determined by the impulse method (22,23) using a pulse of 0.25M KCl solution as tracer and change in conductivity as the signal.

Adsorption experiments using Cadmium-109 tracer were used as a diagnostic tool to evaluate the adsorption characteristics of the amorphous iron oxyhydroxide precipitated under different mixing conditions. Adsorption experiments were conducted as described above.

### Experimental Procedures for Coagulation and Sedimentation Experiments

The coagulation and sedimentation experiments were conducted in a parametric fashion so that the optimal value of each parameter varied in the test run was used in subsequent experiments. The parameters of interest were iron dose, polymer dose, pH, waste dilution, and settling time in the order studied.

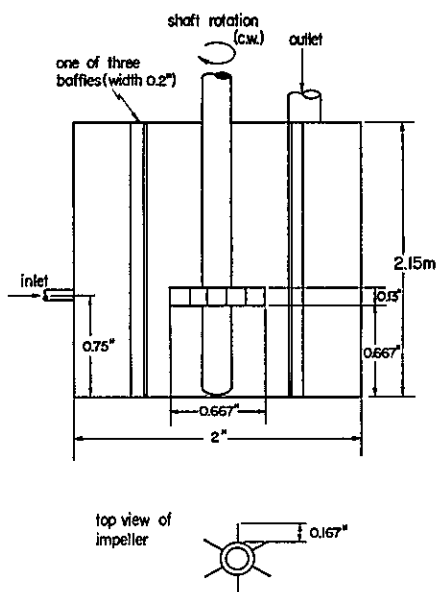


Figure B-4. Mixing tank diagram (cross section)

In each experiment a coagulation/flocculation stirring machine with six stirring bars was set up using 600-ml Pyrex beakers as the reaction vessels. Before addition of the iron dose, somewhat less than 400 ml of waste was added to each beaker, followed by addition of the polymer dose. Upon addition of the iron dose, rapid and equal mixing was initiated in each beaker. During this period of rapid mixing the pH in each beaker was adjusted to the desired value. After rapid mixing, the mixing speed was reduced to allow 15 minutes for flocculation. Solutions were then allowed to settle for forty-five minutes. About 20 ml of supernatant solution was withdrawn at the end of the settling period. A Hach Model 2100A turbidimeter was used to measure the residual turbidity.

#### REFERENCES

1. M. G. MacNaughton. "Adsorption of Mercury(II) at the Solid-Water Interface." Ph.D. Thesis, Stanford University, Stanford, Calif., 1973.
2. J. Vuceta. "Adsorption of Pb(II) and Cu(II) on  $\alpha$ -Quartz from Aqueous Solutions: Influence of pH, Ionic Strength, and Complexing Ligands." Ph.D. Thesis, California Institute of Technology, Pasadena, Calif., 1976.
3. D. E. Yates. "The Structure of the Oxide/Aqueous Electrolyte Interface." Ph.D. Thesis, University of Melbourne, Australia, 1975.
4. P. V. Avotins. "Adsorption and Coprecipitation Studies of Mercury on Hydrous Iron Oxides." Ph.D. Thesis, Stanford University, Stanford, Calif., 1975.
5. J. A. Davis. "Adsorption of Trace Metals and Complexing Ligands at the Oxide/Water Interface." Ph.D. Thesis, Stanford University, Stanford, Calif., 1977.
6. H. J. van den Hull and J. Lyklema. "Determination of Specific Surface Areas of Dispersed Materials. Comparison of the Negative Adsorption Method with Some Other Methods." J. Amer. Chem. Soc., 90, 3010 (1968).
7. P. J. Murphy, A. M. Posner and J. P. Quirk. "Characterization of Partially Neutralized Ferric Nitrate Solutions." J. Coll. Interface Sci., 56, 270 (1976).
8. G. A. Parks. "The Isoelectric Points of Solid Oxides, Solid Hydroxides, and Aqueous Hydroxo Complex Systems." Chem. Reviews, 65, 177 (1965).
9. G. A. Parks and P. L. DeBruyn. "The Zero Point of Charge of Oxides." J. Phys. Chem., 66, 967-976 (1962).
10. W. Stumm, C. P. Huang and S. R. Jenkins. "Specific Chemical Interaction Affecting the Stability of Dispersed Systems." Croat. Chem. Acta, 42, 223-245 (1970).
11. E. Jenné. "Controls on Mn, Fe, Co, Ni, Cu, and Zn Concentrations in Soils and Water: The Significant Role of Hydrous Mn and Fe Oxides." Adv. Chem. Series, 73, 337 (1968).

12. M. MacNaughton and R. James. "Adsorption of Aqueous Mercury(II) Complexes at the Oxide/Water Interface." J. Coll. Interface Sci., 47, 431 (1974).
13. C. G. Armistead, A. J. Tyler, F. H. Hambleton, S. A. Mitchell and J. A. Hockey. "Surface Hydroxylation of Silica." J. Phys. Chem., 73, 3947 (1969).
14. C. P. Huang and W. Stumm. "Specific Adsorption of Cations on Hydrous  $\gamma\text{-Al}_2\text{O}_3$ ." J. Coll. Interface Sci., 43, 409 (1973).
15. H. Hohl and W. Stumm. "Interaction of  $\text{Pb}^{2+}$  with Hydrous  $\gamma\text{-Al}_2\text{O}_3$ ." J. Coll. Interface Sci., 55, 281-288 (1976).
16. C. P. Huang, H. A. Elliott and R. M. Ashmead. "Interfacial Reactions and the Fate of Heavy Metals in Soil-Water Systems." J. Water Poll. Cont. Fed., 49, 745-756 (1977).
17. J. B. Peri. "Infrared and Gravimetric Study of the Surface Hydration of  $\gamma$ -Alumina." J. Phys. Chem., 69, 211 (1965).
18. J. W. Murray. "The Interaction of Metal Ions at the Manganese Dioxide-Solution Interface." Geochim. Cosmochim. Acta, 39, 505-519 (1975).
19. P. Loganathan and R. Bureau. "Sorption of Heavy Metal Ions by a Hydrous Manganese Oxide." Geochim. Cosmochim. Acta, 37, 1277-1293 (1973).
20. M. A. Anderson, J. F. Ferguson and J. Garvis. "Arsenate Adsorption on Amorphous Aluminum Hydroxide." J. Coll. Interface Sci., 54, 391 (1976).
21. Y. G. Bérubé and P. L. DeBruyn. "Adsorption at the Rutile-Solution Interface. I. Thermodynamic and Experimental Study." J. Coll. Interface Sci., 27, 305 (1968).
22. J. B. Gray. "Flow Patterns, Fluid Velocities, and Mixing in Agitated Vessels," Mixing: Theory and Practice, Vol. 1. New York: Academic Press, 1966.
23. O. Levenspiel and K. B. Bischoff. "Patterns of Flow in Chemical Process Vessels." Adv. in Chemical Engineering, Vol. 4. New York: Academic Press, 1963.



**THIS PAGE INTENTIONALLY  
LEFT BLANK**